

# **Classifying sediments on Dutch riverbeds using multi-beam echo-sounder systems**

Proefschrift

ter verkrijging van de graad van doctor  
aan de Technische Universiteit Delft,  
op gezag van de Rector Magnificus prof.ir. K.C.A.M. Luyben,  
voorzitter van het College voor Promoties,  
in het openbaar te verdedigen  
op woensdag 20 november 2013 om 15:00 uur

door

**Dimitrios ELEFTHERAKIS**

Master of Science in Offshore & Ocean Technology  
(specialising in: Diving & Underwater Technology)  
Cranfield University, Verenigd Koninkrijk  
geboren te Athene, Griekenland

Dit proefschrift is goedgekeurd door de promotor:

Prof. dr. D.G. Simons

Copromotor: Dr. ir. M. Snellen

Samenstelling promotiecommissie:

Rector Magnificus,	voorzitter
Prof. dr. D.G. Simons,	Technische Universiteit Delft, promotor
Dr. ir. M. Snellen,	Technische Universiteit Delft, copromotor
Dr. ir. N.A. Kinneging,	Rijkswaterstaat Water Verkeer & Leefomgeving
Prof. dr. ir. W.S.J. Uijtewaal,	Technische Universiteit Delft
Prof. dr. ir. J.C. Winterwerp,	Technische Universiteit Delft
Prof. dr. ir. E.C. Slob,	Technische Universiteit Delft
Prof. dr. J. Greinert,	Christian-Albrecht Universiteit, Duitsland

ISBN 978-90-8891-724-0

Copyright © 2013 by Dimitrios Eleftherakis. All rights reserved.

Cover design: Proefschriftmaken.nl || Uitgeverij BOXPress

Printed by: Proefschriftmaken.nl || Uitgeverij BOXPress

Published by: Uitgeverij BOXPress, 's-Hertogenbosch

*To my mother*

*Στη μητέρα μου*



# Contents

<b>1</b>	<b>Introduction .....</b>	<b>1</b>
1.1	Navigability of Dutch rivers – Motivation of the thesis.....	2
1.2	Systems for mapping the riverbed.....	3
1.3	Research objectives .....	5
1.4	Outline of the thesis.....	6
<b>2</b>	<b>Background .....</b>	<b>9</b>
2.1	Acoustic measurements using MBES .....	10
2.1.1	General information .....	10
2.1.2	Bathymetry.....	12
2.1.3	Imaging .....	13
2.1.4	Resolution .....	13
2.2	Interaction of sound with sediments.....	14
2.2.1	Reflection of sound at interface .....	14
2.2.2	Scattering of sound .....	20
2.2.3	The use of MBES for determining sediment backscatter strength .....	27
2.3	Classification using MBES measurements .....	28
<b>3</b>	<b>Surveyed rivers and equipment.....</b>	<b>31</b>
3.1	Surveyed rivers.....	32
3.2	Equipment .....	34
<b>4</b>	<b>An inter-comparison of sediment classification methods based on multi-beam echo-sounder backscatter and sediment natural radioactivity data.....</b>	<b>37</b>
4.1	Introduction .....	38
4.2	A description of the measurements taken in the area.....	39
4.3	Sediment Classification Methods.....	41
4.3.1	The Bayesian classification method using MBES backscatter data .....	41
4.3.2	A model-based approach for sediment classification .....	42
4.3.3	Medusa method.....	43
4.4	Classification Results .....	45
4.4.1	Bayesian results .....	45
4.4.2	Model-based results .....	46
4.4.3	Medusa results .....	50
4.5	Comparison and Discussion .....	53
4.6	Summary and conclusions.....	56
<b>5</b>	<b>Improving riverbed sediment classification using backscatter and depth residual features of multi-beam echo-sounder systems.....</b>	<b>59</b>
5.1	Introduction .....	60
5.2	Experiments and previous results.....	61
5.2.1	A description of the surveyed areas .....	61

5.2.2	Details of the surveys .....	63
5.2.3	A summary of applying the BCM to the areas .....	63
5.3	Methodology .....	65
5.3.1	Principal component analysis .....	65
5.3.2	K-means clustering .....	67
5.4	Data preparation .....	68
5.4.1	Extracting the features from the surface patches .....	68
5.4.2	Correcting for slopes and angular effect in backscatter data .....	70
5.4.3	Determining the optimum set of features.....	71
5.5	Results and discussions .....	72
5.5.1	Classification based on backscatter strength.....	73
5.5.2	Classification based on LS depth residuals.....	75
5.5.3	Classification using all features .....	78
5.5.4	Discussion of results .....	82
5.6	Summary and conclusions.....	83
<b>6</b>	<b>Potential of multi-beam echo-sounder backscatter strength and depth residuals as classifying parameters for very coarse riverbed sediments .....</b>	<b>87</b>
6.1	Introduction .....	88
6.2	Description of surveys.....	89
6.3	Classification results .....	93
6.3.1	Classification methodology .....	93
6.3.2	Classification maps .....	95
6.3.3	Correlation with grabs.....	95
6.4	Discussion of results.....	98
6.4.1	Observations on the behaviour of backscatter and depth residuals as a function of mean grain size .....	98
6.4.2	A quantitative assessment of backscatter and depth residuals as a function of mean grain size .....	99
6.5	Conclusions .....	106
<b>7</b>	<b>Overview of methodologies for the acoustic classification of sediment distribution in Dutch rivers using multi-beam echo-sounder data .....</b>	<b>111</b>
7.1	Introduction .....	112
7.2	Description of the surveys.....	112
7.3	Classifiers .....	115
7.4	Methods.....	117
7.5	Results .....	118
7.6	Conclusions .....	119
<b>8</b>	<b>Identifying changes in riverbed morphology and sediment composition using multi-beam echo-sounder measurements .....</b>	<b>121</b>
8.1	Introduction .....	122
8.2	A description of the surveyed area.....	123
8.3	Determining changes in riverbed morphology.....	126
8.4	Determining changes in the sediment distribution.....	128
8.4.1	Changes based on grab samples.....	130
8.4.2	Changes based on backscatter values .....	132
8.5	Conclusions .....	135

<b>9</b>	<b>Conclusions and outlook .....</b>	<b>137</b>
9.1	Conclusions .....	138
9.1.1	Conclusions from Chapter 4, the finer sediments .....	138
9.1.2	Conclusions from Chapter 5, intermediate grain size sediments .....	139
9.1.3	Conclusions from Chapter 6, the coarsest sediments.....	140
9.1.4	Conclusions from Chapter 7, overview of classifiers and methods.....	141
9.1.5	Conclusions from Chapter 8, application of classification methods....	142
9.2	Outlook.....	143
<b>A.</b>	<b>Maps of features combinations.....</b>	<b>145</b>
<b>B.</b>	<b>Classification map of Dordtse kil based on Depth Residuals .....</b>	<b>149</b>
<b>C.</b>	<b>Bathymetry maps of Bovenrijn and Meuse.....</b>	<b>153</b>
	<b>Summary.....</b>	<b>157</b>
	<b>Samenvatting .....</b>	<b>161</b>
	<b>Acknowledgements .....</b>	<b>165</b>
	<b>Curriculum vitae.....</b>	<b>167</b>



# 1 Introduction

---

Classification of sediments of river- and sea-beds is of high importance for a large number of applications. The applications are numerous, including e.g. navigation, marine geology, geophysics, marine biology, cable and pipeline laying and maintenance, and coastal engineering. Nowadays acoustic remote sensing systems are available for bathymetric measurements. These systems, however, can also be used for sediment classification, i.e., provide information about the way different types of sediment are distributed over an area. In this thesis focus is on the development of methods for the classification of riverbed sediments. Having available these methods is highly relevant for ensuring safe navigation on the Dutch rivers, as is further addressed in the next section. This motivation is followed by a brief overview of the main systems for mapping the riverbeds, that is the side scan sonar, the single-beam echo-sounder and the multi-beam echo-sounder. This latter system is the system used throughout this thesis. Then the research objectives are summarized, focusing on how the data collected from multi-beam echo-sounders can be used for mapping the sediment distribution on riverbeds. Finally, the outline of the thesis is presented.

## 1.1 Navigability of Dutch rivers – Motivation of the thesis

The Netherlands are part of four international river basins: Rhine, Meuse, Scheldt and Ems. These rivers cross the Netherlands towards the Wadden Sea and the North Sea. The Dutch rivers are used for inland waterway transport inside the Netherlands but also between the Netherlands and their neighbouring countries. For example, the total freight between Rotterdam and Duisburg (Germany) amounted to 165 million metric tons in 1996.<sup>1</sup> Also, about every three minutes, a ship passes the Dutch-German border at Lobith, 24 hours a day and 7 days a week.<sup>1</sup> Therefore the economic importance of the Dutch rivers is very high.

Three factors can affect the water volume in a river: meltwater, precipitation and groundwater. The amounts of precipitation and meltwater are much smaller in the summer than in the winter. Therefore during this period the river stream is narrow, whereas especially during the winter the overflowing river can cover large flood plains.

A minimum depth should be guaranteed to keep the rivers navigable but also to ensure that the ships can carry maximum cargo, as low water levels imply that ships can carry less cargo. For example, maximum cargo can be transported on the river Rhine only when the river's discharge is higher than 1,250 m<sup>3</sup>/s.<sup>1</sup>

Various measures have been taken by the Dutch authorities to control the distribution of water discharges over the branches of the Rhine Delta. The main tools are: the weir at Driel, to control the water flow from the Rhine to the IJssel, the Neder-Rijn and the Waal; the sluice gates in the Afsluitdijk, to regulate the water level in Lake IJsselmeer; and the Haringvliet and Volkerak sluice gates, to control through which 'exit' the water will flow into the sea.

The Rhine river has been trained with groynes, originally with the purpose to reduce the risk of flooding, but in later stages also to improve navigability. In the 1990s, the Waal Programme realized further improvements of navigability by the construction of groyne extensions, maintenance dredging and structural measures in river bends. The latter comprised bendway weirs, fixed layers and bottom vanes. Bottom vanes are vortex generating devices that are mounted on the river bed at an angle to the prevailing flow direction. For the Rhine, the bendway weirs were realized in the bend at Erlecom and fixed layers were constructed in the outer-bend pools of the bends at Nijmegen and St Andries in the river Waal.

The on-going overall bed degradation of the river Waal then arises as a problem, because the fixed layers in the outer-bend pools will not follow the degradation and hence become high obstacles. In general, bed degradation results mainly from a deficit in the sediment supply from upstream and from excessive dredging.

An appropriate measure to arrest overall bed degradation is river bed nourishment by artificial sediment.<sup>2</sup> By supplying coarser sediments than the sediments of the river bed, the amount of required sediment supply will eventually decrease.<sup>2</sup>

The success of the above mentioned measures on keeping the navigation in the Dutch rivers safe is assessed by continuously monitoring the depth of the rivers. This depth depends not only on water discharge but also on river bed topography that changes dynamically in response to discharge fluctuations. The river topography and its dynamics are affected by spatial variations in bed sediment composition. This

spatial sediment distribution, therefore, needs to be known, in order to understand and eventually predict the dynamic behaviour of the river topography. In addition the sediment distribution also needs to be monitored in order to assess the effectiveness of the measures and the long term behaviour of the suppletions.

An attractive system for obtaining information about the riverbed bathymetry is the multi-beam echo-sounder (MBES). The echo-sounder emits short pulses of sound towards the river bed to determine the depth for a large number of beams.

Furthermore, different types of sediment (i.e. differing in grain size), can be discriminated based on their differences with regards to the interaction of sound with the sediments, reflected in the so called backscatter strength. Consequently, the echoes as received by the MBES in theory also allow for discriminating between different sediments. This issue has been extensively studied especially during the last decade when new MBES systems have been developed. This thesis falls within these research efforts to discover the full potential of backscatter measurements for sediment discrimination and characterisation in order to gradually replace the conventional way of mapping the sediment composition of the riverbed by taking a large number of physical grab samples. The MBES provides high spatial coverage of an area within a short time, while the conventional approach is time consuming and with limited coverage of the riverbed.

## 1.2 Systems for mapping the riverbed

The three main acoustic systems for remotely mapping the riverbed are the side scan sonar (SSS), the single-beam echo-sounder (SBES), and the multi-beam echo-sounder (MBES).

The SSS systems are in use since the 1960s. The system (see Fig. 1.1) is towed behind the survey vessel at a short distance above the bottom that enables the system to work in good stability and noise conditions. A side scan sonar insonifies the sediment with two side antennas of narrow directivity in the towing direction (usually  $1^\circ$  or less). The narrow sound beam is intercepting the sediment along a thin strip called swath. The instantaneously insonified area inside this beam footprint is very small due to the very short duration of the transmitted signal (typically 0.1 ms or less). For these systems only the amplitude of the returned echo is recorded as a function of time. Aligning the measurements from subsequent pings and correcting the amplitudes for e.g. propagation effects, an image of the underwater sediment is obtained. Due to the resulting lack of knowledge about the angle of the incoming sound, standard SSS systems cannot determine depths along the full swath.

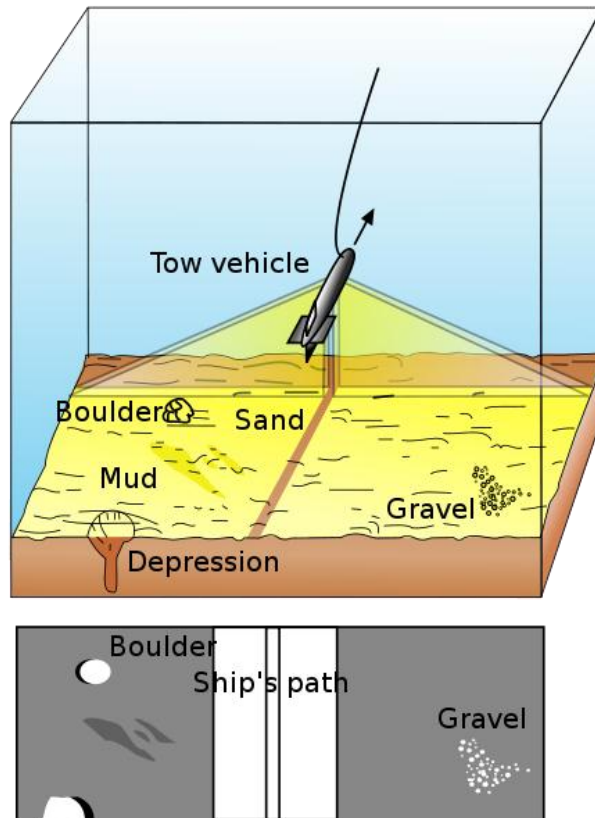


**FIG. 1.1.** Sidescan sonar.<sup>3</sup>

The SBES systems are in use since the 1920s. A single-beam echo-sounder transmits a short signal (duration 0.1 ms to 1 ms), vertically below the ship, in a beam with an angular aperture of typically  $5^{\circ}$ - $15^{\circ}$ . It measures the two-way travel time of the signal, which, if the sound speed is known, provides a single estimate for the water depth for each ping.

The MBES is an extension of the SBES. Contrary to the single-beam echo-sounder, the multi-beam echo-sounder sends out an acoustic pulse (ping) in a wide swath perpendicular to the sailing direction. Beam-steering at reception allows for determining the (two-way) travel-times of the received signals for a set of predefined beam angles. MBES systems measure both the travel time and the intensity of the received signal, which can be used to derive the backscatter strength. The first MBES systems were developed by the US Navy in the 1970s. The first non-military MBES was the Sea Beam, which was put in service in May 1977 on the Australian vessel HMS Cook.<sup>4</sup> This system had an angular resolution of  $2.7^{\circ}$  and maximum operating depth of 11.000 m.

The technology of riverbed mapping systems was further developed during the last three decades. SSS and MBES systems were used in the past simultaneously during a survey to provide complementary information as SSSs were not recording bathymetry but the quality of their imagery was considered higher than the imagery obtained with MBES. Today, use is made of the interferometric SSS that provides a correct positioning of the image of the sediment. Furthermore, high-frequency MBES systems with a large number of beams exist that are suitable for high-resolution mapping in shallow water.

One of the main manufacturers of MBES systems is the Norwegian company Kongsberg (former Simrad). Kongsberg multi-beam echo-sounders were used for acquiring the data analysed in this thesis. The main specifications of the Kongsberg MBES systems that were developed during the last decade are shown in Table 1.1.

For shallow surveys, like the surveys in the Dutch rivers of this thesis where the water depth was less than 20 m, the MBES used was the EM3002. EM3002 was the best – then available – model, since it has been specifically designed for shallow water – high resolution surveys.

**Table 1.1** Specifications of Kongsberg's MBES systems.<sup>5</sup>

<b>Model-[year developed]</b>	<b>Frequency</b>	<b>Depth range</b>	<b>Swath width (degrees)</b>
EM3002-[2004]	300 kHz	0.5 - 250 m	130-200
EM710-[2005]	70-100 kHz	3 - 2000 m	140
EM 302-[2007]	30 kHz	10 - 7000 m	150
EM 122-[2007]	12 kHz	50 - 11000 m	150
EM 2040-[2010]	200-400 kHz	0.5 - 500 m	140-200

### 1.3 Research objectives

In a previous study<sup>6</sup>, a new method was developed employing the backscatter strength data of the MBES for determining seafloor sediment distribution. This method was later used<sup>7, 8</sup> to map the sediment distribution in two parts (Sint Andries and Nijmegen) of the River Waal in the Netherlands. The method gave promising results, but one important artificial riverbed feature, the fixed layer, consisting of large stones, was not identified by the method as a separate sediment type. This indicates that such coarse sediments as the fixed layer cannot be discriminated by the backscatter strength only and that additional measurements are required.

The main objective of the thesis is to fully assess the potential of using the MBES for classification of the Dutch rivers' sediments, leading to the following research objectives:

- 1) It is well established that the amount of backscattering from the sediment, measured by the so called backscatter strength, depends on the sediment properties such as mean grain size. However a variety of methods can be used to employ these backscatter strengths for sediment classification. The objective is to identify the applicability and potential of the different approaches for the sediments encountered in the Dutch rivers.
- 2) In principle, not only the backscatter strength but also bathymetric features contain information that can be used to discriminate between different sediments. Items that will be addressed are:
  - To identify which bathymetric features have classification potential

- To enhance the discrimination potential of the classification methods by using a combination of backscatter and bathymetric features
- 3) Many of the classification methods discriminate the different sediment types that are present in an area as acoustic classes. However, in addition to the distribution of these acoustic classes, also insight in characteristics of the different acoustic classes is highly relevant, allowing for example to order the acoustic classes with respect to their mean grain size. Quantifying the extent to which this characterization is possible is an aim of this thesis research.

In order to fulfil these aims, acoustic data from various Dutch rivers are investigated.

## 1.4 Outline of the thesis

The thesis is comprised of nine chapters. Five of them (Chapters 4-8) can be viewed as stand-alone entities written in the form of journal or conference papers.

Chapter 2 presents the principles behind the measurement techniques that the MBES system is using. The theoretical background of the interaction of sound with sediments is also given. Moreover, the use of MBES for determining the sediment backscatter strengths is explained, and a model for predicting the backscatter strengths for a range of sediments is described. Finally, the main classification methods considered in this thesis are described.

In Chapter 3, details about the parts of the Dutch rivers that were surveyed are given. Moreover, the specifications of the MBES systems used in the surveys are mentioned.

Chapter 4 presents sediment classification results derived from two different sources at the Dordtse Kil river in the Netherlands. The first source is an MBES. For the MBES data, two analysis methods are employed: one uses the average backscatter data per beam and the other matches the measured backscatter curves (i.e. the backscatter strength as a function of angle) to theoretical curves, predicted by a physics-based model. The second source is a gamma-ray scintillation detector, i.e., the multi-element detection system for underwater sediment activity (Medusa), which measures sediment natural radioactivity. The radionuclides (potassium, uranium, thorium, and cesium) are linked to sediment mean grain size, silt content and the presence of organic matter. Moreover, a hydrophone attached to the Medusa system and towed on the riverbed can provide information about the sediment roughness. This chapter presents an inter-comparison between the sediment classification results using the above-mentioned methods.

In Chapter 5 two data sets (in Sint Andries and Nijmegen) are considered, both taken at the Waal River. A new classifier is introduced, that is the depth residuals. Statistical features are calculated for the depth residuals and the backscatter strength. A principal component analysis is used to identify depth residual and backscatter strength features that have classification potential. Clustering is then applied to assign a sediment class to each measurement. The chapter focuses on assessing the

classification potential of combining these two sets of features on providing complementary information on the composition of the riverbed.

Chapter 6 investigates the behavior of the backscatter strength and the depth residuals in very coarse sediment environments. Whereas for the smaller mean grain sizes, in general an increase of backscatter strength with mean grain size is found, this is not the case for the very coarse river sediments. For the coarsest sediments a decrease in backscatter strength with increasing mean grain size is found. Knowing the transition point, i.e. the mean grain size value at which the behavior of the features is reversed, can reduce ambiguity in the classification. The transition point is determined in this chapter.

In Chapter 7 an overview of the results of Chapters 4-6 is given. In the previous chapters two different classifiers and three different classification methods were used for sediment classification based on MBES data. All methods have advantages and limitations. This chapter acts as a guide to which classifier and method can be used when classifying the various sediment types existing in the surveyed Dutch rivers.

Chapter 8 is an application of the experience gained from the previous classification approaches in order to determine the sediment distribution changes in a river that may occur after a period of time. A small part of the Sint Andries area was re-surveyed in 2008 (approximately one year after the first survey). The small part of Sint Andries in 2008 as well as the corresponding part in 2007 are analysed in this chapter and an assessment is given on the observed riverbed morphology and sediment distribution differences.

Finally, Chapter 9 concludes the thesis, restating the main results concerning the sediment classification methods used in Dutch rivers. An outlook on future research is also included.

**REFERENCES**

- <sup>1</sup> “Water management in the Netherlands”, Rijkswaterstaat, (February 2011), [http://www.rijkswaterstaat.nl/en/images/Water%20Management%20in%20the%20Netherlands\\_tcm224-303503.pdf](http://www.rijkswaterstaat.nl/en/images/Water%20Management%20in%20the%20Netherlands_tcm224-303503.pdf) (Date last viewed 25/06/2013).
- <sup>2</sup> E. Mosselman, P. Kerrssens, F. v.d. Knaap, D. Schwanenberg, and K. Sloff, “Sustainable river fairway maintenance and improvement”, Report, (2004).
- <sup>3</sup> <http://woodshole.er.usgs.gov/operations/sfmapping/images/sonartracktextnotow.jpg> (Date last viewed 04/07/2013).
- <sup>4</sup> H. Farr, “Multibeam bathymetric sonar: Sea beam and hydro chart”, *Marine Geodesy*, Volume 4, Issue 2, pages 77 – 93 (1980).
- <sup>5</sup> Kongsberg, [http://www.km.kongsberg.com/ks/web/nokbg0397.nsf/AllWeb/B30F2EE6C225E094C1257746004B7FD8/\\$file/Kongsberg\\_Hydrographic\\_brochure\\_v1\\_lr.pdf](http://www.km.kongsberg.com/ks/web/nokbg0397.nsf/AllWeb/B30F2EE6C225E094C1257746004B7FD8/$file/Kongsberg_Hydrographic_brochure_v1_lr.pdf) (Date last viewed 04/07/2013).
- <sup>6</sup> D.G. Simons, and M. Snellen. “A Bayesian approach to seafloor classification using multi-beam echo-sounder backscatter data”, *Appl. Acoust.* 70, 1258-1268 (2009).
- <sup>7</sup> A.R. Amiri-Simkooei, M. Snellen, and D.G. Simons, “Riverbed sediment classification using multi-beam echo-sounder backscatter data”, *J. Acoust. Soc. Am.* 126, 1724-1738 (2009).
- <sup>8</sup> A.R. Amiri-Simkooei, M. Snellen, and D.G. Simons, “Using multi-beam echo-sounder backscatter data for sediment classification in very shallow water environment”, <http://promitheas.iacm.forth.gr/uam2009/lectures/pdf/29-1.pdf> (date last viewed 09/06/2011).

# 2

## Background

---

In this chapter the background of the multi-beam echo-sounder (MBES) system and its measurements are presented. Section 2.1 describes the principles behind the measurement techniques employed by the MBES systems. Detailed information about the actual MBES system is given in Section 2.1.1. Subsequently, the methods that the MBES uses to determine bathymetry (Section 2.1.2), imagery (Section 2.1.3) and the corresponding resolution (Section 2.1.4) are provided. The second part of this chapter (Section 2.2) discusses the interaction of sound with sediments. First, the basic theory of the reflection of sound at the sediment interface is presented (Section 2.2.1), followed by the theory of scattering of sound at riverbeds (Section 2.2.2). In this section also a model for predicting the backscatter strengths for a range of sediments is described, which will be used for modelling the backscatter strengths in this thesis. The use of MBES for determining the sediment backscatter strengths, one of the main parameters used for sediment classification throughout this thesis, is presented in section 2.2.3. Finally, Section 2.3 of this chapter briefly describes the main ideas behind the classification methods considered in this thesis.

## 2.1 Acoustic measurements using MBES

### 2.1.1 General information

The fan of beams provides, for each ping, a large number of simultaneous depth measurements along a swath of width  $L$  (see Fig. 2.1). For example, a total angular width of typically  $150^\circ$  covers up to  $L=7.5H$ ,  $H$  being the water depth.

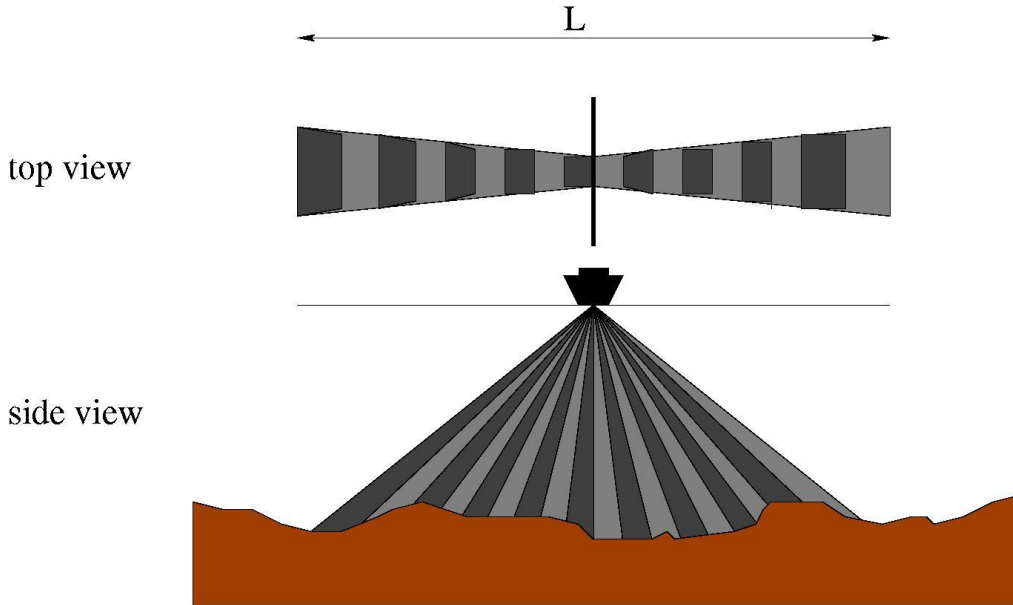


**FIG. 2.1.** Schematic overview of the MBES measurements along a swath with width  $L$  in the across-track direction. Beams in the across-track direction are the result of beam-steering at reception. A depth measurement is taken for every beam.

MBES systems can be divided into three main groups based on their operation frequency:<sup>1</sup>

- Deep water systems operating at a frequency of typically 12 kHz. They can be used only on large vessels due to the large dimensions of their transducer arrays.
- Shallow water systems operating at frequencies of typically 100-200 kHz, used for surveying the continental shelf.
- High-resolution systems operating at frequencies of typically 300-500 kHz, designed for mapping local objects like shipwrecks. They can be installed on small ships, tow fishes or autonomous underwater vehicles (AUV).

The transducer arrays for transmitting the acoustic pulses are designed such that the system has a narrow beam width in the along-track direction, i.e. the sailing direction. This requires a long transmission array along the sailing direction of the supporting platform. Also, a large transmission width is needed to cover as large a swath as possible, corresponding to transmission arrays that are narrow across-track. The along-track discrimination is thus determined by the directivity of the transmission array. The upper plots of Fig. 2.2 show a top and front view of a typical transmitted beam.

Across-track discrimination is accomplished by the reception array, which must be long in the across-track direction (see Fig. 2.2). Applying the principle of beam-steering allows for discriminating between directions from which the sound impinges on the receiving array. The receiver opening angle in the along-track direction is quite large to allow for changes in pitch between transmit and receive. However, this is not reflected in the fore-aft dimension of the individual receiving beams as this is already constrained by the transmission. The final resolution of the MBES is the product of the along-track and across-track resolutions (according to the so-called Mills cross principle<sup>2</sup>).

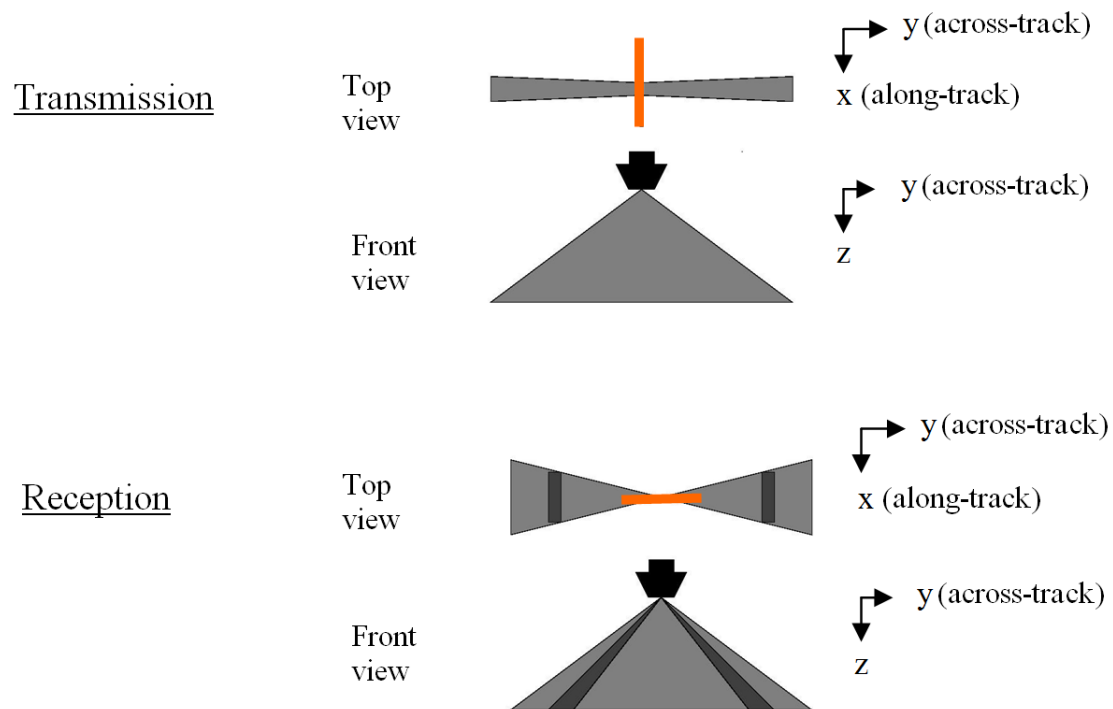


**FIG. 2.2.** Transmission and reception for the MBES. The transducers are indicated by the thick orange lines.

The shapes used for the reception arrays are simple horizontal linear, V-shaped (larger swathe widths possible) or U-shaped (see Fig. 2.3).

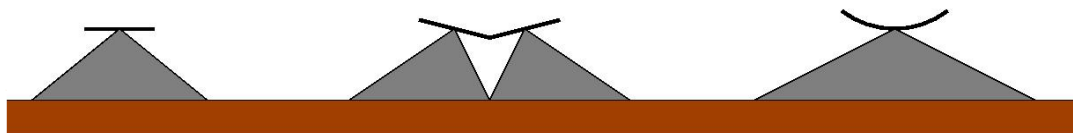


**FIG. 2.3.** Possible shapes of reception arrays.

The MBES provides two-way travel times as function of beam angle relative to the MBES location. Therefore, the ancillary systems of the MBES are significant in order to accurately determine the bathymetry in a required reference system. These are:<sup>1</sup>

- The positioning system which determines the exact geographical position of the ship (GPS, preferably in differential mode);
- The attitude sensor unit providing heading, roll, pitch and heave measurements to compensate for: 1) orientation of the line of depth measurements relative to the ship's axis (heading), 2) orientation of the beams (roll and pitch), and 3) vertical movements of the ship (heave);
- Sound speed profiles to correct for refraction effects;
- Sound speed measurements close to the transducers for correct beam-steering.

### 2.1.2 Bathymetry

The MBES calculates the bathymetry of a point by jointly estimating the two-way travel time  $t$  and beam angle  $\theta$ . Each pair  $(t, \theta)$  is used to determine the position of one depth measurement. When the sound speed profile is constant over the entire water column, the acoustic paths from and to each beam are linear. Then the coordinates  $(y, z)$  of the measurement point, with the origin at the MBES position, are (see Fig. 2.4)

$$\begin{aligned} y &= R \sin \theta = \frac{ct}{2} \sin \theta \\ z &= R \cos \theta = \frac{ct}{2} \cos \theta \end{aligned} \tag{2.1}$$

where  $R$  is the range between the MBES and the sediment (see Fig. 2.4).  $\theta$  is the so called beam angle whereas  $\varphi$  is called the grazing angle of incidence.

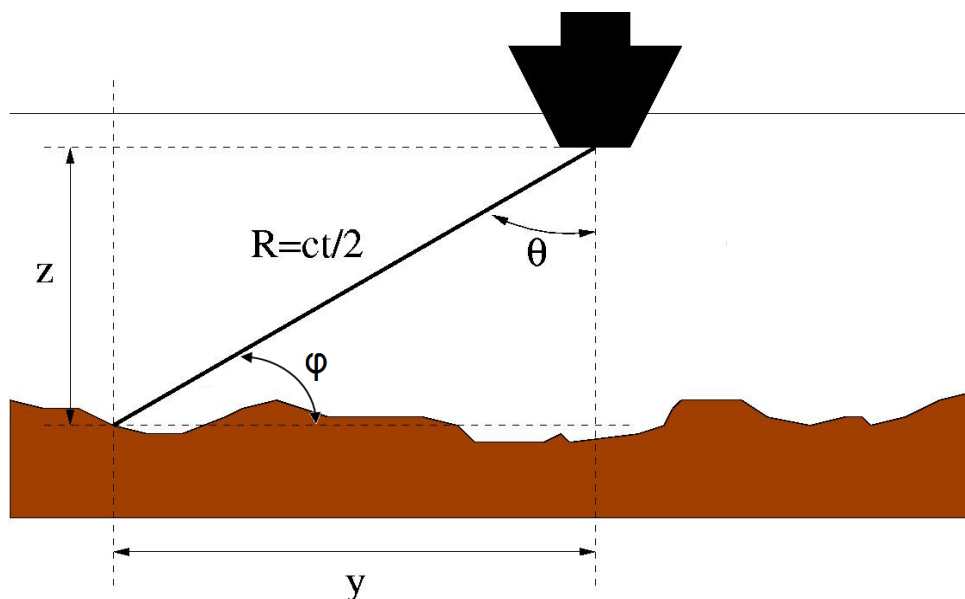


**FIG. 2.4.** Determining bathymetry from  $(t, \theta)$  in the isovelocity situation.

In reality the sound speed profile varies with depth, inducing refraction effects, and therefore the acoustic path has to be reconstructed using geometric ray-tracing software.

As mentioned before, the depth measurement is referenced to the MBES position. It is therefore mandatory to simultaneously know the position and attitude of the support platform, which enables the application of angle corrections (roll in particular) and to associate geographical coordinates with the depth measurements.

Several techniques are being used to measure the couples  $(t, \theta)$ . The maximum amplitude instant (MAI) method was one of the first approaches used for estimating the time of arrival of the backscattered signal. This method of detection is accurate for angles close to normal, since at these angles the signal duration is short and sharp. For decreasing grazing angles of incidence, the time duration becomes larger and more affected by noise. Therefore, for these angles the estimation of arrival time from the MAI becomes troublesome. The commonly applied solution is to divide the receiving array in two sub-arrays and measure the phase difference between the signals as received on these two subarrays, i.e. an interferometric approach. Nowadays modern MBES are based on a combination of the interferometric phase detection approach and MAI time detection from the backscattered signal.

### 2.1.3 Imaging

In addition to the two-way travel times, the MBES also measures the intensity of the echo. These side-scan sonar like measurements are available for each beam. Whereas the side-scan sonar has no information about the location from which the intensities result the MBES does have this information. The MBES therefore combines the  $(t, \theta)$  information with intensity measurements per beam to form a continuous image of the complete swath. To this end, for each beam, first its central point is placed on the swath, and then the image pixels are spread around it, until reaching the boundary of the next beam.

### 2.1.4 Resolution

The along-track resolution  $\delta x$  for bathymetry and imaging is given as

$$\delta x = R\theta_L \quad (2.2)$$

with  $\theta_L$  the beam width of the transducer in the along-track direction, and  $R$  the range between MBES and the sediment (see Fig. 2.4). For example, for beam angle  $45^\circ$ , depth 5 m, and beam width  $1.5^\circ$ , the along-track resolution is 10 cm.

The across-track resolution for backscatter imaging is dependent on the pulse length  $\tau$  as

$$\delta y = \frac{c\tau}{2\sin\theta} \quad (2.3)$$

with  $\theta$  the beam angle, and  $c$  the sound speed. For example, for beam angle  $45^\circ$ , sound speed 1500 m/s, and pulse length  $150 \mu\text{s}$  the along-track resolution is 16 cm.

At the vertical ( $\theta \rightarrow 0^\circ$ ) the across-track resolution for imaging becomes

$$\delta y = \sqrt{Hc\tau} \quad (2.4)$$

where  $H$  is the distance between the MBES and the sediment.

The resolution for bathymetry is determined by the across-track beam width  $\theta_T$  as:

$$\delta y = \frac{H\theta_T}{\cos^2 \theta} \quad (2.5)$$

In practice  $\delta y$  will be in between a value according to this equation and Eq. (2.3), depending on the processing details.

Most MBES systems allow for selecting either an equi-angular or an equi-distant measurement mode. The equi-angular mode corresponds to beam pointing angles at equal angular distances, resulting in a decrease of the sounding density towards the end of the swath. The equi-distant mode selects its beam pointing angles such that the intersection of the individual beams with the ground is at equal distances, resulting in an increasing sounding density towards the end of the swath compared to the equi-angular mode, but also in a decreased sounding density at nadir.<sup>3</sup> In order to obtain the increased sounding density at the outer ends of the swath in the equi-distant mode use is made of interferometry.

## 2.2 Interaction of sound with sediments

### 2.2.1 Reflection of sound at interface

For a perfectly flat sediment, use can be made of the reflection and transmission coefficients for describing the interaction of sound with the sediment. Figure 2.5 shows the reflection of sound at an interface that separates two homogeneous fluid media. Changes in sound speed between the media causes reflection and refraction of the signal.

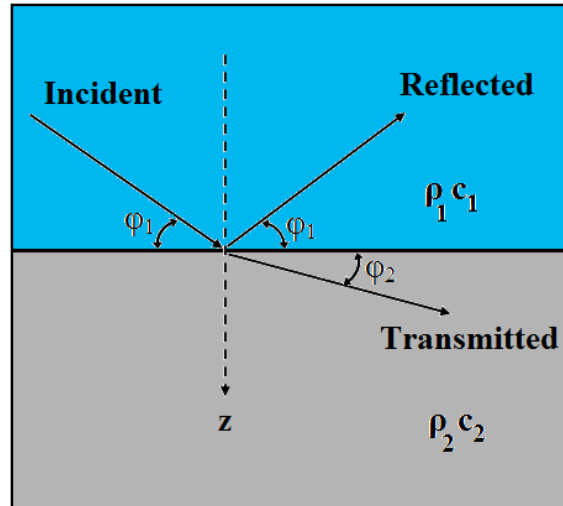


**FIG. 2.5.** Reflection of sound at an interface of two different media.

By applying the continuity conditions at the interface (for pressure and normal velocity) we have Snell's law for determining  $\varphi_2$ , i.e., the angle of the transmitted signal:

$$\frac{\cos \varphi_2}{c_2} = \frac{\cos \varphi_1}{c_1} \quad (2.6)$$

and the expressions for the reflection ( $R_e$ ) and transmission ( $T_r$ ) coefficients:

$$R_e = \frac{\rho_2 c_2 \sin \varphi_1 - \rho_1 c_1 \sin \varphi_2}{\rho_2 c_2 \sin \varphi_1 + \rho_1 c_1 \sin \varphi_2} \quad (2.7)$$

$$T_r = 1 + R_e = \frac{2\rho_2 c_2 \sin \varphi_1}{\rho_2 c_2 \sin \varphi_1 + \rho_1 c_1 \sin \varphi_2} \quad (2.8)$$

If  $c_2 > c_1$ , there exists a critical angle given by

$$\varphi_c = \arccos\left(\frac{c_1}{c_2}\right) \quad (2.9)$$

For  $\varphi_1 < \varphi_c$  no compressional wave can propagate inside medium 2:  $R_e$  becomes complex with unit modulus independent of  $\varphi_1$  ('total reflection'). When  $\varphi_1$  increases while crossing the critical angle,  $R_e$  will suddenly decrease and then varies smoothly with  $\varphi_1$ . At normal incidence ( $\varphi_1 = 90^\circ$ )

$$R_e = \frac{\rho_2 c_2 - \rho_1 c_1}{\rho_2 c_2 + \rho_1 c_1} \quad (2.10)$$

To illustrate the effect of the sediment sound speed on the reflection coefficient, Fig. 2.6 shows the modulus of  $R_e$  versus  $\varphi_1$  where  $c_2$  was varied independently and  $c_1$  was kept constant at 1500 m/s. The thick black line indicates the reflection coefficient for a gravelly muddy sand bottom (see Table 2.1), with a sound speed of 1809 m/s. For illustration purposes the absorption in the sediment is assumed to be zero. The grey lines show the effects of having smaller or larger values for the sediment sound speed,  $c_2$ .

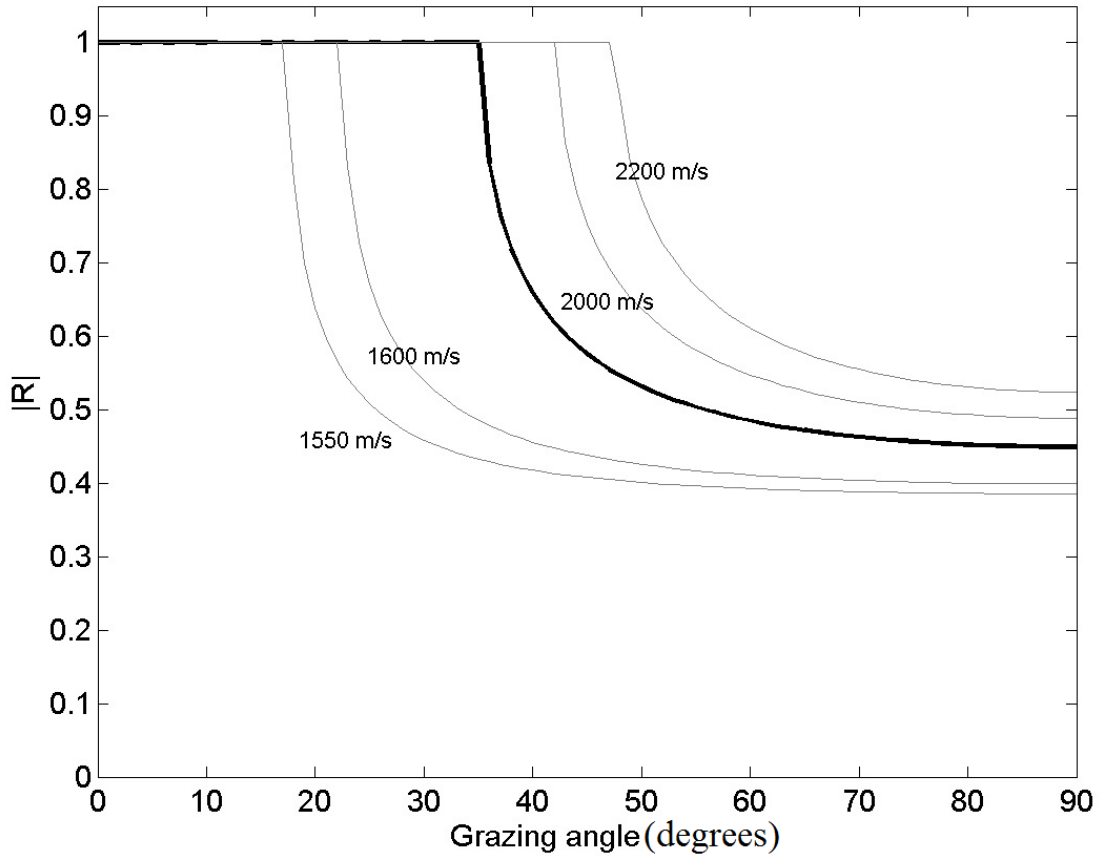


**FIG. 2.6.** Absolute value of the reflection coefficient as a function of grazing angle for a gravelly muddy sand bottom (thick black line). The thin grey lines indicate the absolute reflection coefficients for the same gravelly muddy sand bottom, but now with the sediment sound speed values varied. For all sediments considered the absorption coefficient is taken as 0 dB/ $\lambda$ .

In practice however, absorption is not zero. Absorption in the second medium is accounted for by making the wave number  $k_2$ , and hence the sound speed  $c_2$ , complex. Let  $\alpha_2$  be the absorption coefficient in medium 2 expressed in units of dB/ $\lambda$  (because often  $\alpha_2$  is considered to be proportional with frequency). The absorption coefficient in nepers/m is then given by<sup>4</sup>

$$a'_2 = \frac{a_2}{\lambda_2 20 \log e} \quad (2.11)$$

Here the factor  $20\log e$  converts units nepers/m to dB/m.  $a'_2$  is equal to the imaginary part of the wave number  $k_2$  in the second medium as<sup>4</sup>  $k_2 \rightarrow k_2 + a'_2$ .

The imaginary part of the sound speed in the second medium then becomes:

$$\text{Im}(c_2) \approx \frac{-c_2 a_2}{40\pi \log e} \quad (2.12)$$

The expressions for the reflection and transmission coefficients (Eq. 2.7 and Eq. 2.8) are still valid provided the complex expression for  $c_2$  is used. The implication of absorption in the second medium is that an attenuated wave can always be transmitted and propagate through medium 2, even below the critical angle. Total reflection does not occur below the critical angle;  $|R|$  is slightly below unity, see Fig. 2.7.

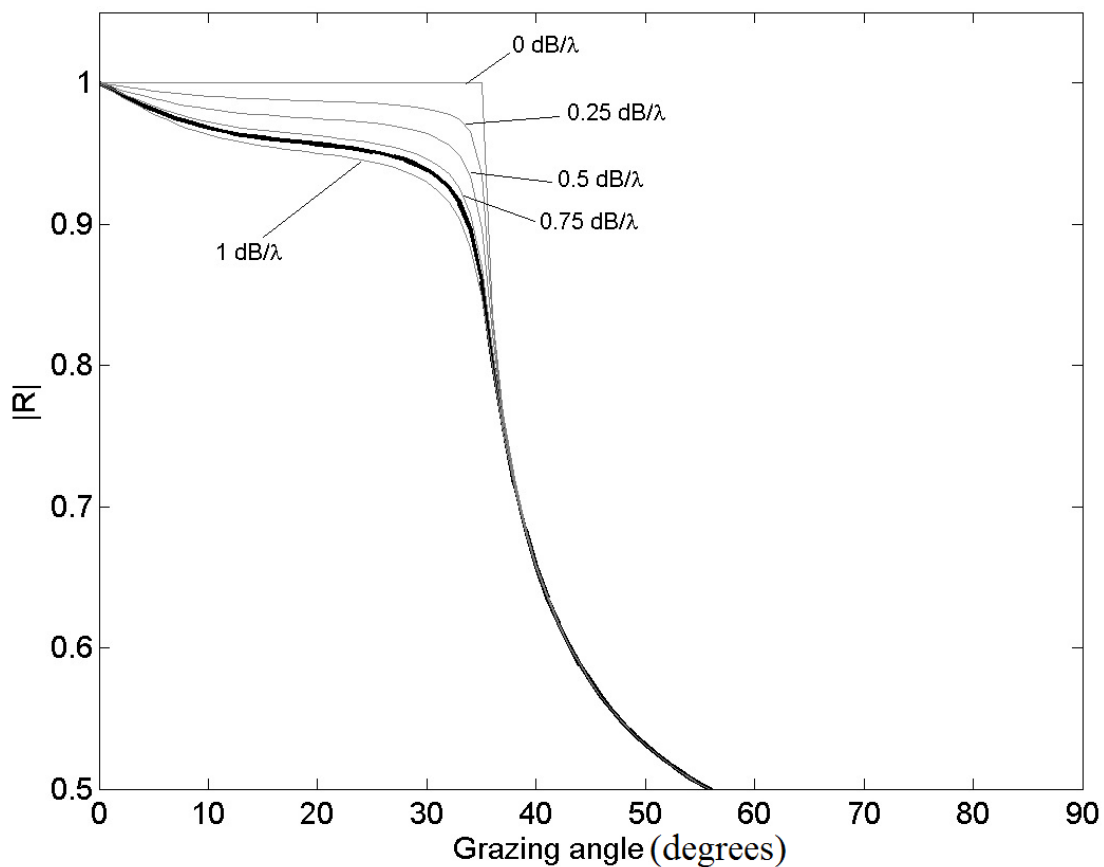


**FIG. 2.7.** Absolute value of the reflection coefficient as a function of grazing angle for a gravelly muddy sand bottom (thick black line,  $a'_2 = 0.86$  dB/λ.). The thin grey lines indicate the absolute reflection coefficients for the same gravelly muddy sand bottom, but now with the values for the absorption coefficient varied.

Sediments parameters affecting the interaction of sound with the sediment are often denoted geo-acoustic parameters. It is well established that different sediments, e.g. sand or mud, correspond to certain values of these geo-acoustic parameters. Table 2.1 provides an overview of the geo-acoustic parameters for many unconsolidated

sediments that are typically found on ocean and riverfloors. This table is actually illustrating the potential of using acoustic systems for sediment classification.

**Table 2.1** Typical values for parameters of various sediment types.

Sediment type	Bulk grain size $M_z$ [phi]	Density ratio $\rho$ [-]	Sound speed ratio $v$ [-]	Loss parameter $\delta$ [-]	Spectral exponent $\gamma$ [-]	Spectral strength $w_2$ [cm <sup>4</sup> ]	Volume parameter $\sigma_2$ [cm <sup>4</sup> ]
Sandy Gravel	-1	2.492	1.337	0.0171	3.25	0.0129	0.002
Muddy Sandy Gravel	0	2.314	1.278	0.0163	3.25	0.0086	0.002
Gravelly Muddy Sand	1	2.151	1.224	0.0165	3.25	0.0056	0.002
Muddy Gravel	2	1.615	1.140	0.0161	3.25	0.0035	0.002
Muddy Sand	3	1.339	1.080	0.0173	3.25	0.0021	0.002
Clayey Sand	4	1.223	1.036	0.0202	3.25	0.0011	0.002
Sandy Silt Gravelly Mud	5	1.169	1.000	0.0126	3.25	0.0005	0.002
Sandy Mud	6	1.149	0.987	0.0039	3.25	0.0005	0.001
Sandy Clay	7	1.147	0.985	0.0024	3.25	0.0005	0.001
Silty Clay	8	1.146	0.982	0.0016	3.25	0.0005	0.001
Clay	9	1.145	0.980	0.0015	3.25	0.0005	0.001

In this table, the mean grain size is given as  $M_z$  in phi units [ $\phi$ ] as

$$M_z = -\log_2(d) \quad (2.13)$$

with  $d$  the average grain diameter in mm.

Density  $\rho$  and sound speed  $v$  ratio in the table are measures of the ratio of sediment density and sound speed relative to the water column sound speed. The dimensionless loss parameter  $\delta$  is related to the absorption coefficient  $\alpha_2$  in dB per wavelength. Parameter  $\delta$  is defined as

$$\delta = \frac{\alpha_2}{k_2} = \frac{\lambda_2}{2\pi} \frac{20 \log e}{\lambda_2} = \frac{\alpha_2}{40\pi \log e} \quad (2.14)$$

The spectral exponent  $\gamma$ , the spectral strength  $w_2$  and the volume parameter  $\sigma_2$  are parameters related to the scattering process and will be treated later on in section 2.2.2.6.

Figure 2.8 gives the reflection coefficient as a function of grazing angle for the sediment types with  $M_z = -1, 0, 1, 2, 3, 4$  and  $5 \phi$  given in Table 2.1.

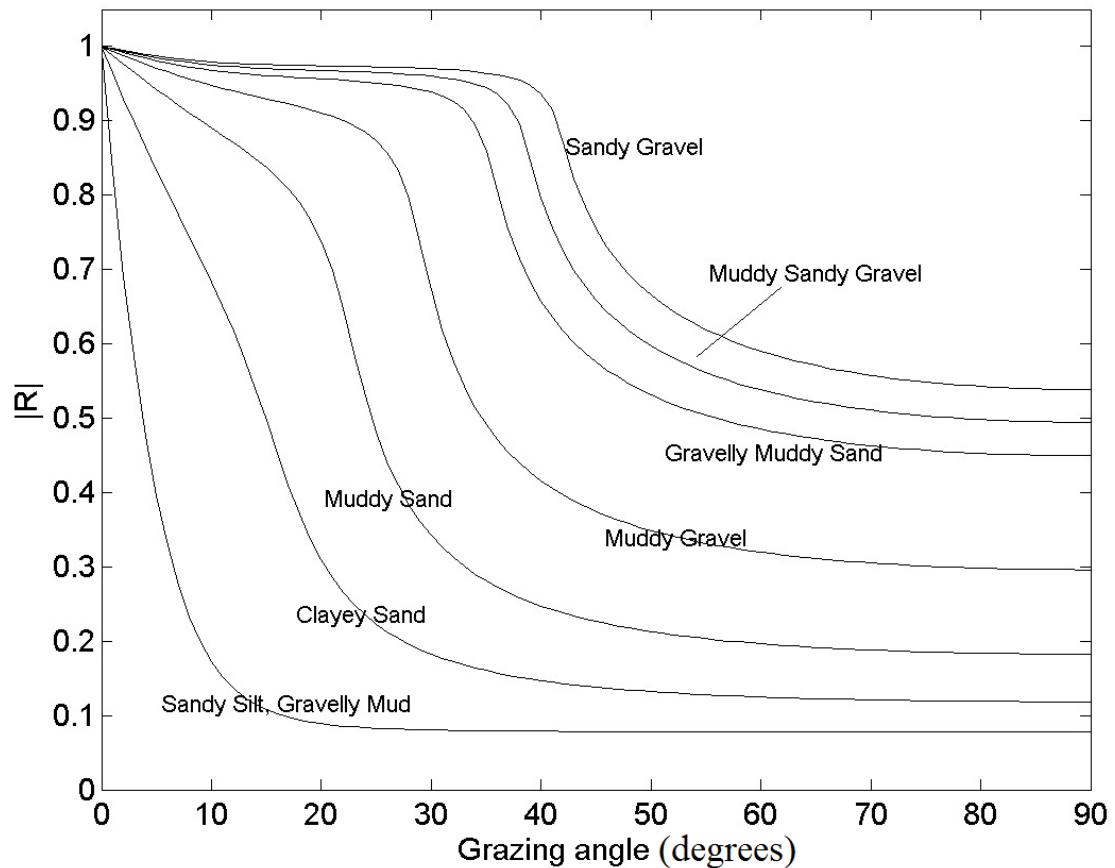


**FIG. 2.8.** Reflection coefficient vs. angle for the Table 2.1 sediment types, corresponding to  $M_z = -1, 0, 1, 2, 3, 4$  and  $5 \phi$ .

It should be noted that if reflection was the sole mechanism affecting the interaction of sound with the sediment, no MBES measurements would be possible, since all sound would be reflected away and no echoes would arrive at the MBES. The fact that echoes are received by the MBES results from the sediments never being perfectly flat. Consequently, in addition to reflection, also scattering is affecting the interaction of sound with the sediment as discussed in the next section.

## 2.2.2 Scattering of sound

### 2.2.2.1 The physics of scattering

As mentioned above, sediments are usually not ideal plane surfaces. Consequently, the interaction of sound with the sediments will be much more complex and considering only reflection and transmission of sound is not sufficient.

As a whole, the sediment surface can still be considered plane. Deviations from this plane surface are represented by the so-called sediment relief.

As the incident wave meets the sediment, a part of it (coherent part) will be reflected in the specular direction. The rest of the energy will be scattered in all directions, included back towards the source (backscattered signal). Figure 2.9 presents some typical patterns for the angular spread of the coherent and scattered part for different combinations of relief characteristics and sediment impedance (equal to  $\rho c$ ). As shown in the figure, low interface roughness, i.e., a smooth bottom, results in a large specular component and the scattering at angles away from the specular direction will be low, while for high interface roughness the specular component will be strongly attenuated.

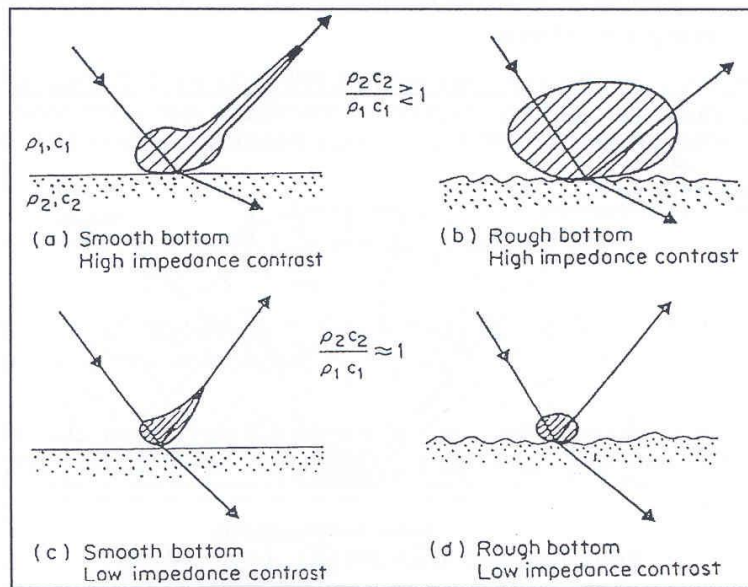


**FIG. 2.9:** Directional echo patterns for different conditions of bottom roughness and impedance contrast.<sup>5</sup>

It should be noted that the effect of the sediment relief is strongly dependent on the sound frequency. Surfaces which appear rough to short acoustic wavelengths can appear smooth to long acoustic wavelengths.

### 2.2.2.2 The spatial roughness spectrum

The sediment's relief is the result of various processes. These processes give rise to the presence of a wide scale of amplitudes coexisting on the same surface.

This situation can be captured through the concept of the spatial spectrum of the relief. This spectrum quantifies the amplitude distribution of the surface and is obtained by Fourier transforming the relief. The spatial wavelengths  $\Lambda_w$  then define the different spatial components. For a situation where the relief is completely random, the spectrum is continuous. In contrast however, the presence of regular sand ripples will result in peaks in the spectrum.

In general it is assumed that the two-dimensional relief spectrum is isotropic and that it can be described by the following expression<sup>6,7</sup>

$$S(\kappa) = w_2 (h_0 \kappa)^{-\gamma} \quad (2.15)$$

Here,  $\kappa$  is the wave number of the relief  $\kappa = 2\pi/\Lambda_w$ ,  $h_0$  is a reference length (1 cm) and  $w_2$  is the spectral strength (see Table 2.1). Parameter  $\gamma$  is the spectral exponent and typically has a value of 3.25.

The expression for the spatial spectrum, equation (2.15) is normalised according to

$$\int S(\kappa) d\kappa = h^2 \quad (2.16)$$

with  $h$  the standard deviation of the relief amplitudes. Assuming a value of 3.25 for parameter  $\gamma$  the following relation between  $h$  and  $w_2$  can be derived<sup>6,7</sup>

$$w_2 = 0.00207 h^2 h_0^2 \quad (2.17)$$

### 2.2.2.3 Reflection revisited – the Rayleigh parameter

Since for a rough surface, part of the sound is scattered in all directions, the reflection coefficient for rough sediments will be lower compared to that of a mirror like surface (Eq. (2.7)). The effect can be addressed through the use of the Rayleigh parameter:

$$P = 2kh \sin \varphi \quad (2.18)$$

with  $k = 2\pi/\lambda$  the acoustic wave number,  $h$  the standard deviation of the relief amplitudes and  $\varphi$  the grazing angle of incidence. Now, the following expression quantifies the reflection coefficient for rough surfaces

$$R_c(\varphi) = R_e(\varphi) e^{-P^2/2} = R_e(\varphi) e^{-2k^2 h^2 \sin^2 \varphi} \quad (2.19)$$

with  $R_e$  the reflection coefficient for the interface without relief. This ‘model’ is valid when  $P$  is small,  $P < \pi/2$ . For larger values of  $P$  the concept of reflection no longer holds and expressions for scattering of sound are required to describe the interaction for sound with the sediment. Figure 2.10 illustrates the effect of interface roughness for a gravelly muddy sand sediment (see Table 2.1 for the parameters) for various frequencies. At 20 kHz the ‘Rayleigh parameter model’ is not valid at all angles (as indicated by the dashed line in the figure).

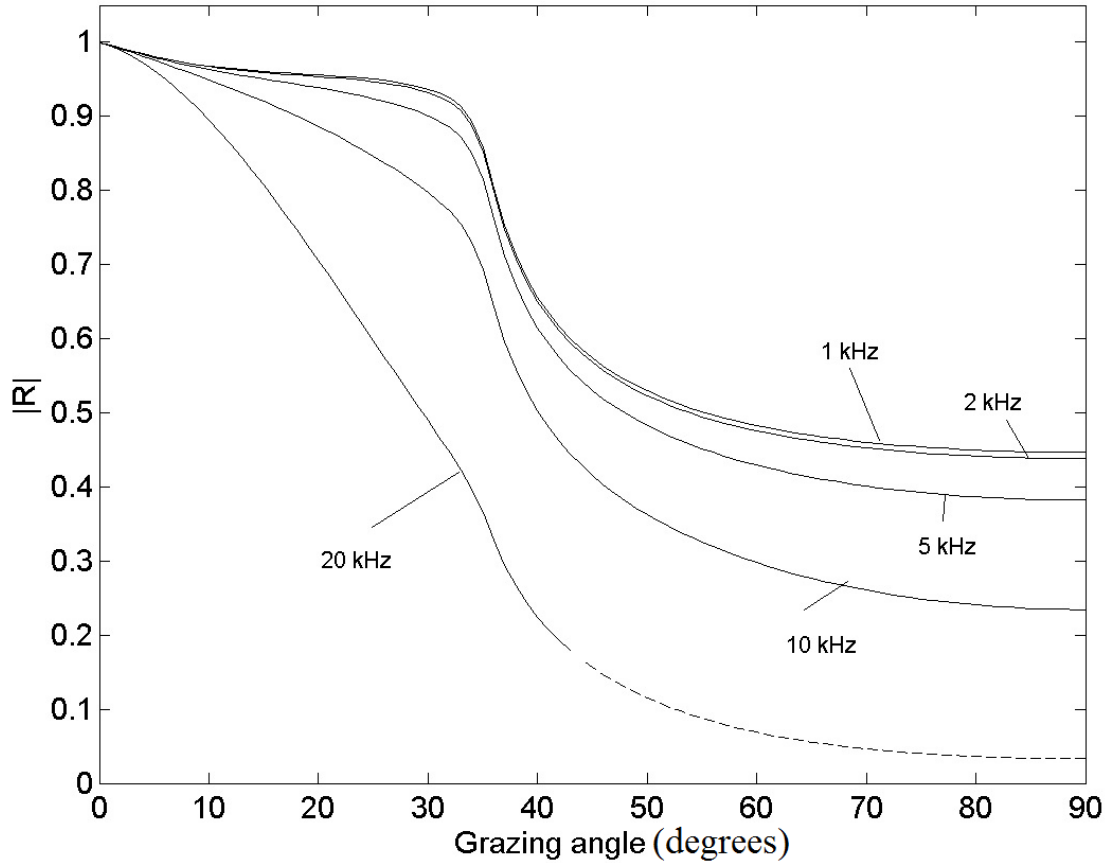


**FIG. 2.10.** Effect of frequency on the reflection coefficient for a gravelly muddy sand sediment (see Table 2.1).

#### 2.2.2.4 The backscattering strength

For MBES measurements, mainly backscattering is of interest. We refer to ‘backscattering’ for the sound scattered in the direction of the source. The corresponding quantity is the so-called backscattering strength defined as

$$BS = 10 \log_{10} \frac{I_s}{I_i} \quad (2.20)$$

i.e., the ratio in dB’s of the intensity  $I_s$  of the scattered sound from a unit area of  $1 \text{ m}^2$  at a distance of 1 m from this unit area in the direction of the source, and the intensity  $I_i$  of the incoming plane wave (see Fig. 2.11).

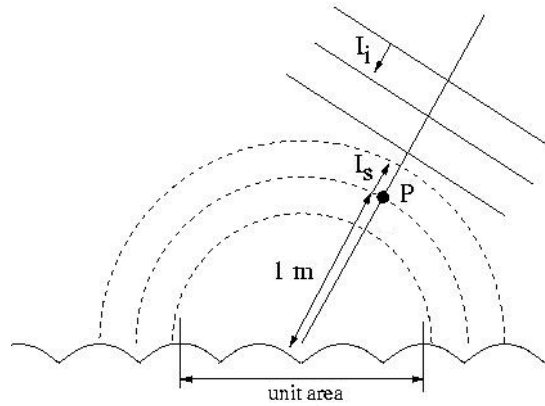


**FIG. 2.11.** Schematic representation of defining the backscatter strength.

The backscatter strength  $BS$  depends on sediment type (roughness), frequency  $f$  and the grazing angle of incidence  $\varphi$ . In general, it increases with increasing  $\varphi$ . Frequency dependence and sediment type dependence is much more complicated. For some types of sediments  $BS$  increases with increasing  $f$ , while other sediment types exhibit hardly any frequency dependence (e.g. when the scale of roughness is large compared to the acoustic wavelength). Apart from sediment roughness, also inhomogeneities in the bottom can contribute to the scattering of sound and hence the backscatter strength.

#### 2.2.2.5 Lambert's rule

A frequently used formula for the backscattering strength is the so-called 'Lambert's rule'. This rule provides a specific angular-dependence according to which many rough surfaces behave.

We consider the situation as depicted in Fig. 2.12.

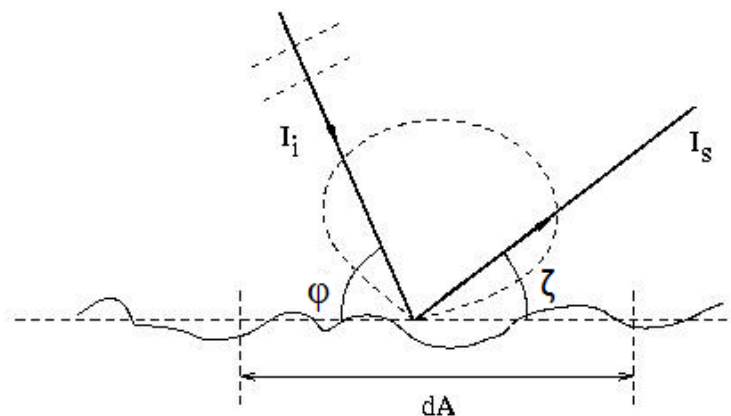


**FIG. 2.12.** Scattering of sound impinging on area  $dA$  with intensity  $I_i$  and angle  $\varphi$ . Angle  $\zeta$  and intensity  $I_s$  denote the angle and intensity of the scattered sound.

$I_i$  is the intensity of a plane wave impinging on a rough sediment at a grazing angle of incidence  $\varphi$ . The power intercepted by the bottom surface  $dA$  is equal to

$I_i \sin \theta dA$ . Lambert's rule assumes this power to be scattered proportional to the sine of the angle of scattering  $\zeta$ . The intensity  $I_s$  in the direction  $\zeta$  at a distance of 1 m from  $dA$  is then given by

$$I_s = \mu(I_i \sin \varphi dA) \sin \zeta \quad (2.21)$$

where  $\mu$  is a proportionality constant. For a unit area  $dA$  of  $1 \text{ m}^2$  we can write

$$10^{10} \log \frac{I_s}{I_i} = 10 \log \mu + 10 \log (\sin \varphi \sin \zeta) \quad (2.22)$$

The backscattering strength, for which  $\zeta = 180^\circ - \varphi$ , then becomes

$$BS = 10 \log \mu + 10 \log (\sin^2 \varphi) \quad (2.23)$$

In principle, the frequency and sediment type dependence can be put in the parameter  $\mu$ . Practically observed values of  $10 \log \mu$  range between  $-40$  dB and  $-10$  dB. At high frequencies there is evidence that  $10 \log \mu$  increases with grain size. A useful starting value for  $10 \log \mu$  for all types of seafloor is  $-27$  dB. Figure 2.13 presents  $BS$  as function of  $\varphi$  for this value of  $\mu$ .

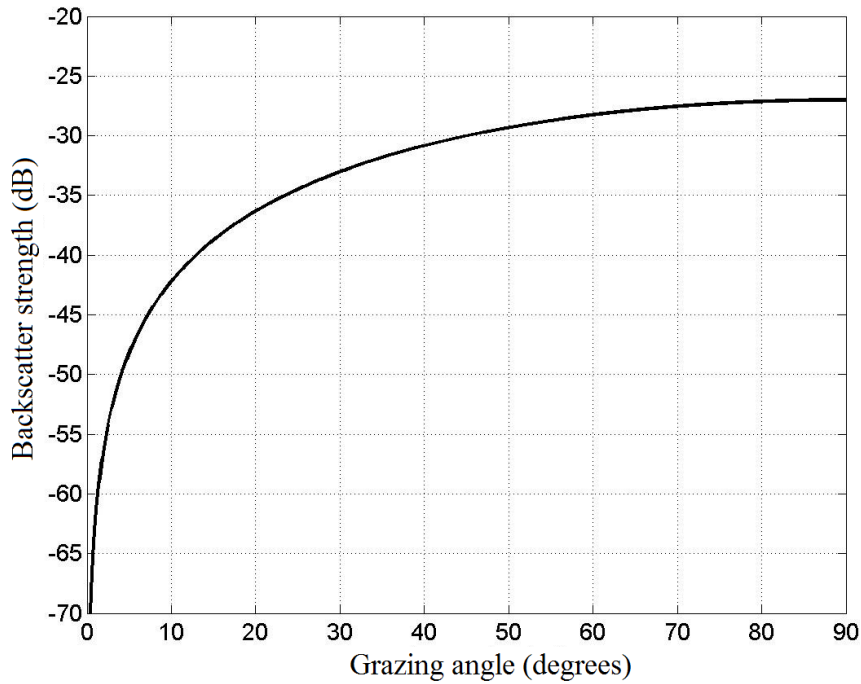


**FIG. 2.13.** Backscatter strength as a function of grazing angle as predicted by Lambert's rule, with  $10 \log \mu$  equal to  $-27$  dB.

### 2.2.2.6 Sophisticated backscatter strength modelling

Lambert's rule yields relatively good agreement with measurements for very rough surfaces such as rocky sediments. For less rough surfaces, the agreement with measurements strongly deteriorates for angles near normal. Therefore, more complex models have been developed. The model described in Ref. 6 is used in Chapter 4. We hereby assume that the model, although developed for frequencies between 10 and 100 kHz, is still applicable for the frequency of 300 kHz, which is the operating frequency of the MBES used for acquiring the data analysed in this thesis. This assumption is based on the research results in Ref. 8, where the model was used for the frequency of 300 kHz. In Ref. 8 there is agreement between modeled and measured backscatter strength.

The total backscatter strength is expressed as a combination of the interface roughness scattering and volume scattering<sup>6</sup>

$$BS(\varphi) = 10 \log_{10} (\sigma_r(\varphi) + \sigma_v(\varphi)) \quad (2.24)$$

with  $\sigma_r$  and  $\sigma_v$  the backscattering cross sections due to the interface roughness and volume scattering, respectively.

$\sigma_r$  is derived by an appropriate interpolation between three approximations<sup>6</sup>:

- The Kirchhoff approximation valid for fine to slightly coarse sediments and at grazing angles close to nadir;
- The composite roughness approximation appropriate for all other angles;
- For rough bottoms (e.g., gravel and rock) use is made of an empirical expression.

All three contributions are a function of the sediment roughness spectrum. A relief spectrum that conforms Eq (2.15) is assumed.<sup>6</sup> Additionally,  $\sigma_r$  is determined by the sediment density, attenuation coefficient, and sound speed.

The following expression for the sediment volume backscattering cross section  $\sigma_v$  is

$$\sigma_{pv} = \frac{5\delta\sigma_2 |1 - R_e^2(\varphi)| \sin^2 \varphi}{\nu \ln 10 |P(\varphi)|^2 \text{Im}(P(\varphi))} \quad (2.25)$$

Here,  $\sigma_2$  is the ratio of sediment volume scattering cross section to attenuation coefficient, and  $P(\varphi) = \sqrt{((1+i\delta)/\nu)^2 - \cos^2 \varphi}$ . In addition to  $\varphi$ ,  $R_e$  is also a function of the sediment parameters  $\nu$ ,  $\delta$  and  $\rho$ .  $\sigma_v$  is determined from  $\sigma_{pv}$  accounting for shadowing and bottom slopes.<sup>6</sup>

Empirical expressions exist that relate  $\sigma_2$ ,  $w_2$ ,  $\rho$ ,  $\nu$ , and  $\delta$  to mean grain size  $M_z$ .<sup>6</sup> However, values encountered for  $w_2$  and  $\sigma_2$  are known to often deviate significantly from the values obtained by these empirical expressions.

As an illustration, Figure 2.14 shows the typical backscatter curves, i.e., backscatter as a function of angle, for a number of sediment types listed in Table 2.1.

From Fig. 2.14 a number of observations can be made:

- The backscatter strength increases when moving from smaller to larger grazing angles;
- Sediments with large mean grain sizes have higher backscatter strength values than sediment with small mean grain sizes. This is due to the fact that larger grains correspond to rougher surfaces so the returned signals are stronger than those in smoother surfaces where a large part of the signal is attenuated in the sediments;
- From  $5\phi$  to  $9\phi$  the difference in backscatter strengths is less pronounced so the potential of discrimination between the sediment types based on backscatter strengths is also less pronounced;
- There is an overlap in the backscatter curves of the different sediment types in the grazing angle ranges  $[0^\circ 20^\circ]$  and  $[70^\circ 90^\circ]$ .

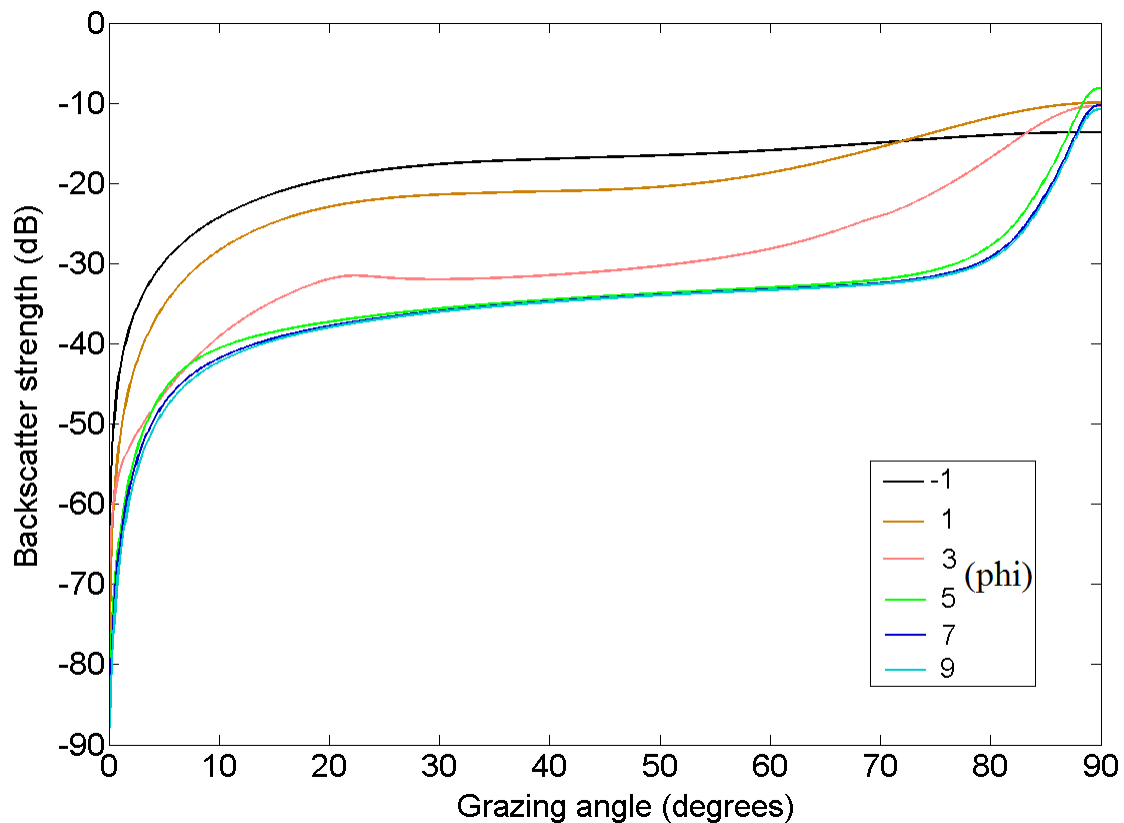


FIG. 2.14. Backscatter curves vs. grazing angle for the sediment types of Table 2.1.

### 2.2.3 The use of MBES for determining sediment backscatter strength

As mentioned in Section 2.1.3 the MBES measures, in addition to the two-way travel times per beam, also the intensities of the echo for each beam. By correcting for propagation and footprint effects, the sediment backscatter strengths can be derived.

The echo level (EL in dB) of the signal backscattered at the riverbed is:

$$EL = SL - 2TL + BTS \quad (2.26)$$

where  $SL$  in [dB re 1  $\mu$ Pa] is the source level of the MBES,  $2TL$  is the transmission loss (two-way) in dB, and  $BTS$  is the bottom “target strength” in dB.

The transmission loss in the water column is the result of two sources: one due to spherical spreading of the signal (first term of Eq. 2.27), and the other due to the energy absorbed by the water (second term of Eq. 2.27):

$$2TL = 40 \log R + 2\alpha R \quad (2.27)$$

The bottom target strength ( $BTS$ ) depends both on properties of the riverbed, but also on the ensonified area. The effect of the sediment properties is reflected by the backscattering coefficient,  $BS$  in dB/m<sup>2</sup>. The ensonified area is dependent on the resolution of the measurements as presented in Section 2.1.4. For angles away from nadir it depends on the alongtrack beam width ( $\theta_L$ ) and the transmit pulse length ( $\tau$ ),<sup>9</sup>

$$BTS = BS + 10 \log(\delta_y \delta_x) = BS + 10 \log\left(\frac{c\tau}{2 \sin \theta} \theta_L R\right) \quad (2.28)$$

For angles close to nadir an expression similar to Eq. (2.4) for the footprint in the across-track direction is used.

Using the expressions (2.26) to (2.28), the backscatter value  $BS$  can be determined from the echo levels as received by the MBES. Filtering is used to reduce the noise contained in the echo. The simplest filter is the moving average filter. For this, short averaging lengths are used and the maximum average level within a beam is chosen to represent the beam  $BS$ .<sup>9</sup>

## 2.3 Classification using MBES measurements

In literature a variety of classification techniques can be found. Significant efforts have been put in using the imaging capabilities of the MBES for discriminating between different sediment types, e.g., using image processing techniques (e.g. Ref. 10). For the current thesis, the backscatter strength is selected as the parameter to be used for sediment classification. Reason is that this parameter is a physical property of the sediment and models such as the one presented in the section 2.2.2.6 are available, predicting backscatter values as a function of sediment type. Practice, however, is cumbersome and imperfections in the MBES measurements result in imperfect measurements of the backscatter strengths. To deal with these imperfections, several classification approaches are considered in this thesis. These MBES classification methods can be divided into phenomenological (or empirical) and model-based (or physical). The model-based methods discriminate between sediment types by matching modelled and measured signals or signal features. These approaches require additional steps to account for the possible imperfections of the backscatter measurements. The empirical approaches, on the other hand, mainly base the classification on the variations in backscatter strengths within the areas surveyed, i.e., they are based on differences instead of absolute values for the backscatter strengths. These methods divide the area into small regions and use statistical features of the bathymetry or the backscatter for identifying the existing sediment classes.

The model-based approaches result directly in sediment types, since the measured signals are related to signals that are expected for different sediment types from experimental knowledge but their implementation is not straightforward. The empirical approaches are easier to implement but their outcome is in general a series of acoustic classes in an area, so ground truth is required for associating the classification results to physical parameters of the sediments (e.g. mean grain size).

Three methods are used in the current thesis; two are model based, and one is empirical:

- Classification based on backscatter strength

A classification approach that is based on the assumption that the backscatter measurements per angle are distributed according to a Gaussian distribution is used in this thesis. The approach that has been developed in Refs. 11, 12 fits a number of Gaussian probability density functions (PDFs) to the histogram of measured backscatter data per beam. The pre-requirement is that the number of measurements used for determining the averaged backscatter strength per beam is large enough to ensure gaussianity. Each PDF corresponds to a different sediment type. More details about this method are given in Chapters 4 and 5 and an example of its application is given in Chapter 4.

- Classification based on bathymetry and backscatter features

The MBES provides the backscatter strengths and the bathymetry of the area. Therefore it is of interest to investigate the potential of using the bathymetry data for classifying riverbed sediments. Moreover, the discrimination performance of the classification methods can be enhanced by combining bathymetric and backscatter data. These cases are investigated in Chapter 5.

- Classification based on acoustic backscatter angular dependence functions

This method makes use of physical models that predict the backscatter strength as a function of angle, i.e., the backscatter curve, for different sediment types. The aim is to maximize the match between modelled and measured backscatter curves. Those model input parameters, corresponding to the maximum match, are taken as being representative for the sediment type. In this thesis such a model-based approach is presented in Chapter 4, where the model described in section 2.2.2.6 is used.

## REFERENCES

- <sup>1</sup> X. Lurton, “An Introduction to underwater acoustics: principles and applications”, Springer (2002).
- <sup>2</sup> Multibeam Sonar Theory of Operation, SeaBeam instruments <http://www.ldeo.columbia.edu/res/pi/MBSsystem/sonarfunction/SeaBeamMultibeamTheoryOperation.pdf> (Date last viewed 07/07/2013).
- <sup>3</sup> J.E. Hughes Clarke, J.V. Gardner, M. Torresan and L. Mayer, “The limits of spatial resolution achievable using a 30 kHz multibeam sonar: model predictions and field results,” in Proceedings of OCEANS (1998).
- <sup>4</sup> F.B. Jensen, W.A. Kuperman, M.B. Porter, and H. Schmidt, “Computational ocean acoustics”, American Inst. Of Physics, (1997).
- <sup>5</sup> R.J. Urick, “Principles of underwater sound”, 3rd. ed., Peninsula publishing (1983).
- <sup>6</sup> “APL-UW high-frequency ocean environmental acoustic models handbook”, Oct. 1994, technical report APL-UW TR9407AEAS 9501, Applied Physics Laboratory, University of Washington, pp. IV1-IV50.
- <sup>7</sup> D.R. Jackson, Third report o. TICIP Bottom Scattering Measurements: Model Development, APL-UW 8708, Sept. (1987).
- <sup>8</sup> D.G. Simons, and M. Snellen, “A comparison between modeled and measured backscatter strength”, In Proceedings of Acoustics conference, June 29 – July 4, Paris, 5307-5312 (2008).
- <sup>9</sup> E. Hammerstad, “Backscattering and Seabed Image Reflectivity”, EM TechnicalNote,(2000),[http://www.km.kongsberg.com/ks/web/nokbg0397.nsf/AllWeb/226C1AFA658B1343C1256D4E002EC764/\\$file/EM\\_technical\\_note\\_web\\_BackscatteringSeabedImageReflectivity.pdf?OpenElement](http://www.km.kongsberg.com/ks/web/nokbg0397.nsf/AllWeb/226C1AFA658B1343C1256D4E002EC764/$file/EM_technical_note_web_BackscatteringSeabedImageReflectivity.pdf?OpenElement) (date last viewed 09/06/2011).
- <sup>10</sup> P. Blondel and O. Gomez Sichi. “Textural analyses of multibeam sonar imagery from Stanton Banks, Northern Ireland continental shelf”, Applied Acoustics, 70, 1288-1297 (2009).
- <sup>11</sup> D.G. Simons, and M. Snellen. “A Bayesian approach to seafloor classification using multi-beam echo-sounder backscatter data”, Appl. Acoust. 70, 1258-1268 (2009).
- <sup>12</sup> A.R. Amiri-Simkooei, M. Snellen, and D.G. Simons, “Riverbed sediment classification using multi-beam echo-sounder backscatter data”, J. Acoust. Soc. Am. 126, 1724-1738 (2009).



# 3

## **Surveyed rivers and equipment**

---

In this chapter the location in the Netherlands and the bathymetry of the various parts of Dutch rivers that were surveyed with MBES systems are presented. Furthermore, the specifications of the MBES systems used in the surveys are given.

### 3.1 Surveyed rivers

The MBES surveys were performed in the Rhine river and the Meuse river between 2007 and 2010. The Rhine river flows through Germany to the Netherlands while Meuse runs through Belgium to the Netherlands. Five parts of the Rhine river were surveyed: Sint Andries, where a large survey was carried out in 2007 with a re-survey of a smaller part of this area in 2008, Nijmegen (2008), Bovenrijn (2008), and the Dordtse Kil (2009). A part of the Meuse river was surveyed in 2010. The location of the rivers on the map of the Netherlands as well as their bathymetry as measured by MBES is shown in Fig. 3.1. All rivers are shallow having similar depth ranges from 1 m to 10 m, except for the Dordtse Kil, which is deeper with depths ranging between 1 m to 19 m.

Grab samples were collected from all surveyed areas. The grab samples were taken from the top 3 to 4 cm of the sediment surface. The reason is that, the acoustic signal of the MBES is sensing only the upper few cm of the sediment.

For obtaining the sediment composition, the grab samples are analysed in a dedicated laboratory. The grab samples are first dried and then are sieved. From this process, gravel and shells are separated from finer material. Then the gravel and shell weight percentage is determined. The grain size distribution of the finer material is determined by optical microscopy.

Figure 3.2 provides an overview of the grab samples' mean grain size per area. It can be seen that there is a gradual shift from fine sediments in Dordtse Kil to coarse sediments in Sint Andries and Nijmegen, and finally to very coarse sediments in Bovenrijn and Meuse. This is also the order that the thesis will follow: from Dordtse Kil (Chapter 4) to Sint Andries and Nijmegen (Chapter 5), and finally Bovenrijn and Meuse (Chapter 6).

Video images and still photographs were taken underwater at each grab sample position. This was done for assisting the interpretation of the classification results in the cases where the laboratory was not able to determine the sediment mean grain sizes (e.g. Meuse, Chapter 6).

Further details about the morphological characteristics of each area can be found in the following chapters of the thesis where the classification results of each area are presented.

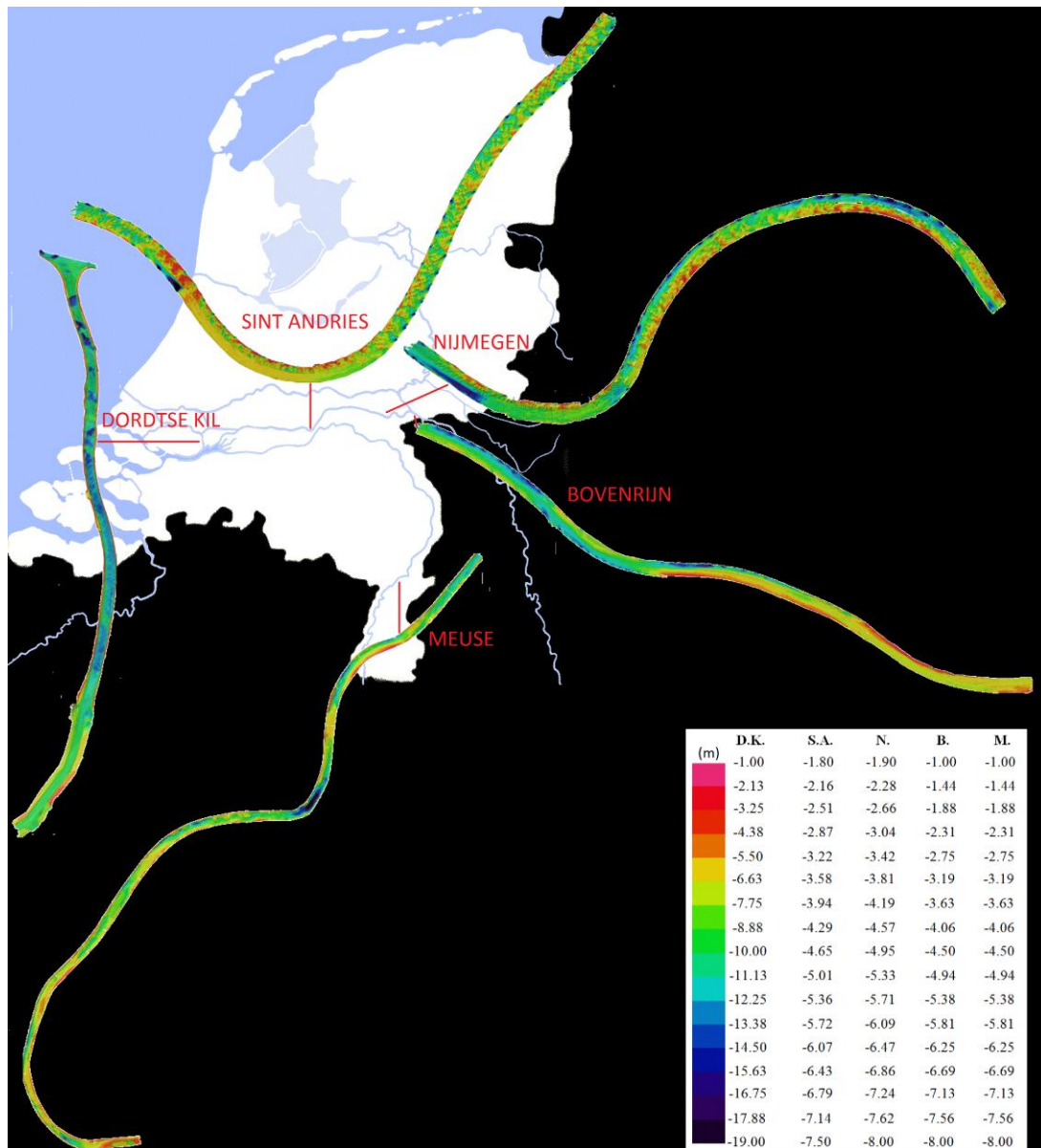


**FIG. 3.1.** Location of the surveyed rivers on the map of the Netherlands and their bathymetry derived from MBES measurements (D.K.=Dordtse Kil, S.A.=Sint Andries, N.=Nijmegen, B.=Bovenrijn, and M.=Meuse).

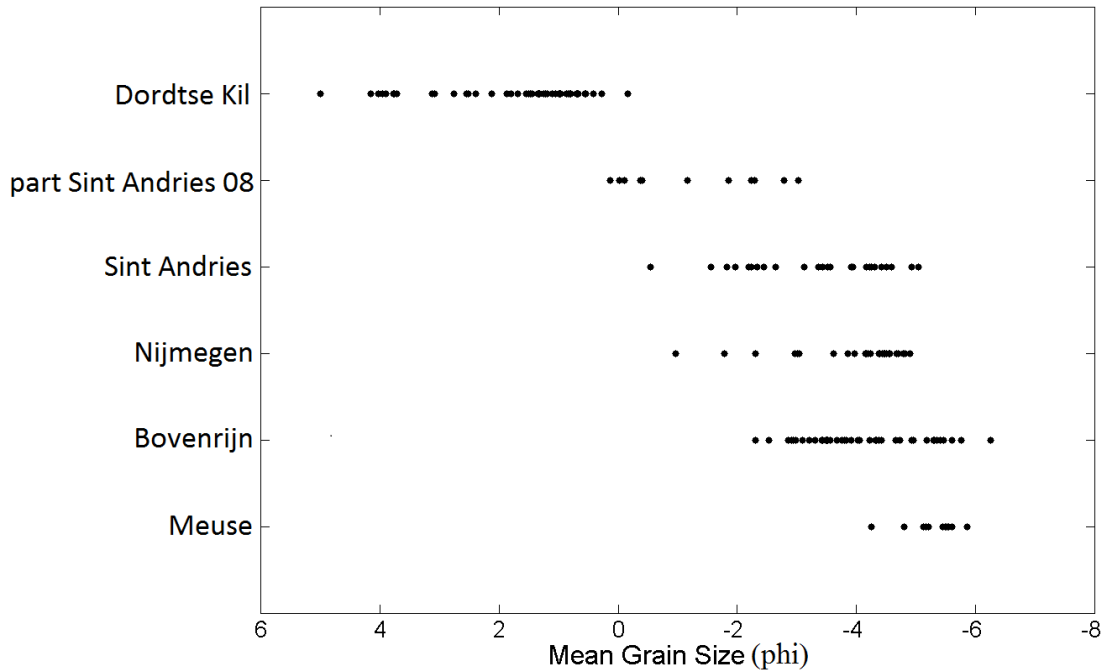


**FIG. 3.2.** Mean grain size of the grab samples taken from the surveyed areas.

## 3.2 Equipment

All the measurements were performed using EM3002 Kongsberg MBES systems. It is a high resolution riverbed mapping and inspection system with minimum operating depth from less than 1 m below its transducers. EM3002 has a very high ping rate of up to 40 Hz, a large number of measurements per ping (up to 254 per sonar head),  $1.5^\circ$  beam-widths, and electronic pitch and roll stabilisation. The pulse length is  $150 \mu\text{s}$  and the sampling frequency of the incoming echo, also denoted range sampling frequency, is 14 kHz. In shallow waters it is possible to achieve 100% coverage of the bottom at vessel speeds of about 10 knots (5.14 m/s) with across-track coverage of up to four times the water depth.<sup>1</sup>

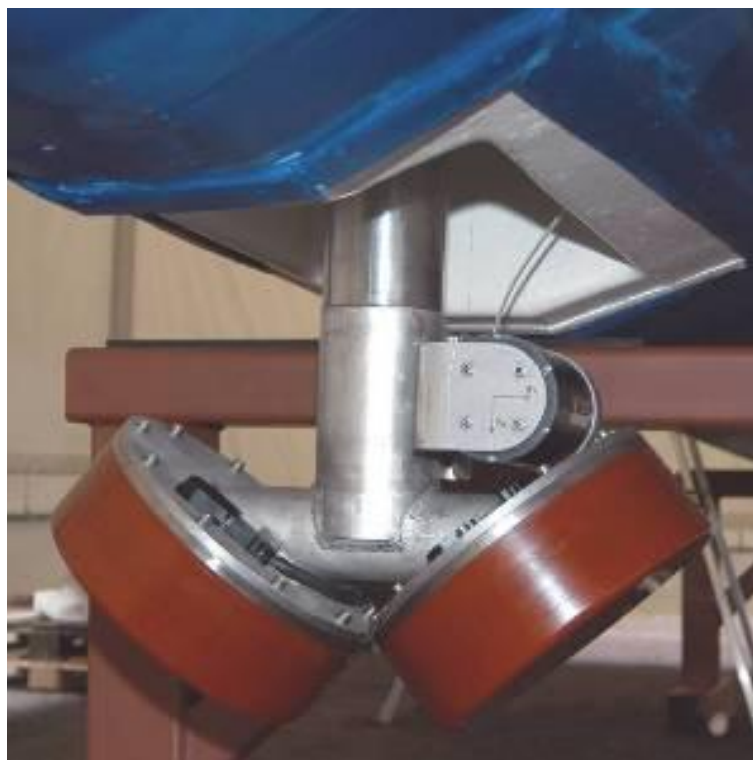
Instead of a single transducer as used for the majority of the measurements, the EM3002 may be also be configured to use two sets of transducers (see Fig. 3.3). This dual configuration was used in the measurements of the Dordtse Kil. This configuration increases the coverage to up to ten times the depth for shallow waters and the number of measurements per ping up to 508.

The system sonar frequency is nominally 300 kHz. Acoustical interference between the two sonar heads of EM3002D (D=dual head) is eliminated by using two different operating frequencies (293 and 307 kHz).

All surveys were performed with equi-distant measurement mode. The average distance between pings per area is given in Table 3.1.

**Table 3.1** Average distance between pings per surveyed area.

Surveyed Area	Ping distance (cm)
Dordtse Kil	21.5
Sint Andries	8.5
part of Sint Andries in 2008	9.7
Nijmegen	9.8
Bovenrijn	8.5
Meuse	8.2

**FIG. 3.3.** Retractable dual head.<sup>2</sup>**REFERENCES**

- <sup>1</sup> EM3002, [http://www.km.kongsberg.com/ks/web/nokbg0397.nsf/AllWeb/7C8510CFA3CD21ABC1256CF00052DD1C/\\$file/164771ae\\_EM3002\\_Product\\_spec\\_lr.pdf](http://www.km.kongsberg.com/ks/web/nokbg0397.nsf/AllWeb/7C8510CFA3CD21ABC1256CF00052DD1C/$file/164771ae_EM3002_Product_spec_lr.pdf) (Date last viewed 26/06/2013).
- <sup>2</sup> <http://www.gserentals.co.uk/details.aspx?product=152> (Date last viewed 26/06/2013).



# 4

## **An inter-comparison of sediment classification methods based on multi-beam echo-sounder backscatter and sediment natural radioactivity data<sup>1</sup>**

---

This chapter presents sediment classification results derived from different sources of data collected at the Dordtse Kil River, the Netherlands. The first source is a multi-beam echo sounder (MBES). The second source are measurements taken with a gamma-ray scintillation detector, i.e., the Multi-element detection system for underwater sediment activity (Medusa), towed over the sediments and measuring sediment natural radioactivity. Two analysis methods are employed for sediment classification based on the MBES data. The first is a Bayesian estimation method that uses the average backscatter data per beam and, therefore, is independent of the quality of the MBES calibration. The second is a model-based method that matches the measured backscatter curves to theoretical curves, predicted by a physics-based model. Medusa provides estimates for the concentrations of potassium, uranium, thorium, and cesium, known to be indicative for sediment properties, viz. mean grain size, silt content and the presence of organic matter. In addition, a hydrophone attached to the Medusa system provides information regarding the sediment roughness. This paper presents an inter-comparison between the sediment classification results using the above-mentioned methods. It is shown that although originating from completely different sources, the MBES and Medusa provide similar information, revealing the same sediment distribution.

---

<sup>1</sup> This chapter has been published as journal paper: *M.Snellen, D. Eleftherakis, A. Amiri Simkooei, R.L. Koomans, and D.G. Simons, "An inter-comparison of sediment classification methods based on multi-beam echo-sounder backscatter and sediment natural radioactivity data", Journal of the Acoustical Society of America 134(2), 959-970 (2013).*

## 4.1 Introduction

Reliable information about the seafloor or riverbed sediment composition is of high interest for a large number of applications such as marine geology, marine biology, off-shore construction projects, and cable and pipeline route planning. Traditionally, obtaining information about the sediment distribution in an area requires an extensive set of grab samples of the sediments and subsequent laboratory analysis, which can be costly and time consuming. Alternatively, acoustic remote sensing techniques can be used for classifying the sediments. Since single- and multi-beam echo-sounders (SBES, MBES) are already in common use for depth measurements, an attractive approach is to use the signals measured by these systems also for sediment classification purposes. Sediment classification potential using the MBES and SBES systems has proven to be high.<sup>1-7</sup>

In general, sediment classification methods using SBES and MBES can be divided into phenomenological (or empirical) and model-based (or physical) methods. In the phenomenological methods, features that are indicative for sediment type (e.g. backscatter strength or features derived from the bathymetric measurements) are used for classification. These methods discriminate the sediments as belonging to different acoustic classes, each with its own acoustic features. These acoustic classes represent the different sediment types that are present in the survey area. However, independent information, e.g. from grab samples taken in the area, is usually needed to assign sediment type, such as mud, sand or gravel, or sediment parameters, such as mean grain size, to the acoustic classes.<sup>6-9</sup> On the contrary, the model-based methods<sup>10-13</sup> determine the sediment type by maximizing the match between modelled and measured signals or signal features, where sediment type, or parameters indicative for sediment type, are input into the model. In principle, no independent information is required for model-based methods, since they provide the sediment type, or properties indicative for sediment type, instead of acoustic classes.

This paper examines two methods for riverbed sediment classification using the MBES. First, a statistical method is applied that utilizes the backscatter strength measurements of an MBES. It uses the backscatter data at a certain angle to obtain the number of sediment classes and to discriminate between them by applying the Bayes decision rule to multiple hypotheses.<sup>14,15</sup> Although this method can be considered as model-based, employing a model for the backscatter histogram, it classifies the sediments as a number of acoustic classes. Second, a method is employed that matches backscatter versus grazing angle as measured by the MBES to model predictions, thereby providing sediment properties.

However, not only acoustic characteristics are indicative for the sediment type, also natural radioactivity levels differ for different sediment types and can as such be used to discriminate between sediments. In this paper, radioactivity levels taken with the Multi-element detection system for underwater sediment activity (Medusa),<sup>16,17</sup> which takes measurements with a gamma-ray scintillation detector, are considered. The system measures gamma-rays being emitted from very low concentrations of a number of radionuclides in the sediment, viz. <sup>137</sup>Cs, <sup>40</sup>K, and radionuclides from the decay series of <sup>238</sup>U and <sup>232</sup>Th. It is towed over the sediment bed behind the vessel. Due to the attenuation of gamma radiation in the sediment, the measured concentrations are characteristic for the top 30 to 50 cm of the sediment. In addition to the radionuclide concentration measurements, Medusa also takes measurements with a hydrophone towed over the sediment. These resulting noise levels can be used to

determine whether or not the system is in contact with the sediment, but are also indicative for the sediment roughness. The measurements taken with the Medusa system and the corresponding data analysis are presented.

The aim of the research presented in this paper is two-fold. (1) In general, the MBES sediment classification methods that classify sediments as a series of acoustic classes are relatively easy to implement and require limited computational efforts. This holds for the phenomenological approaches, but also for the Bayesian method of Ref. 14. The drawback of these methods is that it is not always straightforward to assign sediment type or sediment parameters to the different acoustic classes. Still, this knowledge is considered of high importance for many applications. Therefore, in this paper, the results obtained by applying a model-based method are compared to those obtained with the method of Ref. 14 to investigate the relation between acoustic classes and sediment properties. The results illustrate that although the mean grain size is the most important parameter, the correlation coefficient between mean grain size and acoustic classes is limited impeding a direct conversion of acoustic class to mean grain size. (2) Classification methods based on MBES data can discriminate only sediments that show acoustically distinct behaviour. In this contribution, the acoustic classification results are compared with results of the completely independent Medusa method. The aim is to investigate if there is increased classification potential by using the data of these two independent data sources. The results show that the Medusa measurements and MBES measurements reveal a similar distribution of the different sediment types, thus providing confidence in the reliability of both independent methods. The low correlation between the acoustic classification results (classes and sediment parameters obtained from the model-based method) and concentration of  $^{137}\text{Cs}$  indicates that complimentary information can be derived from this radionuclide which is known to be a proxy for the fraction of organic matter.

This paper is organized as follows. In Section 4.2, details about the experiment are given. Section 4.3 provides a brief description of the acoustic classification methods and the Medusa method. The classification results of each of the methods are presented in Section 4.4. Section 4.5 gives a comparison between the methods and discusses their similarities and differences. Finally, the main conclusions of the paper are summarized in section 4.6.

## 4.2 A description of the measurements taken in the area

The Dordtse Kil is a river in The Netherlands (South Holland) and is an important link and transport axis. The water depths in the Dordtse Kil as acquired by the MBES are presented in Fig. 4.1.

The river area was surveyed in October 2009 over a length of ~10 km and its almost full width of 260 m, using the EM3002D Kongsberg dual head MBES. The total number of beams is 320 (160 per head). The operation frequency was 300 kHz, the pulse length was 150  $\mu\text{s}$ , and the maximum ping rate was 40 Hz. The beam width was  $1.5^\circ \times 1.5^\circ$ . All beams were electronically stabilized for pitch and roll. For each beam and each ping a single backscatter value is given. This value is the result of first applying a moving average over the time series of amplitude values and then selecting the maximum average level of each beam.<sup>18</sup>

During the survey, measurements were taken with the Medusa system measuring the sediment natural radioactivity. This system is towed behind the vessel. For these measurements, contact between the sensor and the sediment is essential. To validate if indeed the sensor was located on the sediment, it is equipped also with a hydrophone. High noise levels indicate good contact between the sensor and the sediment, whereas low noise indicates that the sensor is floating in the water.

In addition, bottom grab samples were collected along the river. For each bottom grab sample the grain size distribution was determined. These results are shown in Fig. 4.2(a), illustrating unimodal behaviour for all grab samples. The grab samples indicate mainly fine-grained sediments with mean grain sizes  $M_z$  ranging from -0.15 to 5 in phi units  $[\phi]$ , with  $M_z = -\log_2(d)$  and  $d$  the mean grain size in mm, see Fig. 4.2(b).

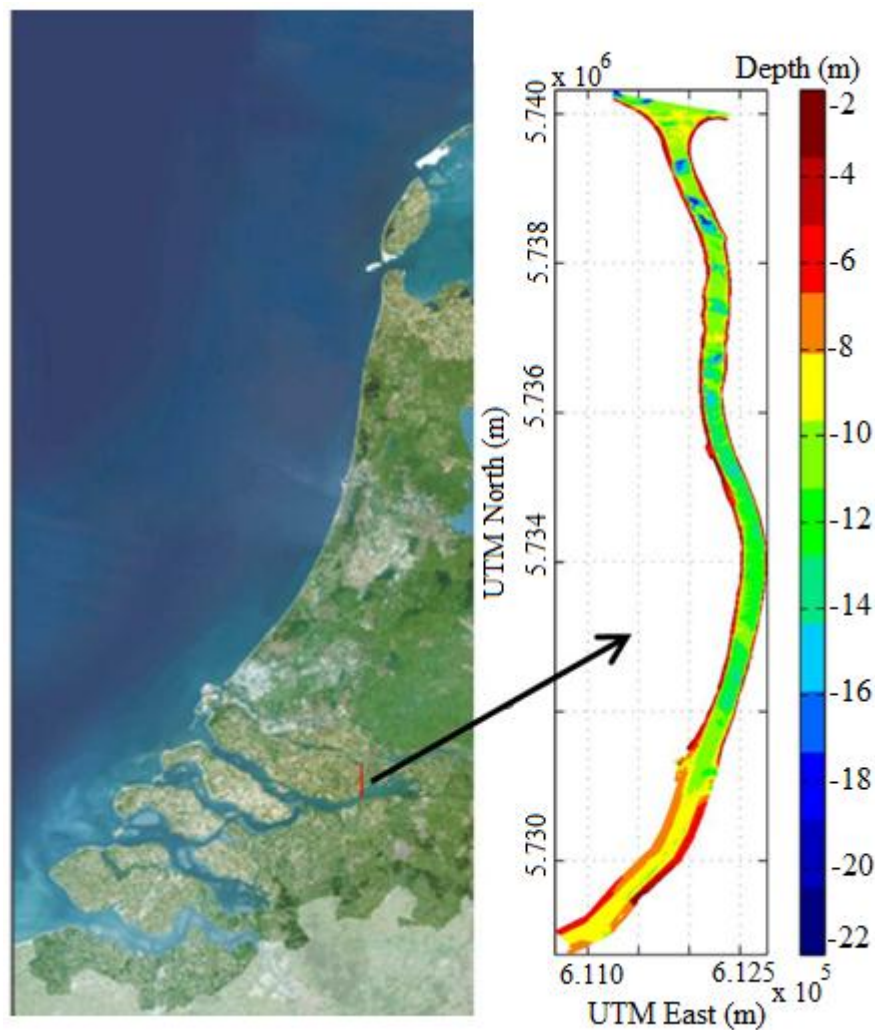


**FIG. 4.1.** The bathymetry of the Dordtse Kil superimposed upon a view of The Netherlands.

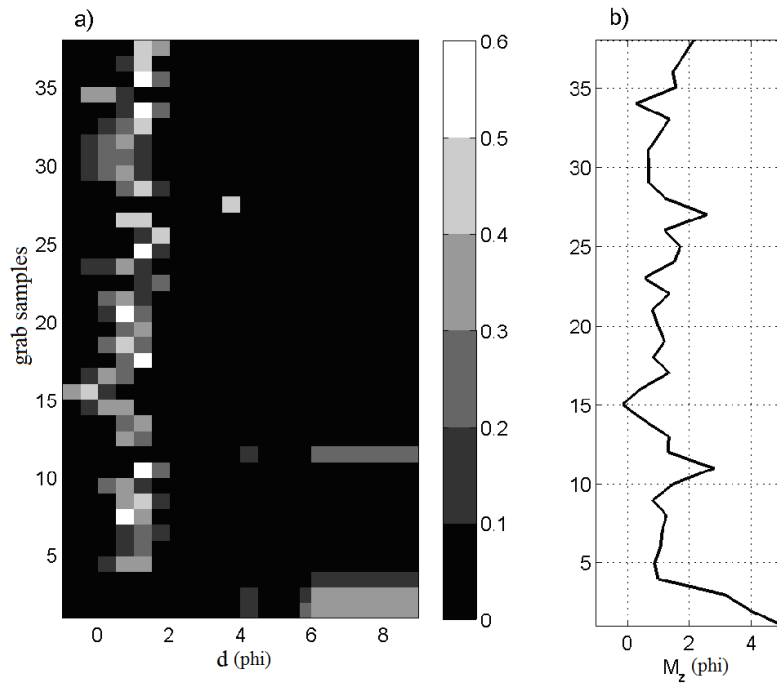


FIG. 4.2. a) Grab sample grain size distribution; b) grab sample mean grain sizes.

## 4.3 Sediment Classification Methods

### 4.3.1 The Bayesian classification method using MBES backscatter data

In Ref. 14 a method is presented for sediment classification using MBES backscatter measurements. The method carries out the classification per angle, which makes it insensitive to variations in sediment type along the swath and to imperfect sonar calibration. It fits a number of Gaussian probability density functions (PDFs) to the histogram of the backscatter strength ( $BS$ ) data at a given angle, i.e.,

$$BS \sim f_{BS}(BS) = \sum_{i=1}^r c_i N(BS; \mu_i, \sigma_i^2) \quad (4.1)$$

where  $\mu_i$  and  $\sigma_i^2$  are the mean and variance of the  $i^{\text{th}}$  Gaussian distribution  $N$ , respectively, and  $c_i$  is the contribution of the individual Gaussian functions to the total PDF.  $f_{BS}$  is the fitted histogram. The number of PDFs is increased until the chi-square distributed test-statistic of the residuals becomes less than a critical value. Based on the resulting  $r$  Gaussian PDFs, the Bayes decision rule is applied to determine the  $r$  regions of backscatter values corresponding to the  $r$  acoustic classes.

The method is based on the assumption that the backscatter values for a single sediment type follow a Gaussian distribution for a sufficiently large number of scatter

pixels in the beam footprint. For shallow river areas, Gaussianity of the distribution is ensured by averaging the measured backscatter values over surface patches, consisting of a small number of beams in the across-track direction and a few pings in the along-track direction.<sup>15</sup> Bottom slopes are accounted for according to the method presented in Ref. 15.

### 4.3.2 A model-based approach for sediment classification

Whereas the Bayesian method makes use of the backscatter values per angle, alternatively use can be made of the complete backscatter curve, i.e., the backscatter as a function of angle. Models exist that predict these backscatter curves as a function of sediment properties and frequency. By searching for those sediment properties that result in an optimal agreement between modelled and measured backscatter curve, the sediments can be classified. In this case, the classification results consist of real sediment properties instead of acoustic classes. For the work presented in this paper, the model described in Ref. 19 and Chapter 2.2.2.6 is employed for predicting the backscatter curve.

As a first step in assessing the agreement between model predictions and measured backscatter curves, backscatter curves measured close to locations of the grab samples are considered. The model is run for mean grain size values as determined from the grab samples, and values for all other model input parameters are derived from the empirical expressions relating them to the mean grain size. Differences (not shown here) between the resulting model predictions and measurements can be attributed to:

- 1) sediment types that change along the swaths;
- 2) values for the  $\sigma_2$ ,  $w_2$ ,  $\rho$ ,  $\nu$ , and  $\delta$  that deviate from those obtained from the empirical expressions;
- 3) imperfect calibration of the MBES backscatter measurements.

To solve for these effects the following procedure is applied. An objective function is defined that quantifies the difference between the modeled and measured backscatter strength:

$$f(\mathbf{x}) = \sum_{\theta} |b_i^{me}(\theta) - b_i^{mo}(\theta; \mathbf{x})| \quad (4.2)$$

where  $b_i^{me}$  and  $b_i^{mo}$  are the measured and modeled backscatter strength, respectively. The use of Eq. (4.2), providing a measure for the absolute discrepancies between the measured and modeled backscatter curves based on the L1 norm, is motivated due to its robustness property compared to the ordinary least-squares (L2) norm.<sup>20</sup> In general,  $\sigma_2$  and  $w_2$  are known to show the largest deviations from the empirical predictions and, therefore, these parameters are considered as unknowns, contained in vector  $\mathbf{x}$ . An estimate for the mean grain size is available from the grab samples, but still this parameter is allowed to vary slightly. Consequently,  $\mathbf{x}$  contains three

unknowns, i.e.,  $\sigma_2$ ,  $M_z$  and  $w_2$ . For minimizing Eq. (4.2) use is made of the differential evolution method as described in Refs. 21 and 22.

Due to the imperfect calibration of the MBES and the noise of the measurements, the objective function will not become zero. The average curve of the differences (between measured and modeled curves) for all grab samples can be considered as the calibration curve. However, as mentioned in item 1 above, measurements can also be affected by variations in sediment types along the swath. Accounting for these measurements will result in differences between modeled and measured backscatter curves that differ significantly from the average, i.e., the calibration curve.

Therefore, an iterative procedure is followed to establish the final calibration curve. In each iteration the measurements are corrected using the calibration curve of the previous iteration. The measurement with maximum discrepancy with the mean curve is masked as an outlier. A new calibration curve is then determined, based on the remaining measurements, as the sum of the old curve and a correction to this curve. After removing more and more outliers, at some iteration the discrepancies become negligible and no further corrections on the calibration curve are required.

The final calibration curve is then applied to all measured backscatter curves, allowing for determination of the three parameters  $M_z$ ,  $w_2$ , and  $\sigma_2$  over the entire area.

### 4.3.3 Medusa method

The Medusa system takes measurements with scintillator-based gamma-ray detectors, towed over the sediment. These measurements allow for: a) measurement of natural background radiation, and b) absolute measurement of radionuclide concentrations in the sediment through deconvolution of the measured signal's spectrum.<sup>23</sup> The deconvolution focuses on estimating concentrations of the radionuclides  $^{238}\text{U}$ ,  $^{232}\text{Th}$ ,  $^{40}\text{K}$ , and  $^{137}\text{Cs}$ , since these are known to be indicative for the sediment properties clay content, organic matter content and mean grain size.

#### Measuring clay content

The  $^{238}\text{U}$  uranium occurs naturally in trace amounts in sediments by its incorporation in silt, sand and in some heavy minerals. In the Netherlands, typical concentrations in silt are higher than in sand. The  $^{232}\text{Th}$  thorium isotope is also present in sediments in approximately similar concentrations in silt and sand.<sup>16</sup> This makes uranium and thorium suited proxies for mapping silt and sand ratio's in the sediment. The correlation between uranium, thorium and silt varies on the scale of a sedimentary basin. Grab sample investigations have shown that these correlations are similar for a delta system as large as the Netherlands.<sup>17</sup>

#### Measuring organic matter content

There is a distinct difference between the natural radionuclides ( $^{40}\text{K}$ ,  $^{238}\text{U}$ ,  $^{232}\text{Th}$ ) and  $^{137}\text{Cs}$  in the way they are distributed in sediments. The natural radionuclides will at least initially be a more or less integral part of the minerals comprising the sediment while  $^{137}\text{Cs}$  is a later surface addition that has been distributed in the environment by atmospheric testing of nuclear weapons in the 1960s and by the Chernobyl accident. The  $^{137}\text{Cs}$  from Chernobyl has been preferentially deposited

along a 150 km broad strip in northwest–southeast direction passing over the centre of the Netherlands. The initially mobile  $^{137}\text{Cs}$  is absorbed by silt and organic matter.<sup>17</sup> This makes  $^{137}\text{Cs}$  a proxy for the organic matter content of the sediments. The correlation between  $^{137}\text{Cs}$  and organic matter depends strongly on the trends in deposition of  $^{137}\text{Cs}$  during the Chernobyl fallout.

#### Measuring grain size

Coarse-grained sediments consist of a mixture of quartz and potassium feldspar. In the process of weathering, feldspars tend to be reduced in size during abrasion, whilst quartz tends to be fragmented and destroyed.<sup>24</sup> This process will cause an increased concentration of feldspar in finer sediments and, consequently, a correlation between the concentration of feldspar and grain size. The Potassium feldspar minerals contain  $^{40}\text{K}$ . Hence, the  $^{40}\text{K}$  concentration can be used as grain size indicator. The exact relation between the  $^{40}\text{K}$  concentration and mean grain size depends on the location.

The concentration of radio-active nuclides in a specific type of sediment is called the radiometric fingerprint of that sediment. To derive a fingerprint for the sediments in a certain area use is made of grab samples taken in the area. These grab samples are analysed both with respect to their sediment properties and the radionuclide concentrations. Based on the resulting relations between the sediment properties and radionuclide concentrations, the radio-active emissions measured by Medusa over the area can be converted to maps of the sediment properties.

In addition to the radiometric measurements, the Medusa system is also equipped with a hydrophone. This hydrophone is towed over the sediment surface with the primary purpose to check whether the Medusa system touches the sediment, resulting in high noise levels, or is floating freely in the water, corresponding to much lower measured noise levels. From experience, it is found that these hydrophone measurements can also be used to assess sediment roughness and the presence of features, such as shells, on the sediment.

## 4.4 Classification Results

### 4.4.1 Bayesian results

Surface patches were created by averaging over approximately eight beams and five pings. The average distance between two consecutive beams is 15 cm and between two pings is approximately 25 cm, and consequently each surface patch is approximately of size 120 cm x 125 cm. After applying corrections for the bottom slope, the average backscatter strength was determined for each of the patches. The assumption of a Gaussian distribution for the backscatter PDFs was tested for areas with a single sediment type and was found to be valid.

From the test statistic, it is observed that the optimal value for the number of classes amounts to five, as illustrated in the left frame of Fig. 4.3, since more classes do not result in a significantly better agreement between model and measurements. The obtained model contains sufficient detail for describing the measurements. The right frame shows the histogram and the Gaussian fit for the averaged backscatter values at the grazing angle of  $30^\circ$  for the left transducer. A similar approach, fitting the histogram with a number of Gaussians, is taken for all other angles, providing for each angle the range of backscatter values corresponding to each of the classes. However, since the discriminative performance is best for the most grazing angles,  $\sim 30^\circ$  in this case, due to their large beam footprint, the number of classes as derived for this angle, i.e., five, is used for the fitting procedure for the other angles. The classification map of the area obtained by accounting for the full range of usable angles ( $26^\circ$ - $70^\circ$  grazing angles) is presented in Fig. 4.4.

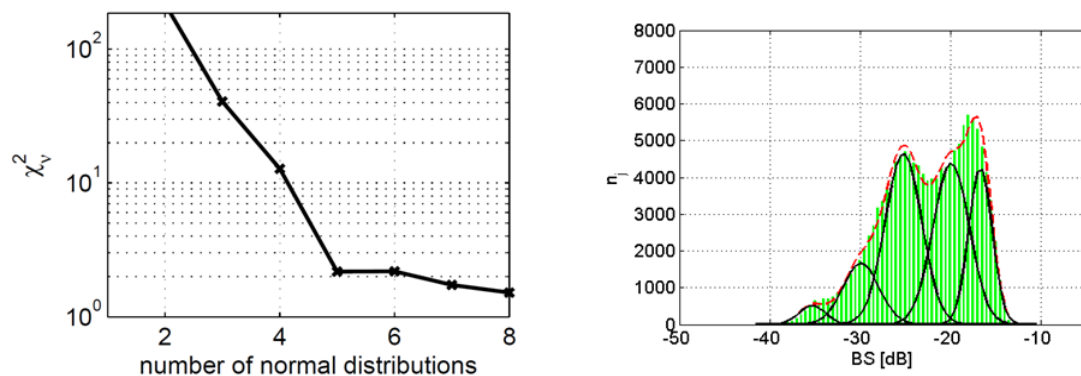


**FIG. 4.3.** Normalized chi-square distributed test statistic versus number of classes (left frame). The right frame presents the histograms of the measured BS data, i.e., number of measurements  $n_j$  as a function of BS, over the entire area (bars), the five Gaussians (solid lines), and its best fit (dashed line) at a grazing angle of  $30^\circ$  (right frame).

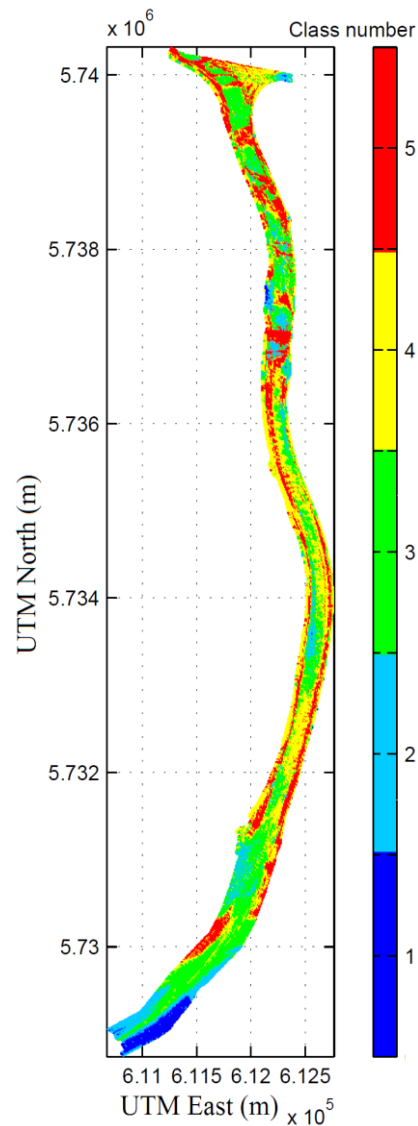


**FIG. 4.4:** Classification of the Dordtse Kil river obtained by applying the Bayesian acoustic classification method.

#### 4.4.2 Model-based results

The strategy explained in section 4.3.2 is now applied to the MBES data acquired in the Dordtse Kil. For all MBES tracks that were sailed over the 38 grab sample positions, mean backscatter curves are obtained over a few consecutive pings. This resulted in 73 combinations of grab samples and mean backscatter curves, as grab sample locations were crossed multiple times while taken the MBES measurements. These curves and the  $M_z$  values of the corresponding grab samples are used to derive the calibration curve. The results are illustrated in Fig. 4.5. The bottom sub-frame at the left shows the (minimized) differences between modelled and observed backscatter curves when accounting for all grab samples. In an ideal case the differences are identical and hence represent the final calibration curve. However, due to variations in sediment type along the swathes and measurement noise, an ideal curve can never be obtained. Therefore the median curve of the differences is

considered to be a first estimate for the calibration curve (thick black line in the left bottom frame of Fig. 4.5). Due to the robustness of the L1 norm minimization, the results presented are not affected by possible outliers. Still, the quality of the estimated calibration curve can be improved by removing some of the outliers. Therefore, the iterative approach of Section 4.3.2 is applied. The approach was stopped after nine iterations after which the L1 norm has decreased from over 80 dB to  $\sim 5$  dB. Additional iterations did not result in a further decrease. It was found that for three grab samples, with mean grain sizes of 1.3, 1.5 and 5.0  $\phi$ , all combinations of these grab samples and backscatter curves were identified as outlier. This can be caused by errors in the measurements, for example due to uncertainties in the exact grab sample locations or backscatter curves that are affected by variations of sediment type along the swath, but can also be due to the backscatter model output not being representative for the sediment at the locations of the grab samples.

The results from the iterative approach are presented in the right frame of Fig. 4.5.

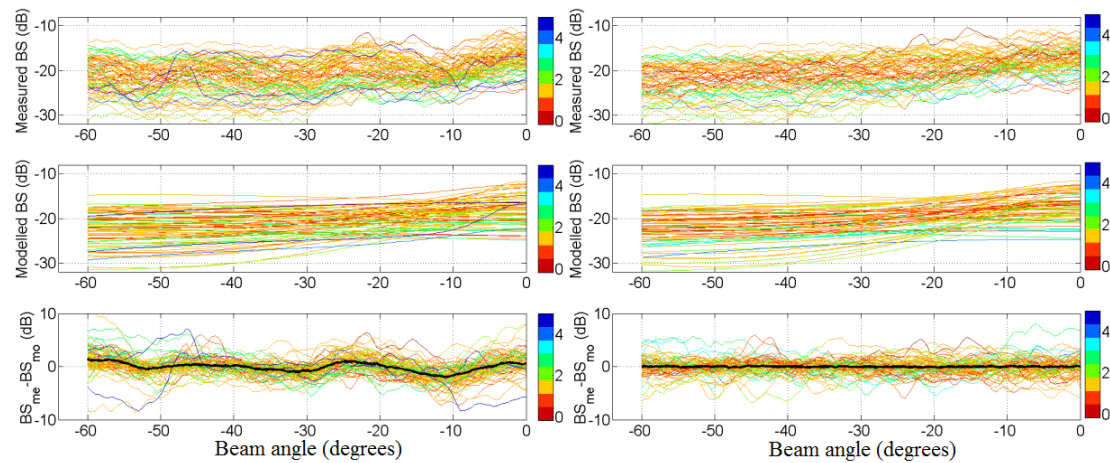


**FIG. 4.5.** Measured backscatter as a function of beam angle  $\theta$  at grab sample positions (top sub-frames), corresponding modelled backscatter versus  $\theta$  (middle sub-frames) and difference between modelled and measured backscatter versus  $\theta$  (bottom sub-frame). The left frames show the result at the first iteration, with all grab samples accounted for. The thick black line in the left bottom sub-frame is the mean of the differences between modelled and measured backscatter, representing the initial calibration curve. The right frames show the result at the final iteration. The measurements (top sub-frame) have been corrected using the calibration curve corresponding to the ninth iteration. The thick black line in the right bottom sub-frame indicates the corrections that would be applied in the next iteration. Colours indicate mean grain sizes in phi unit.

In the next step, the calibration curve is used to correct all measured backscatter curves, obtained by averaging over a few consecutive pings. These are then fed into the optimization process where a search is performed to determine values for  $\sigma_2$ ,  $M_z$ , and  $w_2$  that provide a maximum agreement between modelled and measured backscatter curve from Eq. (4.2). The search bounds were selected as  $-1 \leq M_z \leq 9$ ,  $5 \times 10^{-5} \leq w_2 \leq 2 \times 10^{-2}$ , and  $5 \times 10^{-5} \leq \sigma_2 \leq 5 \times 10^{-3}$ . Figure 4.6 shows two typical examples where this inversion has been applied. The modelled curves fit the

measured curves quite well indicating a reliable optimization method and processing strategy.

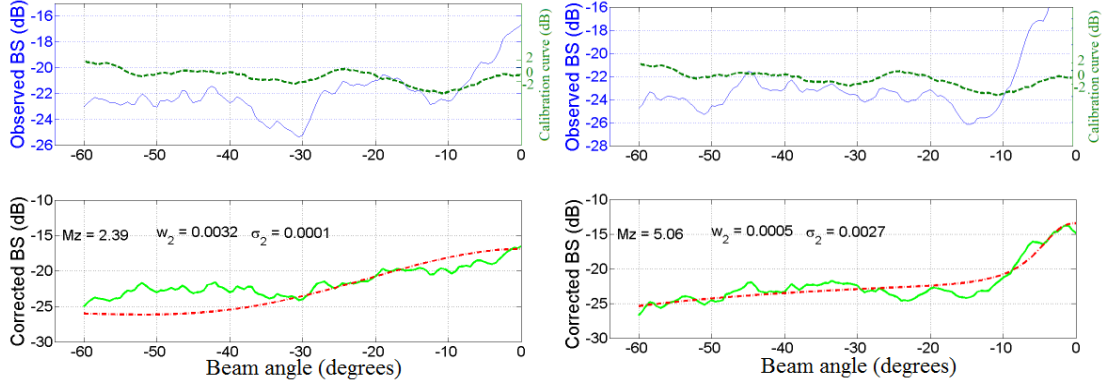


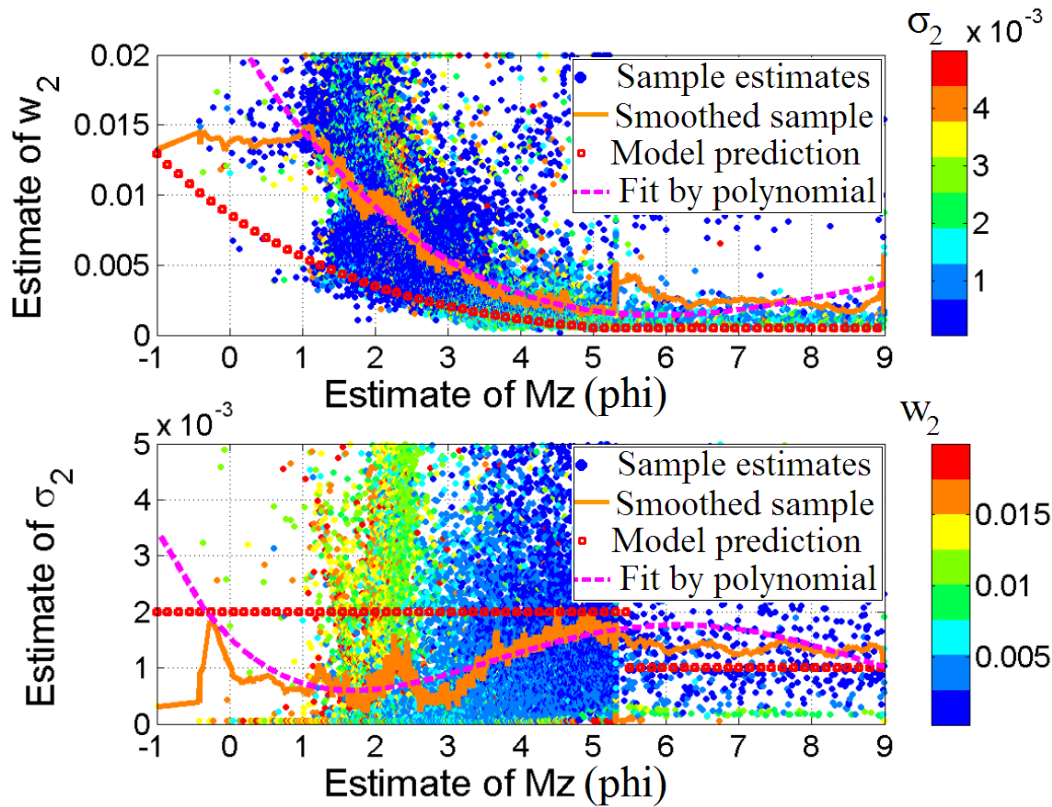
**FIG. 4.6.** Two examples of the optimization problem where the three parameters  $M_z$ ,  $w_2$ , and  $\sigma_2$  are searched for. In each frame the top sub-frame is the calibration curve (thick dashed line) and the observed backscatter curve (thin solid line). The bottom sub-frame is the corrected (thick solid line) and modelled (thick dashed-dotted line) backscatter curve. Indicated in the plots are the estimated parameters for each inversion.

Empirical relations between  $M_z$ ,  $w_2$ , and  $\sigma_2$  are provided in Ref. 19. For  $-1 \leq M_z < 5$ , the relation between  $M_z$  and  $w_2$  is

$$w_2 = 0.00207h^2 \quad \text{with} \quad h = \frac{2.03846 - 0.26923M_z}{1 + 0.076923M_z} \quad (4.3)$$

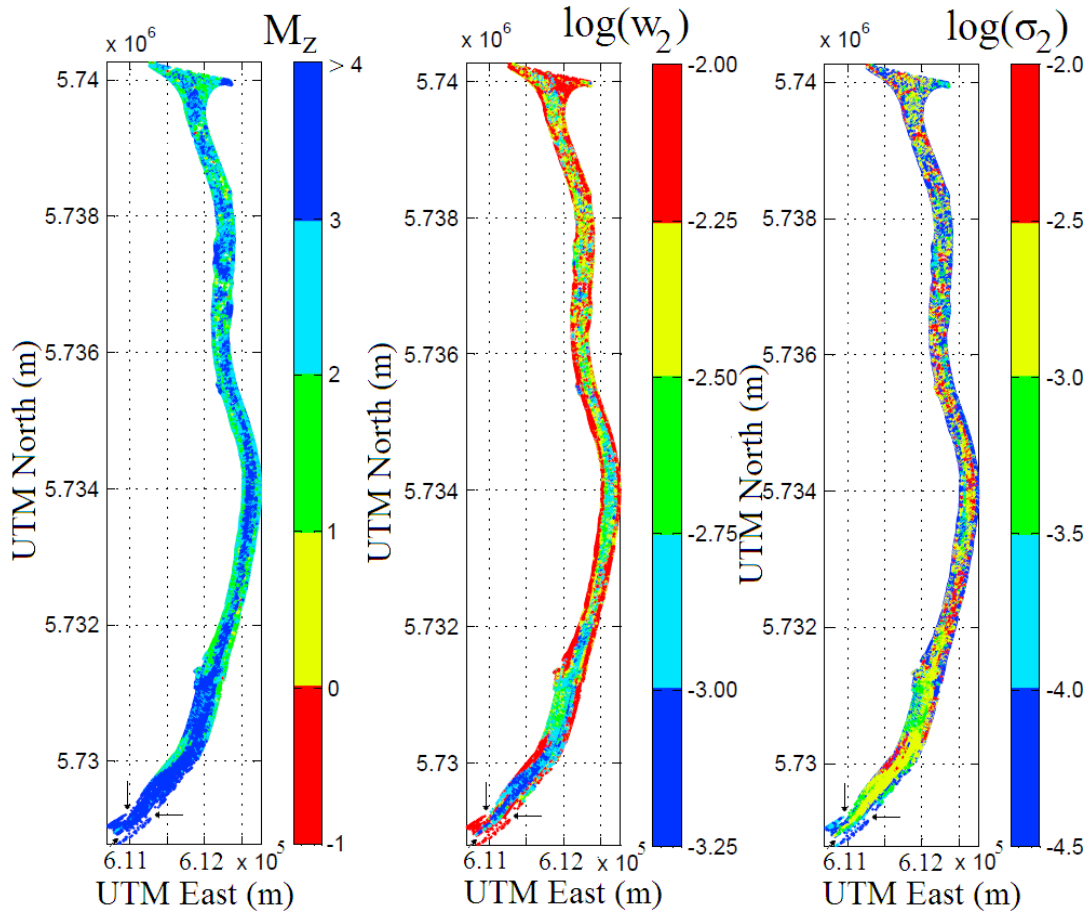
For  $5 \leq M_z \leq 9$  the interface roughness parameter is  $w_2 = 0.00207h^2$ , where  $h = 0.5$ . With regard to  $\sigma_2$ , Ref. 19 indicates a value of  $\sigma_2 = 0.002$  for  $-1 \leq M_z < 5.5$  and  $\sigma_2 = 0.001$  for  $5.5 \leq M_z < 9$ , respectively.

Figure 4.7 presents both the estimates for  $w_2$  and  $\sigma_2$  versus  $M_z$  as obtained from the inversions and predicted from the empirical expressions. It can be seen that, in general, the  $w_2$  values obtained from the inversions are a factor of 2 higher than those predicted by the empirical model. A reverse situation holds for  $\sigma_2$ , where values of  $\sigma_2$  determined from the inversions are a factor 2 lower than those predicted by the empirical expressions for  $-1 \leq M_z < 5.5$ . However, the estimates for  $\sigma_2$  show a large spread, indicating limited sensitivity of the problem to this parameter. This is at least partly due to the high frequencies considered. Another observation is that a discontinuity exists in the behaviour of the estimates for  $\sigma_2$  at  $M_z = 5.3$ . At  $M_z = 5.3$  the empirical relations expressing  $\nu$ , i.e., the ratio of sediment to water sound speed, and  $\rho$ , which is the ratio of sediment to water mass density, as a function of  $M_z$ , change. This might indicate that these relations require corrections when used for the frequency of 300 kHz as considered here.



**FIG 4.7.** Estimated (dots)  $w_2$  versus  $M_z$  (top) and  $\sigma_2$  versus  $M_z$  (bottom). The two frames also show respectively the values of  $w_2$  and  $\sigma_2$  predicted by empirical models (squares), their moving averages (smoothed), and third-order polynomial best fit. In each subplot colours indicate the third estimated parameter, i.e.  $\sigma_2$  (top) and  $w_2$  (bottom).

Finally, Fig. 4.8 presents the estimated values for  $M_z$ ,  $w_2$  and  $\sigma_2$  as a function of position, where for illustrative purposes logarithm scales are used to present  $w_2$  and  $\sigma_2$ . The three maps clearly show areas differencing in sediment types. In general, the three parameters reveal similar spatial patterns. The  $M_z$  values indicate that the softest sediment belongs to the southern part of the Dordtse Kil river. Values for the inverted parameters are found to be at the search bounds for certain areas in the southern part. These results are not included in Fig. 4.8 as the inversion is considered not successful. Since these results are found in distinct regions, i.e. the gaps in the Fig. 4.8 maps as indicated by arrows, we hypothesize that for these regions the backscatter model output is not representative for the sediments of those areas.



**FIG. 4.8.** Maps of inverted mean grain size  $M_z$ , (left frame), spectral strength  $w_2$  (middle frame), and volume scattering parameter  $\sigma_2$  (right frame). Arrows indicate the regions for which the inversions converged to values for  $M_z$ ,  $w_2$ , or  $\sigma_2$  that are at the bound of the search regions.

#### 4.4.3 Medusa results

The total activity of the nuclides was determined by spectrum deconvolution on the measured signal.<sup>23</sup> The activity concentrations in the samples were then determined by the measured activity divided by the mass of the grab sample and the dry matter percentage. The dry matter percentage was determined by the moisture loss in 6 hours at a temperature of 130°C. The silt fraction and organic matter content as determined from the grab samples were compared to the concentrations of  $^{232}\text{Th}$ ,  $^{40}\text{K}$ ,  $^{238}\text{U}$  and  $^{137}\text{Cs}$ . It was found that the  $^{232}\text{Th}$  and  $^{40}\text{K}$  concentrations show positive correlation with the silt fraction. No significant correlation was found with  $^{238}\text{U}$ . Furthermore, a significant correlation exists between  $^{137}\text{Cs}$  and the fraction of organic matter in the grab samples. Both are illustrated in Fig. 4.9. The resulting maps for the silt fraction, as derived from the  $^{232}\text{Th}$  and  $^{40}\text{K}$  concentrations, and organic matter (from  $^{137}\text{Cs}$  concentrations) are presented in Fig. 4.11 (right and centre frames).

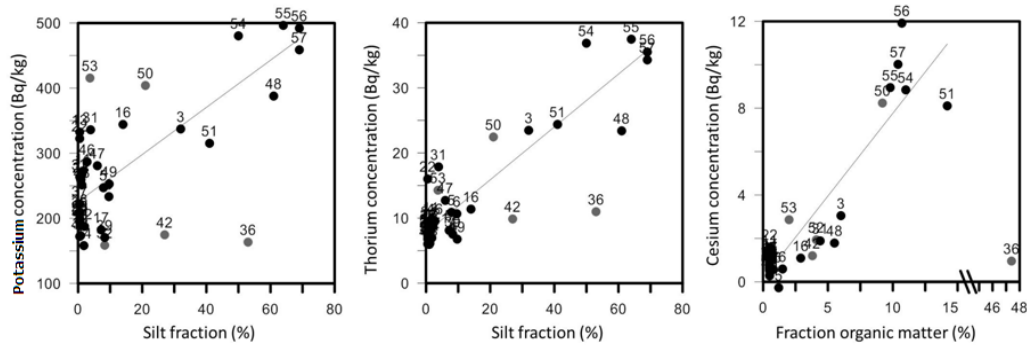


**FIG. 4.9:**  $^{40}\text{K}$  and  $^{232}\text{Th}$  versus silt fraction and  $^{137}\text{Cs}$  versus the fraction of organic matter. The grab samples with low correlation are indicated with grey dots.

Since the  $^{40}\text{K}$  concentrations were found to show the strongest correlation with the mean grain size (80 %), for the current study this parameter was finally used as a predictor of the grain size,  $d_{50}$ , denoting the grain size at which 50 % of the sediments in the grab sample are smaller. This strong correlation is illustrated in Fig. 4.10.

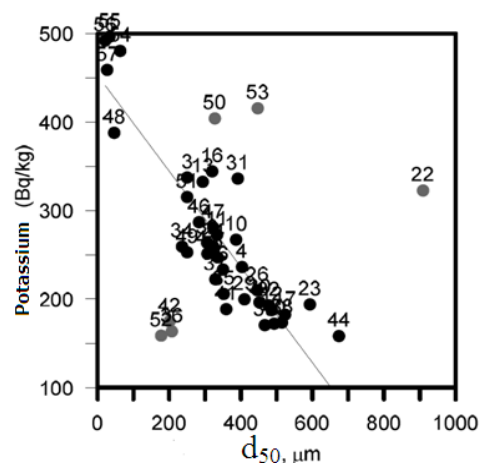


**FIG. 4.10.**  $^{40}\text{K}$  concentration versus  $d_{50}$  for the grab samples taken in the area. The numbers indicate numbers of the grab samples. The grab samples with low correlation are indicated with grey dots.

The following relation between  $^{40}\text{K}$  concentration  $K$  and mean grain size  $d_{50}$  was established by linear regression:

$$d_{50} = -0.54K + 425.5 \quad (4.4)$$

with a coefficient of determination ( $R^2$ ) of 0.8. The grab samples indicated as grey dots in Fig. 4.10 were not accounted for in deriving the above relation as they contain some peat, shells or wood that were removed when determining the radio nuclide concentrations, but were accounted for in the mean grain size determination.

By using Eq. (4.4), a mean grain size map of the full area was derived based on the  $^{40}\text{K}$  concentrations that were measured during the survey, the results of which are presented in Fig. 4.11 (left frame). Note that since the grab sample positions are not

coincident with the Medusa tracks, the range of mean grain sizes encountered in the grab samples differs from the range derived with the Medusa system towed over the sediment. Especially the grab samples corresponding to the smallest mean grain sizes were taken at locations where no measurements were taken with the towed Medusa sensor. All plots contained in Fig. 4.11 have been obtained by Kriging interpolation<sup>25</sup> of the data as acquired along the tracks.

The results of the measurements as taken by the Medusa hydrophone that is towed over the sediment surface, are presented in Fig. 4.12. Their primary use is to indicate whether the Medusa system touches the sediment, or floats freely in the water. However, these measurements are also indicative of the roughness of the sediment, where high noise is associated with rough boundaries and low noise is associated with smooth boundaries. Since the hydrophone is not calibrated, the measured noise intensities can only be used in a relative manner to assess variations in roughness over an area.

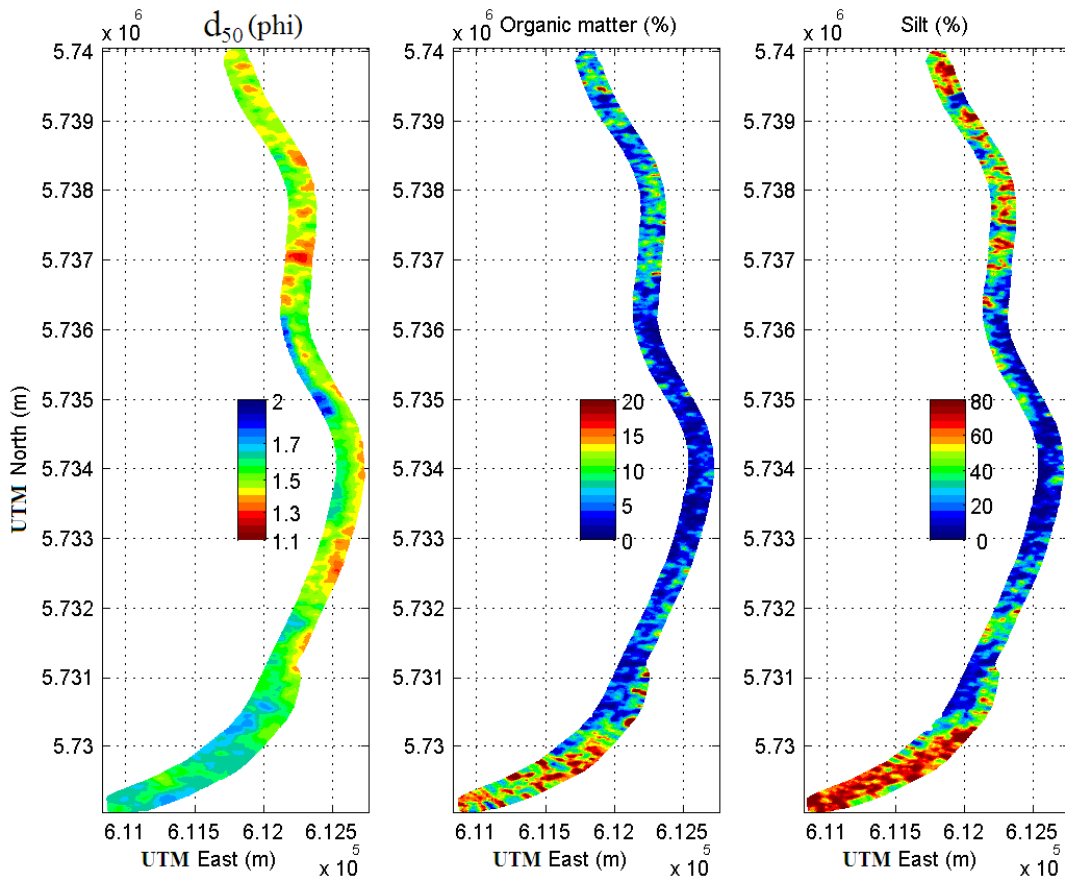


**FIG 4.11.** Maps of the  $d_{50}$  (left) values (in phi units), organic matter (middle), and silt fraction (right) in Dordtse Kil using the Medusa method.

## 4.5 Comparison and Discussion

In Fig. 4.12 an overview of the results of applying the methods for sediment classification described in the previous sections is presented, partly repeating the plots presented in Section 4.4. To allow for comparison, this figure presents only those results that are directly related to the sediment mean grain size. Therefore, the estimates of silt fraction and organic matter are not included. To ease the comparison, similar colormaps are used for all five maps, where blue corresponds to the finer sediment and red to the coarsest sediment. It should be noted that the Medusa measurements were taken only along six lines in the middle of the river with an average distance of 40 m between lines; no measurements are taken at the border of the river, resulting in a low spatial resolution compared to the MBES results. (Note that for the unimodal sediment grain size distribution encountered (Fig. 4.2), differences between  $M_z$  based on  $d_{50}$  (obtained from the Medusa measurements through Eq. (4.4)) and  $M_z$  based on  $d$  (grab samples and model-based method) are negligible ( $<0.3 \phi$ )).

Despite the differences in the range of mean grain size values as obtained for the different methods, with, for example, the model-based results showing an overestimation of  $M_z$  compared to the grab samples, we do observe a similar spatial pattern in the sediment distribution as revealed by all methods. Grain sizes are decreasing towards the southern part of the river, indicated both by the MBES model-based results and the grab sample analysis. Also the  $M_z$  values derived from the  $^{40}\text{K}$  concentrations indicate finer sediments than on the remainder of the river. The Bayesian classification indicates the presence of the first two classes in the areas, corresponding to the lower backscatter strength values. It can also be seen that the noise levels measured with the Medusa hydrophone are low, indicating a smooth sediment surface as expected for these fine-grained sediments.

For the area north of this small grain size region, the Bayesian and model-based MBES results along with the Medusa noise measurements reveal that the middle of the river is mainly fine-grained, interspaced with areas containing coarser sediments. These results indicate coarser sediments also for the border of the river. The grab samples also indicate coarser sediments compared to the southern area, but their limited spatial sampling prevents derivation of more details regarding the sediment distribution. Although the  $^{40}\text{K}$  concentrations indicate coarser sediments compared to the south, these results differ from the other methods as the map based on the  $^{40}\text{K}$  concentration indicates areas with smaller grain sizes in the west of the middle part of the river which is not confirmed by any of the other methods.

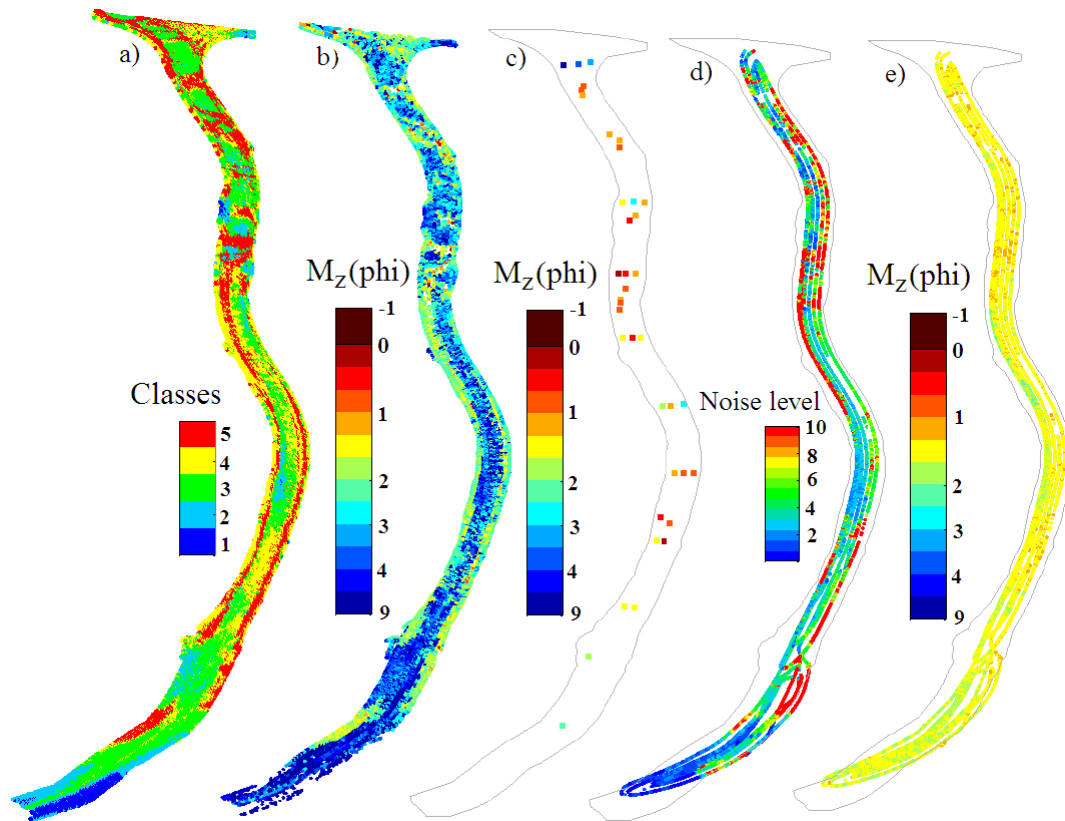


**FIG. 4.12.** Classification maps of Dordtse Kil River using different methods; acoustic classes of the Bayesian method (a), mean grain sizes in phi unit of the model based method (b), mean grain sizes in phi unit of the grab samples (c), noise received by the Medusa hydrophone (logarithmic scale) (d), and the mean grain size in phi unit using the Medusa method (e).

In order to quantitatively assess the correspondence between all measured parameters, Fig. 4.13 presents the cross correlation matrix, where colours indicate the absolute values of the correlation coefficients between the classifiers obtained for all methods considered. All correlation coefficients, except those with the mean grain size from the grab samples, are based on at least 5000 locations, resulting in high confidence levels (100%) for the correlation coefficients. Due to the limited amount of grab samples, correlation coefficients with the grab sample mean grain sizes are subject to lower confidence levels. Only those correlation coefficients with confidence levels exceeding 90 % are presented in Fig. 4.13. (A confidence level of 90 % means that there is a 10 % probability that this correlation coefficient occurs fully by chance.)

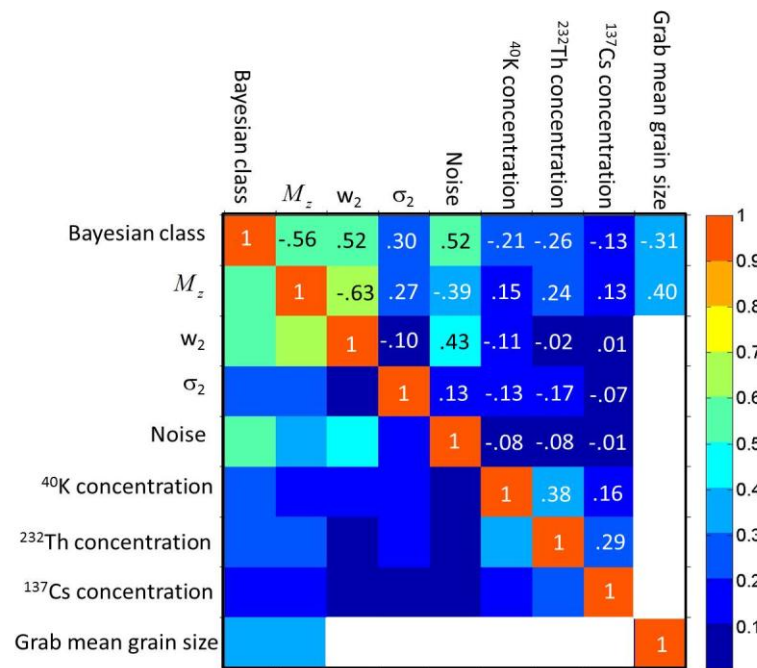


**FIG. 4.13.** Correlation coefficients (the colours indicate the absolute values) between Bayesian classes, the parameters obtained from the model-based method ( $M_z$ ,  $w_2$  and  $\sigma_2$ ), the parameters measured by the Medusa system (Noise,  $^{40}\text{K}$  concentration,  $^{232}\text{Th}$  concentration and  $^{137}\text{Cs}$  concentration) and the grab sample mean grain sizes. Only correlation coefficients with confidence levels exceeding 90 % are indicated.

From the correlations presented, it can be concluded that when considering the Bayesian classes, the highest correlation (-0.56) is found between classes and the mean grain sizes as estimated from the model-based method. This limited correlation coefficient can be caused by a non-linear relation between mean grain size and acoustic classes, but can also be due to the fact that, in addition to sediment mean grain size, also parameters such as the volume scattering parameter and the sediment roughness contribute to the measured backscatter strengths. This impedes the use of a linear relation between acoustic classes and mean grain sizes, for example to convert a map presenting acoustic classes to a map of mean grain sizes. This is also demonstrated by the limited correlation coefficient between the Bayesian classes and the  $M_z$  values of the grab samples (-0.31).

From the Medusa measurements, the noise level is found to have the highest correlation with the Bayesian classes. The concentration of  $^{137}\text{Cs}$  shows the lowest correlations. From Section 4.4.3 it is known that  $^{137}\text{Cs}$  is highly correlated to the concentration of organic matter. Hence, the low correlation between  $^{137}\text{Cs}$  and the acoustic classes is an indication that the presence of organic matter is not revealed by the Bayesian approach. The limited correlation with  $^{40}\text{K}$  and  $^{232}\text{Th}$  with all other parameters, reflects the previous observation (based on Fig. 4.12) that in part of the area, the Medusa mean grain sizes show a spatial pattern that is not conformed by the other methods.

The substantial correlation of 0.43 between the noise levels measured by the Medusa hydrophone and the model-based parameter  $w_2$  results from the fact that both parameters are representative for the sediment surface roughness.

## 4.6 Summary and conclusions

In this chapter three methods for classification of sediments in the Dordtse Kil river in the Netherlands are presented. Two methods base the classification on MBES backscatter data, whereas the third method bases the classification on natural radioactivity. The first method uses the MBES backscatter data collected at a certain angle to obtain the number of acoustic classes and to discriminate between them by applying the Bayes decision rule for multiple hypotheses. The second method is model-based and matches the full measured backscatter versus angle curve of the MBES to the predicted backscatter curve using the model of Ref. 19. The third method, Medusa, bases the classification on measurements of gamma-ray radiation being emitted from very low concentrations of a number of radionuclides in the sediment, i.e.,  $^{137}\text{Cs}$ ,  $^{40}\text{K}$ ,  $^{238}\text{U}$  and  $^{232}\text{Th}$ .

The Bayesian method provides acoustic classes, and is considered to be simple in principle and easy and fast to implement. For the Dordtse Kil area, the Bayesian method identified five acoustic classes. The model-based method provided the sediment parameters mean grain size ( $M_z$ ), spectral strength of sediment surface roughness ( $w_2$ ) and volume scattering parameter ( $\sigma_2$ ). By comparing the classes derived from the Bayesian method and the model-based results, it is found that the model-based mean grain size shows the highest correlation with the acoustic classes. However, this correlation is limited to -0.56. This is an important result, as it indicates the limitations in the potential of using only (grab sample-based) mean grain size for assigning sediment parameters to the acoustic classes. The latter is also illustrated by the limited correlation coefficient (-0.31) between the acoustic classes and the mean grain sizes obtained from grab samples.

The use of model-based methods would eliminate the above-mentioned limitations in converting acoustic class to sediment parameters. However, the model-based results indicate an overestimation of the  $M_z$  values, i.e. too small mean grain size values. This can be due to a still imperfect calibration of the measured backscatter values, caused by a limited number of grab samples available for the calibration. In addition, imperfect modelling of the backscatter curve can play a role. These effects hamper the use of model-based methods for sediment classification.

Analysis of the data taken by the Medusa system provided estimates of the mean grain size based on the concentrations of  $^{40}\text{K}$  and estimates for the silt fraction based on  $^{40}\text{K}$  and  $^{232}\text{Th}$ . Furthermore, concentrations of  $^{137}\text{Cs}$  were used as a predictor for the fraction of organic matter. In addition, noise levels were measured by a hydrophone towed over the sediments. The significant correlation between the Medusa noise level and  $w_2$  indicate that the Medusa noise levels contains information about the sediment roughness. The low correlation between the  $^{137}\text{Cs}$  concentrations and the Bayesian classification results indicates that backscatter measurements do not reveal the presence of organic matter. The Medusa system, however, can provide this information based on the  $^{137}\text{Cs}$  measurements.

## REFERENCES

- <sup>1</sup> C. de Moustier, "Beyond bathymetry: Mapping acoustic backscattering from the deep seafloor with Sea Beam," *Journal of the Acoustical Society of America* 79 (2), pp. 316-331, (1986).
- <sup>2</sup> J.E. Hughes Clarke, "Toward remote seafloor classification using the angular response of acoustic backscattering: a case study from multiple overlapping GLORIA data," *IEEE Journal of Oceanic Engineering* 19(1), pp. 112-126, (1994).
- <sup>3</sup> L. Hellequin, J. Boucher, and X. Lurton, "Processing of high-frequency multibeam echo sounder data for seafloor characterization," *IEEE Journal of Oceanic Engineering* 28(1), pp. 78-89, (2003).
- <sup>4</sup> G. Canepa and E. Pouliquen, "Inversion of geo-acoustic properties from high frequency multibeam data," in: *Boundary influences in high frequency, shallow water acoustics*, N.G. Pace and P. Blondel, Eds., Bath UK, pp. 233 – 240, (2005).
- <sup>5</sup> D.G. Simons and M. Snellen, "A comparison between modeled and measured high frequency bottom backscattering," in: *Proceedings of the European Conference on Underwater Acoustics, June 29-July 4 2008, Paris, France*, pp. 639-644, (2008).
- <sup>6</sup> P.A. van Walree, J. Tegowski, C. Laban, and D.G. Simons, "Acoustic seafloor discrimination with echo shape parameters: A comparison with the ground truth," *Continental Shelf Research*, 25, pp. 2273-2293, (2005).
- <sup>7</sup> A.R. Amiri-Simkooei, M. Snellen, and D.G. Simons, "Principal component analysis of single-beam echo-sounder signal features for seafloor classification," *IEEE Journal of Oceanic Engineering* 36(2), 259-272, (2011).
- <sup>8</sup> C. Wienberg and A. Bartholomä, "Acoustic seabed classification in a coastal environment (outer Weser Estuary, German Bight)-a new approach to monitor dredging and dredge spoil disposal," *Continental Shelf Research* 25, pp. 1143-1156, (2005).
- <sup>9</sup> D. Eleftherakis, A.R. Amiri-Simkooei, M. Snellen, and D.G. Simons, "Improving riverbed sediment classification using backscatter and depth residual features of multi-beam echo-sounder systems", *Journal of the Acoustical Society of America* 131(5), 3710-3725, (2012).
- <sup>10</sup> D.D. Sternlicht and C.P. de Moustier, "Remote sensing of sediment characteristics by optimized echo-envelope matching." *Journal of the Acoustical Society of America* 114(5), pp. 2727-2743, (2003).
- <sup>11</sup> P.A. van Walree, M.A. Ainslie, and D.G. Simons, "Mean grain size mapping with single-beam echosounders," *Journal of the Acoustical Society of America* 120(5), pp. 2555-2566, (2006).
- <sup>12</sup> X. Lurton and E. Pouliquen, "Automated sea-bed classification system for echosounders," in: *Proceedings of the IEEE Oceans 1992 Conference*, pp. 317-321, (1992).
- <sup>13</sup> M. Snellen, K. Siemes, and D.G. Simons, "Model-based sediment classification using single-beam echosounder signals", *Journal of the Acoustical Society of America* 129(5), pp. 2878-2888, (2011).
- <sup>14</sup> D.G. Simons, and M. Snellen, "A Bayesian approach to seafloor classification using multi-beam echo-sounder backscatter data", *Applied Acoustics* 70, pp. 1258-1268 (2009).

- <sup>15</sup> A.R. Amiri-Simkooei, M. Snellen, and D.G. Simons, "Riverbed sediment classification using multi-beam echo-sounder backscatter data", *Journal of the Acoustical Society of America* 126, pp. 1724-1738 (2009).
- <sup>16</sup> M. van Wijngaarden, L.B. Venema, R.J. De Meijer, J.J.G. Zwolsman, B. Van Os, J.M.J. Gieske, "Radiometric sand–mud characterisation in the Rhine–Meuse estuary, Part A. Fingerprinting", *Geomorphology* 43, 87-102, (2002).
- <sup>17</sup> E.R. van der Graaf, R.L. Koomans, J. Limburg, K. de Vries, "In situ radiometric mapping as a proxy of sediment contamination: Assessment of the underlying geochemical and -physical principles", *Applied Radiation and Isotopes* 65, 619-633, (2007).
- <sup>18</sup> E. Hammerstad, "Backscattering and Seabed Image Reflectivity", EM TechnicalNote, [http://www.km.kongsberg.com/ks/web/nokbg0397.nsf/AllWeb/226C1AFA658B1343C1256D4E002EC764/\\$file/EM\\_technical\\_note\\_web\\_BackscatteringSeabedImageReflectivity.pdf?OpenElement](http://www.km.kongsberg.com/ks/web/nokbg0397.nsf/AllWeb/226C1AFA658B1343C1256D4E002EC764/$file/EM_technical_note_web_BackscatteringSeabedImageReflectivity.pdf?OpenElement) (date last viewed 09/06/2011), Norway: Kongsberg, pp. 1-5, (2000).
- <sup>19</sup> "APL-UW high-frequency ocean environmental acoustic models handbook", Oct. 1994, technical report APL-UW TR9407AEAS 9501, Applied Physics Laboratory, University of Washington, pp. IV1-IV50.
- <sup>20</sup> A. R. Amiri-Simkooei, "Formulation of L1 norm minimization in Gauss–Markov models", *Journal of Surveying Engineering*, 129 (1), pp. 37–43 (2003).
- <sup>21</sup> K.V. Price, R.M. Storn, and J.A. Lampinen, "Differential evolution. A practical approach to global optimization," Berlin, Heidelberg: Springer, chapter 2, pp. 37-131 (2005).
- <sup>22</sup> M. Snellen and D.G. Simons, "An assessment of the performance of global optimisation methods for geo-acoustic inversion," *Journal of Computational Acoustics* 16 (2), pp. 199-223 (2008).
- <sup>23</sup> P.H.G.M. Hendriks, J. Limburg, and R.J. de Meijer, "Full-spectrum analysis of natural gamma-ray spectra". *Journal of Environmental Radioactivity* 53, pp. 365-380, (2001).
- <sup>24</sup> R.L. Koomans, "Sand in motion: effects of density and grain size", Phd thesis, RUG, Groningen, 218 pp, (2000).
- <sup>25</sup> R. Webster and M. Oliver, "Geostatistics for environmental scientists", *Statistics in practice*, John Wiley & Sons, Ltd, Chichester, (2001).

# 5

## **Improving riverbed sediment classification using backscatter and depth residual features of multi-beam echo-sounder systems<sup>2</sup>**

---

Riverbed and seafloor sediment classification using acoustic remote sensing techniques is of high interest due to their high coverage capabilities at limited cost. This chapter presents the results of riverbed sediment classification using multi-beam echo-sounder data based on an empirical method. Two data sets are considered, both taken at the Waal River, namely Sint Andries and Nijmegen. This work is a follow-up to the work carried out by Amiri-Simkooei et al., [J. Acoust. Soc. Amer., 126 (4): 1724–1738 (2009)]. The empirical method bases the classification on features of the backscatter strength and depth residuals. A principal component analysis is used to identify the most appropriate and informative features. Clustering is then applied to the principal components resulting from this set of features to assign a sediment class to each measurement. The results show that the backscatter strength features discriminate between different classes based on the sediment properties, whereas the depth residual features discriminate classes based on riverbed forms such as the ‘fixed layer’ (stone having riprap structure) and riverbed ripples. Combination of these two sets of features is highly recommended because they provide complementary information on both the composition and the structure of the riverbed.

---

<sup>2</sup> This chapter has been published as journal paper: *D. Eleftherakis, A.R. Amiri-Simkooei, M. Snellen, and D.G. Simons, “Improving riverbed sediment classification using backscatter and depth residual features of multi-beam echo-sounder systems”, Journal of the Acoustical Society of America 131(5), 3710-3725 (2012).*

## 5.1 Introduction

The morphology and sediment composition of the sea/river bed is of high importance to a large number of offshore activities such as oil and gas exploration, the installation of offshore windmill farms, and the study of marine biology. Furthermore, in countries like the Netherlands, where a great number of rivers are used for navigation, insight into the river morphology and its dynamic behaviour, and sediment composition is essential. An attractive system for obtaining information both for the sea/river bed bathymetry and sediment composition is the multi-beam echosounder (MBES). The sonar emits short pulses of sound towards the sea/river floor to determine the depth and the backscatter strength for a large number of beams. The MBES provides high spatial coverage of an area at moderate costs and within a short time. Therefore, it appears as a good alternative to the conventional, expensive and time-consuming approach of mapping the sea/river floor composition by taking a large number of physical sediment grab samples. A brief overview of the techniques used for determining sediment properties in shallow waters is given in Ref. 1.

The MBES classification methods can be divided into phenomenological (or empirical) and model-based (or physical). Model-based approaches make use of physical models and determine the sediments type by maximizing the match between modelled and measured signals or signal features, where sediments type or parameters indicative of sediment floor type, are input into the model. These approaches allow for direct coupling between the acoustic classes and sediment characteristics if the MBES sensitivity is known. On the other hand, the empirical approaches base the classification on features of the data, after dividing the area into small regions. This approach is considered in the present work. The outcome of this approach is a qualitative description of the sediment distribution of an area (e.g. finer, fine, coarse, coarser), but ground truth is required for associating the classification results to physical parameters of the sediments (e.g. mean grain size). The advantage of the empirical methods is their ease of implementation and use.

The main information provided by an MBES is the backscatter strength and the bathymetry of the area. Both can be treated as individual values or as images by plotting their spatial distributions over an area.<sup>2</sup> The potential of the backscatter for empirical sediment characterization has been highlighted in previous work.<sup>3,4</sup> Significant work in this field has been done by Quester Tangent Corporation (QTC) where 132 features are calculated and processed both from the backscatter amplitude and backscatter texture. Detailed information about QTC can be found in Refs. 5-11. During the last few years, research considered the potential of the information contained in the bathymetry for classification<sup>12,13</sup> and now the interest has focused on how to combine a broader range of information that may include backscatter and bathymetry features in many forms into the clustering models.<sup>14</sup> An extensive review of the different classification approaches can be found in Ref. 15.

In two previous studies<sup>16,17</sup> a new model-based method employing backscatter, denoted as the Bayesian classification methodology (BCM), for deriving the sediment distribution in two parts (Sint Andries and Nijmegen) of the River Waal in the Netherlands gave promising results. However, one important artificial riverbed feature, the fixed layer, was not identified by the method as a separate bottom type. This fixed layer consists of big stones with rip rap structure and is applied for fixation of the sediment. In this chapter a combination of backscatter and a bathymetric feature, namely the residuals of depth, is successfully used to identify the different sediment

classes, including the fixed layer. Principal components analysis (PCA) is used for data reduction and the common K-means method for clustering the data. The importance of the present chapter is twofold: 1) it clearly demonstrates the advantage of the combination of features on capturing the range of different formations on riverbeds, and 2) it provides a physical explanation of the contribution of each feature.

The chapter is organized as follows. Section 5.2 gives information both about the surveyed areas and the details of the surveys. This section also provides a brief description of the methodology of Refs. 16 and 17, and results obtained from the previous studies on the same areas. Section 5.3 provides details on the methodology (PCA and K-means clustering) used for identifying the different sediment types. Section 5.4 describes the data preparation procedures. Section 5.5 presents and discusses the results from the PCA and K-means clustering analysis. Finally, the main conclusions are summarized in Section 5.6.

## **5.2 Experiments and previous results**

### **5.2.1 A description of the surveyed areas**

The MBES data was collected from parts of the Waal River in the Netherlands during surveys conducted by the Directorate General for public works and water management. The Waal River is one of the branches of the Rhine River and the main inland waterway transport artery between the port of Rotterdam and urban and industrial areas of Germany. The Waal River has prominent bends at Nijmegen and Sint Andries. The interplay of water and sediment in these bends had produced characteristic bed topography of deep outer-bend pools and shallow inner-bend point bars. The latter formed obstacles for navigation, despite the large depth available in the pools, because they reduced the space for two-way traffic with possibilities to overtake other ships. The problem has been addressed using three strategies: 1) by dredging in order to remove the shoals, 2) by constructing groynes in order to change the alignment of the river, and 3) by constructing non-erodible layers in order to lower the point bar and increase the navigation width. Therefore the deep pools have been filled and covered with riprap to form a fixed, non-erodible layer in the outer bend. The resulting scour in the inner-bend made the river sufficiently deep over a larger width.

The first fixed layer is located between Sint Andries and Zuilichem (km 925-928). It is 140 m wide and 3.1 km long, and was constructed in the years 1997-1999. It lies 3.5 m below the Dutch river low water reference level (OLR).<sup>18</sup> The bathymetry (not referenced to OLR) of the river at Sint Andries as produced from an October 2007 multi-beam survey is presented in Fig. 5.1 (top). It shows the general pattern of shallow inner bends and deeper outer bends, but also the more detailed forms of underwater dunes as well as local scour holes at the tips of transverse river training structures called “groynes”.

The second fixed layer is located in the Waal river bend at Nijmegen (km 883-885). This fixed layer has a width of 150 m, a length of 2 km and a depth of 3.5 m below the OLR.<sup>18</sup> It was constructed in the years 1986-1988. Figure 5.1 (bottom)

presents the bathymetry of the river in this area as produced from a May 2008 multi-beam survey, again not referenced to OLR.

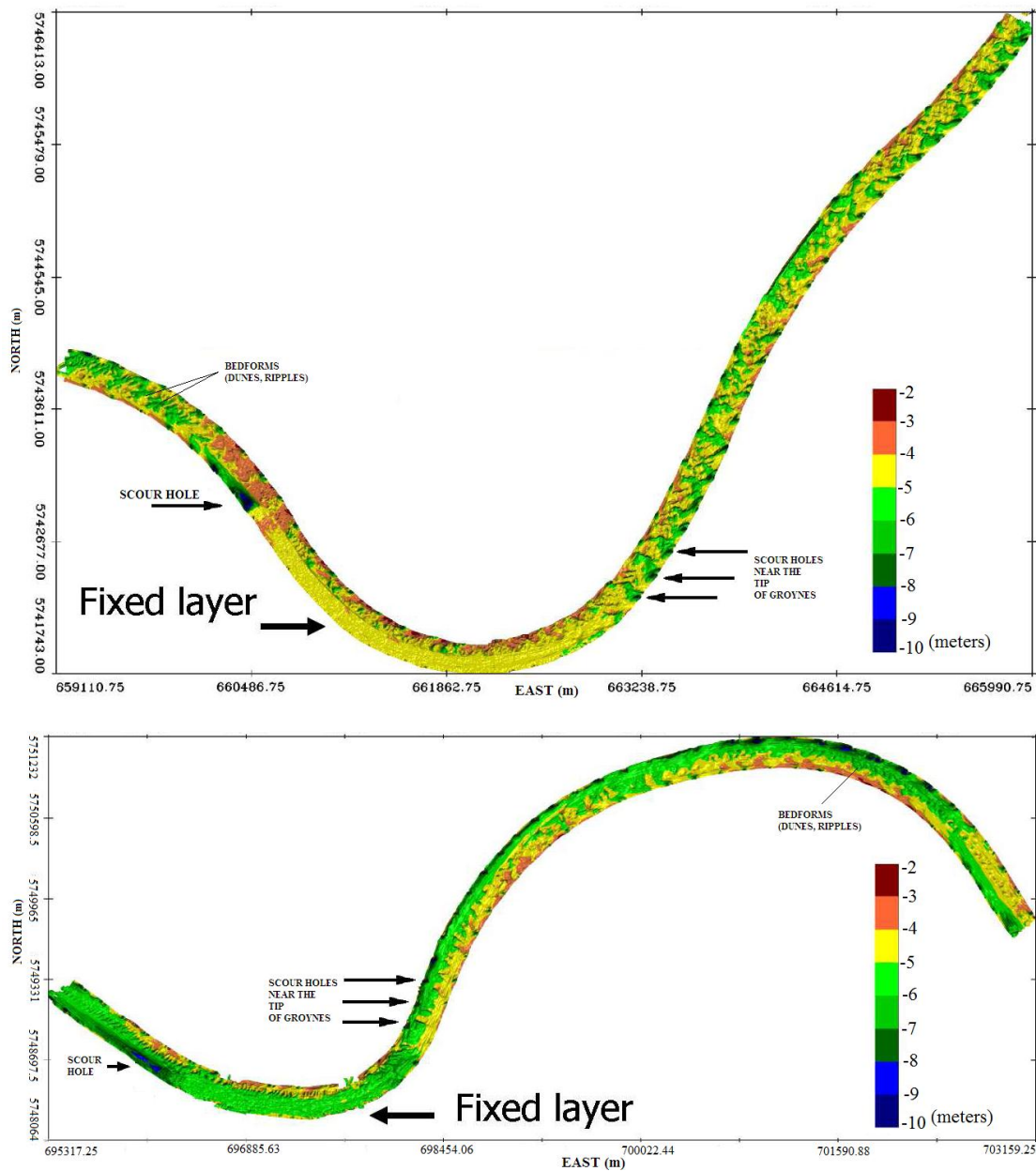


**FIG. 5.1.** Bathymetry of the Waal River at Sint Andries (top) and Nijmegen (bottom). Indicative positions of scour holes behind the fixed layer, scour holes at the tips of groynes, and bed forms (ripples and dunes) are shown in the figure.

Grab samples were collected from both areas, using a bottom grab. Figure 5.2 shows the histograms of the distribution of the mean grain size of the grab samples collected at Sint Andries (left frame) and at Nijmegen (right frame).

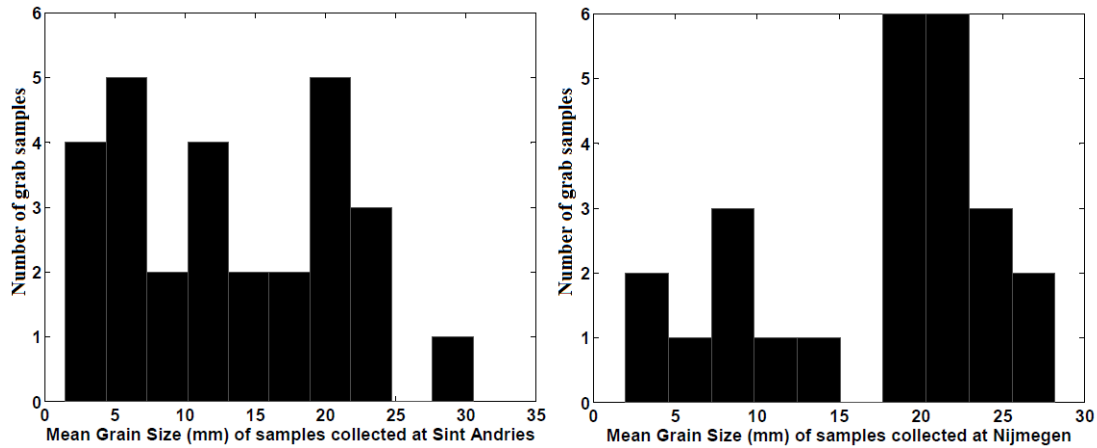


**FIG. 5.2.** Histograms of the mean grain size distribution of the grab samples collected at Sint Andries (left frame), and at Nijmegen (right frame).

### 5.2.2 Details of the surveys

The sonars used in both surveys were of the same type: a Kongsberg EM3002 single-head multi-beam echo-sounder. This sonar is well suited for shallow water depths as its high frequency ensures narrow beams with small physical dimensions. The operational frequency was 300 kHz and the maximum number of beams (of equidistant pattern) per ping was 254. The swath width was  $130^\circ$ , the pulse length 150  $\mu$ s, and the maximum ping rate 40 Hz. The beam width was  $1.5^\circ \times 1.5^\circ$  at nadir. All beams were electronically stabilized for pitch and roll. For each beam and each ping a single backscatter value is given. This value is the result of first applying a moving average over the time series of amplitude values and then selecting the maximum average level of each beam.<sup>19</sup>

### 5.2.3 A summary of applying the BCM to the areas

The method in Refs. 16, 17 and 20 employs the backscatter strength collected at a certain beam angle instead of studying the angular behaviour of the backscatter strength. The classification is performed per angle separately from other angles and hence is considered to be angle-independent. The method is based on the assumption that the backscatter values are an average value of the sample amplitude values. Therefore, according to the central limit theorem -for independent random values- the averaged backscatter value for a single sediment type follows a Gaussian distribution for a sufficiently large number of scatter pixels. Figure 5.3 illustrates this principle. In this figure  $\theta$  is the beam angle and  $\varphi$  the grazing angle of incidence. The required large number of scatter pixels is achieved for shallow waters<sup>16</sup> by averaging the backscatter values over small surface patches, which consist of a small number of beams in the across-track direction and a few pings in the along-track direction. The creation of surface patches, apart from ensuring Gaussianity, has the additional advantage that it allows for two kinds of corrections of the backscatter data due to the presence of slopes: one correction to account for changes of the signal footprint's

area, and a second correction to account for the slope effect on the beam grazing angle.

The method fits a number of Gaussian Probability Density Functions (PDFs) to the histogram of the backscatter data at a given beam angle. The optimum number of PDFs is found by consecutively increasing the number of PDFs until a chi-square distributed test statistic becomes less than a critical value. The number of Gaussians then represents the maximum number of classes that can be discriminated based upon the backscatter values, and the borders of the classes are the intersections of each Gaussian with its neighbour. The backscatter data at a few low grazing angles are processed in order to estimate the mean backscatter strength, the variance and its coefficient per class. These parameters are used as guidance for the statistical processing of all other angles. The surface patches in Refs. 16 and 17 were of size  $0.5 \text{ m} \times 0.5 \text{ m}$ , but the final maps resulted after using weighted moving average for surface patches of  $2 \text{ m} \times 2 \text{ m}$ .

Three classes were identified for each area. The plots can be seen in Refs. 16 and 17. The areas of the fixed layer could not be discerned from the other parts of the river.

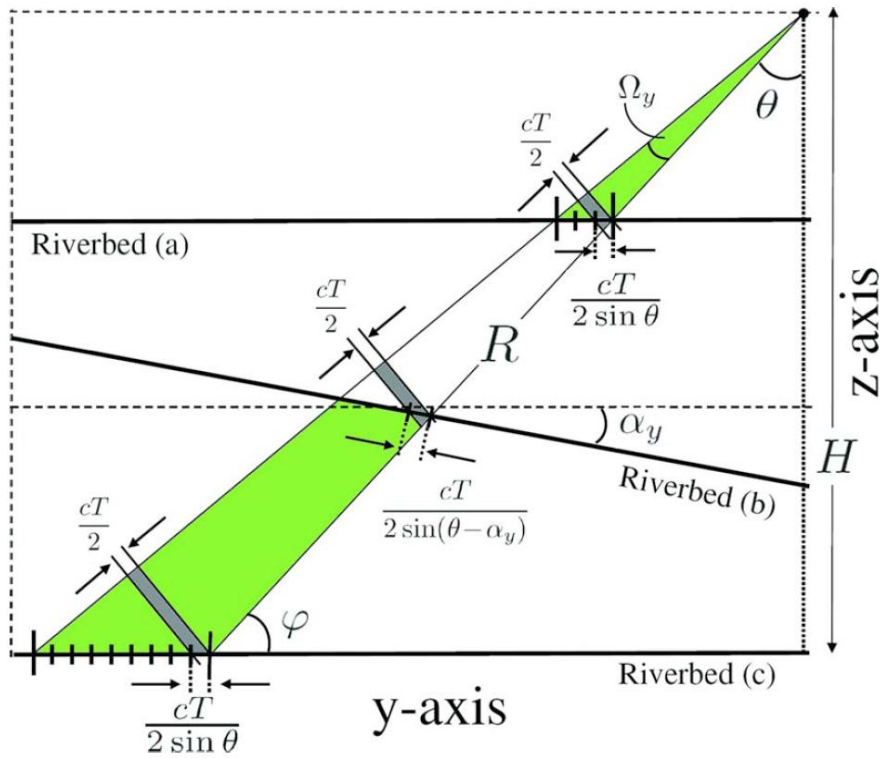


**FIG. 5.3.** Across-track cross section (y-z plane) for signal footprint of an oblique beam for three configurations: (a) shallow water, (b) non-flat bottom, and (c) deep water.  $\theta$  denotes the beam angle and  $\varphi$  the grazing angle. The figure has been taken from Ref. 16.

## 5.3 Methodology

In this section we briefly explain basic concepts of the PCA and the K-means clustering approach. Though the methods are well established, many variations of them exist in the literature, depending on the nature of different investigations. Therefore, the scope of this section is to provide only the necessary details of the methodology followed in this Chapter for creating the sediment distribution maps of the Sint Andries and Nijmegen areas.

### 5.3.1 Principal component analysis

The PCA was first described by Refs. 21 and 22. The aim of the PCA is to reduce a multivariate dataset into a small set of variables called principal components (PCs) that can adequately describe the variability of the whole dataset. The reduction can be achieved if the original variables are at least moderately correlated.<sup>23</sup> Unlike the initial features, the PCs are independent, thus each PC represents a different dimension in the data. Furthermore, they are sorted in descending importance order from the first PC, which explains the largest amount of the data variation to the last one representing the smallest variation. Therefore,  $\text{var}(Y_1) \geq \text{var}(Y_2) \geq \dots \geq \text{var}(Y_p)$ , where  $Y_i$  is the  $i$ -th principal component.

Considering the  $(n \times p)$  matrix  $F$  containing all  $n$  measurements of the  $p$  features, a principal component  $Y_i$  is a linear combination of the  $p$  original features (variables)  $F_1, F_2, \dots, F_p$  ( $F_i$  denoting the  $i$ th column of  $F$ ) as

$$Y_i = a_{i1}F_1 + a_{i2}F_2 + \dots + a_{ip}F_p \quad (5.1)$$

with the condition that its variance,  $\text{var}(Y_i)$ , is maximum, subject to the constraint that<sup>23</sup>  $a_{i1}^2 + a_{i2}^2 + \dots + a_{ip}^2 = 1$ , and that  $Y_i$  is uncorrelated to the other principal components, thus having zero covariance, i.e.  $\text{cov}(Y_i, Y_k) = 0$  for  $i \neq k$ . The calculation of the principal components is performed in four steps:

First, the original features  $f_{ij}$ , where  $i = 1, 2, \dots, p$  (number of features) and  $j = 1, 2, \dots, n$  (size of data) are standardised. This step is necessary when the variables have different scales or common scale with significantly different ranges. The standardization is performed as follows<sup>24</sup>:

$$z_{ji} = \frac{f_{ji} - \mu_{f_i}}{\sigma_{f_i}} \quad (5.2)$$

where  $\mu_{f_i}$  and  $\sigma_{f_i}$  are the sample mean and standard deviation of the feature  $i$ , respectively,

Second, the covariance matrix  $R$  of the standardised data  $Z$  is determined as<sup>24</sup>

$$R = \frac{Z^T Z}{n-1} \quad (5.3)$$

$$\text{where } Z = \begin{bmatrix} z_{11} & z_{12} & \cdots & z_{1p} \\ z_{21} & z_{22} & \cdots & z_{2p} \\ \vdots & \vdots & \ddots & \vdots \\ z_{n1} & z_{n2} & \cdots & z_{np} \end{bmatrix}$$

The diagonal elements of  $R$  are the variances of the features, all having a value of 1 due to standardization, while the non-diagonal elements of  $R$  are the correlation coefficients among the features.

Third, the eigenvalue decomposition of the matrix  $R$  is obtained as

$$R = E\Lambda E^T \quad (5.4)$$

where  $E$  is the square matrix of the eigenvectors of  $R$  and  $\Lambda$  is the diagonal matrix of the corresponding eigenvalues (each column of  $E$  corresponds to one element of  $\Lambda$ ).

Finally, the PC matrix  $Y$  is calculated by multiplying the original data matrix  $F$  with the eigenvectors matrix  $E$  as

$$Y = FE \quad (5.5)$$

After obtaining the  $Y$  matrix, the optimum subset of PCs has to be determined. The subset must consist of the minimum number of PCs that contain most of the original data's information. A large number of tools exist for deciding the optimum number of PCs. An extensive comparison between various tools can be found in Ref. 25.

In the current research we consider one of the simplest but still acceptable tools<sup>26</sup> available for selecting the number of principal components. The criterion is to choose adequate PCs to explain a specific percentage of the total variability in the data. The percentage of the standardised data variance due to the first  $m$  ( $m \leq p$ ) PCs is given as

$$t_m = 100 \times \frac{\sum_{k=1}^m \lambda_k}{\sum_{k=1}^p \lambda_k} \quad (5.6)$$

where  $\lambda$  is the variance explained by each principle component. The threshold percentage varies (70-90%)<sup>26</sup> and frequently depends on the specific details of a data set.

Our application of PCA in this contribution is twofold: 1) PCA was used to determine the most appropriate features among all features, thus reducing the number of the original variables to only the necessary ones, and 2) the optimum set of PCs are grouped into different classes by using K-means clustering.

### 5.3.2 K-means clustering

The K-means<sup>27</sup> unsupervised algorithm partitions  $n$  observations into  $k$  mutually exclusive subsets  $S_j$  (clusters) so as to minimize the sum of point to centroid (point whose parameter values are the average of the parameter values of all points in a cluster) squared Euclidean distances:

$$J = \sum_{j=1}^k \sum_{n \in S_j} |x_n - \mu_j|^2 \quad (5.7)$$

where  $x_n$  is the  $n$ th data point and  $\mu_j$  is the geometric centroid of the data points in  $S_j$ . Detailed information about the algorithm of the K-means clustering can be found in Ref. 28.

In this contribution, two tools are considered in conjunction for determining whether the preselected number of clusters is acceptable or not: 1) the total sum of distances, and 2) the silhouette plot.

The total sum of distances has to decrease for successive ascending values of  $k$  in order to successfully partition the dataset into clusters. However, this sum always decreases with an increasing number of clusters. Therefore, we have selected the relative reduction in the sum, expressed as the percentage reduction. A second tool for determining the quality of the separation between clusters is the silhouette plot, which is mainly a visual measure. One may also define the silhouette coefficient for an individual point as<sup>29</sup>

$$s_i = \frac{b_i - a_i}{\max(a_i, b_i)} \quad (5.8)$$

where  $a_i$  is the average distance (dissimilarity) of the point  $i$  to all other points of its cluster, and  $b_i$  gives the minimum average distance (dissimilarity) of  $i$  to all points of other clusters. Values for  $s_i$  for each cluster fall in the range from -1 to 1. A negative value is undesirable because it corresponds to the case that  $a_i$  is greater than  $b_i$ . A desirable case occurs, in general, when the silhouette coefficient is positive indicating that  $a_i < b_i$ , and, in particular, when it is close to one. Therefore,  $s_i = 1$  indicates that there is a high probability for the points to be successfully clustered. The average silhouette coefficient (aSC) of all the clusters can be used as a quantitative criterion. A proposed (see Table 5.1) interpretation is described in Ref. 29.

In general, a definite selection of an optimal number of clusters is ambiguous. Therefore in this contribution the number of clusters in most of the cases is predefined based on the knowledge gained from Refs. 16 and 17 and the two tools described above are used to determine whether the separation of the selected number of clusters is within the acceptable range or not.

**TABLE 5.1.** Proposed interpretation of the average Silhouette Coefficient (aSC).<sup>29</sup>

aSC	Proposed Interpretation
0.71-1.00	A strong structure has been found
0.51-0.70	A reasonable structure has been found
0.26-0.50	The structure is weak and could be artificial; please try additional methods on this data set
< 0.26	No substantial structure has been found

## 5.4 Data preparation

### 5.4.1 Extracting the features from the surface patches

The data were grouped per beam, in small surface patches, where each surface patch consisted of the mean data values over a few beams in the across-track direction and a few pings in the along-track direction. The typical size of each surface patch was approximately 0.5 m x 0.5 m and all the features were determined for this surface size. This procedure was the same data grouping procedure followed in Refs. 16 and 17. For this contribution, the data size was, at the last stage, further reduced by constructing boxes of 10 m x 10 m in order to be able to process effectively the whole dataset and significantly reduce the fluctuations of the features extracted. For example, the standard deviation of the residuals was calculated for each one of the 0.5 m x 0.5 m boxes and then these values were averaged over 10 m x 10 m boxes to give the final values of the standard deviation of the residuals. For the approach of Refs. 16 and 17 the larger boxes could not be made, because it would result in combining backscatter values over a range interval where the angle dependence cannot be neglected.

For each surface patch the average, the standard deviation, and higher-order statistical moments were determined for both the backscatter strength and the least-squares depth residuals. In addition, the slopes of the surface patches were considered. The backscatter value is an important classification parameter of the sediments on river/sea beds<sup>3,4</sup> and should be accounted for in the classification. The residuals represent the difference between the observed depth values and the fitted surface patch estimated by the least squares method. In fact, they contain information about the sediments size variations in a ‘purer’ way than the depth itself because they take the slopes of the patches into account.

A comment on the estimation of the least squares (LS) depth residuals is in order. The along-track (x) and across-track (y) slopes of each surface patch were calculated based on the method described in Ref. 16. The polynomial used for fitting a surface to each patch has the form:

$$z = f(x, y) = a_0 + a_1x + a_2y + a_3x^2 + a_4y^2 + a_5xy \quad (5.9)$$

The LS method, details of which can be found in Ref. 30, was used to solve the over-determined system of equations. According to LS, the estimate of a linear model  $E(z) = Aa$  is determined as  $\hat{a} = (A^T Q_z^{-1} A)^{-1} A^T Q_z^{-1} z$ , where  $A$  is the design matrix,  $z$  is the vector of depth measurements, and  $Q_z$  is the covariance matrix of  $z$ . The residual vector is calculated as  $\hat{e} = A\hat{a} - z$ .

The first four statistical moments, namely, mean, standard deviation, skewness, and flatness (kurtosis) of the backscatter and depth residuals were computed. The arithmetic mean is the most widely-used statistical parameter. The standard deviation is also an important parameter since it gives a measure of the variability of the data. Skewness is a measure of the asymmetry of the distribution. Kurtosis is the measure of flatness of the data relative to a normal distribution. Skewness and kurtosis were selected because the K-distribution is a potential sediment classification tool based on results from previous research<sup>16</sup> as it can describe the backscatter distribution.

In addition, the median, mode, minimum, maximum, and mean absolute values were used as new features. In cases where the distribution of the backscatter and/or the residuals is not purely symmetric, the median is different from the mean, and can provide the middle point of the distribution. Mode is the value that has the most frequent occurrence within the data set. It shows the main tendency of the features within a surface patch. The minimum and maximum values were included as indicators of the data extremes.

For the residuals of the bathymetry, the mean absolute error (MAE) was calculated instead of the mean. Since the values of the residuals are small and can be positive and negative, the mean value could be each time close to zero. The mean absolute error is an average value for the absolute errors, given by the equation

$MAE = \frac{1}{n} \sum |e_i|$ . Therefore it provides a measure of closeness between the predicted and measured values.

The 17 features that were taken into account for classification are summarised in Table 5.2.

**TABLE 5.2.** Features calculated for surface patches including statistical moments of backscatter values and least-squares depth residuals (16 features). The 17th feature is the total slope of each surface patch.

	#	BS	#	Depth residuals
Mean (MAE)	1	✓	9	✓
Std. dev.	2	✓	10	✓
Skewness	3	✓	11	✓
Kurtosis	4	✓	12	✓
Median	5	✓	13	✓
Mode	6	✓	14	✓
Minimum	7	✓	15	✓
Maximum	8	✓	16	✓
			17	SLOPES

#### 5.4.2 Correcting for slopes and angular effect in backscatter data

Standard corrections to account for slopes were applied. In the present paper the same procedure and equations as those described in Ref. 16 were used for applying the corrections.

Standardisation of the data was applied to account for the angular effect on the backscatter strength, as in performing the K-means clustering method, the data from all angles had to be gathered and processed at the same time. In fact, also the statistical distributions of the backscatter data are angular dependent. To account for this, the data of each angle was first standardised according to Eq. (5.2), allowing simultaneously processing the data corresponding to angles from 20°-70°. This standardization concerns the first and second statistical moments. Standardization of the higher-order moments might also be applied.

The effect of the standardisation procedure followed in this contribution can be seen in Fig. 5.4. The backscatter values versus angles for the complete dataset of Nijmegen have been plotted before standardisation (Fig. 5.4, left), and after standardisation (Fig. 5.4, right). Figure 5.4 (left) shows that there is an angular dependence of the backscatter values. This dependence is eliminated after standardisation, resulting in the mean value of the backscatter measurements for all angles to be zero and the standard deviation to be one (Figure 5.4). The same was done for Sint Andries.

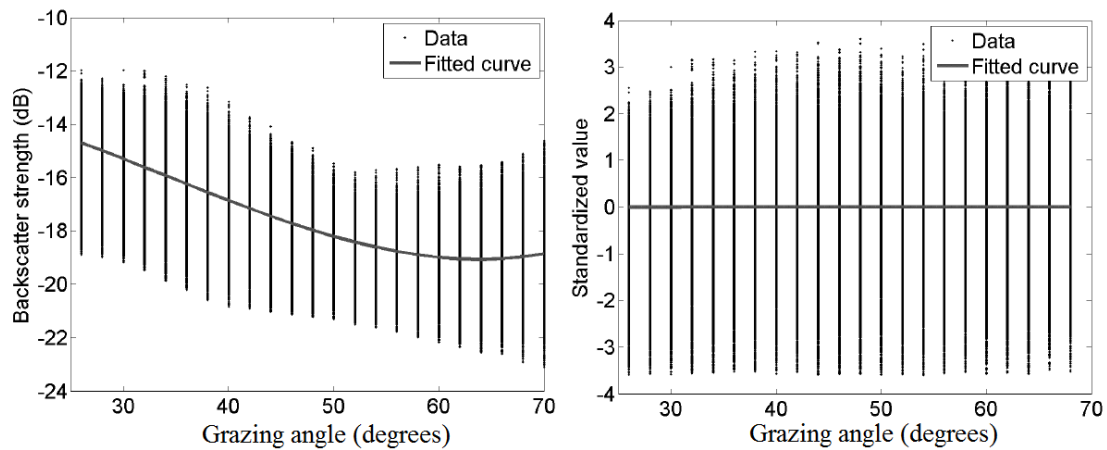


**FIG. 5.4.** Backscatter values versus grazing angles for Nijmegen before standardization (left), and after standardization (right).

### 5.4.3 Determining the optimum set of features

An important step before the classification is to determine those features among the 17 features presented in Table 5.2 that are representative of the river floor sediment. PCA was applied to the available features and the first 3 principal components that expressed most of the variability of the data (around 75%) were obtained using Eq. (5.6). The features were then correlated to these principal components.

Figure 5.5 presents the results obtained following this strategy for Sint Andries (Fig. 5.5, left) and Nijmegen (Fig. 5.5, right) for all the 17 features. From these it can be seen that the most informative features include the mean, median, minimum and mode of the backscatter and the mean absolute error, standard deviation, minimum and maximum of the least-squares depth residuals (Table 5.3). This approach where the number of features is decreased, in this case from 17 to 8, is a relatively standard approach and a variation of it is described in Ref. 26. It, in general reduces the number of PCs needed and consequently eases the interpretation of the results. In fact, using only one feature from each of the two parameters, i.e. reducing the number of features to 2, is found to result in the same map as when using more features (see Sect. 5.5). The balance between the two different sources (backscatter and LS residuals of depth) of information about the sediments was considered to be the optimum for providing reliable and highly discriminative classification results. It has to be noted that the threshold value has been selected in both cases as the value that satisfies three conditions: 1) it is close to the mean value of the ratio of correlations, 2) a sufficient number of features is included for the analysis (in this case 50%), and 3) gives consistent results for both areas.

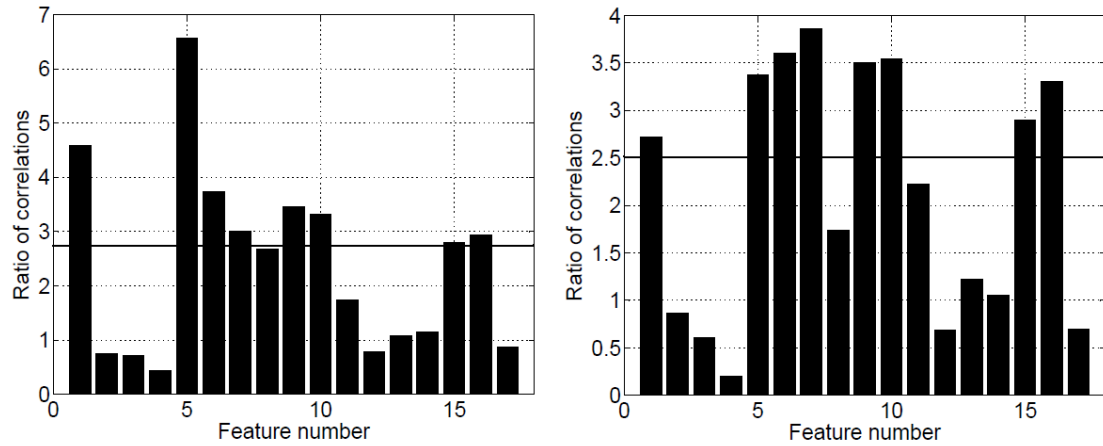


**FIG. 5.5.** Ratio of sum of absolute correlations for the first 3 principal components to sum of absolute correlations for the remaining components; (left) Sint Andries and (right) Nijmegen.

**TABLE 5.3.** Final remaining features; four backscatter features and four LS depth residuals features

# of feature	Backscatter	# of feature	LS depth residuals
1	Mean	5	Mean absolute error
2	Median	6	Standard deviation
3	Minimum	7	Minimum
4	Mode	8	Maximum

## 5.5 Results and discussions

This section is divided into four subsections. The first subsection presents the classification results for the two areas using the PCA and K-means clustering applied to the four extracted features of the backscatter strength. The second subsection presents the classification results based on the LS depth residual features. The third subsection gives the results based on all of the features extracted using the given backscatter and bathymetry data (Table 5.3). Finally the last subsection presents a discussion of the results.

### 5.5.1 Classification based on backscatter strength

The first investigation is to use the four backscatter features only and apply the PCA and K-means clustering to create classification maps of these two areas with three different sediment classes. We hence aim to directly compare the results of the Bayesian classification methodology<sup>16</sup> and the K-means clustering method.

The results in Sint Andries area indicate that the first and second principal components accounts for 96.4% and 2.4% (using Eq. (5.6)) of the variability of the data, respectively. These numbers are 96% and 2.5% for Nijmegen. Because the first PC carries most of the variability, it is an indication for the presence of high correlation among the four backscatter features. Therefore if one tries to obtain the classification map based on each of these features separately the results should be very similar.

The first two PCs are fed to the K-means clustering method. As a first step the clustering is carried out for three clusters equal to the number of sediment types that could be discriminated with the BCM. Figure 5.6 shows the scatter plots of the first PC versus the second PC of the clustered data. We can see that the “cuts” between the clusters are more or less parallel to the second PC. This explains that the first PC has the largest contribution to the clustering, and that the second PC has no significant effect; very similar results can thus be obtained using only the first PC. This supports our remarks made above about the significant correlation among the features.

In general empirical classification approaches provide acoustic classes only. For the situation considered here however the relation between the PCs and a physical parameter, namely backscatter, can be established. Based on this relation, colours have been added to Fig. 5.6, indicating higher backscatter values for lower values of the first PC. Here, green corresponds to fine material (low BS), yellow to intermediate (intermediate BS), and red to coarse (higher BS). This is based on the fact that highest values of the backscatter strength are expected for coarsest grains whereas as the grains become finer as the backscatter strength decreases.

The correspondent sediment distribution maps of Sint Andries and Nijmegen are shown in Fig. 5.7. In the Sint Andries area, the percentage of each class that resulted from the classification procedure is 28.9%, 42.2%, and 28.9% for the fine, intermediate, and coarse sediments, respectively. These numbers change to 12.8% 43.4% 43.8% for Nijmegen. The percentages are different from those obtained using the Bayesian method in Refs. 16 and 17, which were 5% (fine), 40% (intermediate), and 55% (coarse) for Sint Andries, and 5% (fine), 30% (intermediate), and 65% (coarse) for Nijmegen. An important difference between the two methods is the number of measurements over which averaging is performed. For the approach of Refs. 16 and 17 the number of beams which can be averaged is limited due to the angular dependence of the backscatter data. In Ref. 16 a significant overlap existed between the three classes. Here due to the standardisation, averaging was carried out over a much larger number of measurements, improving the discrimination performance.

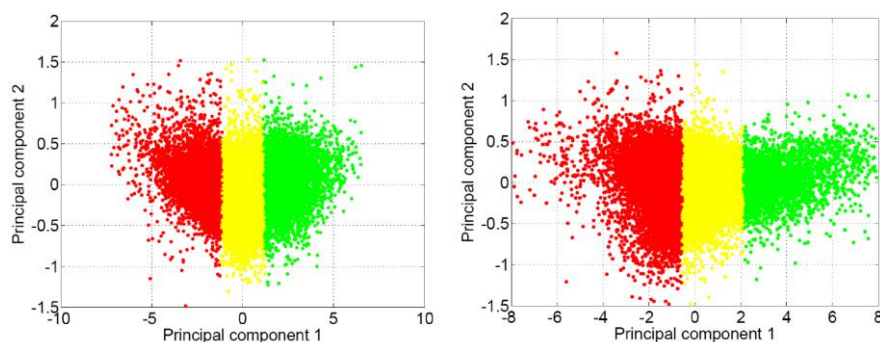


**FIG. 5.6.** Scatter plot of PC1 versus PC2. The colours indicate different clusters resulting from four backscatter features ( $k = 3$ ); (left) Sint Andries and (right) Nijmegen.

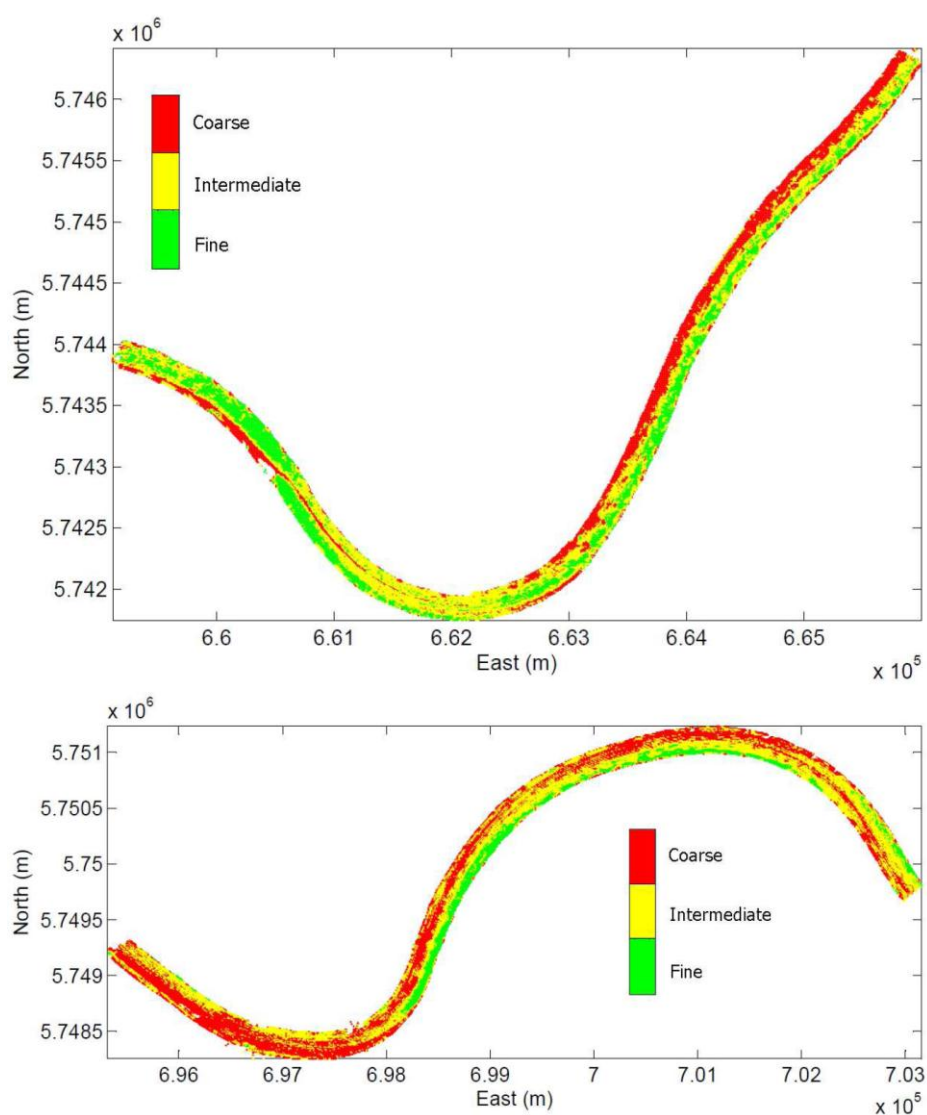


**FIG. 5.7.** Classification map based on the first two PCs and K-means methods applied to only the backscatter features in which the number of clusters was set to  $k = 3$ ; (top) Sint Andries, and (bottom) Nijmegen.

As a second step, it is investigated whether it is possible to further increase the number of clusters. To this end, Fig. 5.8 presents the % reduction (left y-axis) and the average silhouette coefficient (right y-axis) against the number of clusters from 2 to 8 for Sint Andries (Fig. 5.8, left) and Nijmegen (Fig. 5.8, right). It is observed that the maximum % reduction in distances and the largest average silhouette coefficient is achieved for the case of 2 clusters but the value of aSC is still high for 3 clusters (0.66 and 0.63 for Sint Andries and Nijmegen respectively) showing that the separation of the 3 clusters is “almost strong” according to Table 5.1. When increasing the number of clusters to more than 3, the two parameters gradually drop, indicating that further discrimination will be accompanied with less good separated clusters. Therefore, for the current paper the investigation stops at  $k=3$ .

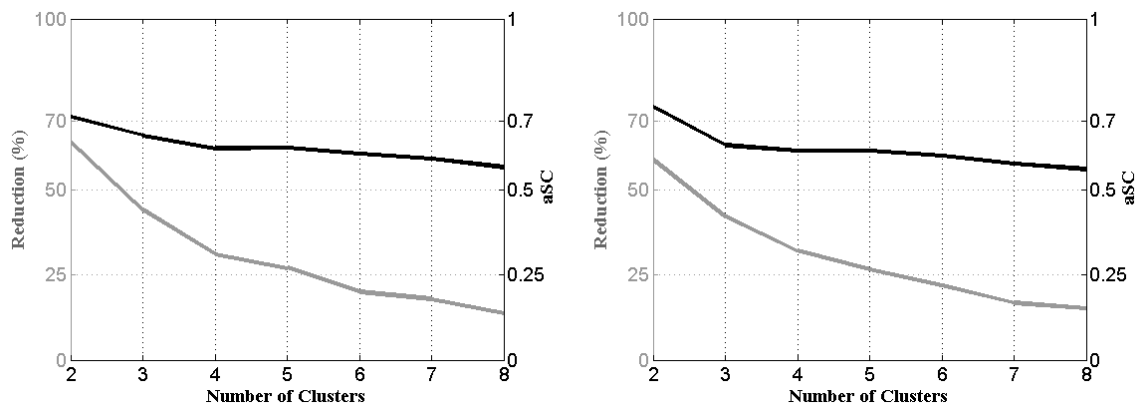


**FIG. 5.8.** Reduction percentage in the sum of distances (left y-axis, grey line) and average silhouette coefficient (right y-axis, black line) versus number of clusters (from 2 to 8) for (left) Sint Andries and (right) Nijmegen, when classifying using backscatter.

### 5.5.2 Classification based on LS depth residuals

The first step is to determine a suitable number of classes that could be obtained by using the four statistical features determined from the LS depth residuals. In Sint Andries, application of the PCA indicates that the first and second PCs account for 99.7% and 0.2% of the variability of the data, respectively. These numbers are 99.4% and 0.38% for Nijmegen. Again it can be concluded that high correlation exists among the four features. Figure 5.9 shows the combined plot of the % reduction in the distances (left y-axis) and the average silhouette coefficient (right y-axis) against the number of clusters for Sint Andries (Fig. 5.9, left) and Nijmegen (Fig. 5.9, right). It is apparent that the case of 4 clusters appears to provide good separated clusters since both the values of the % reduction and the aSC are high (more than 0.7). Therefore, the suitable number of clusters was selected as 4.

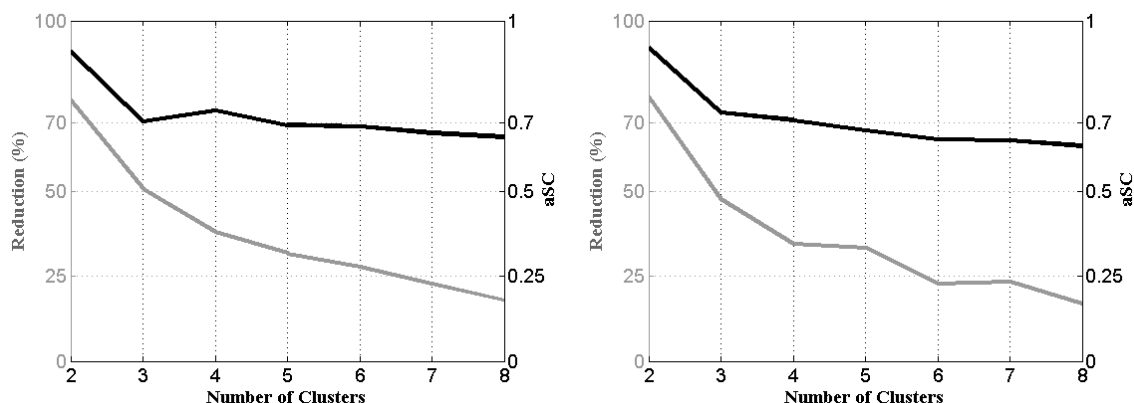


**FIG. 5.9.** Reduction percentage in the sum of distances (left y-axis, grey line) and average silhouette coefficient (right y-axis, black line) versus number of clusters (from 2 to 8) for (left) Sint Andries and (right) Nijmegen, when classifying using LS depth residuals.

For the clustered data, again a “parallel cut” to the second PC appears, indicating that if one uses only the first PC very similar results can be obtained. The sediment distribution maps of Sint Andries and Nijmegen, are shown in Fig. 5.10. Here the first class (blue) has the lowest variations in depth residuals, indicating that the data points can best fit to the surface patch, and class 4 (red) has the highest variations in depth residuals.

We would intuitively expect that coarser sediment gives the highest variations (e.g. highest standard deviations). This however seems not to be the case, because highest variations belong to the finer sediment. That is likely due to the fact that in finer sediment ‘ripples’ can be formed, while coarse sediments will usually form ‘dunes’. Ripples, which are small triangular sand waves, usually are shorter than about 60 cm and not higher than about 60 mm. Ripples typically being about 1 order of magnitude shorter than dunes. Also dunes generally form at larger flow and sediment transport rates, while ripples often form on the upstream slopes of dunes at smaller rates of flow.

The highest depth variations belong to the fixed layer, which is due to the riprap structure. It can therefore be clearly discriminated from the rest of the river. Moreover the northern part of the right-hand side of the fixed layer has been identified as a different class. We hypothesize that this part has been covered by sediments due to the river flow and the resulting sediment transport processes. This leads to lower depth variations with respect to the original fixed layer but higher variations compared to the entire river.

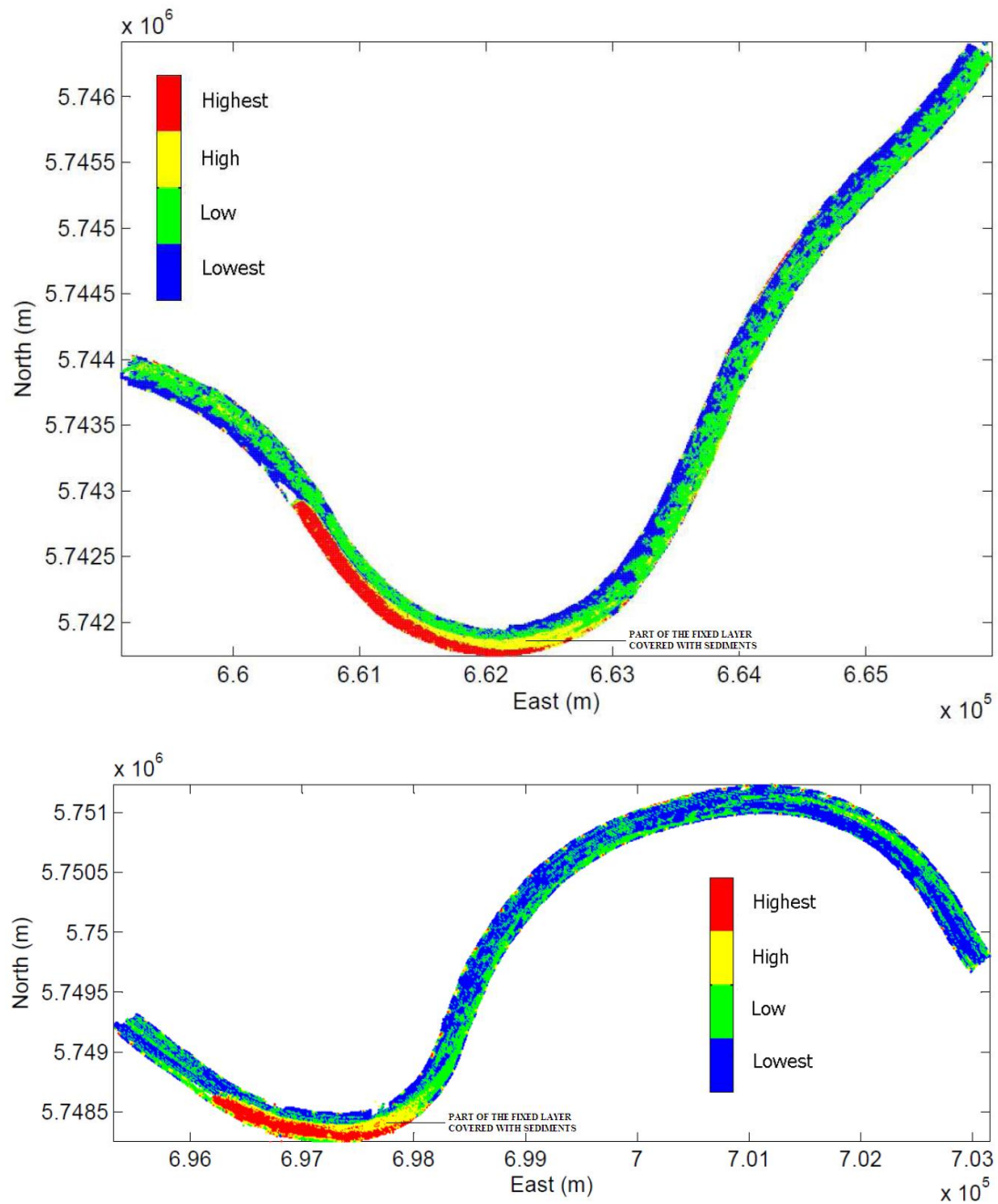


**FIG. 5.10.** Classification map in terms of degree of depth variations based on the first two PCs and K-means methods applied to only the depth residual features in which the number of clusters was set to  $k = 4$ ; (top) Sint Andries, and (bottom) Nijmegen.

### 5.5.3 Classification using all features

This subsection considers all eight features presented in Table 5.3. The objective of this subsection is: 1) to further investigate the nature of all final features considered using the PCA process, 2) to assess the potential of using all features in order to identify the fixed layer, 3) to evaluate the maximum number of classes resulting from all features, 4) to apply this number of classes to both areas and make the classification maps; and 5) to correlate the classification results with the grab samples taken.

The four backscatter features are highly correlated to each other. This holds also for the four residuals features. There is however no significant correlation among the backscatter features and the depth residual features; the average absolute correlation among them for the two areas is around 0.25. This indicates that these two sources of information are independent to a large extent, and hence can provide complementary tools for classification. Therefore any attempt for applying the PCA process on the combined features is expected to give the first two principal components as a combination of backscatter features and a combination of the residual features. This means that any pair of the features of the kind (BS, LS Residuals) can also be used for providing the classification map of the areas that is visually similar to what is presented in this subsection.

Again the PCA is used to combine the information provided from all the features. In Sint Andries, the first, second, and third PCs account for 68.9%, 29.4%, and 1.2% of the variability of the data, respectively. These numbers change to 53.8%, 44.4%, and 0.9% for Nijmegen. Together the first two PCs account for about 98% of the variability and hence will be used for further analysis. The results indicate that the first PC is influenced slightly more by the depth residual features than the backscatter features. The opposite holds for the second PC.

We set the number of classes to 4 based on the results of previous subsections. The first two PCs are fed to the K-means clustering. Figure 5.11 presents the separation of the clusters versus the first and second PCs. A clear distinction between the clusters can be seen for both areas. The sediment distribution maps of Sint Andries and Nijmegen with a fixed number of four classes is given in Fig. 5.12. These results are in fact similar to those with three classes using only the backscatter features (Fig. 5.7) plus the fixed layer. The first three classes are mainly due to the backscatter effect. The fourth class is the fixed layer, which can only be detected if the LS depth residual features are used (cf. Fig. 5.10 with four classes). This implies that the fixed layer has on average a similar backscatter property to the other parts of the river, but it definitely behaves differently on the LS depth residual features.

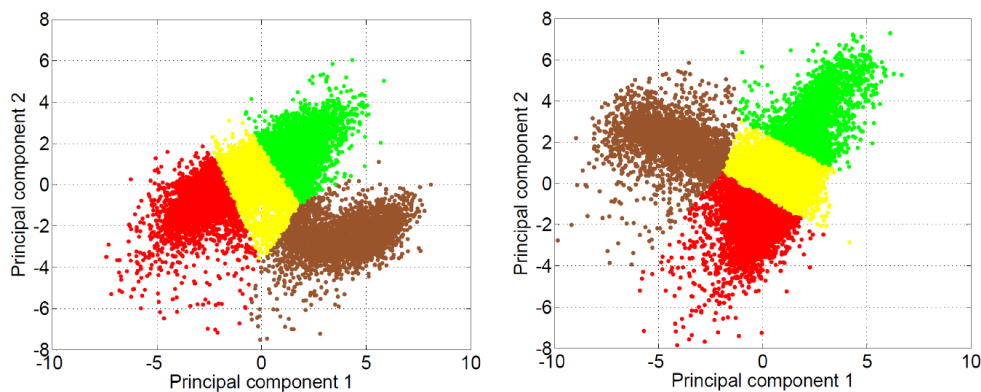


**FIG. 5.11.** Scatter plot of PC1 versus PC2 when K-means clustering is applied to the first two PCs obtained from all features of backscatter and depth residuals ( $k = 4$ ); (left) Sint Andries and (right) Nijmegen.

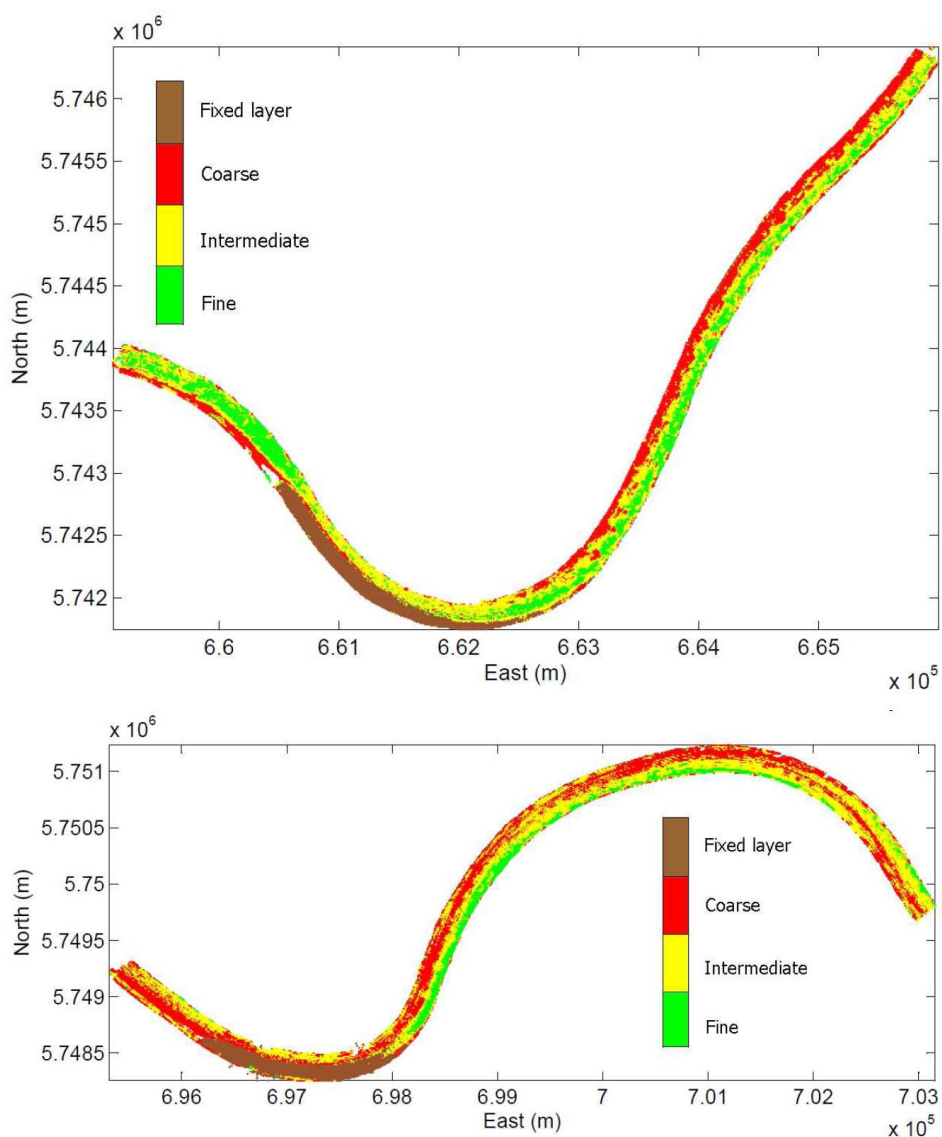


**FIG. 5.12.** Classification maps based on the first two PCs and K-means clustering when all features from backscatter and depth residuals are used ( $k = 4$ ); (top) Sint Andries and (bottom) Nijmegen.

The next step is to assess the possibility of further discrimination. The combined plot of the % reduction in the distances (left y-axis) and the average silhouette coefficient (right y-axis) against the number of clusters for Sint Andries (Fig. 5.13, left) and Nijmegen (Fig. 5.13, right) is given in Figure 5.13. Although there is a drop for 5 clusters, there is another peak for 6 clusters before the values start to gradually drop with increasing clusters number. Therefore the case of six clusters will be further investigated.

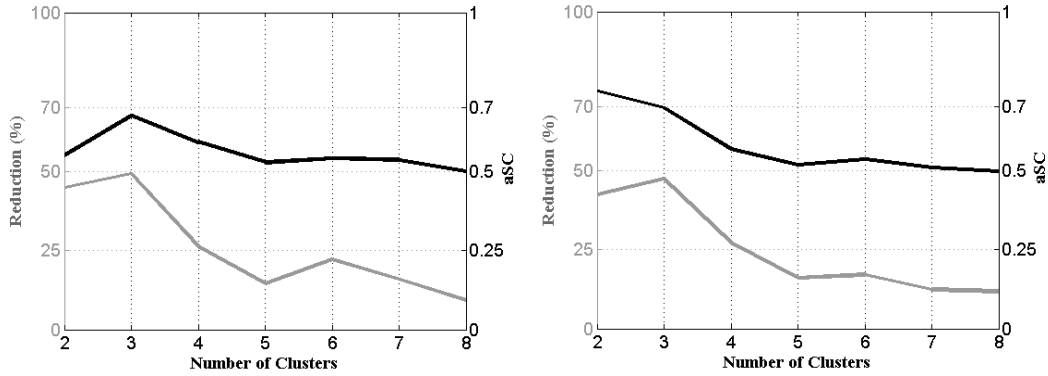


**FIG. 5.13.** Reduction percentage in the sum of distances (left y-axis, grey line) and average silhouette coefficient (right y-axis, black line) versus number of clusters (from 2 to 8) for (left) Sint Andries and (right) Nijmegen, when classifying using both backscatter and LS depth residuals.

Figure 5.14 presents the separation of the clusters versus the first and second PCs for 6 classes. A clear distinction between the clusters can be seen for both areas. The resulting sediment distribution maps of Sint Andries and Nijmegen are shown in Fig. 5.15. These results are in fact similar to those with four classes using only the backscatter features plus two fixed layers given by the depth residual features. Therefore, the first four classes are mainly due to the backscatter effect, and the fifth and sixth classes are mainly due to the depth residual features. This can also be seen in the scatter plots of the first and second PCs in Fig. 5.14. Classes 1 to 4 correspond to the finest to coarsest sediments respectively (as will become clear later in this section where the classification results are compared with the samples). The fixed layer can also be identified here. In addition, for both rivers, on the northern part of the right-hand side of the fixed layer, a separate class can be identified. The degree of depth variations is lower compared with the original fixed layers and probably they (for both rivers) have been covered by sediments. This leads to lower depth variations with respect to the original fixed layer but higher variations compared to the entire river.

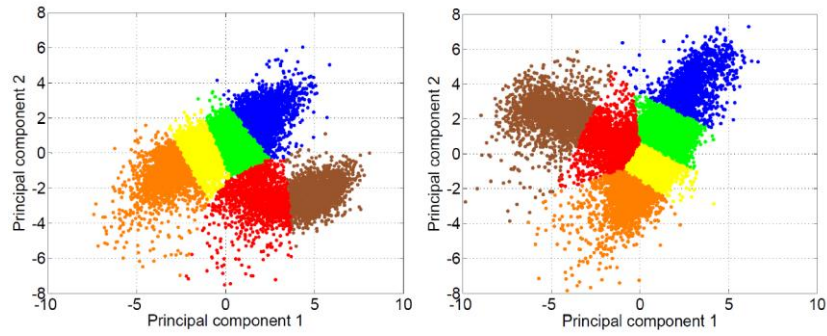


**FIG. 5.14.** Scatter plot of PC1 versus PC2 when K-means clustering is applied to the first two PCs obtained from all features of backscatter and depth residuals ( $k = 6$ ); (left) Sint Andries and (right) Nijmegen.

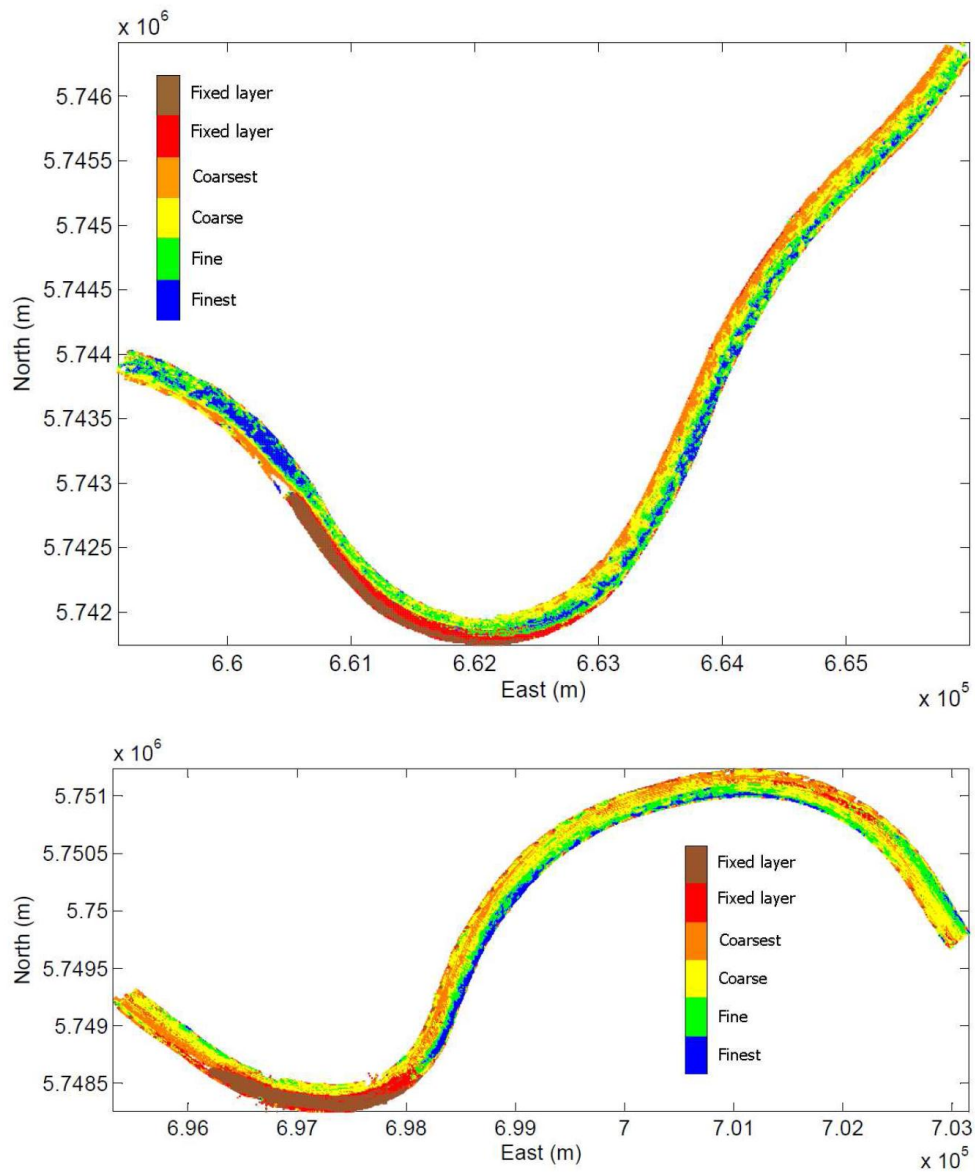


**FIG. 5.15.** Classification maps based on the first two PCs and K-means clustering when all features from backscatter and depth residuals are used ( $k = 6$ ); (top) Sint Andries and (bottom) Nijmegen.

To assess the potential of converting the acoustic classes to riverfloor sediment properties such as mean grain size the classification results are compared with the grab samples.

To make the comparison easier we correlate the mean grain sizes to the acoustic classes 1, 2, 3, and 4; classes 5 and 6 were excluded because they belong to the fixed layer where no grab sample is available. Figure 5.16 shows the best linear fit, using the least squares method, between the classification results (classes) and the mean grain sizes expressed as  $M_z = -\log_2 d$  in phi units, where  $d$  is the diameter of grain in millimeters. A sample is located in an area where surface patches of various classes are present. Each sample took the average class number of the surface patches within a radius of 10 metres from it. The samples without any surface patches within this radius were not used for comparison. The corresponding estimated Pearson correlation coefficients are -0.84 and -0.71 for Sint Andries and Nijmegen, respectively. The same procedure was applied to the three first classes in Fig. 5.12. The correlation coefficients change to -0.84 and -0.75 for these two areas.

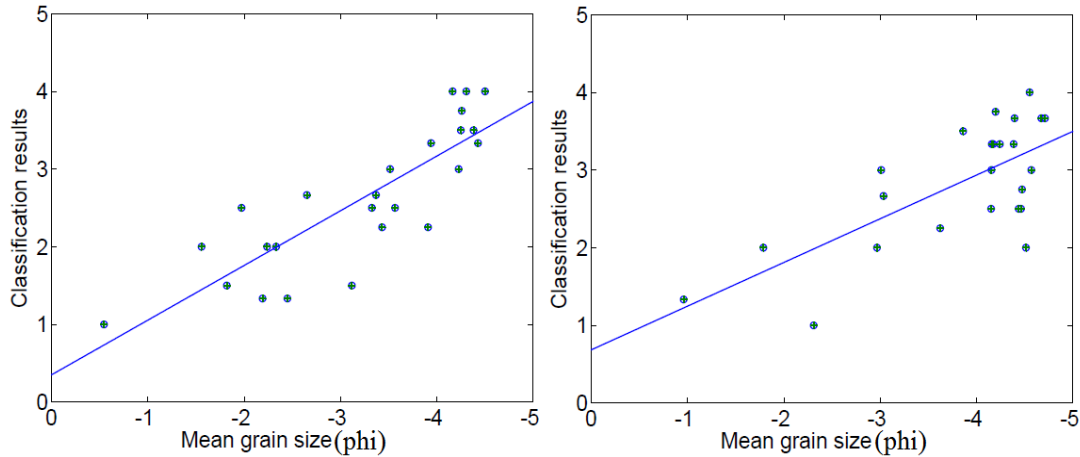


**FIG. 5.16.** Mean grain size of individual grab samples versus classification results of Fig. 5.15, where class numbers 1, 2, 3, 4 belong to the finest, fine, coarse, and coarsest sediment; (left) Sint Andries, (right) Nijmegen.

#### 5.5.4 Discussion of results

The main contribution of this chapter is that it shows that the combination of features can provide insights to the sediment distribution on a riverbed otherwise hidden when only one of the features (backscatter or depth residuals) is used. The fixed layer is clearly visible and clearly highlighted in all maps, when the LS depth residuals or a combination of the LS depth residuals and backscatter were used. This however, is not the case when considering backscatter only. The inadequacy of detecting the fixed layer by using only the backscatter strength has raised many assumptions.<sup>31</sup> The most probable explanation is that the blank areas between the stones and also a thin top layer of the fixed layer is filled with sand, due to transport processes in the outer bend of the rivers, up to a point that this finer layer dominates

the discriminative performance of the sonar. By combining backscatter and bathymetry information it was possible to preserve the main patterns of the classification with 3 classes provided by the backscatter but also adds one more class: the fixed layer.

The depth residual features and the combination of all features gave rise to possible artifacts in the maps. Small areas, at the borders of the river have been classified with the same colour as the fixed layer (brown). This is hypothesized to be the effect of scour holes, resulting in high backscatter values and irregular bathymetry. Because the standard deviations of the depth residuals were larger in the finer sediment than the coarser sediment, we hypothesize that this is due to the riverbed ripples.

The final features used were a combination of 4 backscatter and 4 residual features. Though the final results presented were based on all 8 features, the high correlation among the backscatter features as well as the high correlation among the depth residual features suggested that one can obtain very similar results if for example use is made of only the mean backscatter and the standard deviation of the depth residual.

## 5.6 Summary and conclusions

In this chapter, PCA and K-means clustering were used for the sediment classification of two parts with similar characteristics (groynes, fixed layer) of the river Waal, in the Netherlands. Three cases were investigated: 1) classification with only the backscatter features, 2) classification with only the LS depth residual features, and 3) classification with all backscatter and LS depth residual features. In the first case, the results were compared with previous work,<sup>16,17</sup> where a Bayesian classification methodology was used for the classification process. The results between the two methods are similar: three classes seem to be appropriate for both methods for these particular areas. Deviations in the classification results can be attributed to the different averaging procedures. When averaging, a limited number of beams was used in classification in Ref. 16 due to the angular dependence, whereas in the present contribution, the averaging was performed over a much larger number of measurement, which was made possible due to the standardisation. For the second case, use was made of the LS depth residual features only. It was shown that these features can clearly discriminate between the fixed layer and the remainder of the area. The third case, with all features, could even further discriminate within the fixed layer and within the sediment classes; six classes in total were included. The conclusion here is that the fixed layer can be detected for both areas when use is made of the depth residual features. Using only the backscatter one cannot classify the fixed layer. The following aspects of the research can also be highlighted:

- 1) The depth residual features could detect further than only the fixed layer. Other bottom structures such as the fixed layer covered by sediments and the riverbed ripples can also be identified.
- 2) Due to the high correlation among the features, one can conclude that the combination of only one backscatter feature with only one depth residual

feature can provide results that are very similar to those obtained based on all the features.

- 3) Significant correlation coefficient between the classification results and the mean grain sizes along with the significant slope of the best linear fit (Fig. 5.16) indicate high potential capability of the proposed method for riverbed sediment classification.

## REFERENCES

- <sup>1</sup> M.M. Harris, W.E. Avera, A. Abelev, F.W. Bentrem, and L.D. Bibee. "Sensing shallow seafloor and sediment properties, recent history", Proc. OCEANS 2008 MTS/IEEE, Quebec, 1-11 (2008).
- <sup>2</sup> P. Blondel and O. Gomez Sichi. "Textural analyses of multibeam sonar imagery from Stanton Banks, Northern Ireland continental shelf", Applied Acoustics, 70, 1288-1297 (2009).
- <sup>3</sup> J.M. Augustin, R. Le Suave, X. Lurton, M. Voisset, S. Dugelay, and C. Satra. "Contribution of the multibeam acoustic imagery to the exploration of the sea bottom". Marine Geophysical Researches 18 (2-4), 459-486 (1996).
- <sup>4</sup> B. Chakraborty, H.W. Schenke, V. Kodagali, and R. Hagen. "Seabottom characterization using multibeam echosounder angular backscatter: An application of the composite roughness theory". IEEE transactions on geoscience and remote sensing, 38 (5), Sept. (2000).
- <sup>5</sup> J.M. Preston. "Automated acoustic seabed classification of multibeam images of Stanton Banks", Applied Acoustics 70 (10), 1277-1287 (2009).
- <sup>6</sup> J.M. Preston, A.C. Christney, L.S. Beran, and W.T. Collins, "Statistical seabed segmentation - From images and echoes to objective clustering". In: Proceedings of the seventh European conference on underwater acoustics, Delft, NL, 813-8 (2004).
- <sup>7</sup> J.M. Preston, D.R. Parrot, and W.T. Collins, "Sediment Classification Based on Repetitive Multibeam Bathymetry Survey of an Offshore Disposal Site", in Proceedings IEEE OCEANS 2003, San Diego California, 22-26 Sept. MTS document 0-933957-31-9, 69-75 (2003).
- <sup>8</sup> W.T. Collins, and J.M. Preston, "Multibeam Seabed Classification", International Ocean Systems, 6 (4), 12-15 (2002).
- <sup>9</sup> J.L. Galloway, "Systematic Acoustic Seafloor Habitat Mapping of the British Columbia Coast", Marine Habitat Mapping Technology for Alaska, (eds) J.R. Reynolds, and H.G. Greene, 195-201 (2008).
- <sup>10</sup> C.J. Brown, B.J. Todd, V.E. Kostylev, and R.A. Pickrill. "Image-based classification of multibeam sonar backscatter data for objective surficial sediment

- mapping of Georges Bank, Canada”, *Continental Shelf Research* 31 (2), 100-119 (2011).
- 11 C. McGonigle, C. Brown, R. Quinn, and J. Grabowski. “Evaluation of image-based multibeam sonar backscatter classification for benthic habitat discrimination and mapping at Stanton Banks, UK”, *Estuarine, Coastal and Shelf Science* 81 (3), 423-437 (2009).
  - 12 L. Atallah, and P. Probert Smith. “How useful is bathymetry information in the classification of high frequency sonar surveys?”. In: *Proceedings of the International Conference “Underwater Acoustic Measurements: Technologies & Results”*, Heraklion, Crete, Greece, 2005, [http://www.doc.ic.ac.uk/~latallah/bathy\\_uam.pdf](http://www.doc.ic.ac.uk/~latallah/bathy_uam.pdf) (date last viewed 09/06/2011).
  - 13 G.R. Cutter Jr, Y. Rzhanov, and L.A. Mayer. “Automated segmentation of seafloor bathymetry from multibeam echosounder data using local Fourier histogram texture fixtures”. *Journal of Experimental Marine Biology and Ecology*, 285-286 355-370 (2003).
  - 14 I. Marsh and C. Brown. “Neural classification of multibeam backscatter and bathymetry data from Stanton Bank (Area IV)”, *Applied Acoustics* 70 (10), 1269-1276 (2009).
  - 15 C.J. Brown, S.J. Smith, P. Lawton, and J.T. Anderson. “Benthic habitat mapping: A review of progress towards improved understanding of the spatial ecology of the seafloor using acoustic techniques”, *Estuarine, Coastal and Shelf Science* 92, 502-520 (2011).
  - 16 A.R. Amiri-Simkooei, M. Snellen, and D.G. Simons, “Riverbed sediment classification using multi-beam echo-sounder backscatter data”, *J. Acoust. Soc. Am.* 126, 1724-1738 (2009).
  - 17 A.R. Amiri-Simkooei, M. Snellen, and D.G. Simons, “Using multi-beam echosounder backscatter data for sediment classification in very shallow water environment”, *Proc. Underwater Acoustic Measurements: Technologies & Results*, Nafplion, Greece, June(2009), <http://promitheas.iacm.forth.gr/uam2009/lectures/pdf/29-1.pdf> (date last viewed 09/06/2011).
  - 18 C.J. Sloff, E. Mosselman, and J. Sieben, “Effective use of non-erodible layers for improving navigability”. *Proc. River Flow 2006*, Lisbon, 6-8 Sept., Eds. R.M.L. Ferreira, E.C.T.L. Alves, J.G.A.B. Leal & A.H. Cardoso, Publ. Taylor & Francis, London, ISBN 978-0-415-40815-8, 2 1211-1220, (2006).
  - 19 E. Hammerstad, “Backscattering and Seabed Image Reflectivity”, *EM Technical Note*, (2000), [http://www.km.kongsberg.com/ks/web/nokbg0397.nsf/AllWeb/226C1AFA658B1343C1256D4E002EC764/\\$file/EM\\_technical\\_note\\_web\\_BackscatteringSeabedImageReflectivity.pdf?OpenElement](http://www.km.kongsberg.com/ks/web/nokbg0397.nsf/AllWeb/226C1AFA658B1343C1256D4E002EC764/$file/EM_technical_note_web_BackscatteringSeabedImageReflectivity.pdf?OpenElement) (date last viewed 09/06/2011).
  - 20 D.G. Simons, and M. Snellen. “A Bayesian approach to seafloor classification using multi-beam echo-sounder backscatter data”, *Appl. Acoust.* 70, 1258-1268 (2009).
  - 21 K. Pearson. “On lines and planes of closest fit to systems of points in space”, *Philosophical Magazine* 2 (6), 559-572 (1901).
  - 22 H. Hotelling. “Analysis of a complex of statistical variables into principal components”. *J. Educ. Psychol.*, 24 (7), 498-520, (1933).
  - 23 B.F.J. Manly. “*Multivariate Statistical Methods, A primer*”, Chapman & Hall, 2nd ed. 1994, Chap. 6 pp. 77-79.
  - 24 R.A. Johnson, and D.W. Wichern. “*Applied Multivariate Statistical Analysis*”, 5th ed. Prentice Hall, 2002, Chap. 8 pp. 426-462.

- <sup>25</sup> P.R.Peres-Neto, D.A. Jackson, and K.M. Somers. "How many principal components? Stopping rules for determining the number of non-trivial axes revisited", *Computational Statistics and Data Analysis*, 49, 974-997 (2005).
- <sup>26</sup> I.T. Jolliffe. "Principal component analysis", 2nd ed. Springer, springer series in statistics 2002, Chap. 6 pp. 111-149.
- <sup>27</sup> J. McQuenn. "Some methods for classification and analysis of multivariate observations", in *Proceedings of 5th Berkeley Symposium on Mathematical Statistics and Probability*, Berkeley, University of California Press, p.p. 1:281-297 (1967).
- <sup>28</sup> G.A.F. Seber. "Multivariate Observations". Hoboken, NJ: John Wiley & Sons, Inc, Wiley series in probability and mathematical statistics, 1984, Chap. 7 pp. 379-386.
- <sup>29</sup> L. Kaufman, and P.J. Rousseeuw. "Finding Groups in Data, An introduction to cluster analysis", Wiley series in probability and mathematics, 1990, Chap. 2 pp. 83-88.
- <sup>30</sup> P.J.G. Teunissen, D.G. Simons, and C.C.J.M. Tiberius. "Probability and Observation Theory", Publisher: Department of Earth Observation and Space Systems (DEOS), Faculty of Aerospace Engineering, Delft University of Technology, 2005, Chap. 3 pp. 97-161.
- <sup>31</sup> D. Eleftherakis, E. Mosselman, A.R. Amiri-Simkooei, S. Giri, M. Snellen, and D.G. Simons. "Identifying changes in river bed morphology and bed sediment composition using multi-beam echo-sounder measurements", In: *Proc. of the 10th European conference on Underwater Acoustics*, July 5-9, Istanbul, Turkey, 1365-1373 (2010).

# 6

## **Potential of multi-beam echo-sounder backscatter strength and depth residuals as classifying parameters for very coarse riverbed sediments**

---

This chapter investigates the behavior of two important riverbed sediment classifiers, derived from multi-beam echo-sounder (MBES) data, in very coarse sediment environments. These are the backscatter strength and the depth residuals. Four MBES data sets collected at different parts of rivers in the Netherlands are employed. From previous research the backscatter strength was found to increase for increasing mean grain sizes. Depth residuals, however, are often found to have lower values for coarser sediments. Investigation of the four data sets indicates that these statements are valid only for moderately coarse sediment such as sand. For very coarse sediments (e.g. coarse gravel) the backscatter strength is found to decrease and the depth residuals increase for increasing mean grain sizes. Knowing the transition point, i.e. the mean grain size value at which the behavior of the features is reversed, is of high importance when using these features for sediment classification purposes as the transition in behavior can induce ambiguity in the classification.

## 6.1 Introduction

The Netherlands form the delta for some of the major river systems of Europe, comprising the Rhine, the Meuse, the Scheldt and the Eems. These rivers are valuable parts of national and international ecological networks and are of high economic importance. A minimum depth should be guaranteed to keep the rivers navigable. This depth depends not only on water discharge but also on river bed topography that changes dynamically in response to discharge fluctuations. The river topography and its dynamics are affected by spatial variations in bed sediment composition. This spatial sediment distribution, therefore, needs to be known, in order to understand and eventually predict the dynamic behaviour of the river topography, thereby improving the efficiency of the efforts to ensure safe navigation.

An attractive system to be used for obtaining information on both the river bed bathymetry and sediment composition is the multi-beam echo-sounder (MBES). This sonar emits short pulses of sound towards the river bed to determine the depth and the backscatter strength for a large number of closely-spaced beams. The MBES provides high spatial coverage of an area at moderate costs and within short time. The backscatter strengths are known to be indicative for the sediment types, and consequently have potential with regard to sediment classification (Refs. 1—8). Therefore, the MBES system appears as a good alternative to the conventional, expensive and time-consuming, approach of mapping the river bed composition by taking a large number of grab samples. A brief overview of the techniques used for determining sediment properties in shallow waters is given in Ref. 9.

During the last few years, research considered the potential of the information contained in the bathymetry for classification (e.g. Refs. 10, 11), since only the backscatter cannot be used to predict all sediment characteristics (e.g. Ref. 12), and the use of this additional information might provide improved classification potential. An extensive review of the different classification approaches can be found in Ref. 13.

The work carried out in this contribution is a follow-up to two previous studies (Refs. 14, 15). In Ref. 15, the backscatter and depth residuals, which are the variations in bathymetry relative to a plane fitted through the MBES measured bathymetry, have been used as features for classifying the sediment distribution in two parts of the River Waal in the Netherland, viz. Sint Andries and Nijmegen. The finer sediments in the areas were identified from the backscatter strength. The very coarse sediments, like the fixed layer which consists of rip-rap deposited on top of the original sediments to prevent erosion, could be discriminated from the other sediments only by considering the depth residuals.

This indicates, as also reported in many studies, that coarse sediments do not always correspond to high backscatter strengths.<sup>16-19</sup> In Ref. 20 it is mentioned that the scattering regime can be sub-divided into a number of different zones with respect to the sediment mean grain size. For example, when the grain sizes are smaller (e.g. Ref. 5) or of the same order of magnitude as the acoustic wavelength, the backscattering strength is well understood and models like e.g. Ref. 21 predict the measurements often well. This is not the case when the grain size is much larger than the wavelength since in this case acoustic scattering is determined by facets rather than grains.<sup>20</sup>

To further investigate this, in the present chapter the behaviour of the backscatter strength as well as the depth residuals is assessed over four different datasets collected

in Dutch rivers using a 300 kHz MBES, with sediment types ranging from sandy gravel ( $0 \phi$ ) to very coarse gravel and pebbles ( $-6 \phi$ ). The mean grain sizes ( $M_z$ ) of each area are derived from the grab samples, where  $M_z = -\log_2(d)$  in phi [ $\phi$ ] units and  $d$  the mean grain size in mm. The importance of the present Chapter is that it clearly illustrates the change in the behaviour of the backscatter and depth residuals for the mean grain size (MGS) range from  $0 \phi$  to  $-6 \phi$ .

The chapter is organized as follows. Section 6.2 gives information both about the surveyed areas and the survey settings. Section 6.3 describes briefly the classification methodology using principal component analysis and K-means clustering and gives the classification results based on the backscatter, and classification results based on the depth residuals. The transition point, i.e., the mean grain size at which the behaviour of MBES measured backscatter and depth residuals reverses is determined in Section 6.4. Finally, the main conclusions are summarized in Section 6.5.

## 6.2 Description of surveys

Four areas of two different rivers running through the Netherlands were surveyed during a period of four years (2007-2010). Three surveys involved parts of the Rhine river, and one part of the Meuse river. The positions of the rivers, superimposed on the map of the Netherlands, are shown in Fig. 6.1.

The Rhine river originates in the Alps and flows through Switzerland and Germany to the Netherlands. In the Netherlands, the Rhine is relatively straight with a bifurcation point (Pannerdensche Kop) that divides the flow into the Waal River to the west and the Pannerdensche Kanaal to the north. An MBES survey was performed approximately 1 km upstream of the bifurcation in 2008. This part, known as Bovenrijn, is relatively shallow with an average depth of 3.4 m. After the completion of the Bovenrijn survey, a part of the Waal close to the area of Sint Andries was surveyed with exactly the same MBES and MBES settings as those used in Bovenrijn.

The average water depth at Sint Andries is about 3.8 m and its main characteristic is the presence of deep outer-bend pools and shallow inner-bend point bars (piles of sand and gravel on the inside of sinuous river bends), which form potential obstacles for two-way traffic. Mitigation measures usually involve dredging for removing the shoals, building groynes (artificial structure vertically positioned to the river bank in order to change the direction of the water flow) to avoid lateral erosion, and placing non-erodible layers (fixed layers) comprising of large stone blocks to lower the point bars. A larger part of Sint Andries had been previously surveyed in 2007.

Finally a part of the Meuse river was surveyed in 2010. The river mainly runs close to the Belgian-Dutch border, where it continues its course inside the Netherlands from Maastricht northwards through Venlo closely along the border to Germany. It then turns towards the west, where it joins the Waal river and forms part of the extensive Rhine–Meuse–Scheldt delta. The surveyed part was shallow with mean depth 3.6 m.

For assisting the interpretation of the classification results, grab samples were taken from all surveyed areas. Figure 6.2 presents the resulting mean grain sizes ( $M_z$ ) of each area. As an illustration, Fig. 6.3 shows pictures of some of the grab samples. These figures clearly demonstrate the various ranges of sediment types that are

encountered in the surveyed areas. They include sediments ranging from coarse sand and fine gravel in Sint Andries, to fine gravel and coarse gravel in Bovenrijn, and finally coarse gravel and large stones in Meuse. We note that a number of grab samples in Meuse were so coarse that it was not possible for the laboratory to determine their mean grain sizes.

The sonars used in all surveys were single-head Kongsberg EM3002 multi-beam echo-sounders, a sonar type appropriate for shallow water depths due to the formation of narrow beams ( $1.5^\circ \times 1.5^\circ$ ). The MBESs used for Bovenrijn and the part of Sint Andries that was surveyed in 2008 were exactly the same. However, different MBESs were used in the 2007 survey of Sint Andries and the survey of the Meuse. The frequency of the sonars was 300 kHz. All beams were electronically stabilized for pitch and roll. The backscatter values used in the current work are the backscatter values that resulted of first applying a moving average over the time series of amplitude values and then selecting the maximum average level of each beam. For the details of this processing see Ref. 22.



**FIG. 6.1.** Locations of the surveyed rivers in the Netherlands (modified map of Ref. 23).

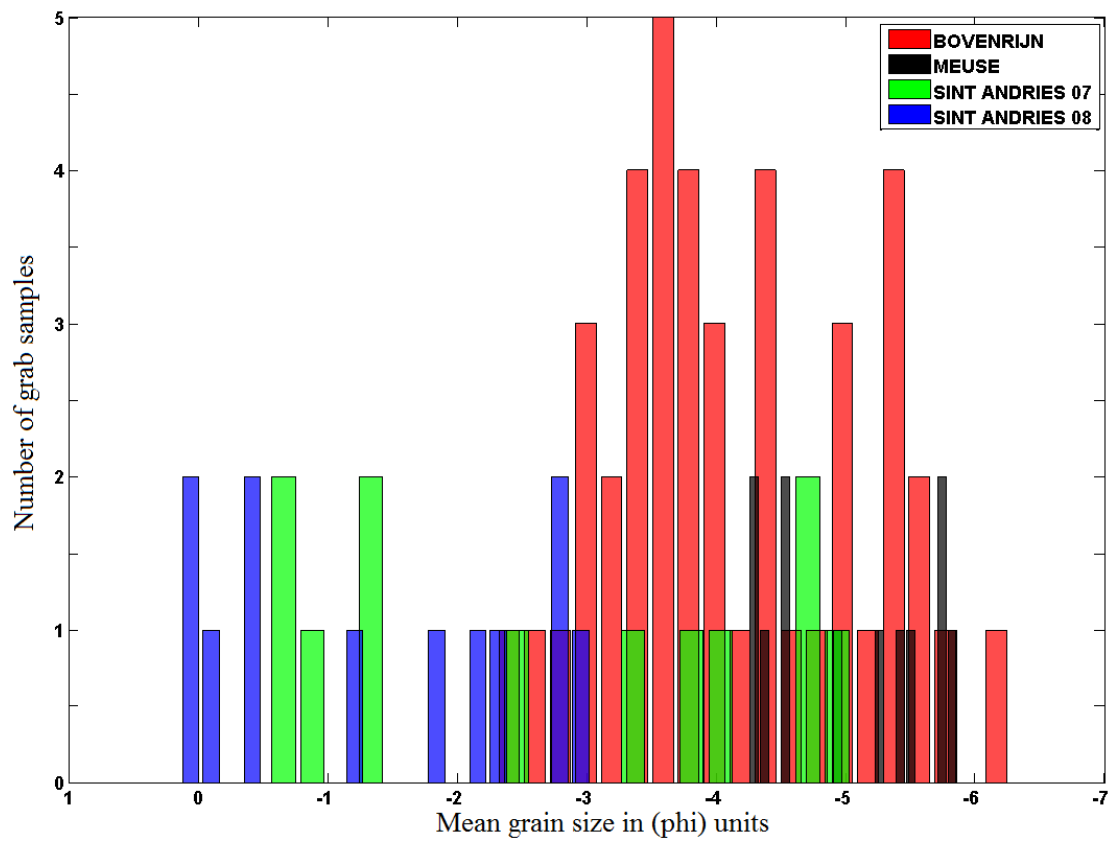


**FIG. 6.2.** Mean grain size of the grab samples taken from the surveyed areas.



**FIG. 6.3.** Pictures of grab samples taken from the surveyed areas.

## 6.3 Classification results

The classification method employed in this contribution is that of Chapter 5 (Ref. 15). In this section, only a short description of the method is presented. For detailed information the reader is referred to Chapter 5 (Ref. 15). Note that classification is done for each area separately.

### 6.3.1 Classification methodology

The pre-processing data procedure can be divided into five phases. In the first phase the sonar data is collected during the survey. In the second phase the data are grouped into small surface patches by averaging over a number of pings and beams. The reason for this is twofold. Not only the noise is reduced, but also the number of measurements inside each surface patch is large enough (minimum ten, typically fifty) for the averaged backscatter values to follow the normal distribution.<sup>14</sup> Since the variation in beam angle over the surface patches is small (approximately  $2^\circ$ ), backscatter angular dependence can be neglected. In this phase 17 statistical features are calculated for each surface patch: eight extracted from the backscatter strength (mean, standard deviation, skewness, kurtosis, median, mode, minimum and maximum), eight extracted from the least-squares (LS) depth residuals (mean absolute error, standard deviation, skewness, kurtosis, median, mode, minimum and maximum), and one is the total slope of the surface patch. The third phase is to use the slopes to account for standard data corrections.<sup>14</sup> Only the data from the beam angle range  $\sim [-60^\circ$  to  $-20^\circ]$  and  $\sim [20^\circ$  to  $60^\circ]$  is used because in this range the backscatter has the highest discriminating power; backscatter curves, i.e. backscatter strength as a function of angle, of different sediment types for angles close to nadir in general overlap.<sup>21</sup>

The concept behind the use of the depth residuals is illustrated in Figure 6.4. The measured depth values are modelled by fitting a 2-D second order polynomial using the least squares principle. The actual measured depths (represented by dots) deviate, however, from the modelled surface. These deviations (vertical lines in Fig. 6.4) are called the depth residuals. They provide measures as to which degree the actual river bottom is smooth. The larger the residuals are, the rougher the bottom will be. Smooth bottoms have small residuals. The mean grain size of the sediments (as very coarse sediments induce a rougher surface) and bottom structures (e.g. riverbed ripples) are two contributing factors to the values of the residuals.

Since the backscatter strengths not only vary as a function of sediment type, but also as a function of angle, the angular dependence needs to be corrected before combining the features of all surface patches into a single dataset. Whereas no angular variation in the depth residual values is expected, still inaccuracies in supporting positioning systems (e.g. attitude sensors) and misregistration between different sensor time series, can induce angular variations.<sup>24</sup> Therefore, the angular correction as applied to the backscatter measurements is also applied to the depth residual values. In phase four, this issue is addressed by standardising the dataset using the method of Ref. 15.

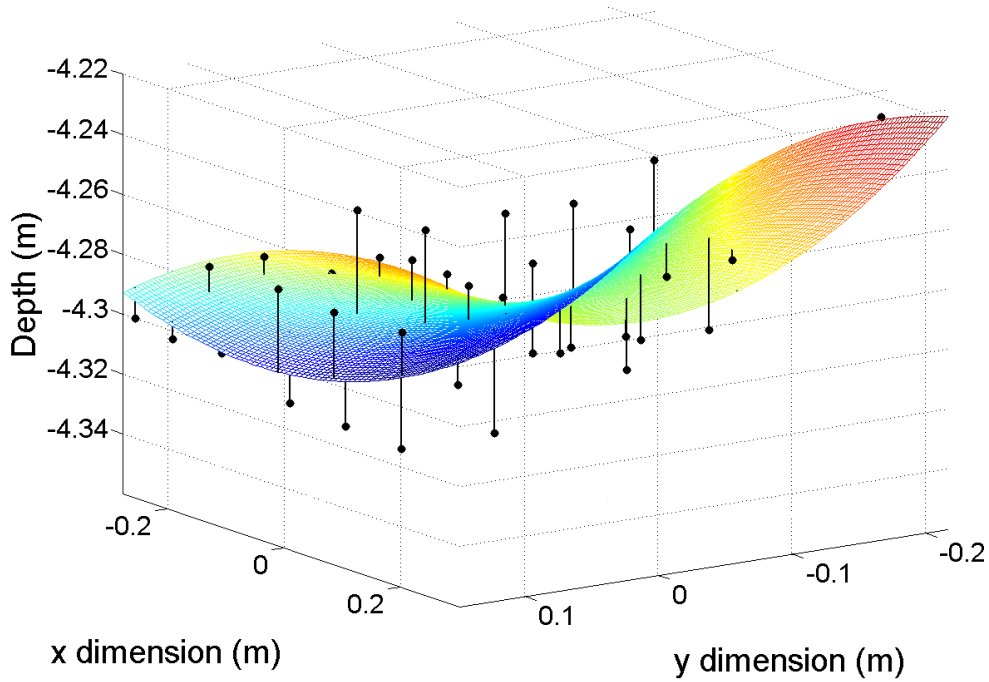


**FIG. 6.4.** Depth residuals (lines) between the measured depth by the sonar (dots) and the fitted surface with second order polynomial (curve).

In the last pre-processing phase a principal component analysis (PCA) is applied to the above-mentioned 17 features. The idea behind PCA is that it converts the set of features to a set of principal components, which are linear functions of the original features that are independent of each other. In general, it is found that a large percentage of the variations found in the original features are represented by a few principal components only. By investigating the correlation between the first three principal components and the original features it was found that for the MBES data considered, 8 out of the 17 features actually contain information. These are: a) the mean, median, mode and minimum of the backscatter data and b) the mean absolute error, standard deviation, minimum and maximum of the depth residuals.

For the subsequent analysis the backscatter and depth residuals are processed separately. Applying PCA to the four backscatter features showed that the first two principal components capture more than 95% of the data variation. Finally, the K-means clustering method was used to partition the first two principal components into different subsets. The optimum number of classes was determined by checking the percentage in the reduction of the distances of the clusters when a new class is added and by the average silhouette coefficient.<sup>15</sup> The same procedure, also indicating the first two principal components to capture more than 95% of the data variation, was applied to the four depth residual features.

### 6.3.2 Classification maps

Using the methodology described in the Section 6.3.1 we obtain two different classification maps: one is based on the 4 backscatter features and the other is based on the 4 depth residuals features. It has to be noted that similar backscatter maps can be obtained using anyone of the backscatter features or the depth residual features separately.<sup>15</sup> The maps are presented in Fig. 6.5. Each class represents a gradual transition from lower to higher backscatter and depth residual values without indicating the exact values. For the ease of comparison the backscatter and depth residuals maps for each area are presented in the same plot. In general these two independent parameters, namely backscatter and depth residuals, provide classification maps that have similar spatial patterns but sometimes with reversed values. For example, the fixed layer in Sint Andries has the largest depth residuals (classification based on depth residuals - red colour) but with lower backscatter values (classification based on backscatter - green colour).

### 6.3.3 Correlation with grabs

To investigate the potential of converting the acoustic classes to riverbed sediment properties such as the mean grain size, the classification results are correlated to the mean grain size values of the grab samples taken from the areas. Figure 6.6 shows linear fits, using the least squares method, between the classification results (classes) and the MGS in  $\phi$  units, for the backscatter and the depth residuals. The correlation coefficients ( $\rho$ ) between the classes (obtained from the backscatter and depth residuals) and the grab samples' mean grain sizes and the corresponding  $p$ -values are shown in Table 6.1. A  $p$ -value of  $6.4 \times 10^{-2}$  (Meuse results) means that there is 6.4% probability that this correlation coefficient (0.50) occurs fully by chance.

A few issues are to be noted: 1) the average of all classes found in a radius of 20 m around each grab sample was used (this averaging will generally result in a fractional class), 2) no outlier removal was used during the fitting process, and 3) in the case of Meuse, there were extremely coarse grab samples for which no mean grain size values were assigned by the laboratory, so these grab samples were not used in the correlations. They however, belong to areas with the highest depth residual values.

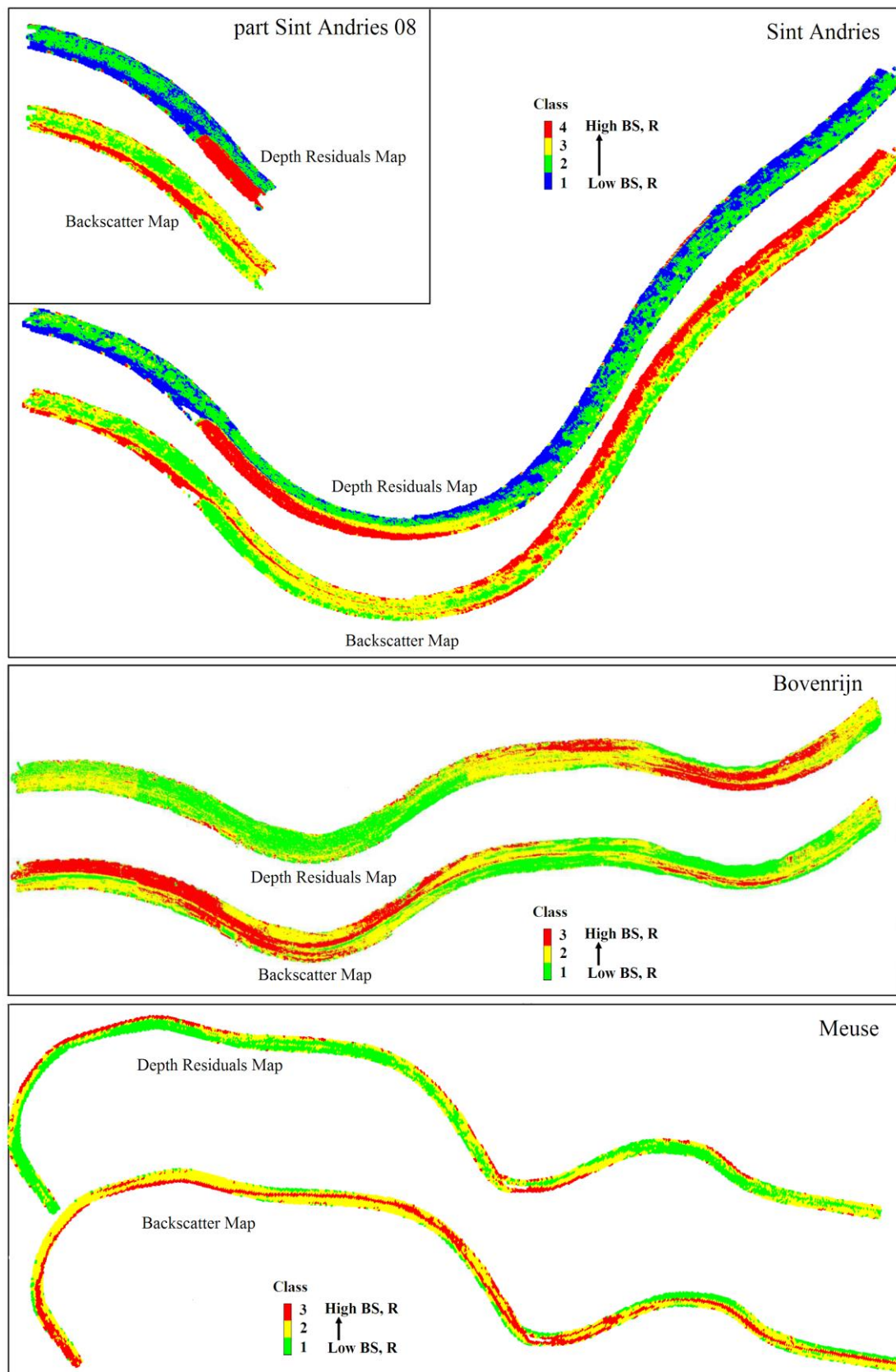


**FIG. 6.5.** Classification maps of (top) Sint Andries, i.e. based on the 2007 survey, and part of Sint Andries 08, (middle) Bovenrijn, and (bottom) Meuse.

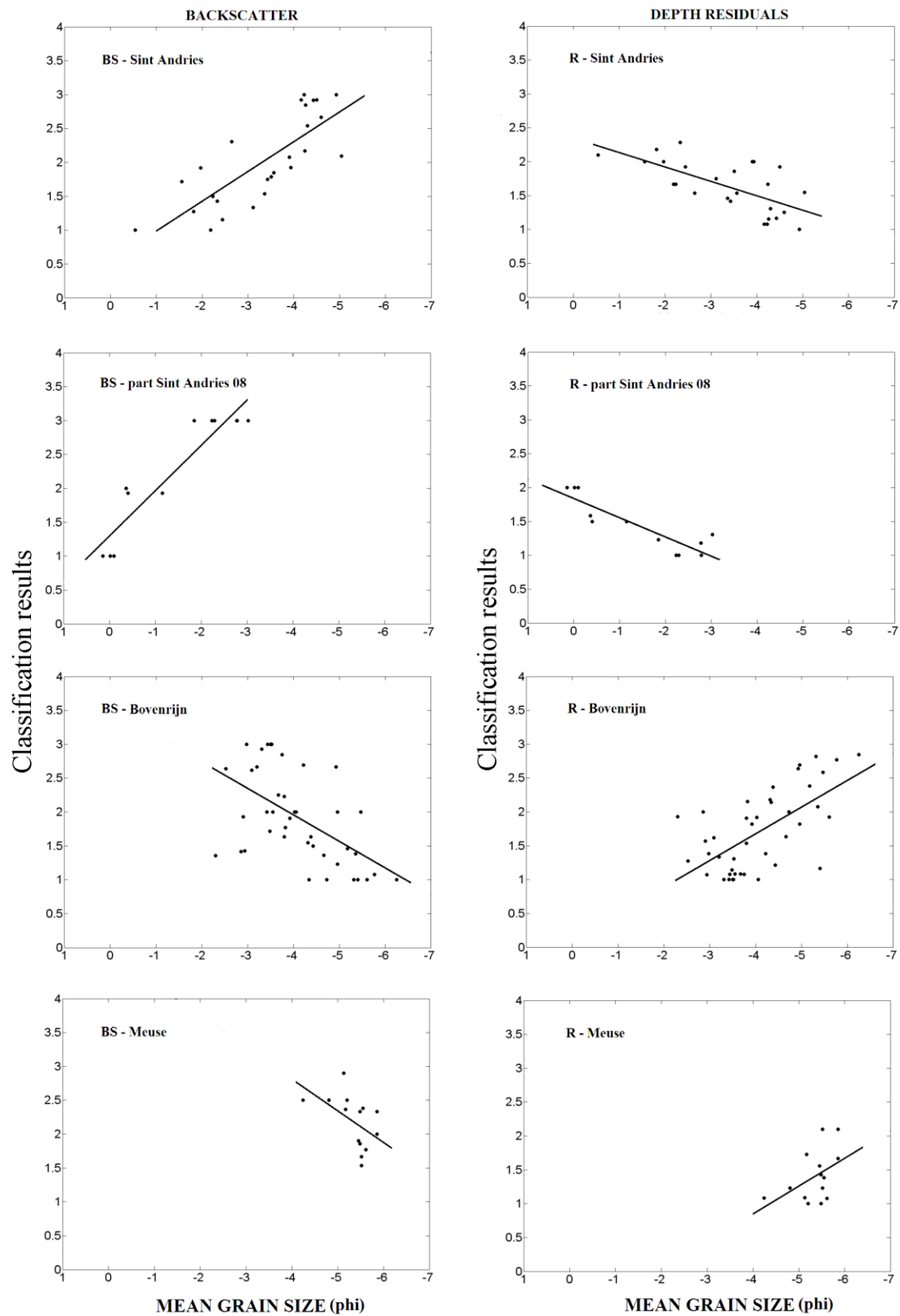


**FIG. 6.6.** Classes based on backscatter and depth residuals versus mean grain size of grab samples (dots). The solid line shows the relation obtained by applying a linear fit. As the class number increases from 1 to 3 (or 4) both the backscatter and depth residual values increase from lower to higher values.

**TABLE 6.1.** Correlation coefficients ( $\rho$ ) and  $p$ -values between the classification results (based on backscatter and depth residual features) and mean grain size of grab samples

Area	Backscatter		Depth Residuals	
	$\rho$	$p$	$\rho$	$p$
Sint Andries	-0.78	$2.2 \times 10^{-6}$	0.66	$2.2 \times 10^{-4}$
part Sint Andries 08	-0.93	$9.1 \times 10^{-6}$	0.88	$1.2 \times 10^{-4}$
Bovenrijn	0.55	$1.6 \times 10^{-4}$	-0.64	$5.6 \times 10^{-6}$
Meuse	0.50	$6.4 \times 10^{-2}$	-0.46	$9.6 \times 10^{-2}$

## 6.4 Discussion of results

### 6.4.1 Observations on the behaviour of backscatter and depth residuals as a function of mean grain size

Based on the results of the previous section, a number of observations can be made.

#### 1) The coupling between features and mean grain sizes is not unique

When considering the behavior of the backscatter as a function of sediment mean grain size, it is observed that for the finer grains as present in Sint Andries backscatter increases with increasing mean grain size, whereas it decreases with increasing mean grain size for the coarser sediments of Meuse and Bovenrijn. The opposite holds for the residuals of depth. The resulting ambiguity where similar values for the features can be found for different sediments, i.e., fine and coarse, can severely hamper an ordering of the classes, where, for example, it is assumed that low class values correspond to finer grains and high class values to coarser grains.

#### 2) The backscatter and depth residuals reflect different sediment physical properties

For all areas the behavior of the backscatter and depth residuals as a function of mean grain size is opposite. For example, in Sint Andries the backscatter strength increases (from class 1 to class 3) with increasing mean grain size, while the depth residual value decreases (from class 3 to class 1). For these fine grain sediments we theoretically expect (e.g. Ref. 21) that an increase in backscatter strength with increasing mean grain sizes is the result of the increase in bottom roughness, sediment

sound speed and density with mean grain size. The corresponding decrease in depth residuals indicates that these residuals are not reflecting the sediment roughness resulting from the grain sizes itself, but rather from the sediment topography. For the Meuse and Bovenrijn the situation is different. Here the increase in the bottom roughness for increasing mean grain sizes does no longer result in an increase of the backscatter values. The increased roughness is, however, contrary to Sint Andries, reflected in increased values for the depth residuals.

### 3) Both features have classification performance

From the classification maps it is seen that both features have sediment classification potential. However, for the areas considered in this paper they contain only limited complementary information, since they reveal a similar distribution of classes. The only exception is the fixed layer in Sint Andries which can be discriminated from the other sediment types only through the use of the depth residuals. Apparently the backscatter values at the fixed layer are such that this very coarse grained area has backscatter values that correspond to the one but lowest class.

## **6.4.2 A quantitative assessment of backscatter and depth residuals as a function of mean grain size**

From the above observations it can be concluded that, for the areas considered, both features contain information that allows for discriminating between different sediments. However, it is also noted that it is not straightforward, for example by using mean grain sizes as derived from grab samples, to order the classes with respect to sediment parameters such as mean grain size. Reason is that the classification results indicate that there is a value of the mean grain size, where a reversal in the relation between features and mean grain size occurs. Knowledge regarding this transition point is of high importance for sediment classification purposes. Taking measurements in an area where sediment mean grain sizes are below and above the transition point will result in an ambiguous classification, since fine and coarse sediments will be attributed to the same acoustic class.

To determine this transition point, the classification results of all areas need to be combined. This is not possible in the current form of Figs. 6.5 and 6.6 because the classes shown do not represent a physical parameter. To this end, values of the features upon which the classification is based need to be used. For this the backscatter (mean over a surface patch) and the depth residuals (mean of the absolute depth residual values over a surface patch) are considered. In the following, for the sake of brevity, we will refer to these features as the backscatter and depth residuals.

Since the backscatter measurements are acquired with different MBES systems for the different surveys, the backscatter measurements cannot be combined directly. Reason is that the MBES calibration is often imperfect, thus requiring an additional calibration. In principle, no calibration is required for the depth residual values since they are derived from the bathymetry measurements, which are independent of the sonar types and sonar settings.

### 6.4.2.1 Calibration of backscatter strengths

The first step is to determine the backscatter curves (backscatter values versus beam angle) that correspond to each one of the classes of Fig. 6.5 for each area. The backscatter values used are the values before removing angular dependence and averaging (over pings and beams). The procedure is as follows. For each of the classes of Fig. 6.5, 50 random locations were selected on the classification maps. An example (Bovenrijn) is shown in Fig. 6.7. The backscatter curves of all 50 locations per class were then averaged for determining the mean backscatter curve per class. These curves are shown in Fig. 6.8 as solid lines for Bovenrijn and part of Sint Andries 08 and with dashed lines for Sint Andries and Meuse. The standard deviation of these 50 curves (as a function of angle) was also computed for later use (results are not shown in Fig 6.8).

A closer inspection of the plots in Fig. 6.8 reveals that the backscatter curves show similar angular behaviour for the three classes in an area but that this behaviour differs significantly among different areas. This is due to the imperfect calibration of the MBES, which is different for different areas.

To correct for the imperfect calibration, thereby allowing for combining the backscatter data as obtained from the different surveys, the Bovenrijn data set is considered as a reference. We then aim to make the other data sets consistent as if all data sets have been measured with the same sonar and sonar settings. This process is called the calibration procedure and it is based on the use of grab samples from the Bovenrijn that indicate a sediment mean grain size also found at either the Sint Andries (2007) area or the Meuse area. These “similar grab samples” are taken as the grab samples that have an absolute maximum difference of  $0.1 \phi$  in their mean grain size values. The grab samples of Sint Andries (2007) were compared to the grab samples of Bovenrijn and 14 cases of “similar grab samples” between the two areas were found. Moreover, 7 “similar grab samples” were identified for the Bovenrijn and Meuse. For each set of similar grab samples the backscatter curves for the two areas are determined from the backscatter curves measured close to the grab samples. The difference between the curves is then determined as a function of angle. Figure 6.9 shows both (top) the mean grain sizes of the “similar grab samples” that were used for the two calibrations and (bottom) the calibration curves that result after averaging the difference curves for all “similar grab samples” per area. The backscatter curves (dashed lines) of Sint Andries and Meuse in Fig. 6.8 were corrected using the corresponding calibration curves of Fig. 6.9 and their corrected backscatter curves are shown in Fig. 6.8 with solid lines. The final appearance of the backscatter curves of Sint Andries and Meuse are now similar to that of the Boverijn area. Bovenrijn and part of Sint Andries 08 surveys were carried out with exactly the same setups (same sonar and same sonar settings); therefore they can be directly combined without any calibration.

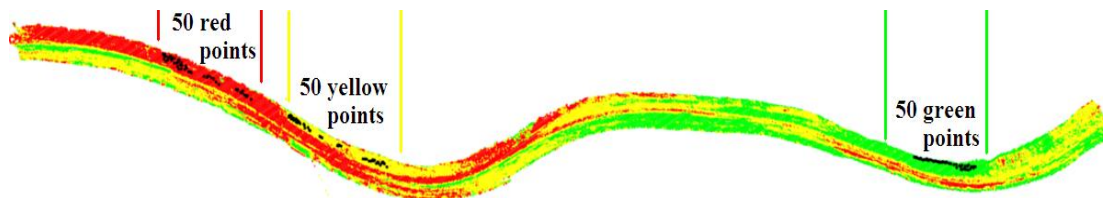


**FIG. 6.7.** Locations from which 50 points (black dots) were selected per class in Bovenrijn.

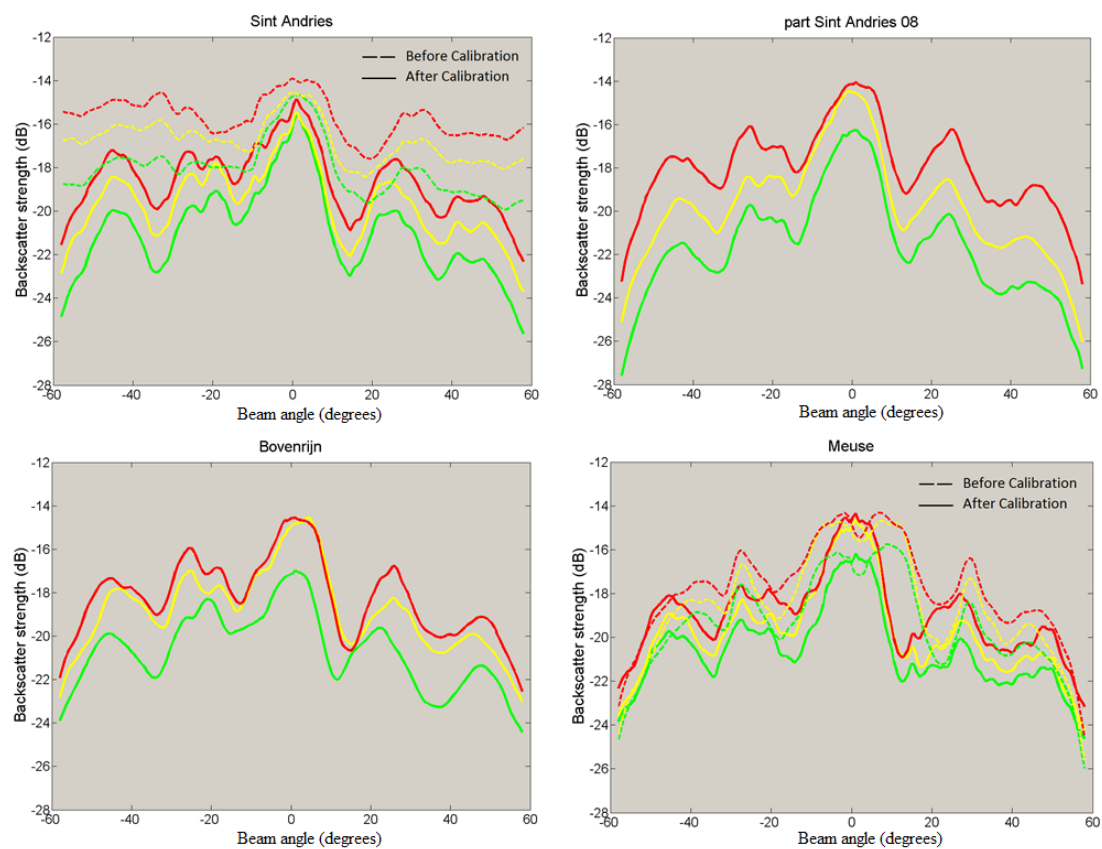


**FIG. 6.8.** Mean backscatter curves for the classes identified in the different areas.

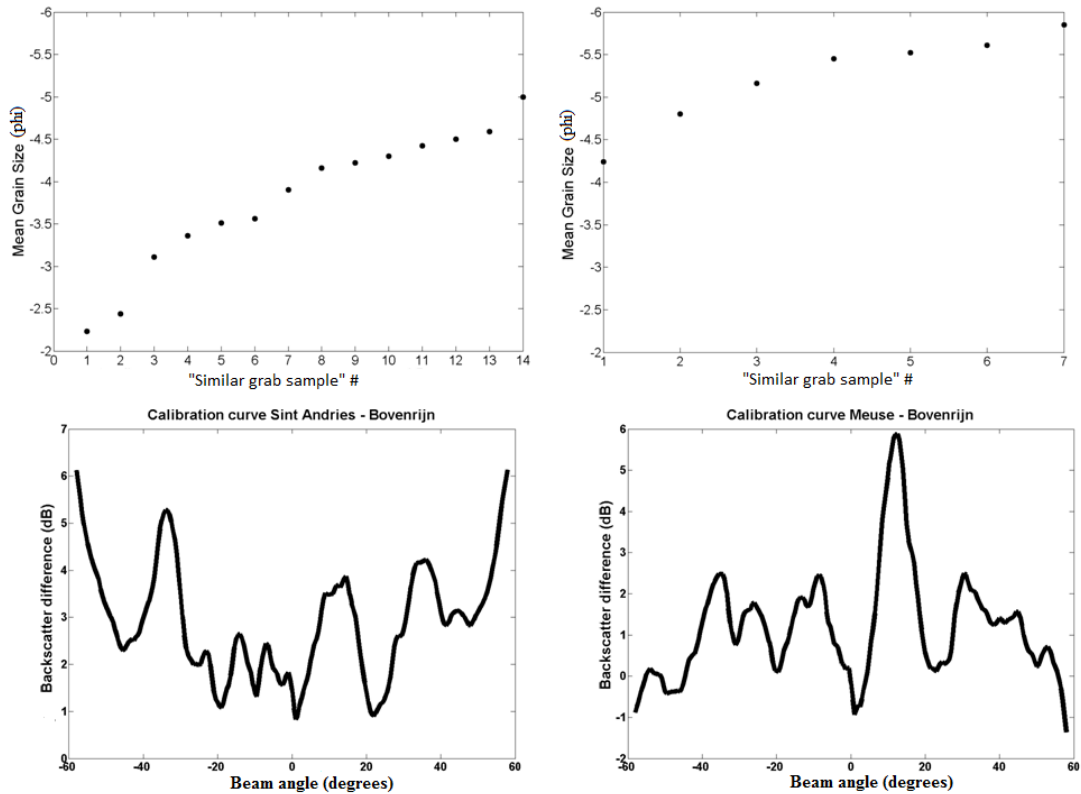


**FIG. 6.9.** (top) Mean grain size values of “similar grab samples” used for calibrating backscatter values between (top left) Sint Andries and Bovenrijn and (top right) between Bovenrijn and Meuse. (bottom) Obtained calibration curves for (bottom left) Sint Andries and (bottom right) Meuse.

#### 6.4.2.2 A closer inspection of the depth residual values

For the depth residuals again for each of the classes 50 points are selected, but this time on the classification map based on the depth residuals (Fig. 6.5). The averages of the selected measurements are shown in Fig. 6.10. As for the backscatter values, the values for the depth residuals are given as a function of angle. The standard deviation of the 50 points (as a function of angle) was also computed for later use (results are not shown in Fig. 6.10). We observe that the depth residual values vary per angle. This, at first sight unexpected, result has also been reported in previous works (e.g. Ref 25) and is due to the bathymetric uncertainty of the sonar systems.<sup>24,25</sup> We note that the classification is not hampered by this effect as the angular change in the depth residual values has been accounted for in the standardization procedure of Section 6.3.1. Still this behavior prevents straightforward combination of the depth residual values from the different areas.

Careful inspection of Fig. 6.10 indicates angle ranges with relative constant values for the depth residuals. For the remaining steps we therefore restrict the analysis to these angle ranges ( $[-44^{\circ} -28^{\circ}]$  and  $[28^{\circ} 44^{\circ}]$ ) assuming that these range allows for combining the measurements from the different areas.

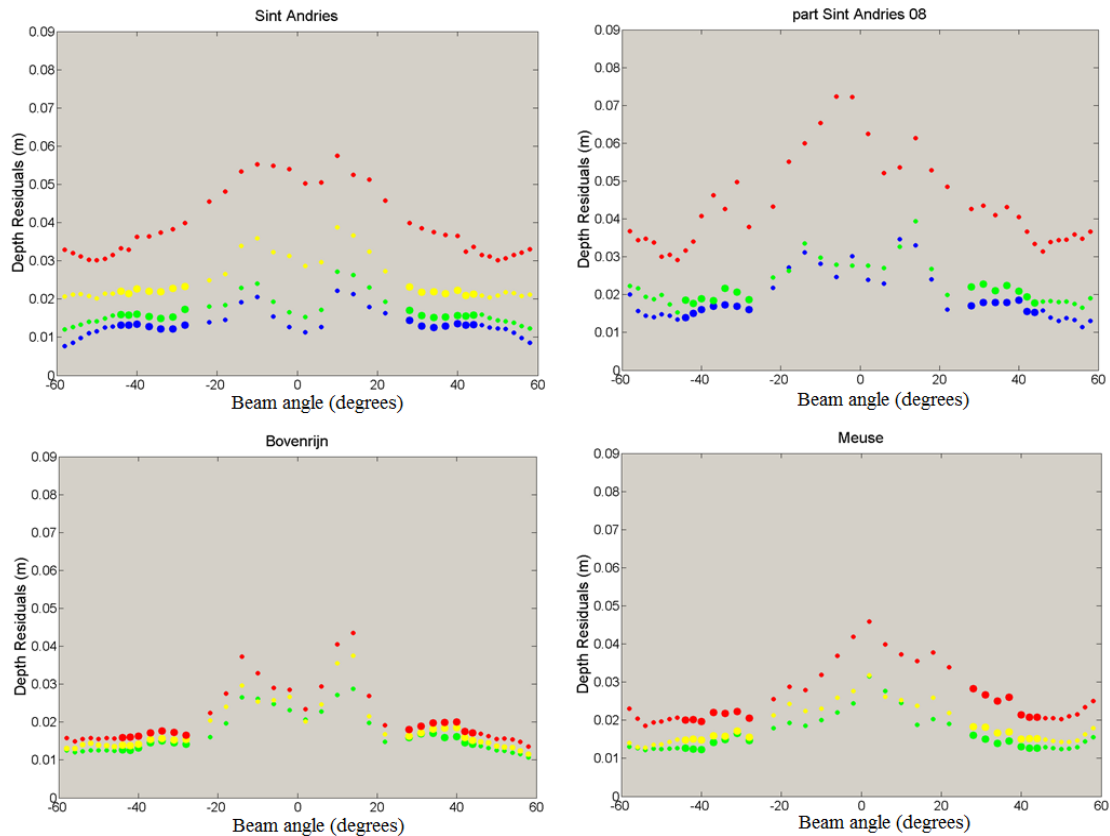


**FIG. 6.10.** Depth residual values for the classes of the depth residual classification maps of Fig. 6.5.

### 6.4.2.3 Combining features from all surveys

By applying the calibration, differences in the calibrated backscatter curves of Fig. 6.8 should be due mainly to variations in the sediment type. To assess this relation between backscatter curve and sediment type, the grab samples that belong almost exclusively to one class (of the backscatter classification maps of Fig. 6.5) are determined per area. The criterion selected is that at least 70% of the surface patches within a radius of 15 m around each grab sample must belong to one class only. The resulting grab samples are then grouped per class and the mean and standard deviation of the mean grain sizes associated to each class are computed. This makes 12 (4 areas x 3 classes) means and 12 standard deviations for the MGS values. Figure 6.11 shows for a number of angles the backscatter (from Fig. 6.8) and standard deviation as a function of this MGS, with the standard deviations in mean grain sizes as error bars in the horizontal axis. For Class 1 (green) in the Meuse area no grab samples were available that met the 70% criterion, resulting in eleven (11) data points (blue dots) in Fig. 6.11 out of the potential 12. The angles are selected in the range  $[-58^{\circ} -20^{\circ}]$  and  $[20^{\circ} 58^{\circ}]$  where the backscatter curves of the different sediment types do not overlap.

The same procedure was used for the depth residuals. First, the grab samples that belong almost exclusively (70% criterion) to one class (of the depth residuals classification maps of Fig. 6.5) are determined per area. Then the average depth residual value for each of the classes in all areas was determined from Fig. 6.10 for the angle range  $[-44^{\circ} -28^{\circ}]$  and  $[28^{\circ} 44^{\circ}]$ . Also these results are depicted in Fig. 6.11,

now as red dots. For the depth residuals, only 9 data points (out of the potential 13) are shown due to the fact that some of the data points did not meet the 70% criterion. For example no grabs samples were taken from the fixed layer of Sint Andries, so the red points of Fig. 6.10 for both Sint Andries surveys are not shown in Fig. 6.11.

The results confirm the existence of a transition point, i.e., a mean grain size value at which the slope of the relation between the features and mean grain size changes sign. To further assess this point, a 2<sup>nd</sup> order polynomial is fitted to the data shown in Fig. 6.11. There are uncertainties (shown by errorbars) in both x (mean grain size) and y (backscatter or depth residuals) axes, which have been taken into account using the weighted total least squares method (see Ref. 26). The resulting fits are also presented in Fig. 6.11 as the solid lines.

All fits show similar appearance. As we move from  $0 \phi$  to  $-3.5 \phi$  the backscatter values increase while the depth residual values decrease. Around the transition point at  $-3.5 \phi$  the values are relatively constant. When moving to very coarse values up to  $-6 \phi$  the backscatter values decrease while the depth residuals increase. Fig. 6.12 shows estimates for the transition point (MGS at maximum values of backscatter fitting curves and minimum values of depth residuals fitting curves) for a large number of angles. For the majority of the cases the transition point is found at  $M_z$  values around  $-3.5 \phi$  (equal to 11 mm) with uncertainty  $\pm 0.5 \phi$ .

The above phenomena can be explained as follows. For the current study on riverbed sediment classification, the depth residuals have larger variations in the finer sediment than the coarser sediment for the range  $[0 \phi$  to  $-3.5 \phi]$ . We hypothesize that this is due to the riverbed ripples that can be formed in finer sediment.<sup>15</sup> In this zone (i.e.  $0 \phi$  to  $-3.5 \phi$ ) the backscatter increases with increasing mean grain size, as expected. For very coarse sediment when the mean grain size is larger than the acoustic wavelength of the sonar (i.e.  $\lambda = -2.3 \phi$ , equal to 5 mm) the backscatter values decrease while the depth residuals increase with mean grain size. In this zone, we would intuitively expect that coarser sediments give the highest variations for the depth residuals. For the backscatter, however, the concept of grain size is no longer valid, because the acoustic scattering is mainly determined by facets rather than the mean grain sizes. When the wavelength is much smaller than the grain size the concept of grain size dependence for the backscatter breaks down. This is also in accordance with the observation of Ref. 20.

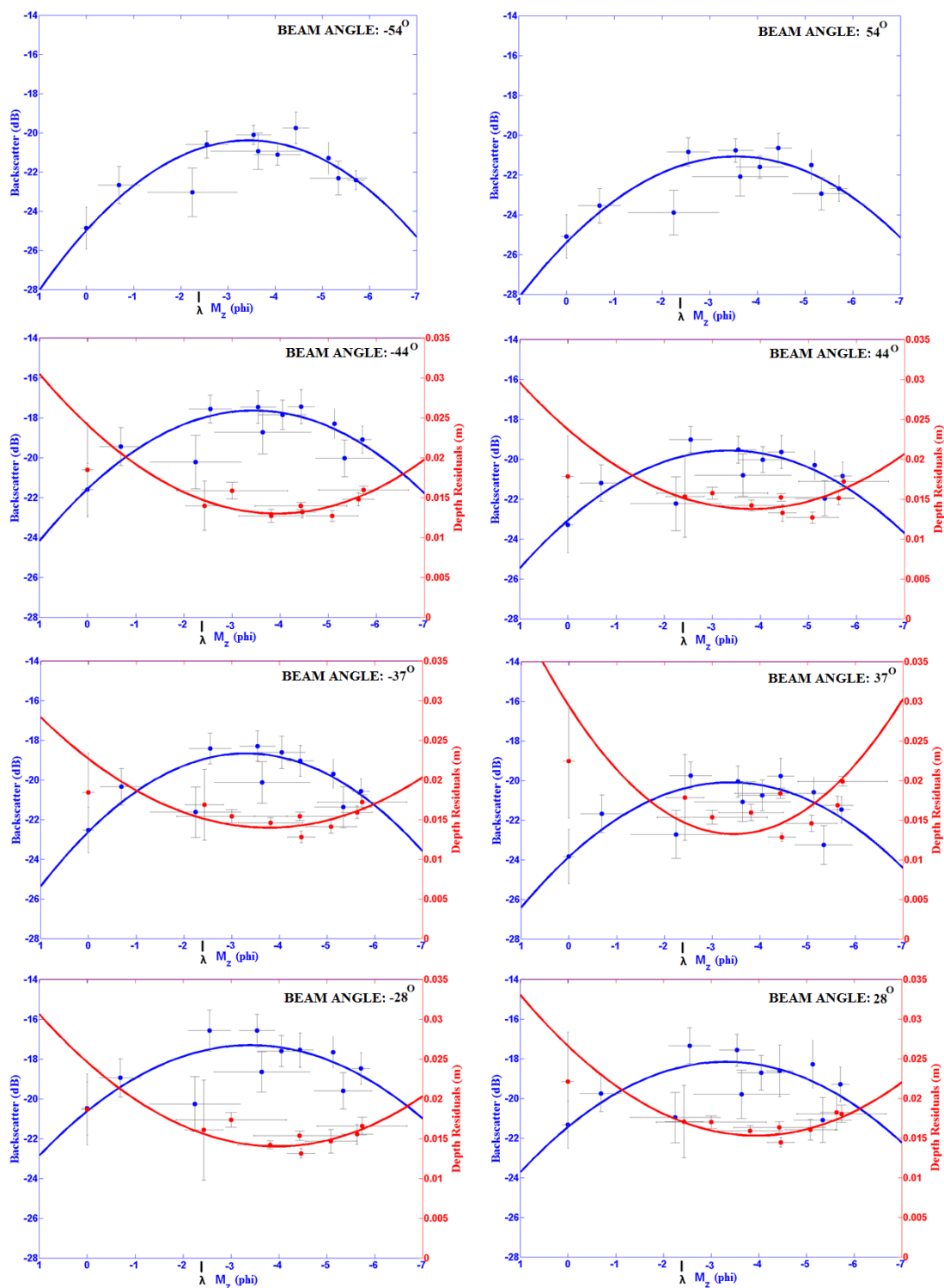


**FIG. 6.11.** Combined plots of (blue dots) backscatter and (red dots) depth residual values vs mean grain size at the grab samples for various beam angles. The fitted curves are shown as solid lines for the backscatter (blue) and the depth residuals (red).

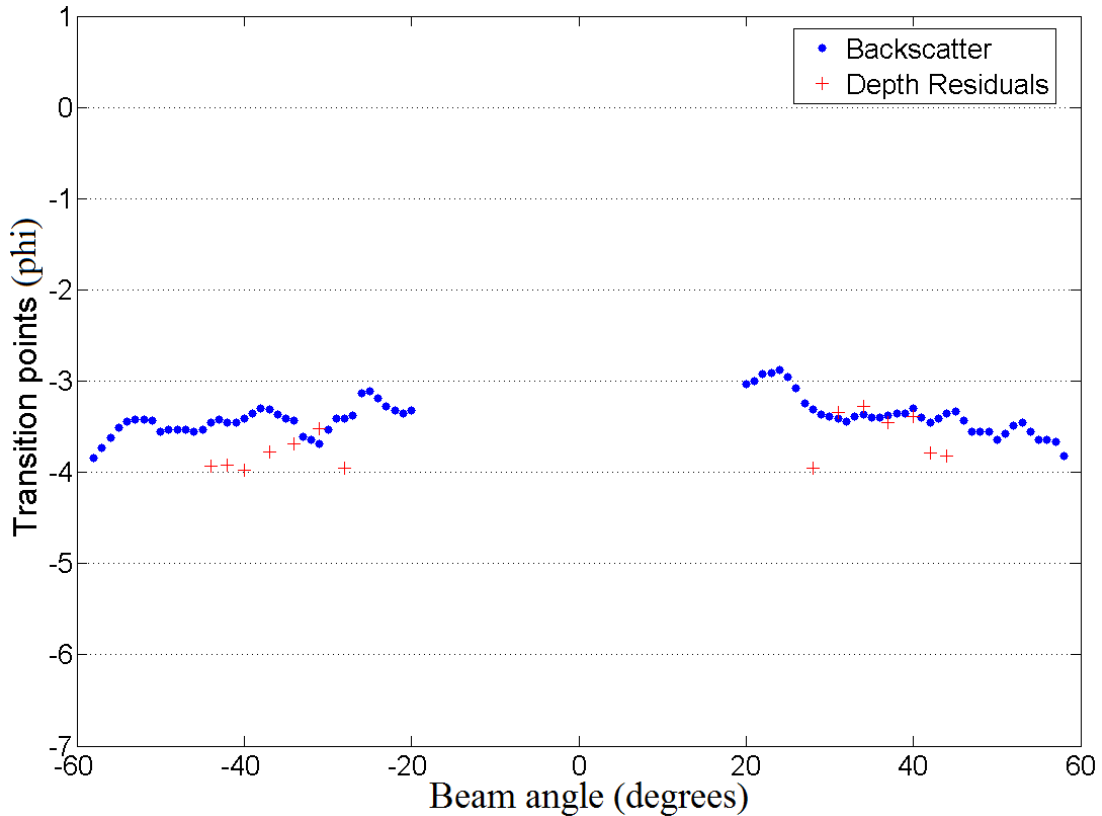


**FIG. 6.12.** Mean grain size values at maximum values of backscatter fitting curves and minimum values of depth residuals fitting curves of Fig. 6.11 for all studied angles.

## 6.5 Conclusions

In this chapter, the behavior of two extracted parameters from MBES measurements, namely the backscatter strength (directly measured) and the depth residuals (calculated from the depth measurements), was investigated for very coarse riverbed sediment in different Dutch rivers. The sediment types range from sandy gravel to very coarse gravel including large stones (fixed layer). The behavior was assessed in two different ways. First, a general assessment was given where the classification results from the backscatter and depth residual maps were correlated to the grab samples in the areas. This indicated that the backscatter and depth residuals show opposite behavior for variations in the mean grain size, but also that their behavior changes when moving from sandy to very coarse gravel sediments. To further assess this behavior, the classes obtained for all surveys were converted into backscatter and depth residual values. This required the backscatter values of the four different river-areas to be calibrated (to eliminate possible effects of imperfect MBES calibrations). For this use was made of grab samples with similar mean grain sizes. The transition point, i.e. the mean grain size at which the dependency of the features on mean grain size changes sign, was estimated to be around  $-3.5 \phi$  (with uncertainty  $\pm 0.5 \phi$ ), that is twice the acoustic wavelength of the MBES used. The results

indicated that the backscatter strengths increase and the depth residuals decrease when the mean grain size increases up to this point, around which the values of both parameters remain relatively constant. Their behavior is then reversed when moving to very coarse sediments. In this zone the backscatter strengths decrease and the depth residuals increase when the mean grain size increases. This knowledge is of high importance when using these features for sediment classification purposes as the transition in behavior can induce ambiguity in the classification.

## REFERENCES

- <sup>1</sup> C. de Moustier, "Beyond bathymetry: Mapping acoustic backscattering from the deep seafloor with Sea Beam," *Journal of the Acoustical Society of America* 79 (2), pp. 316-331, (1986).
- <sup>2</sup> J.E. Hughes Clarke, "Toward remote seafloor classification using the angular response of acoustic backscattering: a case study from multiple overlapping GLORIA data," *IEEE Journal of Oceanic Engineering* 19(1), pp. 112-126, (1994).
- <sup>3</sup> L. Hellequin, J. Boucher, and X. Lurton, "Processing of high-frequency multibeam echo sounder data for seafloor characterization," *IEEE Journal of Oceanic Engineering* 28(1), pp. 78-89, (2003).
- <sup>4</sup> G. Canepa and E. Pouliquen, "Inversion of geo-acoustic properties from high frequency multibeam data," in: *Boundary influences in high frequency, shallow water acoustic*, N.G. Pace and P. Blondel, Eds., Bath UK, pp. 233 – 240, (2005).
- <sup>5</sup> D.G. Simons and M. Snellen, "A comparison between modeled and measured high frequency bottom backscattering," in: *Proceedings of the European Conference on Underwater Acoustics, June 29-July 4 2008, Paris, France*, pp. 639-644, (2008).
- <sup>6</sup> P.A. van Walree, J. Tegowski, C. Laban, and D.G. Simons, "Acoustic seafloor discrimination with echo shape parameters: A comparison with the ground truth," *Continental Shelf Research*, 25, pp. 2273-2293, (2005).
- <sup>7</sup> D.G. Simons, and M. Snellen. "A Bayesian approach to seafloor classification using multi-beam echo-sounder backscatter data", *Appl. Acoust.* 70, 1258-1268 (2009).
- <sup>8</sup> A.R. Amiri-Simkooei, M. Snellen, and D.G. Simons, "Principal component analysis of single-beam echo-sounder signal features for seafloor classification," *IEEE Journal of Oceanic Engineering* 36(2), 259-272, (2011).
- <sup>9</sup> M.M. Harris, W.E. Avera, A. Abelev, F.W. Bentrem, and L.D. Bibee. "Sensing shallow seafloor and sediment properties, recent history", *Proc. OCEANS 2008 MTS/IEEE, Quebec*, 1-11 (2008).
- <sup>10</sup> L. Atallah, and P. Probert Smith. "How useful is bathymetry information in the classification of high frequency sonar surveys?". In: *Proceedings of the International Conference "Underwater Acoustic Measurements: Technologies & Results"*, Heraklion, Crete, Greece, 2005, [http://www.doc.ic.ac.uk/~latallah/bathy\\_uam.pdf](http://www.doc.ic.ac.uk/~latallah/bathy_uam.pdf) (date last viewed 09/06/2011).
- <sup>11</sup> G.R. Cutter Jr, Y. Rzhanov, and L.A. Mayer. "Automated segmentation of seafloor bathymetry from multibeam echosounder data using local Fourier

- histogram texture fixtures”. *Journal of Experimental Marine Biology and Ecology*, 285-286 355-370 (2003).
- <sup>12</sup> V. L. Ferrini and R.D. Flood, “The effects of fine-scale surface roughness and grain size on the 300 kHz multibeam backscatter intensity in sandy marine sedimentary environments”, *Marine Geology* 228, 153-172 (2006).
- <sup>13</sup> C.J. Brown, S.J. Smith, P. Lawton, and J.T. Anderson. “Benthic habitat mapping: A review of progress towards improved understanding of the spatial ecology of the seafloor using acoustic techniques”, *Estuarine, Coastal and Shelf Science* 92, 502-520 (2011).
- <sup>14</sup> A.R. Amiri-Simkooei, M. Snellen, and D.G. Simons, “Riverbed sediment classification using multi-beam echo-sounder backscatter data”, *J. Acoust. Soc. Am.* 126, 1724-1738 (2009).
- <sup>15</sup> D. Eleftherakis, A.R. Amiri-Simkooei, M. Snellen, and D.G. Simons, “Improving riverbed sediment classification using backscatter and depth residual features of multi-beam echo-sounder systems”, *Journal of the Acoustical Society of America* 131(5), 3710-3725, (2012).
- <sup>16</sup> J.C. Borgeld, J.E. Hughes Clarke, J.A. Goff, L. Mayer, J.A. Curtis, “Acoustic backscatter of the 1995 flood deposit on the Eel Shelf”, *Mar. Geol.* 154, 197-210 (1999).
- <sup>17</sup> L. Fonseca, L.A. Mayer, D. Orange, N. Driskoll, “ The high frequency backscattering angular response of gassy sediments: model/data comparisons from the Eel River Margin, California”, *J. Acoust. Soc. Am.* 111 (6), 2621-2631 (2002).
- <sup>18</sup> R. Urgeles, J. Locat, T. Schmitt, J.E. Hughes Clarke, “ The July 1996 flood deposit in the Sguenay Fjord, Quebec, Canada: implications for sources of spatial and temporal backscatter variations”, *Mar. Geol.* 184, 41-60 (2002).
- <sup>19</sup> J.A. Goff, H.C. Olson, C.S. Duncan, “Correlation of side-scan backscatter intensity with grain-size distribution of shelf sediments, New Jersey margin”, *Geo Mar. Lett.* 43-49 (2000).
- <sup>20</sup> N.P. Chotiros, “Seafloor acoustic backscattering strength and properties from published data”, in *OCEANS 2006 - Asia Pacific*, 16-19 May, p.p. 1-6, (2007), <http://ieeexplore.ieee.org/stamp/stamp.jsp?tp=&arnumber=4393905>, (date last viewed 26/06/2013).
- <sup>21</sup> “APL-UW high-frequency ocean environmental acoustic models handbook”, Oct. 1994, technical report APL-UW TR9407AEAS 9501, Applied Physics Laboratory, University of Washington, pp. IV1-IV50.
- <sup>22</sup> E. Hammerstad, “Backscattering and Seabed Image Reflectivity”, EM TechnicalNote,(2000),[http://www.km.kongsberg.com/ks/web/nokbg0397.nsf/AllWeb/226C1AFA658B1343C1256D4E002EC764/\\$file/EM\\_technical\\_note\\_web\\_BackscatteringSeabedImageReflectivity.pdf?OpenElement](http://www.km.kongsberg.com/ks/web/nokbg0397.nsf/AllWeb/226C1AFA658B1343C1256D4E002EC764/$file/EM_technical_note_web_BackscatteringSeabedImageReflectivity.pdf?OpenElement) (date last viewed 09/06/2011).
- <sup>23</sup> A.A. Markus, J.R. Parsons, E.W.M. Roex, G.C.M. Kenter, and R.W.P.M. Laane, “Predicting the contribution of nanoparticles (Zn, Ti, Ag) to the annual metal load in the Dutch reaches of the Rhine and Meuse, *Science of the Total Environment*, 456-457, 154-160 (2013).
- <sup>24</sup> C. De Moustier, “Field evaluation of sounding accuracy in deep water multibeam swath bathymetry”, *OCEANS*, 2001, MTS/IEEE Conference and Exhibition, vol3, pp. 1761-1765 (2001).
- <sup>25</sup> T. Hiller, L.N. Brisson, and S. Wright. “Measuring Bathymetric Uncertainty of the Edgetech 4600 Sonar”, In *Conference Proceedings: Hydro12 – (2012)*,

[http://proceedings.utwente.nl/241/1/Hiller\\_et\\_al\\_4600Paper.pdf](http://proceedings.utwente.nl/241/1/Hiller_et_al_4600Paper.pdf) (date last viewed 02/04/2013).

- <sup>26</sup> A. Amiri-Simkooei, and S. Jazaeri , “Weighted total least squares formulated by standard least squares theory”, *Journal of Geodetic Science* (2), 113-124 (2012).



# 7

## **Overview of methodologies for the acoustic classification of sediment distribution in Dutch rivers using multi-beam echo-sounder data<sup>3</sup>**

---

Maintaining the Dutch rivers on a sufficient depth is essential for safe navigation. Various measures such as coarse sediment suppletions are taken to ensure these depths. In order to assess the effectiveness of these measures, knowledge on riverbed sediment composition is of high importance. At current, using acoustic remote sensing techniques, together with grab samples, is an accepted approach for mapping the distribution of sediment types over an area. A range of methods exist for extracting the required information from the acoustic measurements. All methods have advantages and limitations. To assess these advantages and limitations, six parts of various Dutch rivers, spanning a large range of sediment types, were surveyed during a period of 4 years using multi-beam echo-sounder (MBES) sonars operating at 300 kHz. Physical grab samples were also taken from the rivers to assist the classification. The mean grain size of the grab samples of the rivers vary from relatively fine ( $\sim 5 \phi$ ) to extremely coarse ( $< -6 \phi$ ). This chapter presents an overview of the different classification methods and their results that were applied to determine the distribution of sediment types on the river beds.

---

<sup>3</sup>This chapter has been published as conference paper: *D. Eleftherakis, M. Snellen, A.R. Amiri-Simkooei, and D.G. Simons, "Overview of methodologies for the acoustic classification of sediment distribution in Dutch rivers using multi-beam echo-sounder data", In Proceedings of 1<sup>st</sup> International Conference and Exhibition on Underwater Acoustics, 23-28 June, Corfu, Greece, 1407-1414 (2013)*

## 7.1 Introduction

Knowledge about the composition of the sea- or river floor is essential to a large number of applications such as off-shore construction projects, marine geology, and cable route planning. Especially in the Netherlands monitoring changes in the river floor, both in bathymetry and composition, is extremely important since most of the rivers are used for navigation. At current, the use of acoustic remote sensing systems, such as multi-beam echo-sounders (MBES), in addition to collecting grab samples of the sediment, is an accepted approach.

In general, sediment classification techniques using acoustic remote systems can be divided into phenomenological (or empirical), where information of features indicative of sediment types (e.g. backscatter strength, bathymetry) are combined and used for classification, and model-based (or physical), where the sediment type is determined by maximizing the match between modelled and measured signals. In the first approach ground truth is needed to convert the sediment classes to sediment types, whereas, in principle, no independent measurements are needed for the model based methods.

Over the last years various sediment classification methods were developed and applied to classify the sediments present on Dutch river beds. Six different areas were surveyed using MBES. The sediment types were ranging from slightly gravelly sandy mud (5  $\phi$ ) to very coarse gravel (-6  $\phi$ ). The mean grain size was determined from grab samples taken from the areas. For the classification two riverbed sediment classifiers were employed, the backscatter strength and the depth residuals. Furthermore three different methodologies were used; two model based and one empirical. One of the model based methods, however, provides classes instead of sediment parameters.

The present work gives an overview of the methods and classifiers used for sediment classification and assesses the applicability of each method and classifier over the sediment mean grain size encountered, i.e., from approximately 5  $\phi$  to -6  $\phi$ .

## 7.2 Description of the surveys

Six MBES surveys took place between 2007 and 2010 mainly involving parts of the Rhine river in the Netherlands. The Rhine river flows through Switzerland and Germany to the Netherlands. In the Netherlands, the Rhine River is relatively straight with a bifurcation that divides the flow into the Waal River to the west and the Pannerdensch Kanaal to the north. The first survey was performed in 2007 when a part of the Waal close to the area of Sint Andries was surveyed. It was followed by another survey in 2008 in Nijmegen (also part of Waal). The third MBES survey was performed approximately 1 km upstream of the bifurcation of Rhine, viz. the Bovenrijn, in 2008. Subsequently, a small part of Sint Andries was re-surveyed with exactly the same MBES and MBES settings as those used in Bovenrijn. In 2009 the Dordtse Kil river survey took place. Dordtse Kil is a tidal and very busy river that connects the Hoeksche Waard and the Hollandse Diep. Finally, the Meuse river was surveyed in 2010. It mainly runs close to the Belgian-Dutch border, but turns to the west at Maastricht from where it continues its course inside the Netherlands northwards through Venlo closely along the border to Germany. Figure 7.1 shows the

position of the rivers in the Netherlands. Table 7.1 gives an overview of the specifics of the surveyed areas.

For assisting the interpretation of the classification results physical samples were taken from all the surveyed areas. Figure 7.2 illustrates the mean grain sizes ( $M_z$ ) as derived from the samples in phi [ $\phi$ ] units, with  $M_z = -\log_2(d)$  and  $d$  the mean grain size in mm.

The sonars used in all surveys were single- and dual-head Kongsberg EM3002 multi-beam echo-sounders, a sonar type appropriate for shallow water depths due to the formation of narrow beams with small physical dimensions. All beams were electronically stabilized for pitch and roll. The backscatter values used in all cases are the backscatter values resulting of first applying a moving average over the time series of amplitude values and then selecting the maximum average level of each beam.

**TABLE 7.1.** Overview of the specifics of the surveyed areas.

<b>Area</b>	<b>Area specifics</b>	<b>Measurement specifics</b>
1. Sint Andries	Fixed layer present; Mean water depth 3.8 m.	Surveyed in 2007. Sonar: EM3002S @ 300 kHz.
2. Nijmegen	Fixed layer present; Mean water depth 4.2 m.	Surveyed in 2008. Sonar: EM3002S @ 300 kHz.
3. Bovenrijn	Mean water depth 3.4 m.	Surveyed in 2008. Sonar: EM3002S @ 300 kHz.
4. Sint Andries (part)	Mean water depth 4.3 m.	Surveyed in 2008; same sonar as in Bovenrijn. Sonar: EM3002S @ 300 kHz.
5. Dordtse Kil	Part of the river has irregular surface due to the presence of deep holes (~ 16 m deep). Mean water depth 8.6 m.	Surveyed in 2009. Sonar: EM3002D @ 300 kHz. Additional measurements with device measuring sediments' radioactivity were taken.
6. Meuse	Very coarse riverbed. Mean water depth 3.6 m.	Surveyed in 2010. Sonar: EM3002S @ 300 kHz.

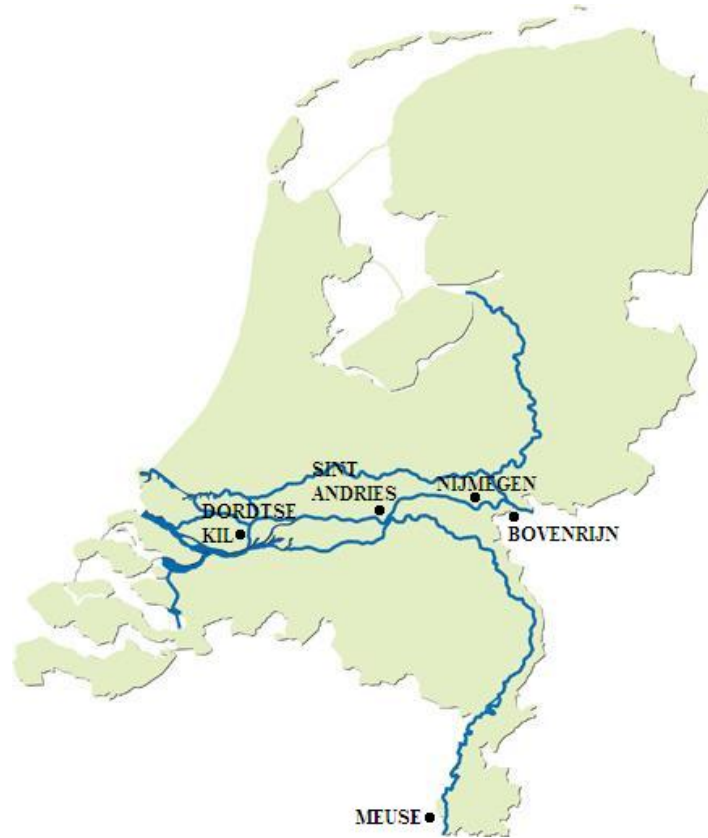


**FIG. 7.1.** Locations of the surveyed rivers in the Netherlands.

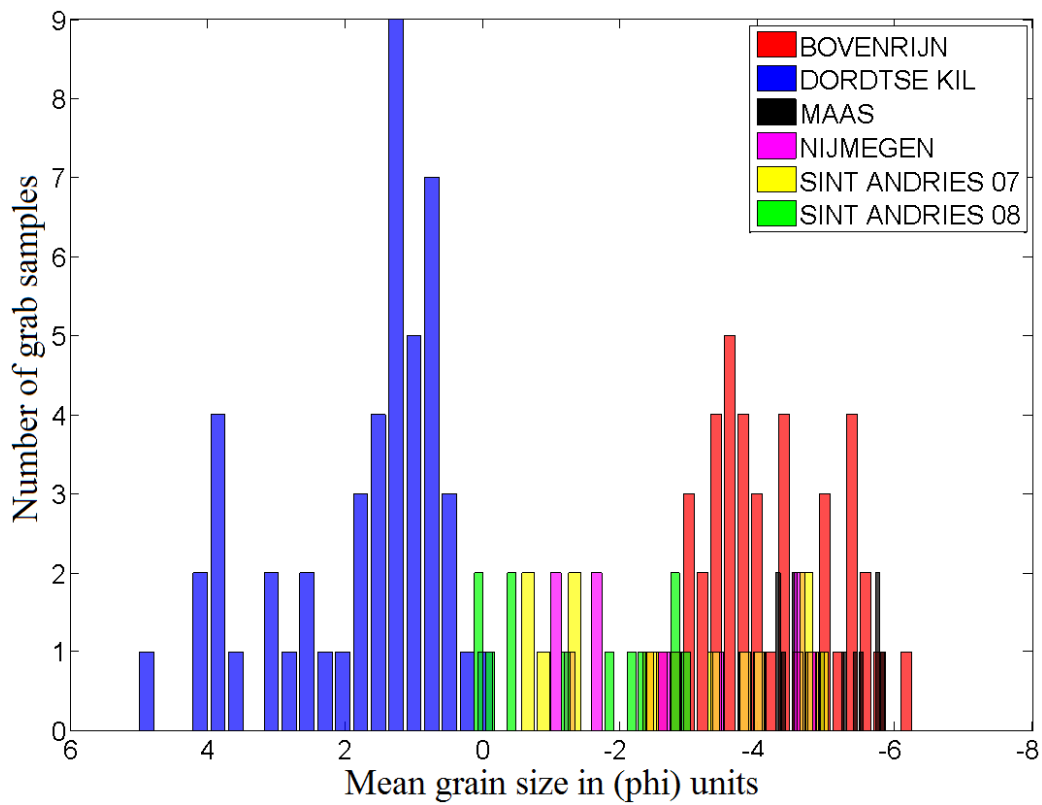


**FIG. 7.2.** Mean grain sizes of the physical samples present in the areas.

### 7.3 Classifiers

The research work investigated the behavior of two important riverbed sediment classifiers, one directly and one indirectly derived from multi-beam echo-sounder (MBES) measurements. These are the backscatter strength (direct), which is derived from the intensity of the received signal, and the depth residuals (indirect), which are the variations in bathymetry relative to a plane fitted through the MBES measured bathymetry.

**Backscatter:** The scattering process of an acoustic wave when it comes in contact with unregular interface (like the riverbed) is shown in Fig. 7.3. As the incident wave meets the sediment on the riverbed, a part of it (coherent part) will be reflected in the specular direction. The rest of the energy will be scattered in all directions, included back towards the source (backscattered signal). It is known that the backscatter strength is different for different sediment types.<sup>2</sup> As an illustration, Fig. 7.4 presents modelled backscatter strength curves for part of sediment types encountered in the Dutch rivers.

**Depth Residuals:** The depth residuals concept is presented in Fig. 7.5. The measured depth values are modelled by fitting a 2-D second order polynomial using the least squares principle. The actual measured depth variations (represented by dots) deviate, however, from the modelled surface patch. These variations (lines in Fig. 7.5) are denoted as ‘depth residuals’. They provide measures as to which degree the actual river bottom can be represented by the second order polynomial. The larger the residuals are, the larger the variation around the fit, indicating roughness on spatial scales smaller than the surface patch. Smooth bottoms have small residuals as all bathymetric variations are well described by the fit. The mean grain size of the sediments (for very coarse sediments which induce a rougher surface) and the bottom structure (e.g. riverbed ripples) are two factors contributing to the values of the residuals.

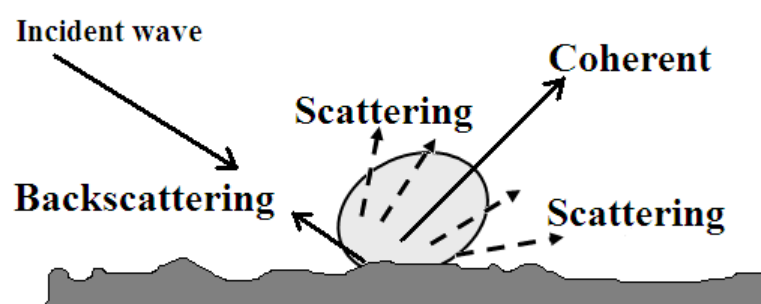


FIG. 7.3. Scattering process.<sup>1</sup>

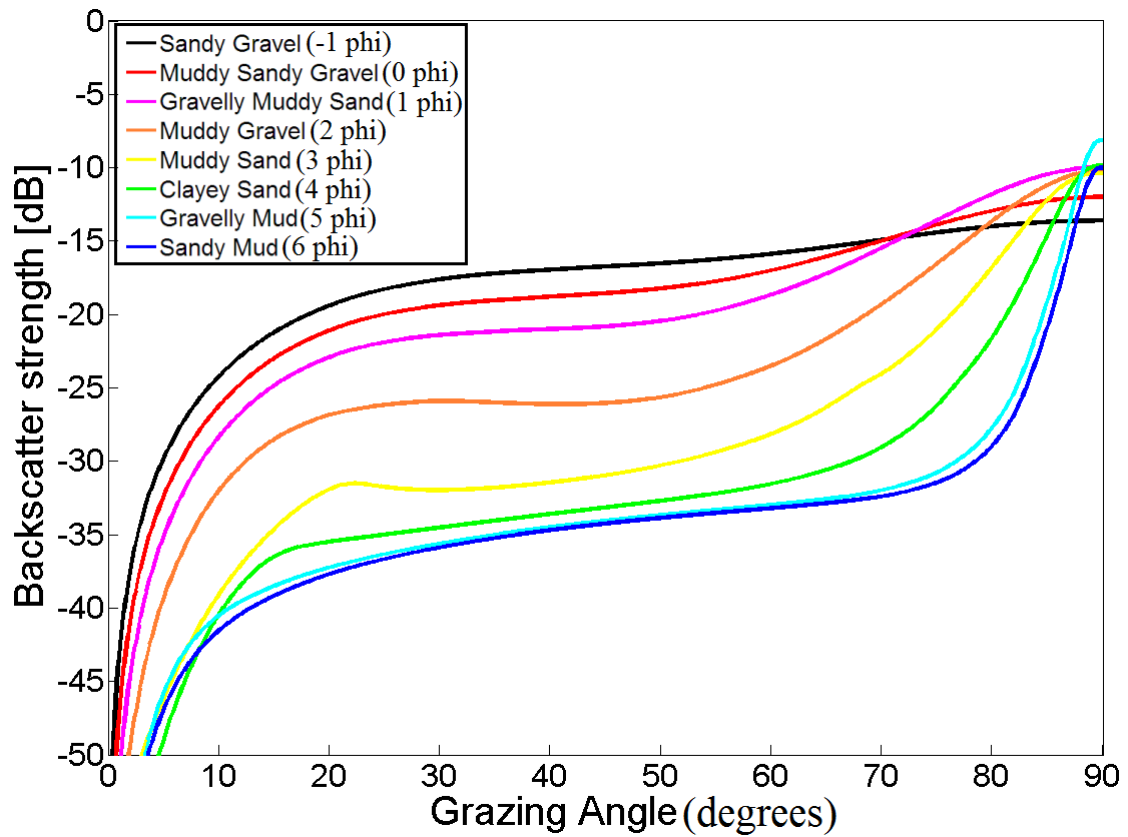


FIG. 7.4. Mean backscatter curves vs grazing angle for mean grain sizes from  $-1 \phi$  to  $6 \phi$ .

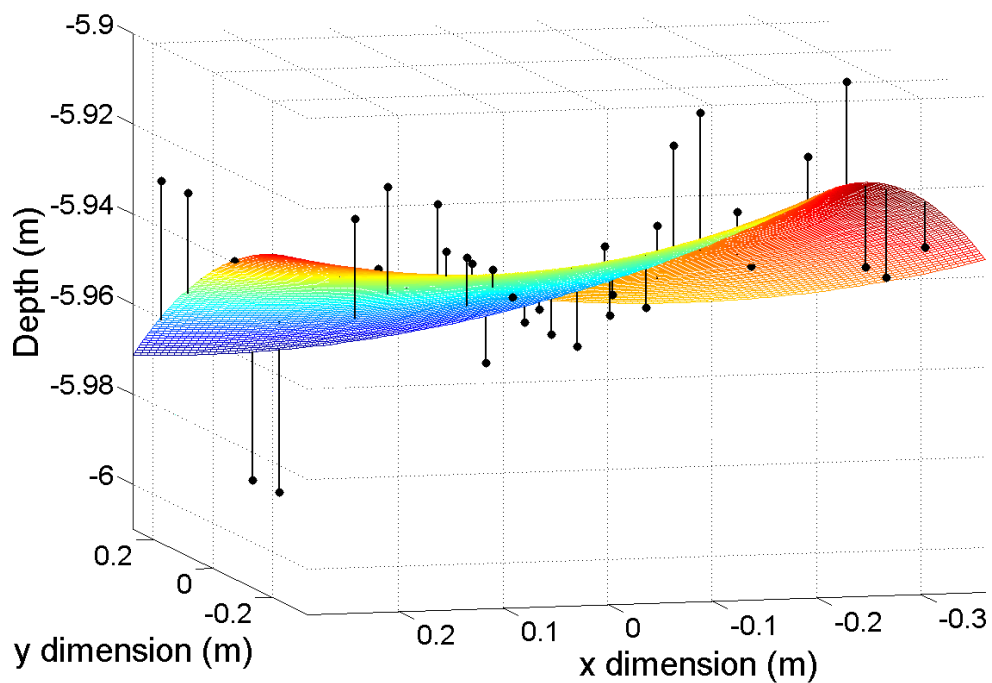


FIG. 7.5. Depth residuals (lines) between the measured depth by the sonar (dots) and the fitted surface with second order polynomial (curve).

## 7.4 Methods

Three methods were used for processing the classifiers in order to get maps of the spatial distribution of sediments on the various riverbeds. The first two methods are model based, while the other is empirical.

### A. Model-based (APL)

The method makes use of the model in Ref. 2. It uses the complete backscatter curve, i.e., the backscatter as a function of angle. The total backscatter strength is expressed as a combination of the interface roughness scattering and volume scattering. By searching for those sediment properties that result in an optimal agreement between modelled and measured backscatter curve, the sediments can be classified. In this case, the classification results consist of real sediment properties instead of acoustic classes. The model can be applied to mean grain sizes ranging from  $-1 \phi$  to  $9 \phi$ . As, often, the MBES calibration for backscatter is imperfect, a calibration step is needed to eliminate MBES induced effects on the backscatter measurements. To this end, backscatter curves measured close to locations of the grab samples are considered. The model is run for mean grain size values as determined from the grabs, and values for all other model input parameters are derived from the empirical expressions relating them to the mean grain size. The average curve of the differences (between measured and modelled curves) for all grab samples is taken as the calibration curve. The calibration curve is then applied to correct all measured backscatter curves, allowing for determination of the three parameters, that is the mean grain size, the spectral strength and the volume scattering strength, over the entire area. The differential evolution method is used for finding those parameters that minimize the differences between modelled and measured curves.

### B. Bayesian Classification Methodology (BCM)

The Bayesian Classification Methodology (BCM) was developed in Ref. 3 and carries out the classification per angle, which makes it insensitive to variations in sediment type along the swath. The method is based on the fact that the backscatter values are an average value of the sample amplitude values. Therefore, according to the central limit theorem –for independent random values– the averaged backscatter value follows a Gaussian distribution for a sufficiently large number of scatter pixels in the beam footprint. The method then fits a number of Gaussian probability density functions (PDFs) to the histogram of the backscatter strength data at a given angle until the chi-square distributed test-statistic of the residuals becomes less than a critical value. Based on the resulting Gaussian PDFs, the Bayes decision rule is applied to determine the regions of backscatter values corresponding to the acoustic classes. The number of Gaussians is then the number of classes, and the borders of the classes are the intersections of each Gaussian with its neighbour. For shallow river areas, the central limit theorem is violated since small beam footprints result in a limited number of scatter pixels per beam. To overcome this problem, the method was extended in Ref. 4. The Gaussianity of the distribution is now ensured by averaging the measured backscatter values over surface patches, consisting of a small number of beams in the across-track direction and a few pings in the along-track direction.

### C. PCA and K-means clustering

This empirical method was applied in Chapter 5 (Ref. 4). The backscatter and depth residual data are grouped into small surface patches and for each surface patch 17 statistical features are calculated: eight (mean, standard deviation, skewness, kurtosis, median, mode, minimum and maximum) extracted from the backscatter strength, eight (mean average error, standard deviation, skewness, kurtosis, median, mode, minimum and maximum) extracted from the least-squares depth residuals, and one is the total slope of the surface patch. Since the backscatter strength is angle dependent it has to be corrected. This is addressed by standardising the dataset using the method in Ref. 5. After this correction the measurements from all angles can be combined. A principal component analysis (PCA) is then applied to the above-mentioned 17 features. The idea behind PCA is that not only does it convert the set of features to a set of principal components but it can also be used to identify the most informative features among the original seventeen. By correlating the principle components to the original features it was found that for the MBES data considered, 8 out of the 17 features contain most information. These are: a) the mean, median, mode and minimum of the backscatter data and b) the mean absolute error, standard deviation, minimum and maximum of the depth residuals. The final step is to apply the K-means clustering method to partition the first two principal components (which capture more than 95% of data variability) into different subsets. The optimum number of classes is determined by calculating both the percentage in the reduction of the clusters' distance and the average silhouette coefficient when adding a new class. The K-means clustering can be applied: a) only to the backscatter features, b) only to the depth residual features, and c) to the combination of backscatter and depth residual features.

## 7.5 Results

In this section, the plot of Figure 7.2 is used as a guide to describe the classification results across the sediment mean grain size range present in the Dutch rivers.

First, we consider the results of the area with the finest sediments that is the Dordtse Kil (Chapter 4),<sup>6</sup> with mean grain sizes from  $\sim 5 \phi$  to  $\sim 0 \phi$ . The appropriate classifier was found to be the backscatter strength, since it can discriminate successfully the sediments types present on the riverbed. All three methods were used, that is the APL based, the Bayesian, and the K-means for the backscatter, all revealing a similar distribution of sediments. On the other hand, the depth residuals were found to be not a good classifier (see Appendix B), indicating that for these fine sediments, differences in mean grain sizes are not reflected in this feature.

The areas considered next are Sint Andries, Nijmegen (Chapter 5),<sup>5</sup> and the small part of Sint Andries that was resurveyed (Chapter 6).<sup>7</sup> These areas are similar with sediment mean grain sizes in the range  $\sim [0 \phi$  to  $-5 \phi]$ . This range is outside the capability of the APL model, so the model based method was not used. The Bayesian method and the K-means for the backscatter were found to capture successfully the sediment distribution in the area, except for an artificial structure in the river; the

fixed layer was not identified from the backscatter. This was achieved by using the depth residuals. Moreover when the two classifiers were combined using PCA and K-means clustering (Chapter 5),<sup>5</sup> the resulting map captures successfully the complete sediment distribution in the areas, where three sediment classes were identified from the backscatter strength and the fixed layer was shown from the depth residuals. This clearly demonstrates the increased discrimination performance by combining the two classifiers.

For all areas considered above the backscatter and the depth residuals showed consistent behaviour: with increasing mean grain size, the backscatter increases and the depth residuals decrease. When moving to the coarser areas of Bovenrijn and Meuse this behaviour reversed: the depth residuals increase and the backscatter decreases with increasing mean grain size (Chapter 6).<sup>7</sup>

## 7.6 Conclusions

The conclusions on the classification potential of the two classifiers as well as the applicability of each method for the range of sediment types encountered in the current work is presented in Figure 7.6. From  $5 \phi$  to  $-1 \phi$  the appropriate classifier is the backscatter strength and all the three methods can be used. From  $-1 \phi$  to  $\sim -3.5 \phi$  the backscatter can still be used but the depth residuals start to have discriminative potential. As the sediments become coarser the backscatter can still discriminate but its behaviour becomes unpredictable so the depth residuals are the most appropriate classifier. This is due to the fact that the mean grain size becomes gradually larger than the acoustic wavelength of the MBES ( $= -2.3 \phi$  for 300 kHz, indicated by  $\lambda$  in Fig. 7.6) so in this case acoustic scattering is determined by facets rather than grains.

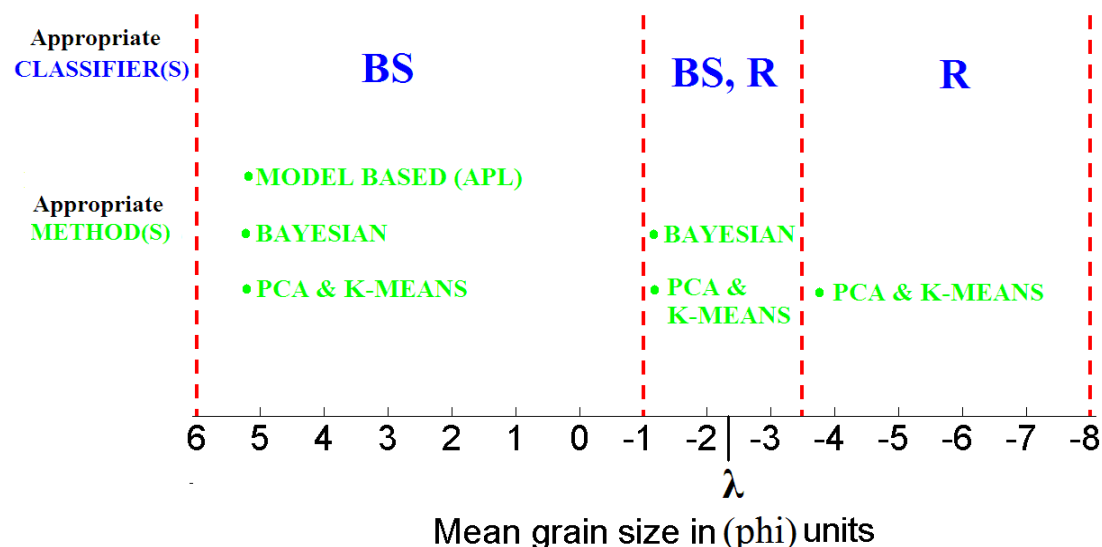


**FIG. 7.6.** Overview plot of appropriate classifier(s) and method(s) for the different mean grain size ranges.

**REFERENCES**

- <sup>1</sup> X. Lurton, “An Introduction to underwater acoustics: principles and applications”, Springer (2002).
- <sup>2</sup> “APL-UW high-frequency ocean environmental acoustic models handbook”, Technical report APL-UW TR9407AEAS 9501, Applied Physics Laboratory, University of Washington, pp. IV1-IV50, (1994).
- <sup>3</sup> D.G. Simons, M. Snellen, "A Bayesian approach to seafloor classification using multi-beam echo-sounder backscatter data", *Appl. Acoust.* 70, 1258-1268 (2009).
- <sup>4</sup> A.R. Amiri-Simkooei, M. Snellen, and D.G. Simons, “Riverbed sediment classification using multi-beam echo-sounder backscatter data”, *J. Acoust. Soc. Am.* 126, 1724-1738 (2009).
- <sup>5</sup> D. Eleftherakis, A.R. Amiri-Simkooei, M. Snellen, and D.G. Simons, “Improving riverbed sediment classification using backscatter and depth residual features of multi-beam echo-sounder systems”, *Journal of the Acoustical Society of America* 131(5), 3710-3725, (2012).
- <sup>6</sup> M.Snellen, D. Eleftherakis, A. Amiri Simkooei, R.L. Koomans, and D.G. Simons, "An inter-comparison of sediment classification methods based on multi-beam echo-sounder backscatter and sediment natural radioactivity data”, accepted for publication to *J. Acoust. Soc. Am.*, July (2013).
- <sup>7</sup> D. Eleftherakis, M.Snellen, A. R. Amiri Simkooei, D.G. Simons, “Potential of multi-beam echo-sounder backscatter strength and depth residuals as classifying parameters for very coarse riverbed sediments”, submitted to the *J. Acoust. Soc. Am.*, July (2013).

# 8

## Identifying changes in riverbed morphology and sediment composition using multi-beam echo-sounder measurements<sup>4</sup>

---

Riverbed topography and sediment composition respond to natural changes and human interventions. For the river Waal in the Netherlands, these changes affect safety against flooding, navigability and river habitat. In a part of the river Waal, close to St. Andries, multi-beam echo-sounder (MBES) measurements have been taken at two different moments in time, approximately one year apart. Two different MBES systems (still of the same type) were used for these measurements. For both datasets, grab samples are available. We present and discuss the bathymetry and sediment classification maps that have been produced after processing the two-way travel time and backscatter strength data. Only minor differences in riverbed morphology between the two different surveys are observed. Two approaches are used for assessing the presence of differences in sediment composition.

---

<sup>4</sup> This chapter is an updated version of the conference paper: *D. Eleftherakis, E. Mosselman, A.R. Amiri-Simkooei, S. Giri, M. Snellen, and D.G. Simons. "Identifying changes in river bed morphology and bed sediment composition using multi-beam echo-sounder measurements", In: Proc. of the 10th European conference on Underwater Acoustics, July 5-9, Istanbul, Turkey, 1365-1373 (2010).*

## 8.1 Introduction

Insight in the instantaneous river morphology and its dynamic behaviour is important for understanding how river channels are changing over time. This is especially true for countries like the Netherlands, where a great number of rivers are used for navigation. Therefore there is an imperative need for monitoring the morphological changes occurring in these rivers. Multi-beam echo-sounder (MBES) systems are a very promising solution to this requirement due to their high spatial coverage at limited cost. These systems have already been successfully used to measure the bathymetry of the rivers but moreover their backscatter data can be employed to obtain information about the physical properties of the riverbed.

It has been proven that both backscatter strength and bathymetric features have the potential to characterize the sediment types present on river/sea beds.<sup>1,7</sup> A special research case is when an area is revisited in order to assess changes in the morphology but also in the sediment distribution that occurred in the time interval between the surveys. Since the MBES provides high resolution bathymetry the first task is relatively straightforward and differences in morphology can be accurately determined (e.g. see Ref. 8). Using the MBES backscatter data for assessing differences in sediment distribution is in general more cumbersome. This is especially the case when the classification method discriminates between the different sediment types as acoustic classes since relating classes with sediment types pre-requires very good knowledge of the sediments present in an area. The uncertainty is reduced only if a large number of samples, or/and photographs,<sup>9</sup> and/or divers are used to assist the interpretation.

In this chapter the riverbed morphology and sediment distribution differences of a part of the Waal river (close to Sint Andries) surveyed in October 2007 and re-surveyed in November 2008 are assessed. The classification maps were constructed using the method described in Chapter 5 (Ref. 10). A combination of backscatter strength and depth residuals is used to identify the different sediment classes, including the fixed layer. Principal components analysis (PCA) is used for data reduction and the common K-means method for clustering the data. The importance of the present chapter is twofold: a) it highlights the difficulties of accurately determining changes in the sediment distribution of riverbeds when assigning sediment parameters to acoustic classes based on limited number of grab samples, and b) it provides an alternative approach for assessing the differences with more confidence.

The chapter is organized as follows. Section 8.2 gives information about the surveyed areas and the details of the surveys. In Section 8.3 the changes in the riverbed morphology are determined. Section 8.4 briefly describes the classification methodology (PCA and K-means clustering) used and presents the resulting classification maps. The different approaches for assessing the differences in sediment distribution between 2007 and 2008 are also given in Section 8.4. Finally, the main conclusions are summarized in Section 8.5.

## 8.2 A description of the surveyed area

The surveyed area is a part of the Waal River, close to Sint Andries, the Netherlands. This river carries 65% of the total flow of the Rhine and flows through the central Netherlands for about 80 km before joining a former branch of the Meuse near Woudrichem to form the Boven Merwede. It is the main transport artery between major urban and industrial areas of Germany and the port of Rotterdam. The river has a right bend at Sint Andries (km 920-930, km 0 refers to a bridge in Constance, Switzerland<sup>11</sup>). A fixed layer was constructed here in the period of January 1997 to February 1999 to improve the navigability of the river. The fixed layer has a width of 140 m and a length of 3100 m. Its 0.8 m thick top layer consists of stones with sizes from 70 to 260 mm. The surveyed area involved the part of St. Andries from km 927 to km 930, as shown in Fig. 8.1. The fixed layer is indicated with the blue rectangle.

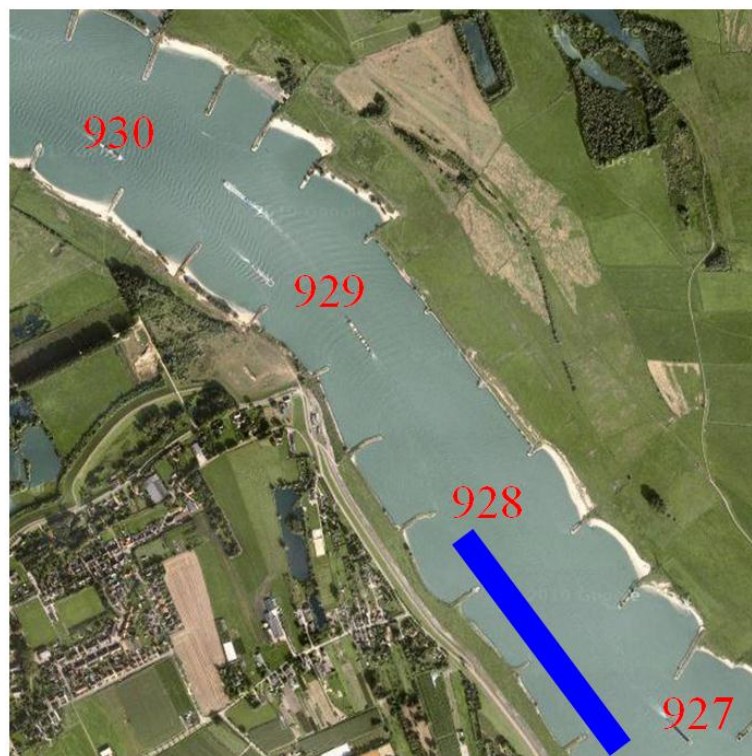


**FIG. 8.1.** Aerial photo of the surveyed part of the Waal river close to Sint Andries. The fixed layer is indicated with the blue rectangle.

The second survey took place on 10 and 12 November 2008, when the part between km 927 to 930 was resurveyed. The first survey took place in October 2007 when the whole area of the Waal river, close to St. Andries (km 920 – 930), was surveyed. The part corresponding to the second survey was surveyed in 22 October 2007. For both measurements a Kongsberg EM3002 single-head multi-beam echosounder was used. All beams were electronically stabilized for pitch and roll. The operation frequency was 300 KHz and the maximum number of beams (of equidistant pattern) per ping was 254. The difference between the two surveys was on the maximum angular coverage. It was 130° (from -65° to 65°) in 2007, and 120° (from -60° to 60°) in 2008.

For assisting the interpretation of the classification results, physical grab samples were taken from the surveyed areas. The number of grab samples in 2007 was limited to only five. Figure 8.2 shows the histogram of mean grain sizes for 2007 and 2008 as derived from the grab samples in phi [ $\phi$ ] units. The location of the grab samples on the map of the area is presented in Fig. 8.3. It can be seen that the grab samples were taken in different locations in 2007 and 2008. Furthermore, the grab samples in 2008 are per three located very close to each other with three of them located inside the scour hole behind the fixed layer (see Figure 8.4).

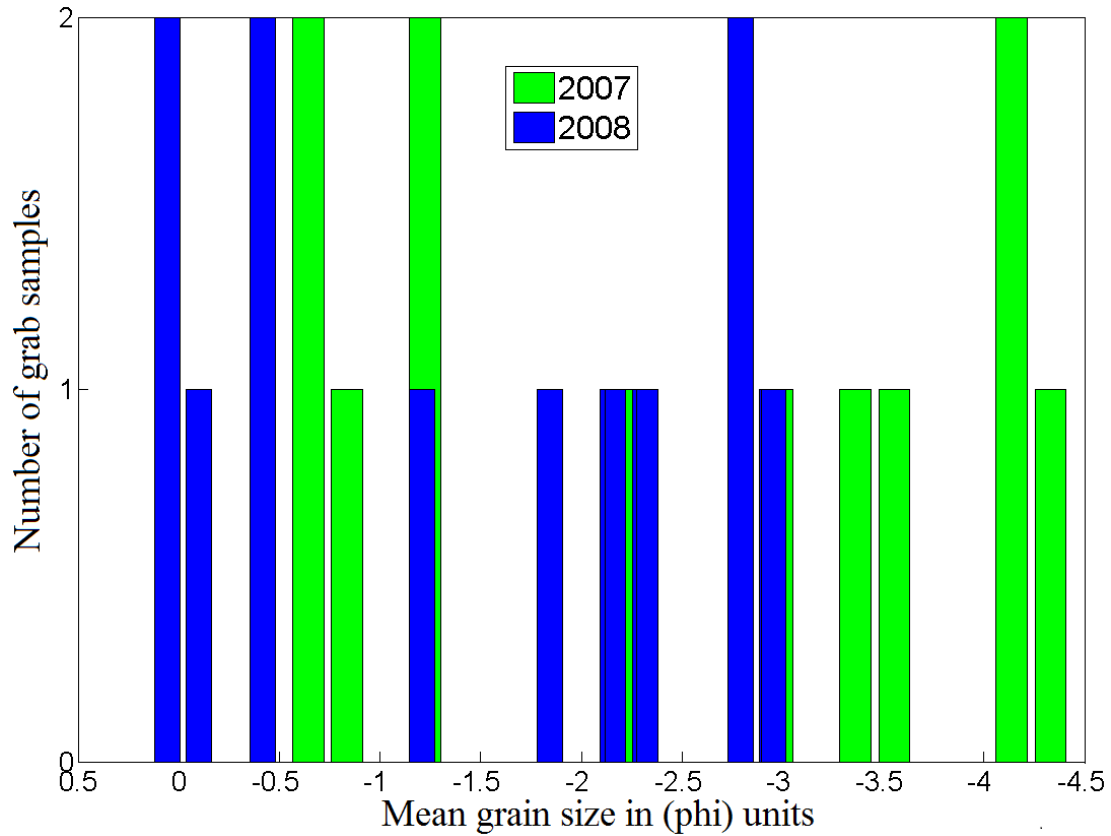


**FIG. 8.2.** Histogram of grab samples mean grain sizes in 2007 (green) and 2008 (blue).

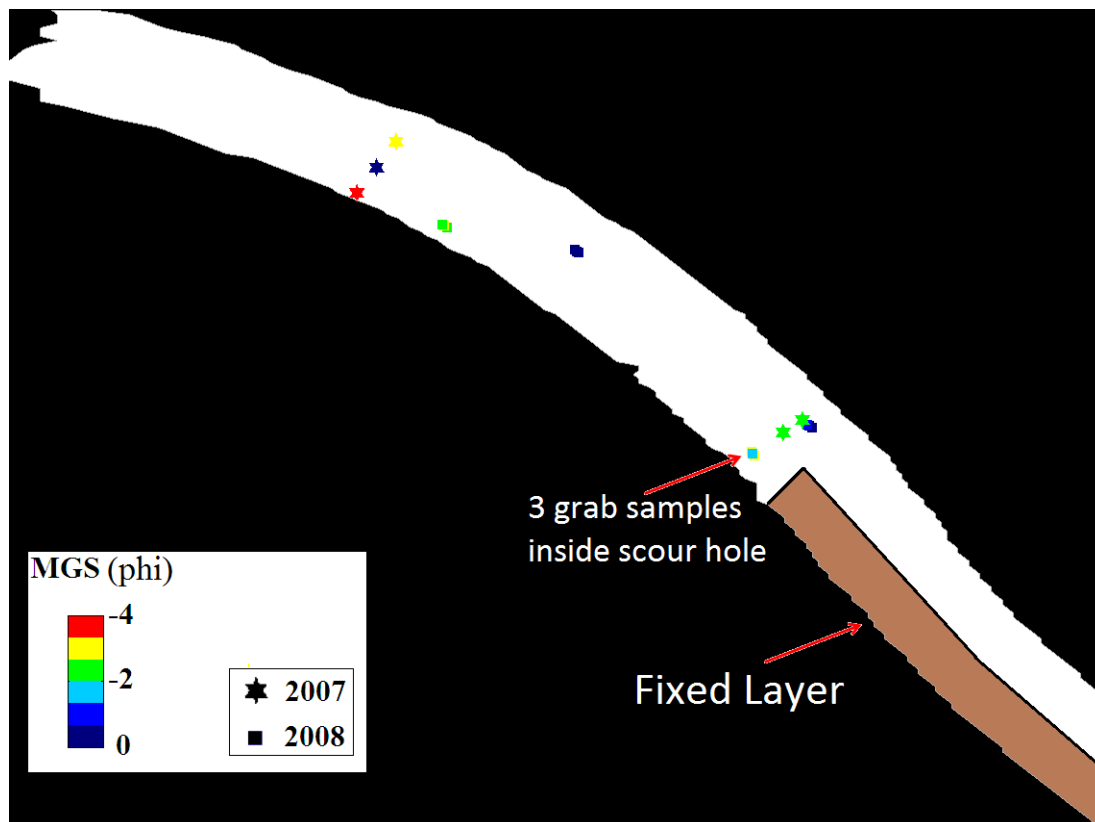


**FIG. 8.3.** Location of the grab samples taken in 2007 (stars) and 2008 (squares) on the map of the area. Colours indicate the grab samples' mean grain size.

### 8.3 Determining changes in riverbed morphology

The two bathymetry maps derived from the MBES measurements are shown in Figure 8.4. The resolution of the maps is 20 cm x 20 cm. A first comparison might suggest that the area was different in 2008. However, this conclusion would be unfounded without checking the water level during the two periods, since the sonar provides depth values with respect to the water surface rather than elevation values with respect to a predefined datum.

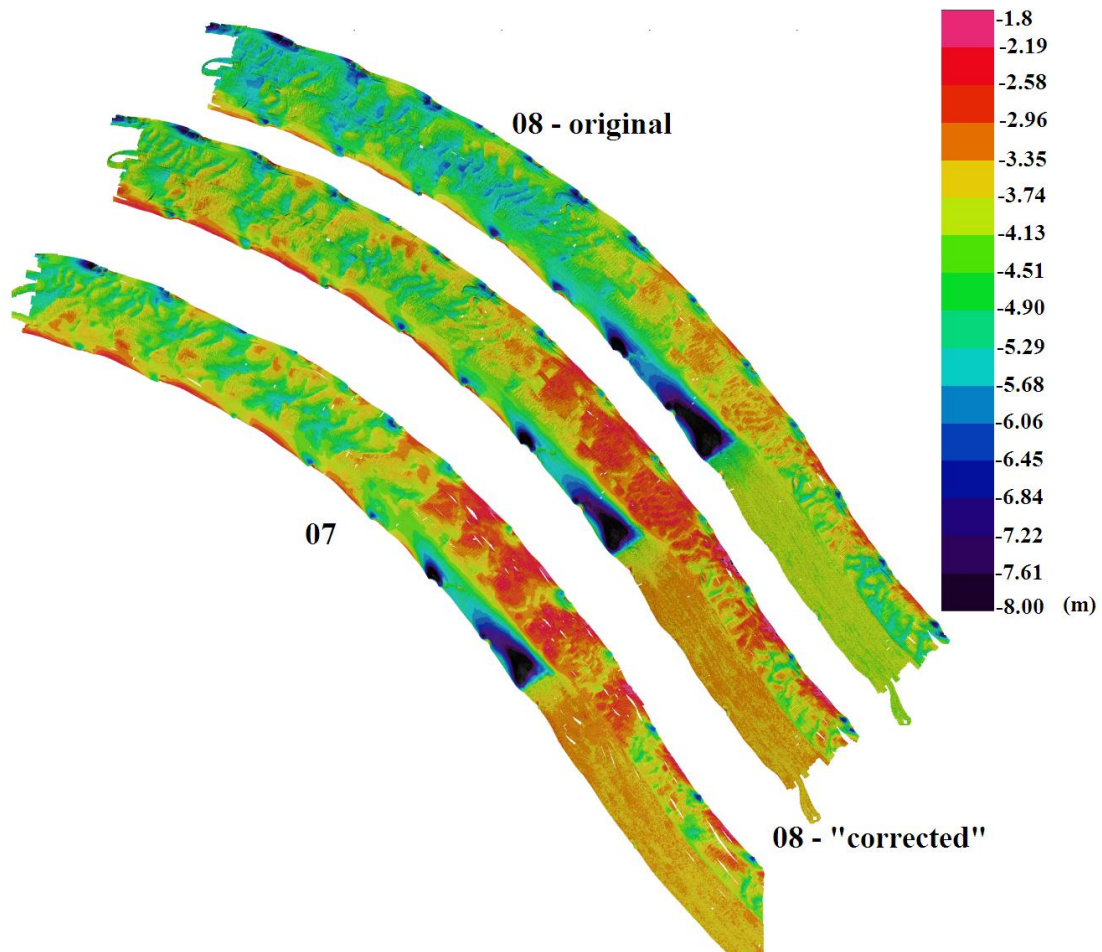


**FIG. 8.4.** Bathymetry maps in 2007 (07) and 2008 (08-original), where depths are relative to the water surface. The map indicated by “08-corrected” provides the depths of the 2008 survey relative to the 2007 water level.

We used water level data from the Tiel gauge station at a distance of about 12 km upstream. The water level (averaged value) was 330 cm NAP on 22 October 2007 and 413 cm on 10 and 12 November 2008. Subsequently, we used the calibrated 1D Sobek model of the Rhine branches to deduce the corresponding water levels at St. Andries. The Sobek runs were made for the flow conditions observed during the two surveys. A constant discharge at the upstream boundary and tidal-averaged water levels at downstream boundaries were imposed (based on observation data). The water level for the two years is presented in Fig. 8.5.

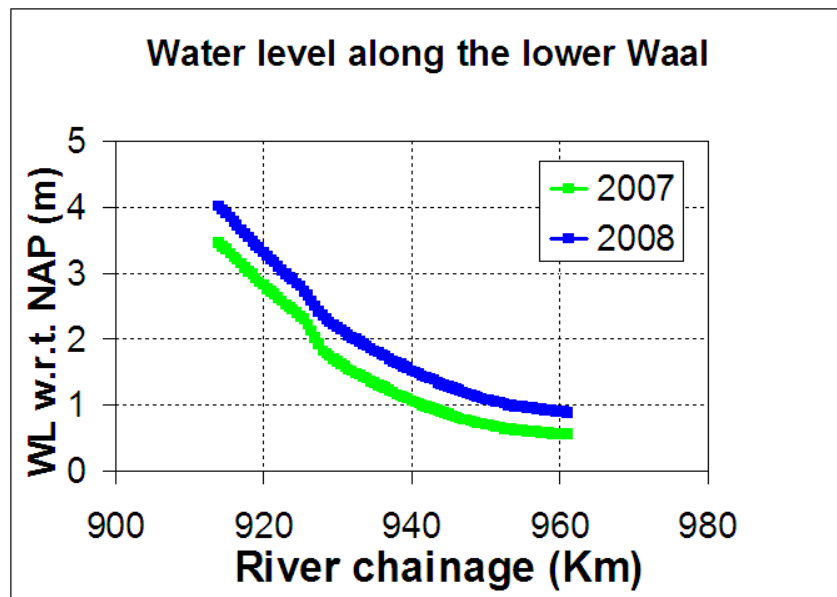


**FIG. 8.5.** Water level of lower Waal for 2007 and 2008.

From Fig. 8.5 it was calculated that the water level at Tiel was 55 cm higher in 2008, while the water level at St. Andries was 52 cm higher in 2008. By extrapolating the information for the water levels from the gauge station at Tiel and the Sobek model (at Tiel and at St. Andries) it was calculated that the water level at St. Andries was higher in 2008 by approximately 78 cm.

Therefore, for proper comparison of the bathymetry maps of 2007 and 2008, we subtract 78 cm from the depth measurements of 2008 and the “corrected” map is also presented in Fig. 8.4. The new comparison reveals that the morphology of the riverbed in 2007 and 2008 is very similar, with small differences that can be ascribed to moving bedforms on the riverbed.

## 8.4 Determining changes in the sediment distribution

The classification methodology applied is the method of Chapter 5 (Ref. 10) where the whole area of Sint Andries was analysed. In the current chapter only part of the Sint Andries data, acquired in 2007, and all data of 2008 is analysed.

The data was first grouped in small surface patches of approximately 0.5 m x 0.5 m by averaging 7 pings by 8 beams together in order to reduce the noise in the data. For each surface patch 8 statistical features (mean, standard deviation, skewness, kurtosis, median, mode, minimum and maximum) were calculated for the backscatter strength and 8 (mean absolute error, standard deviation, skewness, kurtosis, median, mode, minimum and maximum) for the depth residuals. Also the slope of the patches is used as a feature, resulting in 17 features in total. Since the backscatter is angle dependent and the range of values of the features is different it was necessary to standardise the data according to the method as described in Chapter 5.

For all features their potential in discriminating between the different sediments was assessed. Hereto a principal component analysis was applied on the standardised features. Then each one of the features was correlated to the first three principal components that account for 75% of the data variability. From this correlation 4 backscatter and 4 depth residual features were identified as the most informative ones. These are: a) the mean, median, mode and minimum of the backscatter data and b) the mean absolute error, standard deviation, minimum and maximum of the depth residuals.

The top frame of Fig. 8.6 shows the maps based only on the 4 backscatter features. The bottom frame shows the classification maps resulting after combining the 4 backscatter with the 4 depth residual features. In both cases the first two principal components were used and the different classes (sediment types) were determined using the K-means clustering method. The optimum number of classes was determined by checking the percentage in the reduction of the distances of the clusters, and the average silhouette coefficient. (For the classification based on depth residuals only two classes are found in the area outside the fixed layer. This lower discrimination performance is expected from Chapter 6 for this area with intermediate mean grain sizes. Therefore these results are not considered further in this chapter).

From Fig. 8.6 it can be seen that the maps derived from backscatter and from combining backscatter and depth residuals are almost identical except the region where the fixed layer is located. The fixed layer in the combined plots results from the contribution of the depth residual features on the classification.

By comparing the classification maps for 2007 with those for 2008 it seems that the sediments in the area remained almost unchanged. This conclusion can be misleading since the maps are referring to classes which do not constitute common ground for comparison. For example class 1 in 2007 can belong to a different sediment type than class 1 in 2008. Therefore, classification maps that present classes cannot be compared directly. In the following two sub-sections two approaches are used for overcoming this problem.

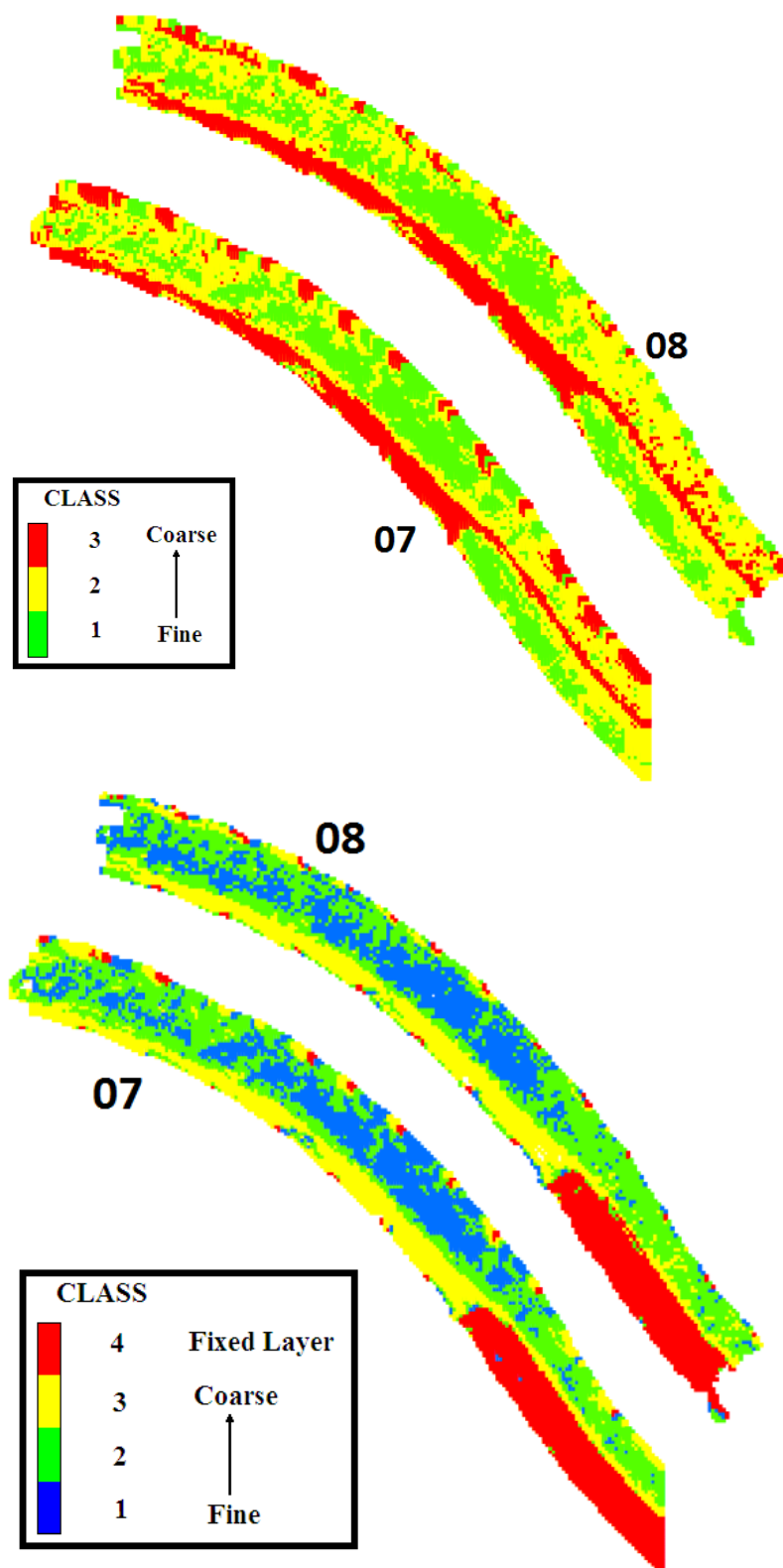


**FIG. 8.6.** Classification maps for Sint Andries 07 & 08 from only the backscatter features (top), and the combination of backscatter and depth residual features (bottom).

### 8.4.1 Changes based on grab samples

The first approach is to assign mean grain size values to each of the classes using the availability of the grab samples. This can be achieved by correlating the classes derived from the MBES classification to mean grain sizes from the grab samples and then determine the best linear fit using the least squares method.

A sample is usually located in an area where surface patches of various classes are present. The approach taken is to assign to each grab sample the average class of all surface patches located within a radius of 50 metres from it. The results for 2007 and 2008 are presented in Figure 8.7. The estimated Pearson correlation coefficients are -0.66 and -0.94 for 2007 and 2008, respectively.

The relations found between classes and mean grain sizes are as follows:

$$x = \frac{1.0405 - y}{0.2990} \text{ in (2007)} \quad (8.1)$$

$$x = \frac{1.2440 - y}{0.6844} \text{ in (2008)} \quad (8.2)$$

with  $x$  the mean grain size in  $\phi$  units, and  $y$  the class.

By applying these relations, the mean grain size values that correspond to classes one to three of Figure 8.6 are presented in Table 8.1. By comparing the values it can be concluded that the river in 2008 has substantially finer sediments in 2008 compared to 2007. The difference is so large that it could be explained only if an extraordinary event had happened in 2008, e.g. a flood. However, from investigating the river flow conditions no indication for such an event is found. It is concluded that the large difference is likely to result from the limited number of samples used for the correlations, inducing large uncertainties in the coefficients of Equations (8.1) and (8.2).

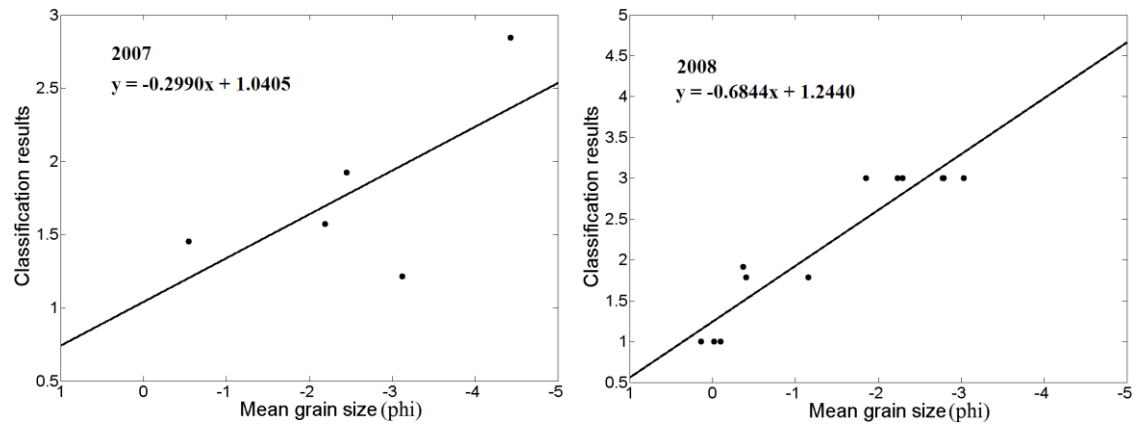


**FIG. 8.7.** Mean grain size of individual samples versus classification results for (left) 2007 and (right) 2008.

**TABLE 8.1.** Mean grain for the sediment classes of 2007 and 2008 as derived from Equation (8.1) and (8.2) respectively.

	<b>Sint Andries 2007</b>	<b>Sint Andries 2008</b>
	(phi)	(phi)
<b>Class 1</b>	0.13	0.35
<b>Class 2</b>	-3.20	-1.10
<b>Class 3</b>	-6.55	-2.56

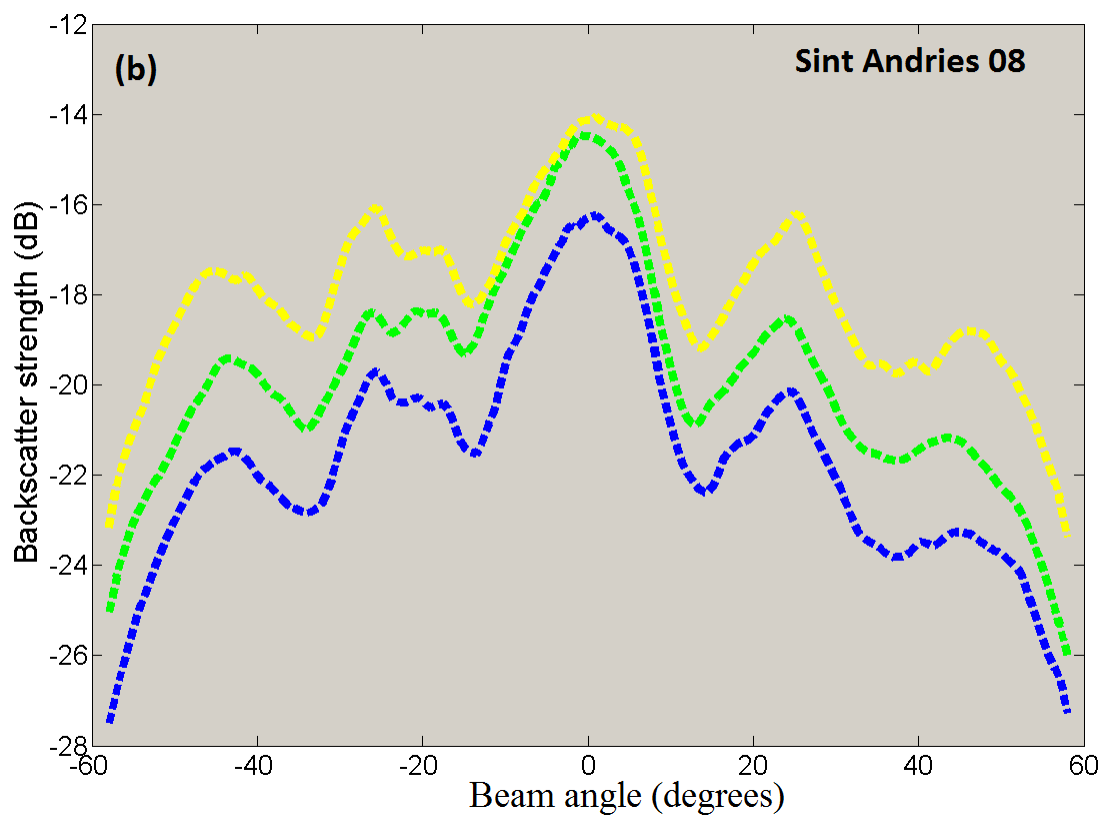
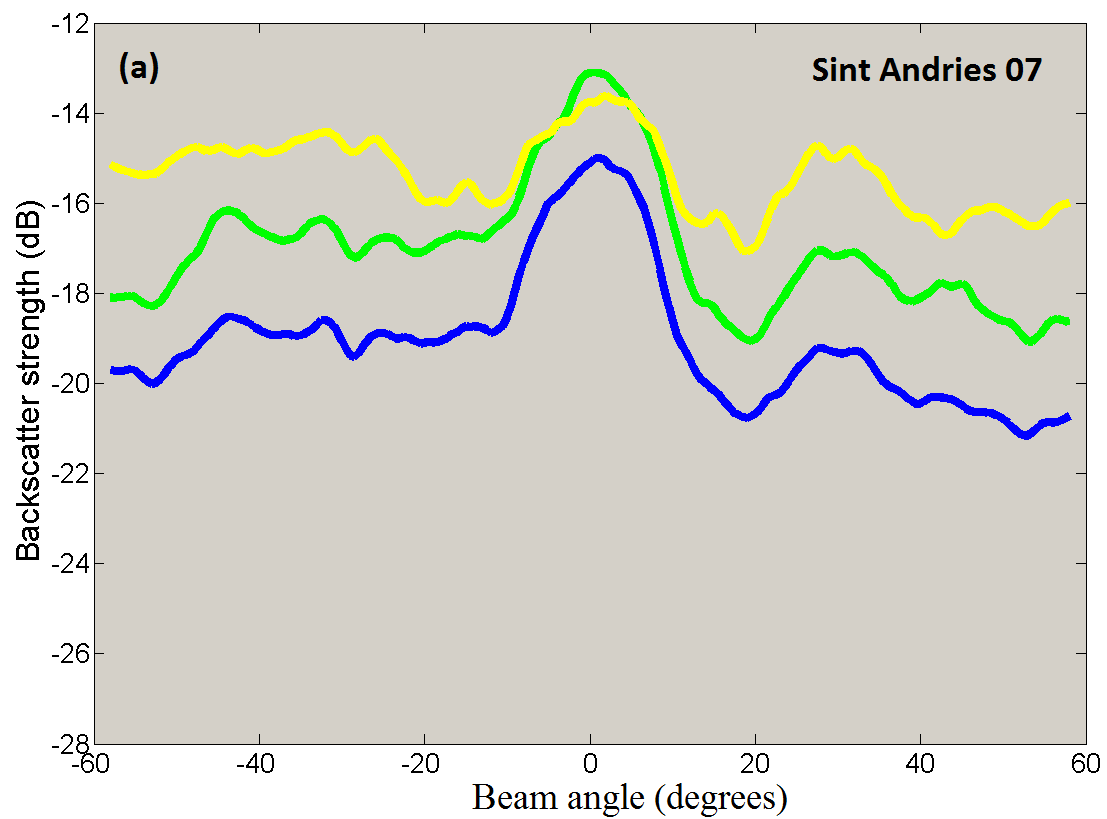
### 8.4.2 Changes based on backscatter values

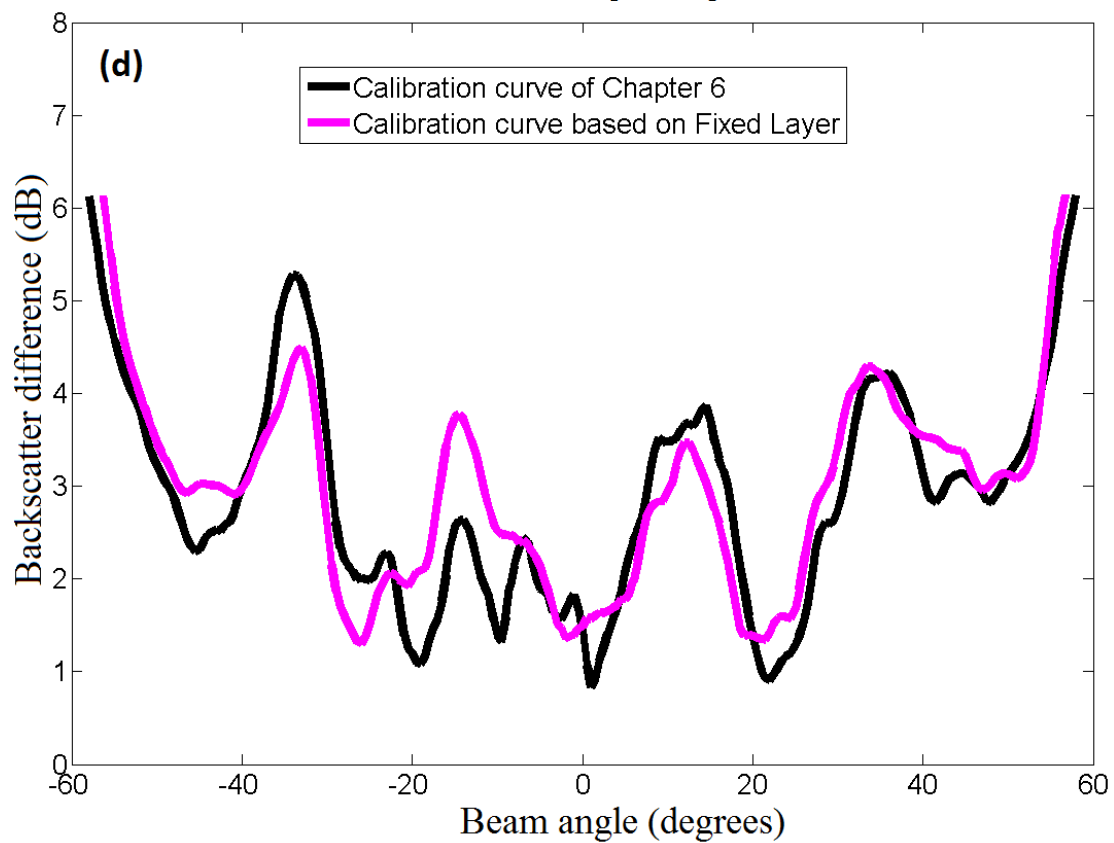
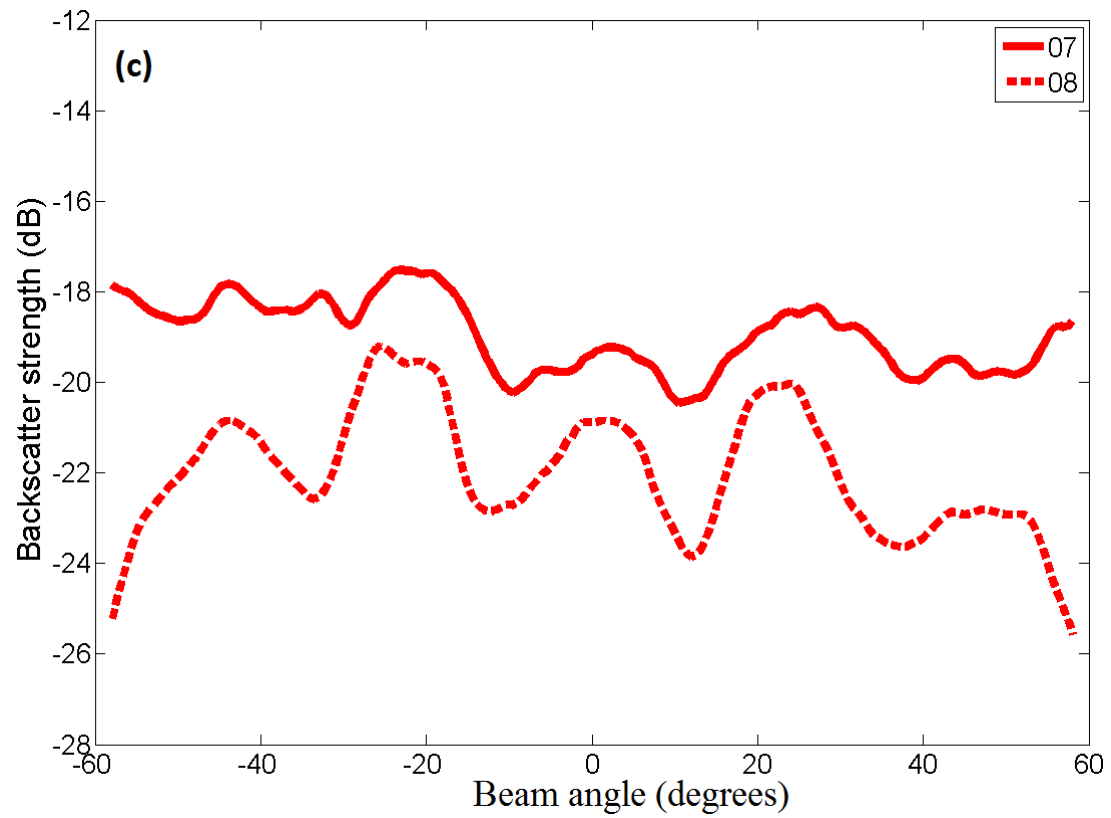
As a second approach the potential differences between the sediments present in the two subsequent years are assessed without making use of the grab samples. Instead, differences are assessed by looking at the measured backscatter values, since these values are known to be indicative for the sediment types. The approach taken is to determine for each of the classes the backscatter curve i.e. backscatter strength as a function of angle.

These are determined as follows: 50 locations were selected for each of the classes on the classification maps of Figure 8.6. For each of the 50 locations, the backscatter strength per angle i.e. the backscatter curve was determined. These 50 curves per class were then averaged. The procedure is the same as the calibration procedure of Chapter 6.

By comparing the backscatter curves for 2007 (Fig. 8.8a) and 2008 (Fig. 8.8b) it can be seen that not only there is a difference in the backscatter values between 2007 and 2008 but also the shape of the curves is different. This is due to the imperfect calibration of the MBES used for the surveys with respect to the backscatter strength. To counteract this, the measured backscatter strength needs to be calibrated. For this, use is made of the backscatter measurements taken on the fixed layer, where it is assumed that no changes in sediment type have taken place from 2007 to 2008. The backscatter curves on the fixed layer for 2007 and 2008 are shown in Fig. 8.8c. Then their difference is calculated and it is used as a calibration curve to shift the 2007 backscatter values, allowing for comparing them with the values in 2008. The calibration curve (magenta) is presented in Fig. 8.8d, where also the calibration curve (black) of Chapter 6 is plotted for comparison. The calibration curve of Chapter 6 resulted from a completely different approach as it is based on the use of “similar grab samples” between Sint Andries and Bovenrijn. The two calibration curves are very close, giving confidence in their applicability.

Figure 8.8e presents the calibrated backscatter curves of 2007 and the original backscatter curves of 2008. We conclude that the classes of 2007 and 2008 correspond to similar sediments, since the calibrated backscatter curves of 2007 and the original backscatter curves of 2008 are very close. Therefore, the classification maps in Fig. 8.6 of 2007 and 2008 can be directly compared. It is apparent that the maps are very similar so the area remained almost unchanged except small changes that can be ascribed to moving bedforms.





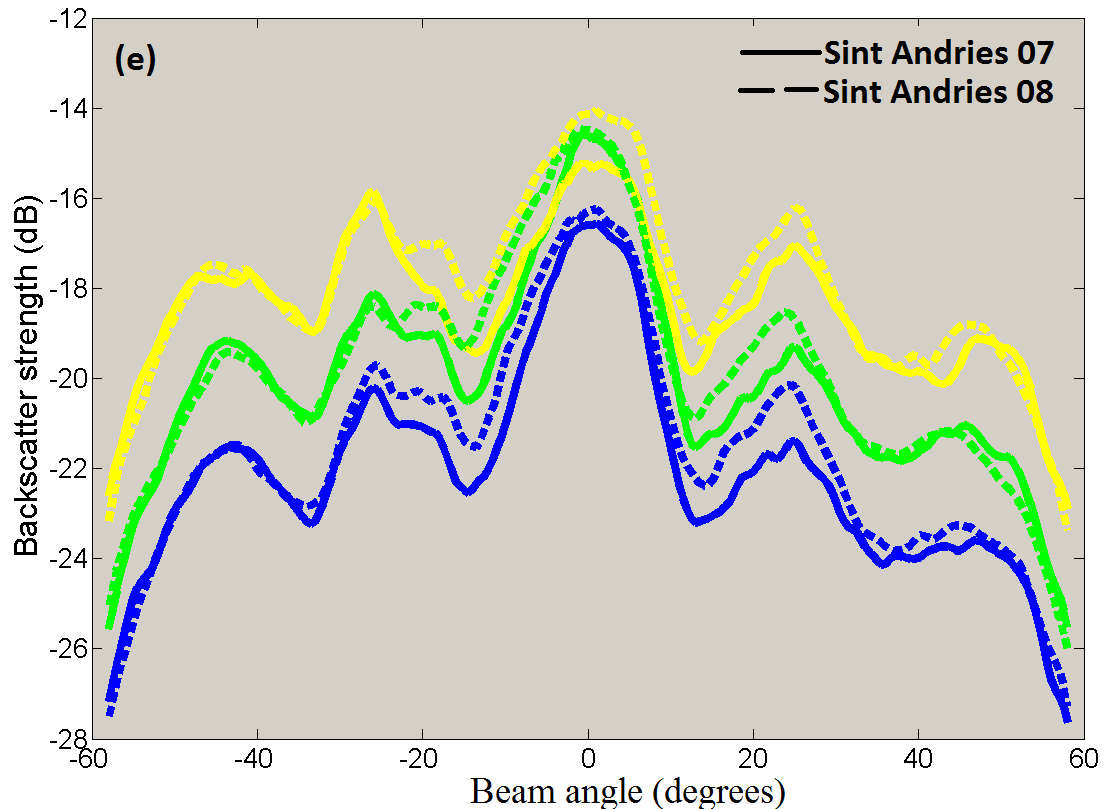


**FIG. 8.8.** (a) Mean backscatter curves of the three classes identified in Sint Andries in 2007, (b) Mean backscatter curves of the three classes identified in Sint Andries in 2008, (c) Mean backscatter curves on the fixed layer of the area in 2007 and 2008, (d) Calibration curves from (black) Chapter 6 and (magenta) present procedure, (e) Combined plot of the mean backscatter curves in (solid line) 2007 and (dashed line) 2008 after calibration.

## 8.5 Conclusions

In this chapter the differences in a river that was surveyed twice, using MBES systems were evaluated both regarding the riverbed morphology and the sediment distribution. The time interval between the surveys was one year.

Regarding the riverbed morphology the critical point was to correct the bathymetry for the different water levels in the two periods since MBES systems provide depth measurements with respect to the water level. The final bathymetry maps after the correction revealed minor morphological differences between 2007 and 2008.

The classification method of Chapter 5 was used for classifying sediments in the area based on: a) the backscatter strength, and b) the combination of backscatter and depth residuals. The method provides acoustic classes, hampering a direct comparison between the sediments present in the area in 2007 and 2008, respectively. To overcome this problem two approaches were used. The first was to correlate the classification results with the mean grain size of the grab samples taken during the surveys and use the resulting relations to convert classes to mean grain size values.

This approach indicated that the area has become significantly finer in 2008. Since the flow conditions both in 2007 and 2008 were similar and no extreme events had happened, the difference in sediment mean grain sizes between the two years is attributed to the limited number of available grab samples. The second approach was to determine the backscatter curves for the classes 1 to 3. For this, the backscatter values were calibrated based on the fixture present in the area that is expected to remain unchanged with time, the fixed layer. The results of this approach showed that the area in 2007 and 2008 remained almost unchanged.

## REFERENCES

- <sup>1</sup> P. Blondel and O. Gomez Sichi. "Textural analyses of multibeam sonar imagery from Stanton Banks, Northern Ireland continental shelf", *Applied Acoustics*, 70, 1288-1297 (2009).
- <sup>2</sup> M. Augustin, R. Le Suave, X. Lurton, M. Voisset, S. Dugelay, and C. Satra. "Contribution of the multibeam acoustic imagery to the exploration of the sea bottom". *Marine Geophysical Researches* 18 (2-4), 459-486 (1996).
- <sup>3</sup> B. Chakraborty, H.W. Schenke, V. Kodagali, and R. Hagen. "Seabottom characterization using multibeam echosounder angular backscatter: An application of the composite roughness theory". *IEEE transactions on geoscience and remote sensing*, 38 (5), Sept. (2000).
- <sup>4</sup> J.M. Preston. "Automated acoustic seabed classification of multibeam images of Stanton Banks", *Applied Acoustics* 70 (10), 1277-1287 (2009).
- <sup>5</sup> D.G. Simons, and M. Snellen. "A Bayesian approach to seafloor classification using multi-beam echo-sounder backscatter data", *Appl. Acoust.* 70, 1258-1268 (2009).
- <sup>6</sup> A.R. Amiri-Simkooei, M. Snellen, and D.G. Simons, "Riverbed sediment classification using multi-beam echo-sounder backscatter data", *J. Acoust. Soc. Am.* 126, 1724-1738 (2009).
- <sup>7</sup> I. Marsh and C. Brown. "Neural classification of multibeam backscatter and bathymetry data from Stanton Bank (Area IV)", *Applied Acoustics* 70 (10), 1269-1276 (2009).
- <sup>8</sup> P.L. Manley and J.K. Singer, "Assessment of sedimentation processes determined from side-scan sonar surveys in the Buffalo River, New York, USA", *Environ Geol* 55, 1587-1599 (2008).
- <sup>9</sup> J.M. Preston, D.R. Parrot, and W.T. Collins, "Sediment Classification Based on Repetitive Multibeam Bathymetry Survey of an Offshore Disposal Site", in *Proceedings IEEE OCEANS 2003*, San Diego California, 22-26 Sept. MTS document 0-933957-31-9, 69-75 (2003).
- <sup>10</sup> D. Eleftherakis, A.R. Amiri-Simkooei, M. Snellen, and D.G. Simons, "Improving riverbed sediment classification using backscatter and depth residual features of multi-beam echo-sounder systems", *Journal of the Acoustical Society of America* 131(5), 3710-3725, (2012).
- <sup>11</sup> International Committee of the hydrology of the Rhine basin (CHR), *Hydrological monograph*, The Hague, The Netherlands, (1977).

# 9

## Conclusions and outlook

---

The Dutch rivers are heavily used for navigation. For safe navigation a minimum river depth has to be ensured by taking measures such as suppletions of coarse sediment. For monitoring the effectiveness of these measures, regular measuring campaigns are carried out. Multi-beam echo-sounder (MBES) systems are used for determining the bathymetry in the areas. Grab samples of the sediments are taken to assess the spatial distribution of sediment types. The efficiency of these monitoring surveys can be highly increased if, in addition to bathymetry, the MBES system can also be used for classifying the river bed sediments. In this thesis methods have been developed that allow for classifying the river sediments using the MBES measurements. The methods employ the sediment backscatter strength, derived from the measured echo intensities, supported by the MBES bathymetric measurements, i.e. the depth residuals. The depth residuals are the variations in bathymetry relative to a plane fitted through the MBES measured bathymetry and are a measure for the sediment roughness. To assess the advantages and limitations of the classifiers, i.e. backscatter and depth residuals, six parts of various Dutch rivers, spanning a large range of sediment types, were surveyed during a period of 4 years, using multi-beam echo-sounder (MBES) sonars operating at 300 kHz. Physical grab samples were also taken from the rivers to assist the classification. This work has demonstrated the applicability of acoustic remote sensing methods using MBES measurements for classifying Dutch rivers' sediments. It has identified the strengths and limitations of the various acoustic classification methods, given the characteristics of the area of interest. Employing this knowledge allows for selecting for each area the optimal acoustic classification method. In the remainder of this chapter conclusions are presented for each of the chapters separately, ending with recommendations for future work.

## 9.1 Conclusions

### 9.1.1 Conclusions from Chapter 4, the finer sediments

The measurements considered in this chapter were taken in the Dordtse Kil area, which has the finer sediments (see Fig. 9.1). The fine grained sediments allow for applying a model-based approach where the measured backscattered curves (i.e. backscatter strength vs. angle) are compared with modelled backscatter curves. Model input parameters that provide a maximum match between modelled and measured curves are considered as the true sediment parameters. The other MBES classification method (called Bayesian) is also model based and also makes use of the measured backscatter strengths. However, here the backscatter strengths are considered per MBES beam and are modelled as a Gaussian distributed random variable per sediment type. The MBES measurements were supported not only with grab samples but also with measurements taken from the Medusa system. The Medusa system measures sediment radioactivity, known to be indicative for sediment properties.

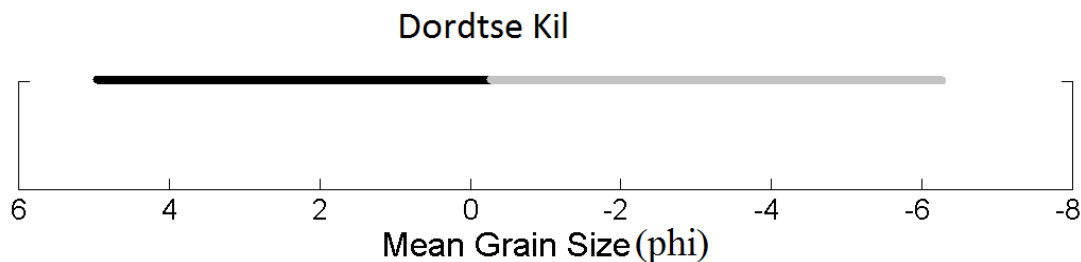


**FIG 9.1:** Range of mean grain size values at Dordtse Kil river (black line). The grey line indicates the full range of sediment mean grain sizes encountered during all surveys considered in this thesis.

The main conclusions are:

- The Bayesian method provides acoustic classes, and its implementation is relatively straightforward. On the other hand grab samples are necessary to assign sediment parameters to the acoustic classes. The limit of this conversion is demonstrated by comparing the Bayesian classes with the model based results, i.e., mean grain size ( $M_z$ ), spectral strength ( $w_2$ ) and volume scattering parameter ( $\sigma_2$ ). It is shown that the mean grain size is the most important parameter that can be attributed to the different classes. However, also the other parameters  $w_2$  and  $\sigma_2$  affect the acoustic classes. This indicates the limitations of using only grab sample-based mean grain size for assigning sediment parameters to the acoustic classes.
- Implementation of the model-based method requires calibration of the measured backscatter curves, i.e. accounting for the imperfect calibration of the MBES with respect to backscatter strength. The advantage of this method is that the results are physical parameters of the sediments. An overestimation of  $M_z$  values is found, indicating imperfect calibration of the backscatter

values due to the limited number of grab samples. In addition, imperfect modelling of the backscatter curve can play a role. Current understanding of the backscattering process at sediments with grain sizes  $> -1 \phi$  is well developed, reflected in well validated models.

- The Medusa system provided estimates of the mean grain size based on the concentrations of  $^{40}\text{K}$  and estimates for the silt content based on  $^{40}\text{K}$  and  $^{232}\text{Th}$ . Furthermore, concentrations of  $^{137}\text{Cs}$  were used as a predictor for the fraction of organic matter. The noise levels measured with a hydrophone attached to the Medusa system and towed on the riverbed provided a measure for the roughness of sediments. The Medusa system and the MBES are partly complementary where Medusa can quantify the presence of organic matter based on the  $^{137}\text{Cs}$  measurements.

### 9.1.2 Conclusions from Chapter 5, intermediate grain size sediments

For the Sint Andries and Nijmegen areas, which have intermediate sediments (see Fig. 9.2), a combination of backscatter and depth residuals features was used for discriminating between the different sediments.

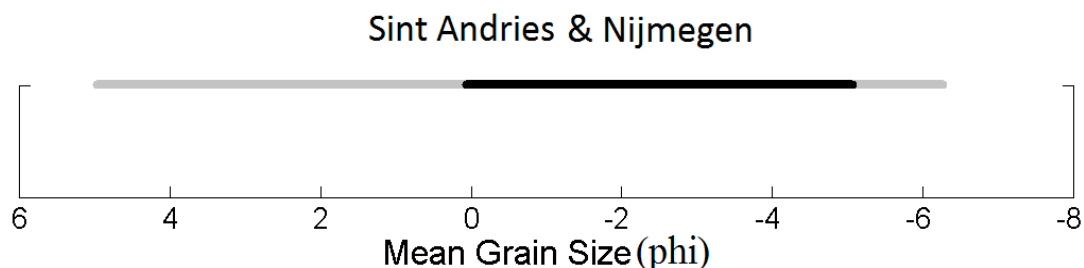


**FIG 9.2:** Range of mean grain size values at Sint Andries and Nijmegen (black line). The grey line indicates the full range of sediment mean grain sizes encountered during all surveys considered in this thesis.

The main conclusions are:

- The Bayesian method can be applied and is capable of discriminating between three different sediment types.
- The other method used for classifying the sediments in the area bases the classification both on measurements of the backscatter strength, but also on the depth residuals. The combination of backscatter strength and depth residuals is achieved by using principal component analysis (PCA) to remove feature inter-dependency and the K-means clustering method to assign feature ranges to the different sediment types.
- Only when the two classifiers were combined (backscatter and depth residuals) using PCA and K-means clustering the resulting map captures successfully the complete sediment distribution in the areas. That is the three sediment types plus the fixed layer, a man-made structure consisting of large

stones. This clearly demonstrates the increased discrimination performance by combining the two classifiers.

- The three sediment classes (finer material) were identified from the backscatter strength, whereas the fixed layer (coarser material) was identified from the depth residuals.

### 9.1.3 Conclusions from Chapter 6, the coarsest sediments

For the Bovenrijn and Meuse areas, which have coarse and very coarse sediments (see Fig. 9.3), the backscatter and depth residuals features were used separately for classifying the sediments in the areas.

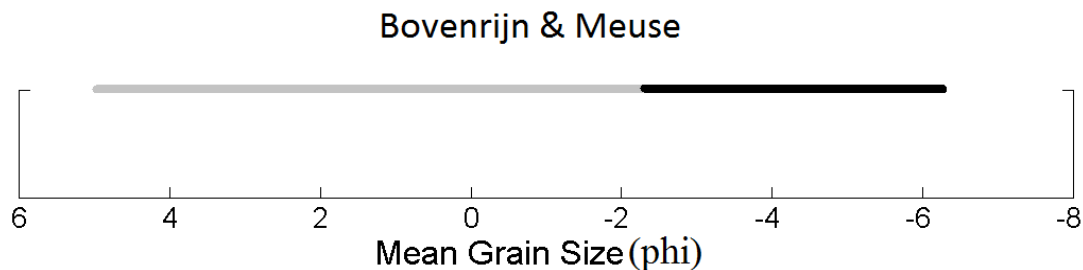


**FIG 9.3:** Range of mean grain size values at Bovenrijn and Meuse (black line). The grey line indicates the full range of sediment mean grain sizes encountered during all surveys considered in this thesis.

The main conclusions are:

- Both the backscatter strength and the depth residuals have the potential to discriminate the different sediment types in these very coarse areas.
- For the areas with finer and intermediate sediments, the backscatter and the depth residuals showed consistent behaviour: with increasing mean grain size, the backscatter strength increases and the depth residuals decrease. When moving to the coarser areas this behaviour reversed. The depth residuals increase and the backscatter strength decreases with increasing mean grain size.

The classification results from Sint Andries, part of Sint Andries 08, Bovenrijn, and Meuse were combined to determine the value of the mean grain size point at which the behaviour of the backscatter strength and depth residuals start to change. Since different MBES systems, although of the same type, were used for the surveys a calibration step is needed to account for the imperfect MBES calibration. The classification results based on the backscatter features were combined after calibrating the backscatter values of the areas.

The main conclusion is:

- The transition point is determined to be approximately  $-3.5 \phi$ . There, the mean grain size becomes gradually larger than the acoustic wavelength of the sonar ( $\lambda=5$  mm, corresponding to  $-2.3 \phi$  for 300 kHz). In this case acoustic scattering is determined by facets rather than grains.

### 9.1.4 Conclusions from Chapter 7, overview of classifiers and methods

In this chapter, all research outcomes of the previous chapters are combined in order to establish an overview of the applicability of the methods to the various river environments encountered. The classifiers are the backscatter strength and the depth residuals. The methods are: the Bayesian, the model-based, and the PCA & K-means.

The result is displayed in Fig. 9.4. This schematic can be used for selecting for each river environment the most suitable classification approach.

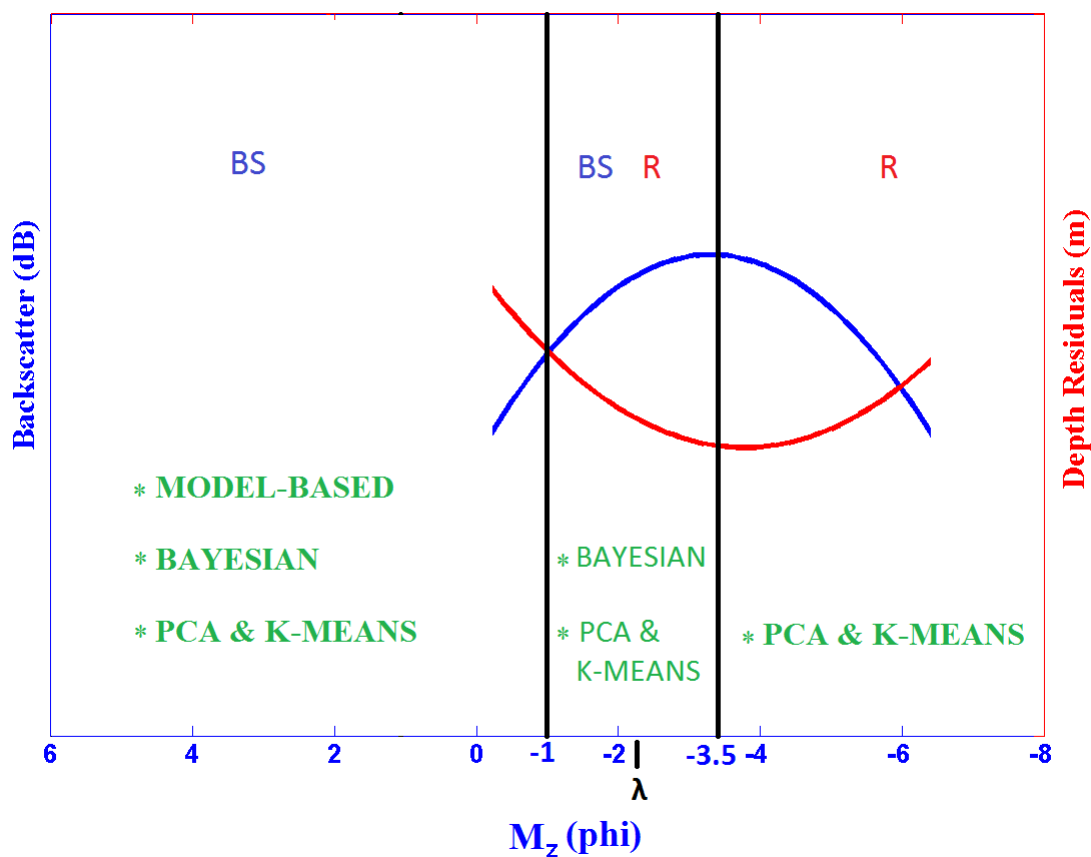


**FIG 9.4:** Overview plot of appropriate classifier(s) and method(s) for the different mean grain size ranges.

### **9.1.5 Conclusions from Chapter 8, application of classification methods**

In this chapter the sediment distribution differences in a part of Sint Andries that was surveyed in 2007 and re-surveyed in 2008 are assessed. For this area the classification methods that can be used are the Bayesian classification method and the method using PCA and K-means clustering. Both methods provide results as classes. Classes do not have a physical meaning so they cannot be used for directly comparing the sediment distribution maps in 2007 and 2008. Two approaches are used to assess the differences in the sediment distribution between the two surveys: a) to use the grab samples' mean grain size for deriving the relation between class and mean grain size, and b) to convert the classes into backscatter values. The latter, however, requires correcting for the imperfect calibration of the MBES with respect to backscatter.

The main conclusions is:

- The two different approaches used for assessing the differences in the sediment distribution of the area between 2007 and 2008 lead to different conclusions regarding the changes in sediment types present in the area. The mean grain size maps (based on the grab samples) showed that the area became substantially finer in 2008 compared to 2007. On the other hand, when using the calibrated backscatter curves of the areas, the differences are estimated to be very small. The first approach employed a very limited number of grab samples for converting acoustic classes to sediment mean grain size, and consequently the relation between them is subject to uncertainty. In addition, as mentioned in 9.1.1, care has to be taken when using grab samples to assign mean grain size values to the acoustic classes, as also other parameters affect these acoustic classes. The second approach shows that the area remained relatively unchanged during this one year. Since no exceptional flow phenomenon (e.g. flood) occurred in the area during this one year most probably the results of the second approach are closer to the truth.

## 9.2 Outlook

The methods for sediment classification using MBES data, as developed in this thesis, have been applied to various river environments, demonstrating their applicability. Compared to the traditional methods of using grab samples to map the river sediment distribution, the use of acoustic classification methods provides a huge increase in the detail with which this information is obtained. Use of the classification methods, and the resulting highly detailed maps, is expected to assist strongly in a further understanding of the river dynamics. This insight will, if incorporated in the morpho-dynamic models, add to the current capabilities of predicting the river dynamics. Useful insights on appropriate methods to assess differences on the sediment distribution of areas over a period of time can be gained when planning regular surveys of the same area using the same MBES systems.

Although the methods are at a stage that they allow for practical use, the on-going developments of the multi-beam system technology will give rise to further developments of classification methodologies. First of all, if MBES systems become well-calibrated with respect to backscatter strengths, the potential of assigning sediment characteristics to acoustic classes will strongly increase. This is the case for the sediment range for which models, predicting the backscatter strengths, exist, but alternatively, for well-known areas, a database can be established that contains for each sediment type the expected backscatter curve.

Another development in MBES systems that is of high interest for classification purposes is the possibility of registering for each beam the full incoming signal. This allows for applying model-based approaches, where the model used predicts the incoming signal per beam as a function of sediment characteristics.

Also developments in the classification methods are ongoing.

For the model-based approach in this thesis the theoretical model as developed by the Applied Physics Laboratory<sup>1</sup> was used since it is currently the most reliable and validated model. Developing new models valid for predicting backscatter for larger mean grain sizes will allow for using the model-based approach for the full range of mean grain sizes encountered in the Dutch rivers.

The Bayesian classification method fits Gaussian probability density functions on the histograms of the backscatter strength values per beam. Pre-requirement to this process is that the number of pixels in the beam footprint is large enough to ensure gaussianity. However, this degrades resolution. If use would be made of the non-averaged data, maximum resolution is kept, but another probability density function has to be assumed when fitting the histogram of the measured backscatter.

The behaviour of both the backscatter strength and the depth residuals can be further investigated by surveying areas that cover a large range of sediments (e.g. from  $9 \phi$  to  $-9 \phi$ ). For this it would be advantageous to use the same MBES and MBES settings.

**REFERENCES**

- <sup>1</sup> “APL-UW high-frequency ocean environmental acoustic models handbook”, Oct. 1994, technical report APL-UW TR9407AEAS 9501, Applied Physics Laboratory, University of Washington, pp. IV1-IV50.

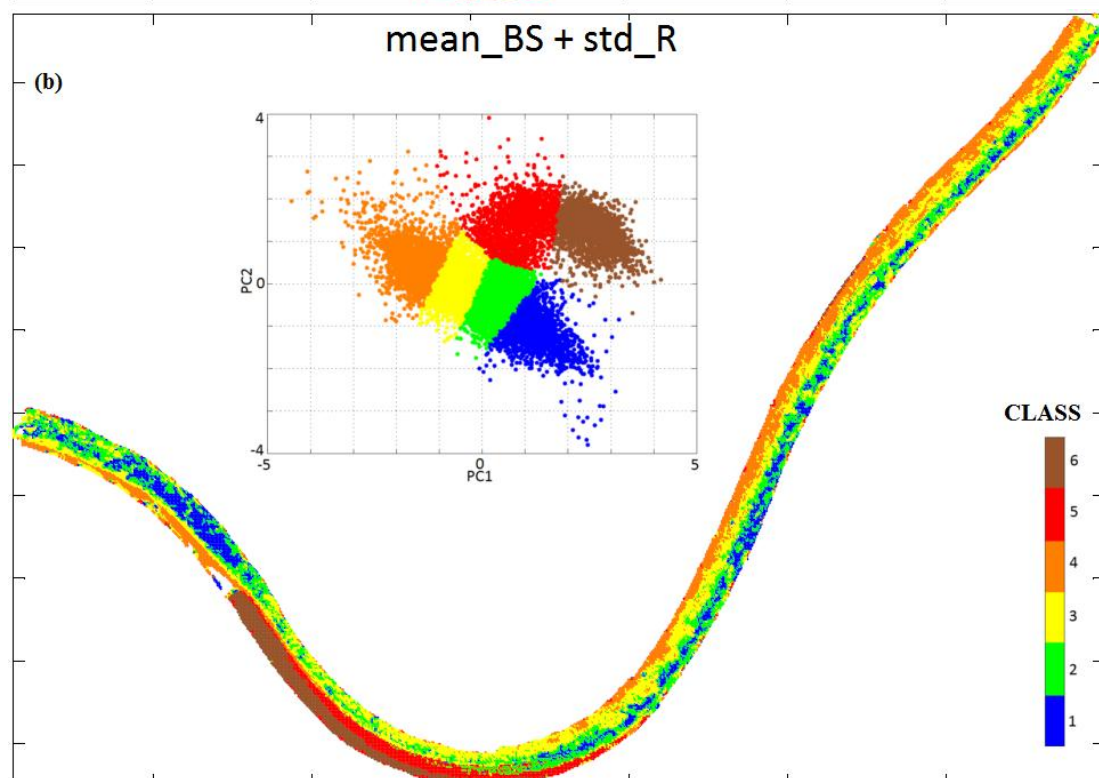
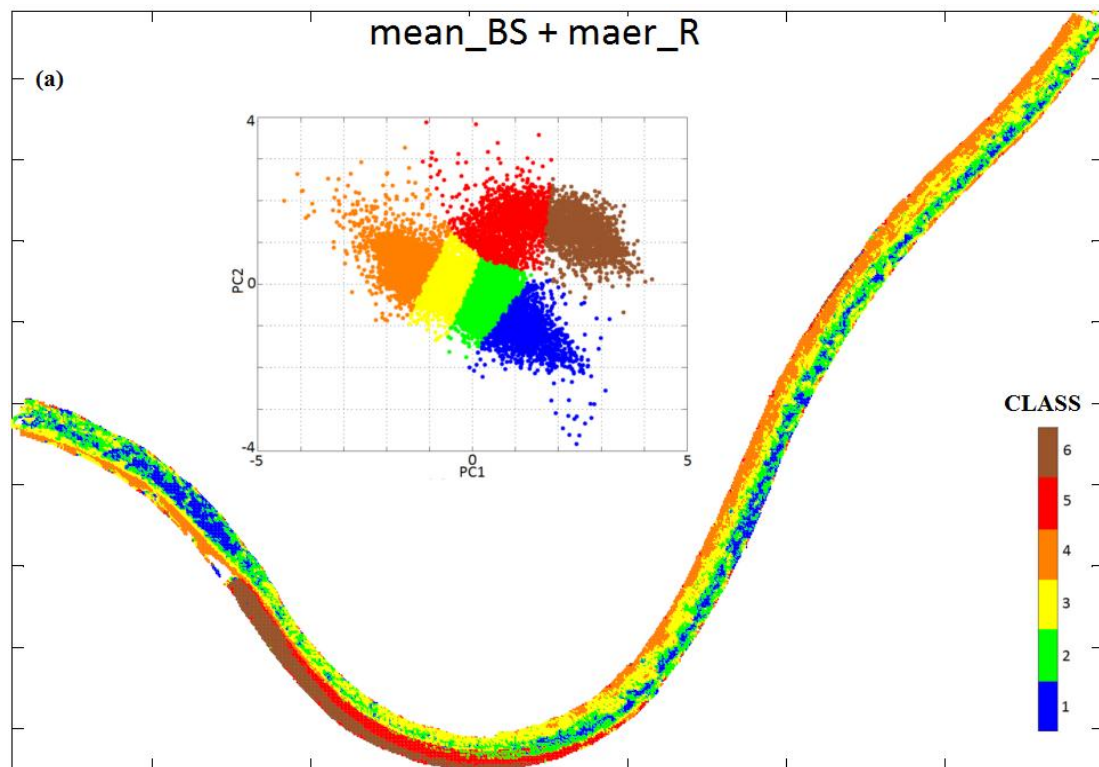
# A ● Maps of features combinations

---

The classification maps created with the PCA and K-means method were based on eight statistical features; four from the backscatter values and four from the depth residual values. These features are: the mean, median, minimum and mode of the backscatter and the mean absolute error (maer), standard deviation, minimum and maximum of the least-squares depth residuals. In Chapter 5 it is stated that any pair of the features of the kind (BS, Residuals) can also be used for providing the classification map of the areas that is visually similar to maps created from all eight features.

To illustrate this, in this section we use all possible combinations between one of the backscatter features (e.g. the mean backscatter) with each one of the four depth residual features in order to create the Sint Andries map (Fig. 5.15 top) with six different classes.

The resulted four maps are shown in Fig. A.1. All four maps in Fig. A.1 and the map in Fig. 5.15 top are very similar justifying the validity of the statement that any combination between any backscatter and any depth residual feature can be used to create classification map of an area very similar to the map created by the combination of all features.



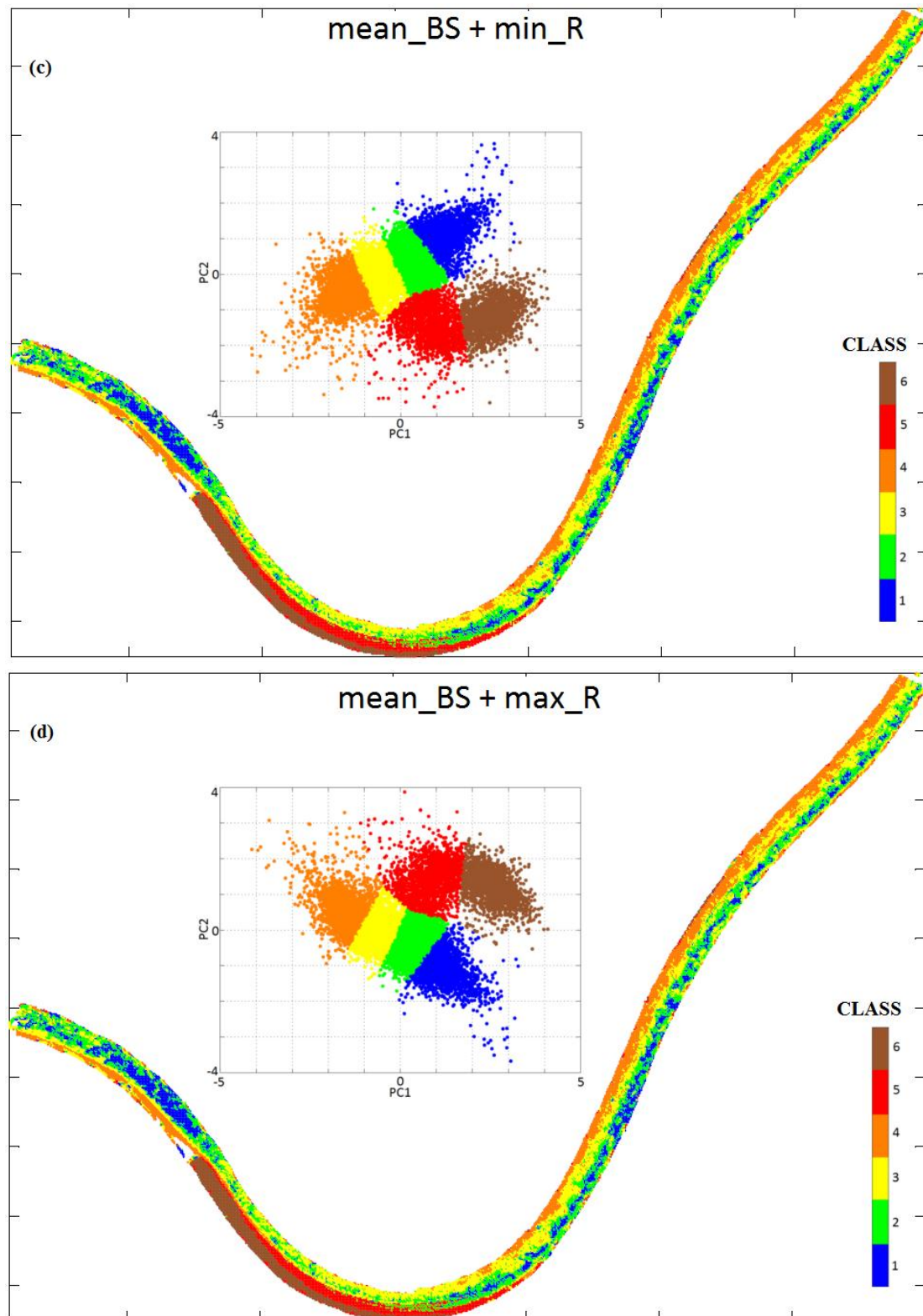


**FIG. A.1.** Classification map of Sint Andries based on the combination between (a) mean backscatter and mean absolute error of depth residuals, (b) mean backscatter and standard deviation of depth residuals, (c) mean backscatter and minimum of depth residuals, and (d) mean backscatter and maximum of depth residuals. In all plots also the clusters of the 6 different classes are shown.



# **B** • **Classification map of Dordtse kil based on Depth Residuals**

---

In Appendix B we will briefly give the results of the classification analysis of Dordtse Kil based on only the depth residuals. The analysis followed the PCA and K-means method described in Chapter 5.

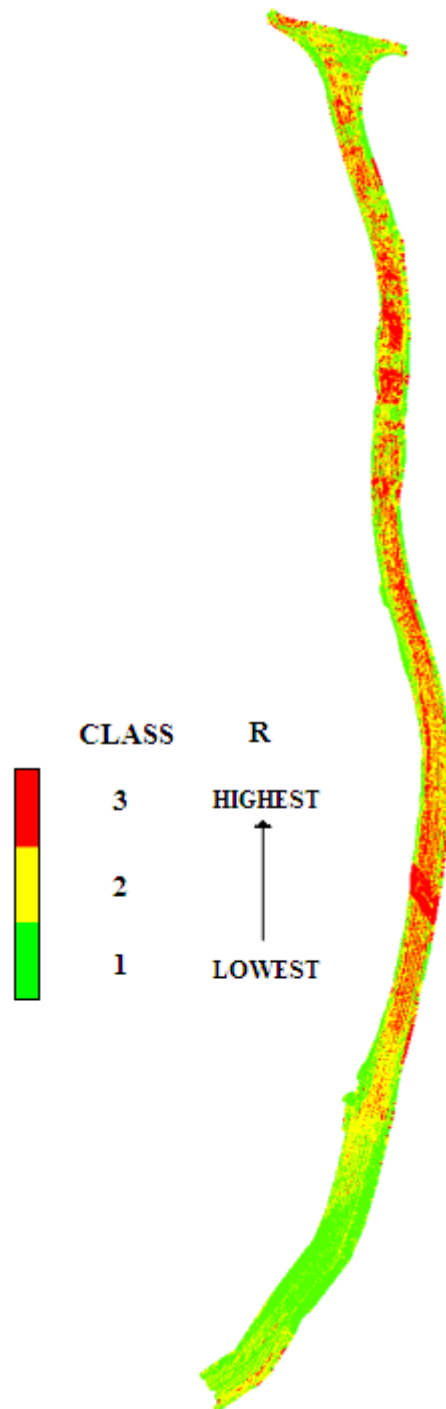
Four statistical features of the depth residuals contain most of the data information. These are: the mean absolute error, the standard deviation, the minimum and the maximum.

We select three classes as the optimum number of classes. For three classes both the percentage in the reduction of the distances of the clusters, and the average silhouette coefficient have maximum values.

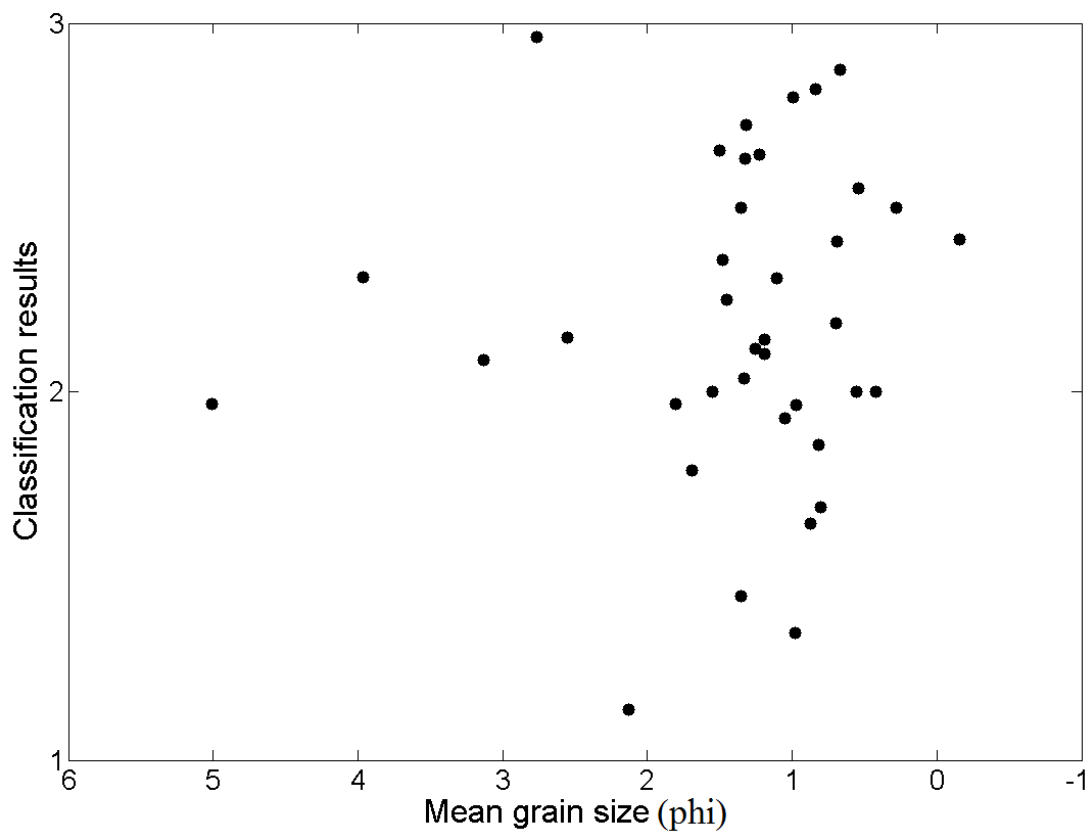
Figure B.1. presents the classification map of Dordtse Kil based on the four depth residual statistical features.

Figure B.2. shows the correlation between the classification results (classes) and the mean grain sizes (MGS) of the grab samples collected at Dordtse Kil. Each grab sample took the average class number of the surface patches within a radius of 30 metres from it. No outlier removal was performed.

From Fig. B.2. it is obvious that there is no correlation between the classification results and the grab samples.



**FIG. B.1.** Classification map of Dordtse kil based on the depth residual features.



**FIG. B.2.** Mean grain size of individual grab samples versus classification results of Fig. B.1., where class numbers 1, 2, 3 belong to the smaller, intermediate, and higher depth residual values.



# **C** ● **Bathymetry maps of Bovenrijn and Meuse**

---

In Appendix C the bathymetry maps of Bovenrijn (Fig. C.1.) and Meuse (Fig. C.2.) are presented as reconstructed by MBES measurements.

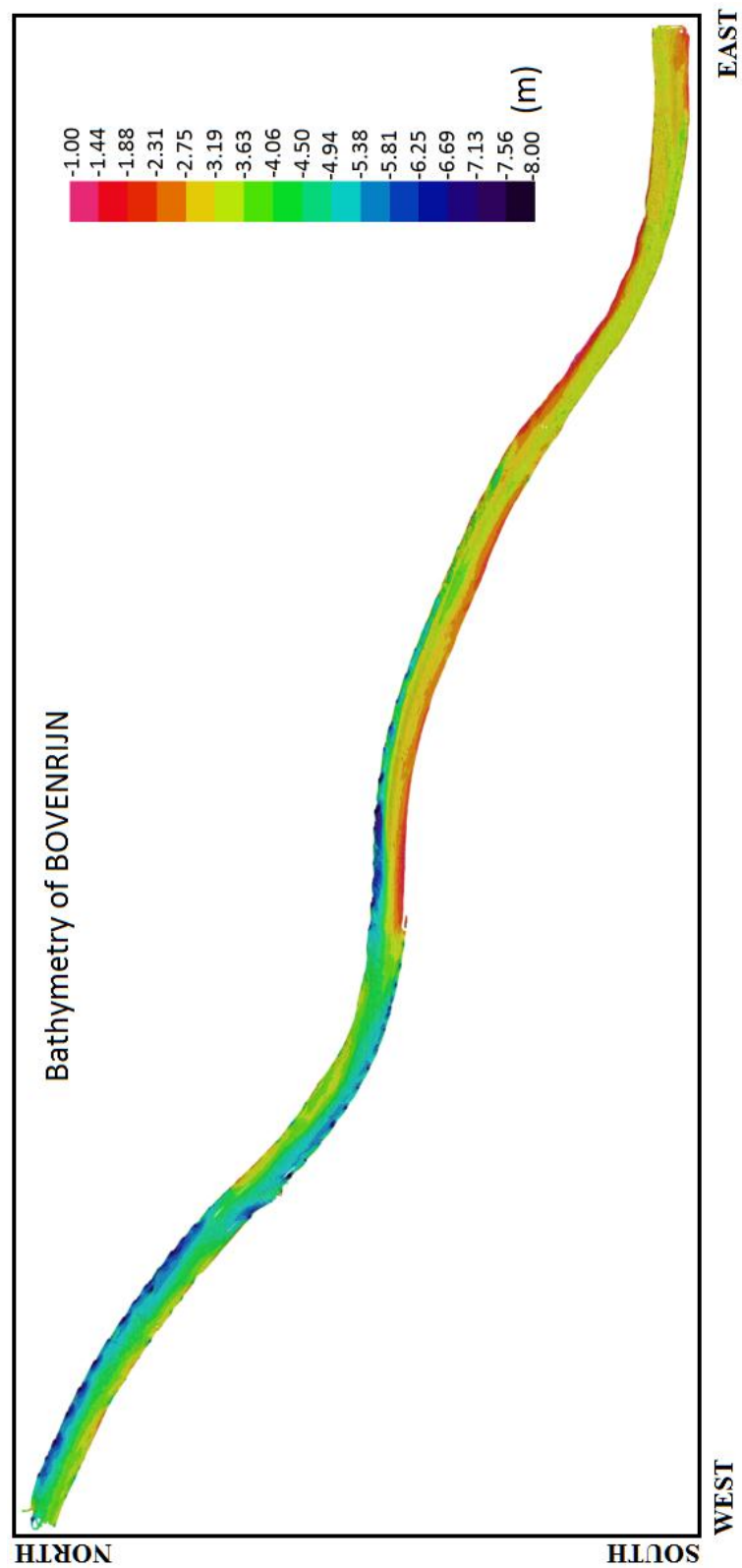


FIG. C.1. Bathymetry map of Bovenrijn.

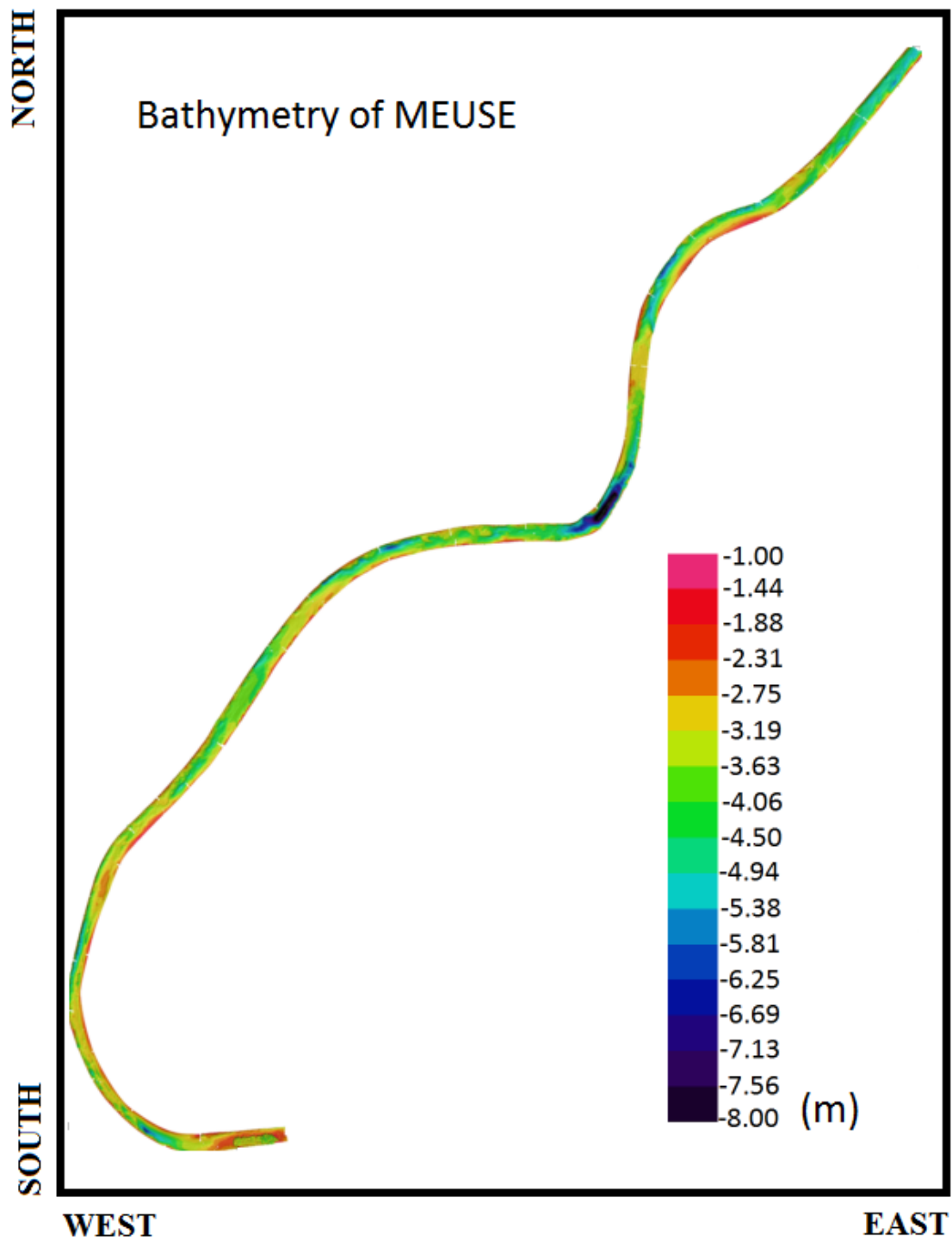


FIG. C.2. Bathymetry map of Meuse.



## Summary

---

The Netherlands are part of four international river basins: Rhine, Meuse, Scheldt and Ems. The economic importance of the Dutch rivers is very high as they are heavily used for inland waterway transport between the Netherlands and their neighbouring countries.

A minimum depth must be guaranteed to keep the rivers navigable but also to ensure that the ships can carry maximum cargo. The Rhine river has been trained with groynes, originally with the purpose to reduce the risk of flooding, but in later stages also to improve navigability. In the 1990s, the Waal Programme realized further measures to ensure navigability e.g. by constructing fixed layers consisting of large stones on top of the sediment. For the Rhine, fixed layers were constructed in the outer-bend pools of the bends at Nijmegen and St Andries in the river Waal.

The on-going overall bed degradation of the river Waal then arises as a problem, because the fixed layers in the outer-bend pools will not follow the degradation and hence become high obstacles. River bed nourishment by artificial sediment supply is considered as an appropriate measure to arrest overall bed degradation. The success of the measures on keeping the navigation in the Dutch rivers safe is assessed by continuously monitoring the depth of the rivers. In addition the sediment distribution also needs to be monitored in order to assess the long term behaviour of the suppletions.

An attractive system for obtaining information about the riverbed bathymetry is the multi-beam echo-sounder (MBES). Furthermore, the MBES received echoes due to acoustic backscatter from the sediments in theory also allow for discriminating between different sediments. This method gained significantly in potential especially during the last decade when new MBES systems have been developed. This thesis falls within these research efforts to discover the full potential of backscatter measurements for sediment discrimination and characterisation in order to gradually replace the conventional way of mapping the sediment composition of the riverbed by taking a large number of physical grab samples. The MBES provides high spatial coverage of an area within a short time, while the conventional approach is time consuming and provides information at the grab samples positions only.

The aim of the research presented in this thesis was to develop methods for discriminating between different river sediments using MBES measurements. In order to fulfil this aim, MBES surveys were performed in the Rhine river and the Meuse river between 2007 and 2010. Five parts of the Rhine river were surveyed: Sint Andries, where a large survey was carried out in 2007 with a re-survey of a smaller part of this area in 2008, Nijmegen (2008), Bovenrijn (2008), and the Dordtse Kil (2009). A part of the Meuse river was surveyed in 2010. All rivers are shallow having similar depth ranges from 1 m to 10 m, except for the Dordtse Kil, which is deeper with depths ranging between 1 m to 19 m.

Grab samples were collected from all surveyed areas. Based on the grab samples mean grain size there is a gradual shift from fine sediments in Dordtse Kil to coarse sediments in Sint Andries and Nijmegen, and finally to very coarse sediments in Bovenrijn and Meuse. Video images and still photographs were taken underwater at each grab sample position to assist interpretation of the results.

All the measurements were performed using EM3002 Kongsberg MBES systems. The system sonar frequency is nominally 300 kHz.

The research shows that indeed the MBES system can be used for discriminating between the different sediments present in the river areas. In addition an important finding is that areas differing in sediment type require different classification approaches. The classification approaches employed in the thesis are

- 1) The so-called Bayesian classification approach that uses the MBES backscatter data collected at a certain angle to obtain the number of acoustic classes and to discriminate between them by applying the Bayes decision rule for multiple hypotheses. This method is found to discriminate between different sediment types (Chapter 4). However, it is found that a transition point exists at which the behaviour of backscatter as a function of mean grain size reverses. For small grain sizes backscatter increases with mean grain size whereas it is found to no longer increase with increasing mean grain size for sediment with mean grain sizes larger than this transition point. Discrimination between sediments is possible as long as the range of sediment types encountered in the area is below or above this transition point. For environments with sediment mean grain sizes both below and above the transition point, there is ambiguity, resulting in both finer and coarser sediments being assigned to a single acoustic class.
- 2) The second method solves this ambiguity, at least partly. In addition to backscatter now also features of the bathymetric measurements are used for discriminating between the different sediments. These bathymetric features are derived from the so-called depth residuals. They are calculated by modelling the measured depths through a 2-D second order polynomial fit using the least squares (LS) principle. However, the actual measured depths deviate from the modelled surface. These deviations are the depth residuals. They provide measures as to which degree the actual river bottom is smooth. The combination of backscatter strength and depth residuals is achieved by using principal component analysis to remove feature inter-dependency and the K-means clustering method is used to assign feature ranges to the different sediment types. An example, showing the strength of adding these bathymetric features to the classification is given in Chapter 5. Three cases were investigated: i) classification with only the backscatter features, ii) classification with only the LS depth residual features, and iii) classification with both backscatter and LS depth residual features. When using only the backscatter strength three classes were identified but the fixed layer was not discriminated as a separate class. Adding the depth residual features, however, shows the fixed layer as a fourth class.
- 3) The third method is model-based and matches the full curve of measured backscatter strength versus beam angle of the MBES to a predicted backscatter curve. The agreement between measured and modelled curves is maximised by searching for the unknown model input parameters, using the global optimisation method of differential evolution. The model-based method provides values for the unknown parameters, i.e. the sediment parameters mean grain size ( $M_z$ ), spectral strength of sediment surface

roughness ( $w_2$ ) and a volume scattering parameter ( $\sigma_2$ ). At current however, the imperfect calibration of the MBES backscatter strengths measurements, prevents the direct application of this method. In this thesis calibration was performed based on grab samples and by using the data obtained at the fixed layer. Both calibration approaches show similar results. Still, applying the model based results to the Dordtse Kil area (Chapter 4) indicates offsets in the estimated  $M_z$  values compared to those derived from the grab samples. This can be due to a still imperfect calibration of the measured backscatter values, caused by a limited number of grab samples available for the calibration. In addition, imperfect modelling of the backscatter curve can play a role.

Next to deriving the optimal classification strategy, another important topic investigated in this research is the potential of assigning characteristics of the sediments, such as mean grain size, to the different sediment classes. This item is of relevance mainly for the methods 1 and 2 as listed above. An obvious approach may be to use the grab samples and apply a linear fit to the acoustic classes vs. mean grain size from the grab samples. It is however demonstrated that this approach is hampered by several factors. The first is the fact that backscatter strengths are determined not only by mean grain size, but also by other sediment parameters such as sediment roughness and volume inhomogeneities as shown in Chapter 4. Secondly, there is a transition point at which the behaviour of backscatter vs. sediment mean grain size reverses, impeding an unambiguous relation (Chapter 6). Also for the depth residuals a transition point is found (Chapter 6). However, here depth residual values decrease with increasing mean grain size for the finer sediments and increase for the coarser sediments. Although from this research it is clearly shown that assuming a linear fit between mean grain size and acoustic class is subject to errors, still an ordering of classes with respect to mean grain size, for example finer, less fine, coarser, is possible. This is only the case if the sediments encountered in the surveyed area all fall below or above the transition point. Otherwise additional knowledge, e.g. knowing that there is a fixed layer present, is needed to make such an ordering.

When applying the acoustic classification method to investigate changes in the spatial sediment distribution and sediment types, the ordering of classes in general will not suffice. A solution is presented in Chapter 8. In this chapter the differences in a river that was surveyed twice using MBES are evaluated both regarding the bathymetry and the sediment distribution. The time interval between the surveys is one year (2007 and 2008). For both surveys three classes were found in the area. The classes were compared using the backscatter curves per class. From this it is found that the backscatter curves for the classes of 2007 very closely resemble the classes of 2008, indicating similar sediment types.

Another classification method considered in this thesis (Chapter 4) is classification based upon the levels of gamma-ray radiation being emitted from very low concentrations of a number of radionuclides in the sediment, i.e.,  $^{137}\text{Cs}$ ,  $^{40}\text{K}$ ,  $^{238}\text{U}$  and  $^{232}\text{Th}$ . The system used for taking these measurements is the ‘Multi-element detection system for underwater sediment activity’ (Medusa). Also a hydrophone is towed over the sediments measuring noise levels. This measurement is used mainly for monitoring whether or not the Medusa system is in contact with the river bottom, but is found to also provide a measure for the roughness of the sediment. It is found that the MBES and Medusa measurements show similar spatial distributions of different sediment types, but that Medusa can also reveal the presence of organic matter in the sediment based on the  $^{137}\text{Cs}$  measurements.



## Samenvatting

---

Nederland is onderdeel van vier internationale rivierbekkens: de Rijn, Maas, Schelde en Eems. Het economische belang van de Nederlandse rivieren is zeer groot, want ze worden intensief gebruikt voor vervoer over binnenwateren tussen Nederland en de naburige landen.

Om de rivieren bevaarbaar te houden en ervoor te zorgen dat schepen de maximum lading kunnen vervoeren, moet er een minimum diepte worden gegarandeerd. In de Rijn zijn golfbrekers aangelegd, oorspronkelijk met de bedoeling om het risico van overstromingen te verkleinen, maar later ook om de bevaarbaarheid te verbeteren. In de jaren negentig werden in het kader van het Waal-programma verdere maatregelen genomen om de bevaarbaarheid te garanderen, bijvoorbeeld door een vaste laag aan te brengen in de vorm van grote stenen op het sediment. Voor de Rijn werden vaste lagen aangelegd in de diepe gedeelten van de bochten (in de buitenbocht) in de Waal bij Nijmegen en Sint Andries.

De voortdurende erosie van de bedding van de Waal zorgt echter voor een probleem, want de vaste lagen in de diepe gedeelten in de buitenbocht eroderen niet en worden daardoor hoge obstakels. Het storten van kunstmatig sediment op de rivierbedding wordt als een adequate maatregel beschouwd om de erosie van de bedding tegen te gaan. Er wordt gecontroleerd of de maatregelen voor een veilige bevaarbaarheid van de Nederlandse rivieren succesvol zijn door continu de diepte van de rivieren te meten. De verdeling van het sediment moet ook worden gevolgd om te bepalen wat het gedrag van de suppleties op de lange termijn is.

Een aantrekkelijk middel om informatie te verkrijgen over het diepteprofiel van de rivierbedding is het multibeam echolood. Bovendien kunnen met de multibeam echo's t.g.v. akoestische verstrooiing aan het sediment in theorie ook verschillende sedimenten worden onderscheiden. Deze methode is met name in de laatste tien jaar steeds interessanter geworden door de nieuwe multibeam echoloodsystemen die werden ontwikkeld. Dit proefschrift valt binnen het kader van het onderzoek om het volledige potentieel te ontdekken van het meten van deze akoestische verstrooiing voor het onderscheiden en karakteriseren van sedimentlagen. Het doel is dat deze methode de conventionele methode geleidelijk gaat vervangen. Nu wordt de samenstelling van sedimenten van rivierbeddingen bepaald door een groot aantal fysieke monsters van de bodem te nemen. Met een multibeam echolood kan snel een nauwkeurig volledig dekkend beeld worden verkregen van een heel gebied, terwijl de conventionele methode tijdrovend is en alleen informatie oplevert over de posities waar de bodemmonsters zijn genomen.

Het doel van het in dit proefschrift beschreven onderzoek was het ontwikkelen van methoden voor het onderscheiden van verschillende riviersedimenten met behulp van metingen met een multibeam echolood. Daarvoor is tussen 2007 en 2010 onderzoek verricht met een multibeam echolood in de Rijn en de Maas. Vijf gedeelten van de Rijn zijn onderzocht: Sint Andries, waar in 2007 een groot onderzoek werd uitgevoerd en in 2008 een nieuw onderzoek plaatsvond van een kleiner gedeelte van dit gebied, Nijmegen (2008), Bovenrijn (2008) en de Dordtse Kil (2009). In 2010 werd een gedeelte van de Maas onderzocht. Al deze rivieren zijn ondiep en hebben vergelijkbare diepten van 1 tot 10 meter, behalve de diepere Dordtse Kil, waar de diepte varieert van 1 tot 19 meter.

In alle onderzochte gebieden werden bodemmonsters genomen. Uit de gemiddelde korrelgrootte van de bodemmonsters blijkt dat er een geleidelijke

overgang is van fijne sedimenten in de Dordtse Kil naar grove sedimenten bij Sint Andries en Nijmegen en uiteindelijk naar zeer grove sedimenten in de Bovenrijn en de Maas. Er werden onder water videobeelden en foto's gemaakt van iedere plaats waar bodemonsters werden genomen om de resultaten beter te kunnen interpreteren. Alle metingen werden verricht met het Kongsberg EM3002 multibeam echoloodstelsel. De sonarfrequentie van het systeem is nominaal 300 kHz.

Uit het onderzoek bleek dat het multibeam echoloodstelsel inderdaad kan worden gebruikt om verschillende sedimenten in de riviergebieden te onderscheiden. Een andere belangrijk resultaat is dat gebieden met verschillende sedimenttypen verschillende classificatiemethoden vereisen. De volgende classificatiemethoden zijn voor dit proefschrift gebruikt:

- 1) De zogenaamde Bayesiaanse classificatiemethode, waarbij gebruik wordt gemaakt van data van het terugverstrooide signaal die onder een bepaalde hoek zijn verzameld. Het aantal akoestische klassen en het onderscheid tussen die klassen kunnen worden bepaald met behulp van de beslissingsregel van Bayes voor meerdere hypothesen. We constateerden dat met deze methode verschillende sedimenttypen kunnen worden onderscheiden (hoofdstuk 4). Er is echter ook vastgesteld dat er een overgangspunt is waarbij de akoestische verstrooiingssterkte als functie van de gemiddelde korrelgrootte tegenovergesteld gedrag gaat vertonen. Bij kleine korrelgrootten neemt de verstrooiing toe met de gemiddelde korrelgrootte, terwijl dat niet het geval is voor sedimenten waarbij de gemiddelde korrelgrootte voorbij dit overgangspunt ligt. Er kunnen sedimenten worden onderscheiden zolang de korrelgrootte van de sedimenten in het onderzochte gebied zich onder of boven dit overgangspunt bevinden. In gebieden met sedimenten met gemiddelde korrelgrootten die zowel onder als boven het overgangspunt liggen, zijn de resultaten dubbelzinnig, want zowel fijnere als grovere sedimenten kunnen worden gekoppeld aan dezelfde akoestische klasse.
- 2) De tweede methode biedt een oplossing voor deze dubbelzinnigheid, in ieder geval ten dele. Naast verstrooiingsgegevens worden ook kenmerken van de bathymetrische metingen gebruikt om verschillende sedimenten te onderscheiden. Deze bathymetrische kenmerken worden afgeleid van de zogenaamde diepteresiduen. Deze worden berekend door van de gemeten diepten een model te maken met behulp van een tweedimensionale tweede orde polynoomfit waarbij de kleinste-kwadratenmethode wordt toegepast. De werkelijk gemeten diepten wijken echter af van dit model. Deze afwijkingen zijn de diepteresiduen. Op grond daarvan kan worden bepaald in hoeverre de werkelijke rivierbodem glad is. De verstrooiingssterkte en de diepteresiduen worden gecombineerd door met behulp van 'principle component' analyse de onderlinge afhankelijkheid van verschillende kenmerken te elimineren en door met de K-means clustermethode een bereik van kenmerken toe te kennen aan de verschillende sedimenttypen. Een voorbeeld in hoofdstuk 5 laat de kracht zien van het toevoegen van deze bathymetrische kenmerken aan de classificatie. Er werden drie gevallen onderzocht: i) classificatie met alleen de verstrooiingskenmerken, ii) classificatie met alleen de kenmerken van de diepteresiduen die met de kleinste-kwadratenmethode zijn verkregen, en iii) classificatie met zowel alle verstrooiingskenmerken als alle kenmerken van de diepteresiduen. Met gebruikmaking van alleen de verstrooiingssterkte werden

drie klassen geïdentificeerd, maar de vaste laag werd niet als een afzonderlijke klasse onderscheiden. Wanneer de kenmerken van de diepteresiduen werden toegevoegd, werd de vaste laag echter wel als een vierde klasse gevonden.

- 3) Bij de derde, modelgebaseerde methode wordt de volledige curve van de gemeten verstrooiingssterkte als functie van de bundelhoek (t.o.v de normaal) gematcht aan een voorspelde verstrooiingscurve. De overeenstemming van de gemeten curven en de modelcurven wordt gemaximaliseerd door te zoeken naar de onbekende invoerparameters van het model, waarbij gebruik wordt gemaakt van een globale optimalisatiemethode, genaamd 'differentiële evolutie'. Met de modelgebaseerde methode kunnen waarden worden gevonden voor de onbekende parameters, dat wil zeggen de sedimentparameters gemiddelde korrelgrootte ( $M_z$ ), spectrale sterkte van de oppervlakteruwheid van het sediment ( $w_2$ ) en een volumeverstrooiingsparameter ( $\sigma_2$ ). Op dit moment kan deze methode echter niet direct worden toegepast vanwege de niet perfecte ijking van de verstrooiingssterktemetingen met het multibeam echolood. Voor dit proefschrift werd geijkt door middel van bodemmonsters en door gebruik te maken van de vaste laag. Beide ijkingmethoden leverden vergelijkbare resultaten op. Toepassing van het modelgebaseerde resultaat op het gebied van de Dordtse Kil (hoofdstuk 4) wijst echter op systematische verschillen tussen de met de modelgebaseerde methode geschatte  $M_z$  ten opzichte van de  $M_z$  waarden die zijn afgeleid uit de bodemmonsters. Dit kan het gevolg zijn van een nog steeds niet optimale ijking van de gemeten verstrooiingswaarden doordat maar een beperkt aantal bodemmonsters beschikbaar was voor de ijking. Daarnaast kan het model van de verstrooiingscurve niet precies genoeg zijn.

Naast het bepalen van de optimale classificatiestrategie was een ander belangrijk onderwerp van dit onderzoek de mogelijkheid om kenmerken van de sedimenten zoals gemiddelde korrelgrootte toe te kennen aan de verschillende sedimentklassen. Dit onderwerp is voornamelijk van belang voor de hiervoor genoemde methode 1 en 2. De voor de hand liggende methode is om bodemmonsters te gebruiken en een lineaire fit toe te passen op de akoestische klassen als functie van de gemiddelde korrelgrootte, maar er is aangetoond dat deze methode door verschillende factoren wordt belemmerd. Het eerste probleem is dat de verstrooiingssterkten niet alleen afhangen van de gemiddelde korrelgrootte, maar ook van andere sedimentparameters zoals de ruwheid van het sediment en de volume-inhomogeniteiten in het sediment, zoals in hoofdstuk 4 wordt aangetoond. Ten tweede is sprake van een overgangspunt waarbij het verstrooiingsgedrag als functie van de gemiddelde korrelgrootte omslaat, waardoor een ondubbelzinnige relatie niet mogelijk is (hoofdstuk 6). Ook voor de diepteresiduen is een overgangspunt gevonden (hoofdstuk 6). De diepteresiduuwaarden nemen af met toenemende gemiddelde korrelgrootte voor de fijnere sedimenten en nemen toe voor de grovere sedimenten. Uit dit onderzoek blijkt duidelijk dat het uitgangspunt van een lineaire fit tussen gemiddelde korrelgrootte en akoestische klasse tot fouten leidt. Het is echter nog wel steeds mogelijk om klassen te ordenen op grond van de gemiddelde korrelgrootte, bijvoorbeeld fijner, minder fijn en grover. Dit is echter alleen het geval als de sedimenten die in het onderzochte gebied zijn gevonden allen onder of boven het overgangspunt zitten. Anders is aanvullende

kennis nodig om deze ordening uit te voeren, bijvoorbeeld weten dat er een vaste laag is.

Wanneer de akoestische classificatiemethode wordt toegepast om veranderingen in de ruimtelijke sedimentverdeling en sedimenttypen te bestuderen, is het ordenen van klassen over het algemeen niet voldoende. Een oplossing voor dit probleem wordt besproken in hoofdstuk 8. In dat hoofdstuk worden de verschillen geëvalueerd die zijn geconstateerd bij resultaten van een rivier die tweemaal met een multibeam echolood is onderzocht, zowel wat betreft het diepteprofiel als de sedimentverdeling. De periode tussen de twee meetcampagnes is één jaar (2007 en 2008). Bij beide campagnes werden in het gebied drie klassen gevonden. De klassen werden vergeleken met behulp van de verstrooiingscurven per klasse. Op grond daarvan werd vastgesteld dat de verstrooiingscurven voor de klassen van 2007 in hoge mate lijken op die voor de klassen van 2008, hetgeen wijst op vergelijkbare sedimenttypen. In dit proefschrift wordt ook een classificatiemethode toegepast welke gebaseerd is op het meten van de niveaus van gammastraling afkomstig uit zeer lage concentraties van een aantal radionucliden in het sediment, namelijk  $^{137}\text{Cs}$ ,  $^{40}\text{K}$ ,  $^{238}\text{U}$  en  $^{232}\text{Th}$  (hoofdstuk 4). Deze metingen worden met het Medusa (Multi-element detection system for underwater sediment activity) systeem verricht. Er wordt ook een hydrofoon over de sedimenten gesleept die de geluidsniveaus meet. Deze meting wordt voornamelijk gebruikt om te controleren of het Medusa-systeem wel in contact is met de rivierbodem, maar uit deze meting bleek ook de ruwheid van het sediment te kunnen worden afgeleid. De multibeam metingen en de metingen met Medusa bleken vergelijkbare ruimtelijke verdelingen van verschillende sedimenttypen op te leveren, maar met Medusa kan ook de aanwezigheid van organisch materiaal in het sediment worden vastgesteld op grond van de  $^{137}\text{Cs}$ -metingen.

## Acknowledgements

---

The research presented in this thesis is financially supported by Deltares.

First and foremost, I would like to thank my supervisor Prof. Dick G. Simons for giving me the chance to participate in this very interesting project. I would especially like to thank him for his continuous support and encouragement to participate in many international conferences in order to quickly become a member of the scientific community. Also, his advice and feedback, based on his undeniable expertise on the field, was always critical on improving the quality of the work carried in this thesis.

I would like to express my deepest gratitude to my daily supervisor Dr. M. Snellen, for her continuous help and guidance throughout the project. Her vast scientific knowledge combined with her hard working attitude was important on achieving successful research outcomes. Furthermore, her open door policy, and meticulous reviewing are highly appreciated.

One of the most important persons who contributed to the completion of the research work was Dr. Alireza Amiri-Simkoei. Alireza continued the work of Prof. Simons and Dr. Snellen on sediment classification and I tried to follow his path. Alireza is a wonderful person and a real expert. He was always positive and he was trying to efficiently guide and help me in –unfortunately– the limited time that he was present in the Delft University during the project.

The members of the doctoral committee are highly acknowledged for their thorough review of this thesis.

I would like to acknowledge Dr. Arjan Sieben for initiating the project after realising the significant potential of the acoustic remote sensing methods on riverbed sediment classification. Arjan's help throughout the thesis was invaluable.

I would also like to thank Ir. Ben Dierikx for coordinating the project and for his help when it was needed.

Sincere thanks to Dr. Niels Kinneking for the cooperation that we had for preparing the paper for and his excellent presentation in Hydro12 conference.

Dr. Erik Mosselman is one of the key contributors for giving a “morphological” insight to the classification results of the thesis. With his expertise he helped me link the classification results to river processes. He was always friendly and his guidance was priceless.

Special thanks belong to Adri Wagener for ensuring the success of the river surveys. With this opportunity I would like to thank all the crew members of the ships that participated in the river surveys. They were extremely helpful, trying to do everything in order to acquire “good” data.

I would like to thank deeply Ronald Koomans and all Medusa members for the excellent cooperation that we had in the Dordtse Kil survey and the journal paper to JASA.

I would like to thank Dr. S. Giri, Dr. A. Blom, Dr. Y. Huismans and Cl. Orru with whom we cooperated on interesting topics trying to understand the usefulness of our classification results to river engineering.

I am grateful to T. Eldevik, service engineer in Kongsberg for his prompt help in all issues that arose with regard to the sonar operation. Also, I would like to thank St. Berendse and P. Bijl from Kongsberg for their help during the surveys.

I would like to thank Dr. Z. Lubniewski from the Gdansk University of Technology for providing data with the water column of the MBES.

Warmest thanks to all my colleagues (Air Transport and Operations group) and former colleagues (Laser remote sensing group and Mathematical geodesy and positioning group) for their support. In particular I would like to thank my roommates over these years: Laslo Evers, Brenda Hooiveld, Kerstin Siemes, Julius Fricke, Michael Arntzen, Mathieu Colin, Bert van Midden and Edo van Dijl. Special thanks to Wim Verhagen for his helpful information regarding the format of the thesis.

I would also like to thank Dr. N. El Allouche, an excellent person and very good scientist for the co-operation that we had in the acoustic instrument experiments. Many thanks also to Paul Keijzer for his technical support on the same project.

Many thanks to the experts from the technical computer support department in Aerospace Engineering. They were always keen to fix as soon as possible problems with crashed hard drives (happening usually close to deadlines of papers submissions). Moreover, many thanks to the technicians in the Fluid mechanics laboratory for their help with the swimming pool experiment.

Special thanks to all secretaries taking care of the formalities concerning my work. Starting with Lidwien de Jong whom I first met when I joined the University and of course Vera van Bragt and Geeta van der Zaken, who helped me in the final stages of my thesis.

Finally, words are not enough to express my love to my family and friends for their moral support.

## Curriculum vitae

---

Dimitrios Eleftherakis was born on the 5<sup>th</sup> of March 1974. He graduated as mechanical engineer from the University of Patras, Greece, in 1998. After completing his military service in the Greek Air-force (20 months), he continued his studies obtaining an MSc degree at UMIST (University of Manchester Institute of Science and Technology) in 2000-2001. There he specialised in Advanced Manufacturing Technology and Systems Management.

Then, he worked for one year (2002-2003) in Saudi Arabia as mechanical engineer for a Dutch-Greek construction company. He was managing and motivating multi-national teams to effectively maintain and repair company's land and marine equipment. After Saudi Arabia he worked for almost 2 years (2003-2005) in the Agricultural University of Athens as researcher, where he was using computationally fluid dynamics to analyse low structures for plant protection.

His great passion for the sea and especially underwater activities led him to study a second MSc course in Offshore and Ocean Technology (specialized in diving and underwater technology) at Cranfield University in 2005-2006.

He joined the Delft University of Technology in 2009 to study underwater acoustics in depth.

## Bibliography

### Peer-reviewed journals

D. Eleftherakis, A.R. Amiri-Simkooei, M. Snellen, and D.G. Simons, "Improving riverbed sediment classification using backscatter and depth residual features of multi-beam echo-sounder systems", *Journal of the Acoustical Society of America* 131(5), 3710-3725 (2012).

M.Snellen, D. Eleftherakis, A. Amiri Simkooei, R.L. Koomans, and D.G. Simons, "An inter-comparison of sediment classification methods based on multi-beam echo-sounder backscatter and sediment natural radioactivity data", *Journal of the Acoustical Society of America* 134(2), 959-970 (2013).

**Conference proceedings**

D. Eleftherakis, E. Mosselman, A.R. Amiri-Simkooei, S. Giri, M. Snellen, and D.G. Simons. "Identifying changes in river bed morphology and bed sediment composition using multi-beam echo-sounder measurements", In: Proc. of the 10th European conference on Underwater Acoustics, July 5-9, Istanbul, Turkey, 1365-1373 (2010).

A. Amiri-Simkooei, D. Eleftherakis, M. Snellen, and D.G. Simons, "Inversion of bottom parameters in riverbed soft sediment using multi-beam backscatter strength", In: Proc. Of the 4<sup>th</sup> International Conference and Exhibition on Underwater Acoustic Measurements: Technologies and Results, 20-24 June, Kos, Greece, 1267-1274 (2011).

D. Eleftherakis, A.R. Amiri-Simkooei, M. Snellen, R.L. Koomans and D.G. Simons, "Determining riverbed sediment composition using multi-beam echo-sounder backscatter data and natural radio activity", In: Proc. Of the 4<sup>th</sup> International Conference and Exhibition on Underwater Acoustic Measurements: Technologies and Results, 20-24 June, Kos, Greece, 1275-1282 (2011).

D. Eleftherakis, M. Snellen, A.R. Amiri-Simkooei, and D.G. Simons, "Determining sediment composition of coarse riverbeds using multi-beam echo-sounder backscatter and bathymetric features", In Proceedings of the 11<sup>th</sup> European Conference on Underwater Acoustics, 2-6 July, Edinburgh, UK, 619-626 (2012).

N. Kinneging, M. Snellen, D. Eleftherakis, D.G. Simons, E. Mosselman, and A. Sieben, "Riverbed classification using multi-beam echo-sounder backscatter data", In Proc. Hydro12 - Taking care of the sea, 13-15 November, Rotterdam, The Netherlands (2012).

D. Eleftherakis, M. Snellen, A.R. Amiri-Simkooei, and D.G. Simons, "Overview of methodologies for the acoustic classification of sediment distribution in Dutch rivers using multi-beam echo-sounder data", In Proceedings of 1st International Conference and Exhibition on Underwater Acoustic, 23-28 June, Corfu, Greece, 1407-1414 (2013).